In today's technology, when there is an avalanche of increasingly sophisticated, more electronic and mechatronic systems, a very important thing for the intelligent control of some physical quantities, which can be: heat, vibrations, forces, moments of friction, is intelligent measurement and control systems. These systems are made by combining computerized, on-line control with various intelligent materials, whose physical properties change depending on the various external physical quantities. In the technique of dynamic behavior optimization, a special role is played by the complex auxiliary components with spring, damper type elements, which are inserted into the structure of industrial robots, RI. Vibration isolators and shock absorbers are used in common to reduce the vibrations of machines and installations. Isolating elements are usually passive and are generally designed to reduce vibrations with unwanted frequencies. Often, in many applications, the excitation frequency varies over a wide range, which is why it is necessary to adjust the damping during system operation.

The research team is made up of a university professor specialised in the field of assisted research of dynamic behaviour in Robotics, a scientific researcher with a doctorate in science in the field of magneto-rheological dampers and a scientific researcher with a doctorat in the military field of optimization of the intelligent servo-actuators.

9 786206 156918

Serban Olaru, Adrian Olaru, Adrian Alexei

Serban Olaru
Adrian Olaru
Adrian Alexei

Modelling, simulation and optimisation in Robotics

Appling magneto-rheological dampers in the robots structure

LAP LAMBERT Academic Publishing

Serban Olaru
Adrian Olaru
Adrian Alexei

Modelling, simulation and optimisation in Robotics

Serban Olaru
Adrian Olaru
Adrian Alexei

Modelling, simulation and optimisation in Robotics

Appling magneto-rheological dampers in the robots structure

LAP LAMBERT Academic Publishing

Imprint
Any brand names and product names mentioned in this book are subject to trademark, brand or patent protection and are trademarks or registered trademarks of their respective holders. The use of brand names, product names, common names, trade names, product descriptions etc. even without a particular marking in this work is in no way to be construed to mean that such names may be regarded as unrestricted in respect of trademark and brand protection legislation and could thus be used by anyone.

Cover image: www.ingimage.com

Publisher:
LAP LAMBERT Academic Publishing
is a trademark of
Dodo Books Indian Ocean Ltd. and OmniScriptum S.R.L publishing group

120 High Road, East Finchley, London, N2 9ED, United Kingdom
Str. Armeneasca 28/1, office 1, Chisinau MD-2012, Republic of Moldova, Europe
Printed at: see last page
ISBN: 978-620-6-15691-8

Content

Introduction

In today's technology, when there is an avalanche of increasingly sophisticated, more electronic and mechatronic systems, a very important thing for the intelligent control of some physical quantities, which can be: heat, vibrations, forces, moments of friction, is intelligent measurement and control systems. These systems are made by combining computerized, on-line control with various intelligent materials, whose physical properties change depending on the various external physical quantities. Intelligent multifunctional materials are defined as those materials that have intrinsic and extrinsic properties to react to external stimuli in a useful manner. External stimuli, which are sensed, can cause changes in the environmental conditions of materials, such as light, temperature, pressure, humidity, electric field, magnetic field, etc. The response to a change in the environment will produce a change in one or more physical properties of the material, such as: size, shape, color, structure, conductivity, magnetization or polarization, etc. In the technique of dynamic behavior optimization, a special role is played by the complex auxiliary components with spring, damper type elements, which are inserted into the structure of industrial robots, ***RI***. Vibration isolators and shock absorbers are used in common to reduce the vibrations of machines and installations. Isolating elements are usually passive and are generally designed to reduce vibrations with unwanted frequencies. Often, in many applications, the excitation frequency varies over a wide range, which is why it is necessary to adjust the damping during system operation. Such systems are the semi-active components, to which the stiffness and the damping coefficient can be adjusted, during operation, on-line. By changing the stiffness of the element or the system, it is possible to move the critical frequencies of the system (eigenfrequency values of the system) in the attenuation range, thus bypassing the resonance frequencies. A safe control of the system involves monitoring the critical points and knowing the frequency spectrum of the system. This adaptive isolation modality can change the operating conditions according to the dominant load in improving the vibration isolation compared to the passive attenuation system. Unwanted vibrations are reduced for various load conditions, in a very wide frequency range. Numerous concepts have recently been studied through the use of smart materials within adaptive structures through the simultaneous use of multiple sensor-actuator-accelerometer systems. Magneto-rheological (***FMR***) fluids and elastomers, shape memory alloys (***SMA***) and piezoelectric materials are some of the smart materials whose properties can be controlled online. These materials use the mechanical response (stretch-compression) coupled with other physical quantities such as the magnetic or electric field, heat, etc., which is why it is possible to develop with the help of these materials some adaptive structures without too many complicated mechanisms (Angeles, 2000). Magneto-rheological materials (***MMR***s) are materials whose rheological properties (flow properties) are rapidly modified by the application of a magnetic field. This change is proportional to the applied magnetic field and is reversible in a very short time. ***MMR*** rapidly transforms from a fluid state to a semi-solid state upon application of the magnetic field, returning abruptly to the initial state after the application of the magnetic field ceases. ***MMR*** are the fastest and simplest interfaces between the electrical control system and the mechanical system, for moving the vibrations of a structure in the attenuation domain (Li et al., 2000). ***MMR***s are used in many applications due to the wide range in which their properties can be modified. Among these, the following applications can be noted: active suspensions in the automotive industry Toyota ***TEMS*** (Toyota Electronic Modulated Suapension), the piezoelectric motor with surfing wave propagation, actuators for dot matrix printers, magnetostrictive actuators for reducing low vibrations, silencers, of vibrations both for cutting processes and for civil construction, naval construction and military applications, adaptive shape control in aeronautics or in optoelectronic and laser systems or in the construction of antennas, telescopes and large reflectors, monitoring the integrity of the structure and the wear of ***HUMS*** (Health and Usage Monitoring Systems) of both the engine and the landing gear, the control system and the aircraft structure, to the ***BMS*** (Biological Motor System) biological engine type systems, controllable valves, controllable brakes and clutches, finishing devices of big precision, for special shock absorbers used in the construction of buildings, bridges, in the construction of prostheses, etc. All these applications denote the fact that magneto-rheological damping is still not

sufficiently applied, especially in top fields of automation of manufacturing processes, such as industrial robots and peri-robotic components. As it can be seen, the work covered a very important, topical subject, with great importance in optimizing the dynamic behavior of robotic structures, and with a very easy interface between command and servo actuation.

In chapter 1, intelligent materials are described in detail with their structure, definitions and terminology and, respectively, their physical-mechanical properties, highlighting the relatively easy way of interfacing these materials, between electronic command and control, and the type execution elements mechanic of robotic systems. The performances of different smart materials in their use as actuators and sensors are exemplified in a table. The definitions for intelligent structures and for adaptive structures are addressed, as well as the components of such systems. Some theoretical contributions refer to the schematization of such intelligent control and optimization systems, as well as the LabVIEW virtual instrumentation created especially for the assisted theoretical research of various amortization schemes or complex command and control laws.

Chapter 2 presents the technological comparison of magnetorheological and electrorheological materials with the presentation of the advantages and disadvantages of each type. The modes of operation with magnetorheological fluids and a series of representative applications and characteristics of magnetorheological dampers in optimizing the dynamic behavior of buildings are presented, as suspensions in the automobile industry, as seismological research systems, in medicine, as locomotive recovery systems, as well as in technique, as vibration damping systems for installations, mechanisms and machines.

Chapter 3 deals with researching the dynamic behavior of robotic structures. A series of matrix-vector mathematical models are presented, some relationships being the result of the research carried out within the present work and are contributions to the complex mathematical modeling of dynamic systems.

In chapter 4, the critical conclusions of the bibliographic research are presented, both regarding the researched mathematical models, as well as how to optimize the dynamic behavior of robotic structures, and the research directions of the work are established.

In chapter 5, the theoretical contributions of the work are presented. Virtual vibration simulation tools, active, passive, semi-active vibration controllers, as well as acceleration signal simulation tools, composite periodic signal, with at least ten natural frequencies, considered as the first natural frequencies, in general, are presented , are more important in the process of optimizing the dynamic behavior. The research methods addressed are highlighted, among which we mention: the parameterization of the characteristics of the damping force vs. travel speed, simulation of continuous dynamic systems with multiple reactions and different corrections and control laws, simulation of simple and complex attenuation elements and complex mechanical systems with several springs, seismic masses and shock absorbers.

Chapter 6 includes the research methods approached and their brief description, as well as the equipment and programs made under the LabVIEW kernel, for undertaking the theoretical and experimental research of magnetorheological dampers.

Chapter 7 includes the presentation of the results of the theoretical and experimental research of magnetorheological dampers and the optimization of the dynamic behavior of the structures and servoactuations of industrial robots through their application. This chapter contains a series of experimental characteristics of the behavior of the researched didactic robot in various damping and vibration attenuation variants, as well as with various laws of motion, with and without time delay within a phase or when changing direction. Numerous Fourier spectra are presented to highlight the results of applying intelligent damping. The research also includes the optimization approach through the use of an intelligent damping, using in its own design an intelligent magneto-rheological damping scheme that includes: the accelerometer as a sensor, the acquisition and control board as an interface and amplification element, the virtual instrument created as a soft element, the amplifier with three amplification stages, the connection to the shock absorber coils, the magneto rheological shock absorber as an actuator element.

Among the theoretical and experimental contributions, the following can be mentioned: (i) the realization and testing of an intelligent shock absorber on a didactic structure of an articulated arm type robot; (ii) obtaining the reduction of amplitude of oscillations by using magnetorheological damping; (iii) obtaining the transfer of low-frequency vibrations to higher frequencies, transfer limited by the three-stage construction of the voltage amplifier supplying the shock absorber coils, which is about 10-15Hz; (iv) obtaining a new, modern mathematical model, validated by comparison with experimentally obtained results; -realization of a proprietary Fourier analyzer, analyzer used in the theoretical and experimental research technique addressed in the thesis; (v) realization of numerous virtual instruments with the help of LabVIEW virtual instrumentation, instruments for simultaneous acquisition on five channels, digital control of the movements of the didactic robot structure, with 6 and 8 bit control, instruments for the theoretical research of the comparative characteristics of the magnetorheological damper, as well as of the Fourier spectrum, of the online generation of the Amplitude-frequency and Phase-frequency Bode characteristics for various motion commands, of the electronic command and control equipment and of adjusting the voltage signal applied to the shock absorber coils, tools for simulating the dynamic behavior of the shock absorber in anticipatory or inertial variants, variants obtained by changing the position of the shock absorber within the mechanical scheme, depending on the springs used; (vi) the introduction and use of the parameterization of the damping force vs. speed characteristic in order to identify the coefficients of the mathematical model used; (vii) the assisted identification of all the coefficients of the mathematical model through comparative theoretical and experimental research and through the use of LabVIEW virtual instrumentation, created especially for comparative analysis; (viii) the use of the validated mathematical model, in the assisted optimization technique of the dynamic behavior, by using the LabVIEW virtual instrumentation and the matrix-vector mathematical model completed with the expression of the viscous damping force.

Approaching such a subject, as well as the research undertaken, opens new horizons towards the implementation on a larger scale of intelligent systems in servo-actuator technology, through the use of intelligent materials, systems that interface optimally and relatively simply with electronic command and control systems.

CHAPTER 1
Introduction to the Field of Materials and Intelligent Structures

In the technique of dynamic behavior optimization, a special role is played by the auxiliary, complex components, with spring, shock absorber elements, which are inserted into the structure of industrial robots, RI. Vibration isolators and shock absorbers are used in common to reduce the vibrations of machines and installations. Isolating elements are usually passive and are generally designed to reduce vibrations with unwanted frequencies. Often, in many applications, the excitation frequency varies over a wide range, which is why it is necessary to adjust the damping during system operation. Such systems are the semi-active components, to which the stiffness and the damping coefficient can be adjusted, during operation, on-line. By changing the stiffness of the element or the system, it is possible to move the critical frequencies of the system (eigenfrequency values of the system) in the attenuation range, thus bypassing the resonance frequencies. A safe control of the system involves monitoring the critical points and knowing the frequency spectrum of the system. This adaptive isolation modality can change the operating conditions according to the dominant load in improving the vibration isolation compared to the passive attenuation system. Unwanted vibrations are reduced for various load conditions, in a very wide frequency range. Numerous concepts have recently been studied using smart materials within adaptive structures. Magnetorheological (***FMR***) fluids and elastomers, shape memory alloys (***SMA***) and piezoelectric materials are some of the smart materials whose properties can be controlled online. Smart materials use the mechanical response (stretch-compression) coupled with other physical quantities such as magnetic or electric field, heat, etc., which is why it is possible to develop adaptive structures with these materials without too many complicated mechanisms (Angeles, 2000). Magneto-rheological materials (***MMR***s) are materials whose rheological properties (flow properties) are rapidly modified by the application of a magnetic field. This change is proportional to the applied magnetic field and is reversible in a very short time. ***MMR*** rapidly transforms from a fluid state to a semi-solid state upon application of the magnetic field, returning abruptly to the initial state after the application of the magnetic field ceases. ***MMR*** are the fastest and simplest interfaces between the electrical control system and the mechanical system, for moving the vibrations of the structure in the attenuation domain (Li et al., 2000). ***MMR***s are used in many applications due to the wide range in which their properties can be modified.

Materials for smart structures. Definitions and terminology. In piezoelectric transducers, the material characteristics depend on the direction of electric field application, displacement, mechanical stresses and strains. The polarization direction is generally identified with the Z axis of the orthogonal crystallographic system. The X, Y and Z axes are represented as the directions 1, 2 and 3, and the rotations on these axes are 4, 5 and 6.

Fig.1.1.Poloarized directions

The variation of the constants of piezoelectric materials are generally expressed by writing some indices. The first index expresses the direction of the electric field associated with the applied electric voltage or the electric charge produced, the second index expresses the direction of the mechanical stresses and strains, and the third index indicates certain conditions of the mechanical or electrical constants.

Actuators. The evolution of piezoelectric actuators from disc and tube type to more elaborate flexible systems with different mechanical torque of the piezoelectric element, in accordance with the elastic

properties to be measured. However, a large displacement due to a flexural system becomes expensive for low frequency and low force operations.

Multifunctional materials for sensors and actuators [4,5,6,7]. Among the materials used in the construction of intelligent structures are the following materials: piezoceramics; piezopolymers; electrostrictive; magnetostrictive; shape memory materials; rheological fluids.

Piezoceramic materials. Lead-Zirconate-Titanate (***PZT***). This material has the property of interaction between the electric field and the mechanical force, both with a direct and inverse effect. It is a very good exciter, has a high modulus of elasticity, wide bandwidth, moderate response to stress, appreciable exposure to hysteresis. It can be processed into many shapes for very wide applications (discs, cylinders, tubes, bars, hemispheres, etc.).

Piezopolymers [11,12,13,14]. Vinyl-fluoride monomer (***CH2-CF2***) has been known for over 90 years and forms the basic element for the semi-crystalline polymer, polyvinyl-fluoride (***PVDF***). It is processed into thin shapes and is flexible and light. It is an excellent sensor. It has a high dielectric constant, is temperature dependent, and has a high loss factor. It can be used as an optical sensor, in hydrophonic measurements, or any non-destructive testing.

Electrostrictive Materials. Lead-Magnesium-Niobate (***PMN***) and Lead-Lanthanum-Zirconate-Titanate (***PLZT***). The exciting force results from the interaction between the electric field and the electric dipoles. It is a self-polarizing material. It has a high modulus, hysteresis at low frequencies and moderate temperatures, high dielectric coefficient, precise optical adaptivity. It is used to create active bars.

Magnetostrictive materials. Terbium-Dysprosium-Iron (***Terfenol-D***). The exciting forces are obtained from the interaction of the magnetic field and the magnetic dipoles. It is self-polarizing, has a high modulus of elasticity, prompt response, low hysteresis and a relative insensitivity to temperature variations. The material is bandwidth limited, both by mechanical resonance and by eddies of magnetic currents.

Shape memory alloys. Nickel-Titanium (***Nitinol***). This material has the ability to recover a particular shape when activated by an external stimulus. The material phase changes between martensite and austenite as a result of exceeding the thermal transformation point. It has high strength, high sensitivity to temperature variations, high hysteresis limit and low bandwidth. It is frequently used as dental floss, medical devices and composite materials.

Rheological fluids [11,13,14,15,16,39,44,61,68]. Silicone and starch. Rheological fluids are formed by particles in suspension in viscous fluids, and which react to the application of magnetic or electric fields to the fluid. The particles have constant dielectric polarization and are suspended in hydrophobic liquids. Viscosity increases by 40% when applying an electric field of 4V/mm. These materials are commonly used in clutches, engine oils, high response valves and active dampers.

General intelligent structures [71,72,73,74,95]. Intelligent structures are structures that have incorporated in their construction exciters, sensors with a high level of integration, as well as feedback and command links to a computerized surveillance system. Intelligent structures contain a high level of logic control, signal conditioning and electronically controlled amplification. Currently, signal processing elements (from sensors) are incorporated inside structures, in order to influence their condition, characteristics and performances.

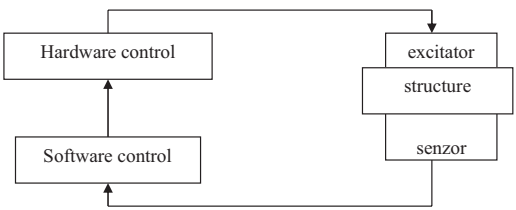

Fig.1.2. Block schema of the smart structure

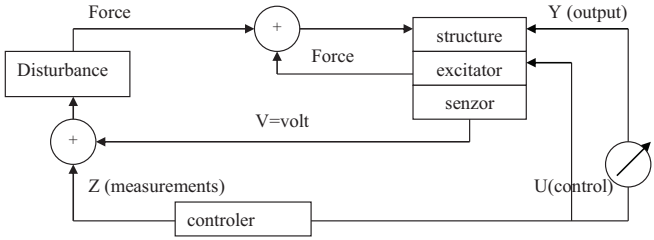

Fig.1.3. Detailed schema of the smart system

Vibration control has been a challenge over time in both research fields: academic and industrial. Virtually, vibrations can be found everywhere, in vehicles, buildings or machines. Most of all, vibrations are undesirable because they produce unpleasant noises, unwanted tensions in structures and cause the system to malfunction or fail. Numerous controllers have been designed to solve vibration control problems. Most vibration control problems are nonlinear in nature, so the performance of traditional control techniques cannot be satisfactory. In these cases, non-linear, adaptive or neural control techniques are required to achieve the required performance. The successes of the ***CMAC*** (Cerebellar Model Articulation Controller) neural network in various control applications from the University of New Hampshire, presented the advantages of neural networks, as an adaptive controller next to another neural network-based controllers and traditional adaptive controllers. Next, a simulation study is presented, using the ***CMAC*** neural network as an intelligent vibration controller, in the two-mass vibration problem, which has various multi-frequency disturbances, measurement noise, and nonlinearities. Fig. 1.4 schematically shows the system with two masses. A source of vibration moves table 1. The energy is transferred to table 2, via a suspended platform. Under each table is placed a composite panel, called ***SmartPanel***, containing a piezoelectric sensor, a piezoelectric actuator and accelerometers. The ***CMAC*** reads the force and acceleration of mass 2 and calculates a control signal to compensate for the disturbing force. The purpose of ***CMAC*** is to minimize the energy transferred through the platform so that mass 2 is isolated from the vibration source [124,146,148].

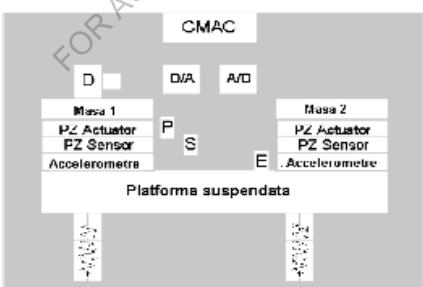

Fig.1.4. Schematic of the two-mass system in smart structure

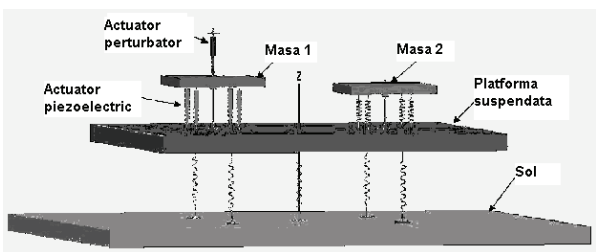

Fig.1.5. The simulation model of the two-mass system with a 3D simulation program

The analysis of the results showed that the ***CMAC*** neural network represents an effective approach to reducing vibrations and isolation problems. Due to its self-learning property, ***CMAC*** is a very good controller in the nonlinear system, which has unexpected changes for a disturbance and noise in the measurements. Research continues to extend these results to real-time experiments but also to much more complicated dynamical systems.

Adaptive structures. Generalities. Adaptive structures represent a new approach in an engineering sense, which integrates the action of sensors, actuators and control circuit elements, in a single system that reacts to changes in the environment. Such integrated systems, which have the ability to adapt to changes in the environment, bring significant values to materials, technologies or finished products, which they transform into high-performance systems, which would not be possible in a classical approach.

History has been deeply influenced by materials, so that distinct time periods (Stone Age, Bronze Age and Iron Age) were defined based on the materials used. The current era of synthetic materials (plastics and composites) can be defined as the dawn of a new era, the era of multifunctional materials, which will use these materials in order to research some new technologies, for the synthesis of adaptive systems. The degree of sophistication of this new generation of materials will mainly depend on each individual application, however, it is anticipated that these innovative methods and technologies will be used in several scientific fields, such as nanotechnology, biomaterials, neural networks, molecular electronics, etc. Self-repair, self-diagnosis, self-multiplication and self-regulation are also some anticipated characteristics of adaptive structures.

An adaptive structure is an intrinsic system of sensors, actuators and control mechanisms that sense external stimuli, respond to these stimuli, in a predetermined and reversible manner to the initial state, after their removal. Adaptive structures use materials with advanced functionalities, whose properties can be used to sense an external stimulus and/or respond to this stimulus. Such materials are commonly used in numerous devices and for a wide range of applications.

The problem that arises is to review the state-of-the-art of materials in the technology of adaptive structures, and to identify the evaluation criteria for sensors, actuators and control systems in order to be used in the structure of adaptive systems.

Multifunctional materials and adaptive structures [155,156,157]. Multifunctional materials are defined as those materials that have intrinsic and extrinsic properties to react to external stimuli in a useful manner. External stimuli, which are sensed, can cause changes in the environmental conditions of materials, such as light, temperature, pressure, humidity, electric field, magnetic field, etc. The response to a change in the environment will produce a change in one or more physical properties of the material, such as: size, shape, color, structure, conductivity, magnetization or polarization, etc. There are numerous examples of adaptive structures made. Broadly speaking, these are classified into structures with precise shape control: active dampers, adaptive noise dampers, and applications for real-time monitoring of structural integrity.

Technologies for adaptive structures. An adaptive structure has three basic components: sensors, actuators, and control system. The performance of these systems is dictated by the performance of the adaptive structure. Important research and activities have been directed towards the realization of sensors, actuators and control systems for controlling applications with adaptive structures. The technologies used to make sensors and actuators are primarily based on physical phenomena, project concepts and sketches, material properties, and technological properties of materials. Control systems technology is based on control theory, electronics and computing techniques.

Sensors [174]. Applying an electric field to a material sensor generates a change in its characteristics. In sensor materials, a small change in the energy field can produce a significant change in one or more characteristics, and these changes can be detected. The response of a material sensor can be: mechanical, electrical, optical, magnetic, thermal or chemical. For an adaptive structure, the most useful response is the electrical one, because it can be monitored and analyzed by a control system. Most of the sensor technologies used in adaptive structures are well established. Optical strain sensors were developed several years ago for the aerospace industry.

Strain sensors [174]. Strain sensors measure changes in an object's length by detecting changes in mechanical, optical, acoustic and/or electrical properties. The strain sensors usually used in adaptive structures are strain gauges, optical fiber strain sensors (***FOSS***), and piezoelectric strain sensors. Strain Gauges are often used to measure surface stresses. They work on the principle of piezo resistance, by changing the resistance of a material when it is subjected to an effort. The ratio between the change in resistance and the change in length is defined as a measurement factor. Other characteristics are the measured length, the type and value of the measured stress (bending, axial stress, mean stress, torsion), and the operating temperature. The best-known technique for measuring changes in resistance, with strain gauge sensors, is used in the Wheatstone bridge structure, with four sensors, one on each branch. The best-known stress sensors are the wire, foil and semiconductor stress sensors. ***FOSS*** prove to be excellent strain sensors because they are immune to electromagnetic field interference. They can be fixed on the surface of the structures or incorporated into the structure. ***FOSS*** can be used under high temperature conditions (800^0C for silicon fibers, and 1700^0C for sapphire fibers). They use intrinsic changes in material fiber properties, such as frequency, phase, wavelength, modal index, polarization state, refractive index, attenuation coefficient, etc. to measure effort. However, signal processing is complicated and expensive, which leads to a reduced use of these types of sensors. Fiber optic strain measurement uses two interferometric techniques (wavelength measurement through interference phenomena) Fabry-Perot and Mach-Zehnder. Piezoelectric strain sensors have the ability to convert mechanical energy into electrical energy. When a piezoelectric material is subjected to a stress, the voltage generated is proportional to the thickness of the material and the magnitude of the applied force. However, sensors are usually limited to small sizes due to the fact that they must interact with the structure without affecting its properties. The best-known coefficients used to characterize piezoelectric materials are d31 and d33. The coefficient d31 describes the traction and compression behavior of the piezoelectric disc in the x-z plane when an electric field is applied in the z direction, while the d33 coefficient describes the traction and compression behavior in the z-axis direction. Another useful factor is the electromechanical torque coefficient k, which connects the induced mechanical energy and the resulting electrical energy, their ratio being k2. Piezoelectric sensors are used in the construction of adaptive structures. ***PVDF*** are flexible piezoelectric polymers with a stress coefficient 20 times higher than ceramic materials ***PZT*** type. ***PVDF*** type sensors operate better in the dynamic case because the load imbalance created by the stress on the material is dissipated over time. For applications that require low frequency domains, piezoceramic materials are the best option. The advantage of membrane type sensors compared to those made of piezoceramic materials is that they have a precise response over a wide frequency limit, of the order of GHz.

Displacement sensors. Displacement sensors are used to measure the amplitude of the deformation of a structure, at any point, caused by static loads or excitation vibrations. Various types of sensors can be used. These are Potentiometric Displacement Transducers (***PDT***), Linear Voltage Differential Transducers (***LVDT***), Eddy Current Transducers (***ECT***), and Variable Capacitance Transducers (***VCT***).

PDTs are made from either a coil-type element with uniform windings or from a film of high resistivity material whose resistance is directly proportional to the length of the potentiometer. The amount of output from the potentiometer is proportional to the voltage difference between one of the ends of the potentiometer and the point of contact with the object and is therefore proportional to its deformation. The performances of these sensors depend on: thermal stability, coil wires, and non-linearity produced by an impedance mismatch with the voltage source, potentiometer and measurements in the circuit.

Force and acceleration sensors. The force acting on an object can be measured with a piezoelectric force sensor or a load cell (Load Cell-***LC***), and the acceleration can be measured with a piezoelectric accelerometer. Piezoelectric force sensors use a piezoelectric transducer to obtain an electrical output quantity that is proportional to the applied force. The force sensor is mounted in series with the force transmitting element, in order to expose the piezoelectric element directly to the measured force. Since the piezoelectric element is prestressed, the sensor can measure both tensile

and compressive forces. A high stiffness also implies a high resonance frequency and therefore the sensor will have minimal effect on the integrity of the structure. A load cell consists of a strain gauge mounted on a metal plate that will bend as a result of a load. These cells can be adjusted for different forces by varying the properties of the metal plate used. Piezoelectric accelerometers are based on the piezoelectric effect of generating an electrical output quantity, which is proportional to the applied acceleration. Piezoelectric accelerometers are of several types. These configurations are defined according to the sense of the inertial force, the acceleration being measured, etc. There are currently 3 configurations available for: compression, distributed stress, and flexible beam.

Temperature sensors. Thermocouples are the best known temperature sensors. Temperature transducers are made up of two dissimilar metal wires joined at one end by a spot weld. When a thermocouple is subjected to a certain temperature, a voltage appears that changes proportionally with the temperature change, and which can be measured at the two free ends of the thermocouple. Although the effect is dependent on the nature of the metals used, a number of bimetals have been standardized for different temperature ranges. Thermocouples are effectively an inexpensive solution for temperature measurement for a large number of applications. Thermistors operate on the principle of variation of the resistivity of a material with temperature. Resistive temperature detectors (***RTD***s) can be made in the form of coils or films. The negative temperature coefficient (***NTC***) for a p-type ceramic semiconductor thermistor expresses the decrease in resistivity with increasing temperature. The positive temperature coefficient (***PTC***) for an n-type ceramic semiconductor thermistor expresses the increase in electrical resistance with increasing temperature. Regardless of the nature of the measurements, the performance of any type of sensor can be evaluated according to the characteristic performances: sensitivity, length measurement, bandwidth, response time, working temperature, accuracy, power, weight, and cost.

Actuators [25,154]. Excitation can be defined as a controlled release of energy. The excitation process converts a form of energy (conductive) into actuating energy. Conductive energy can be in the form of electric field, magnetic field, thermal energy, mechanical effort, or it can be stored as a hydrocarbon fuel. The excitation energy can be in the form of light, heat, radiation, or mechanical stress. Micro-positioning of actuators based on mechanical excitation technologies is considered suitable for adaptive structures. A wide range of materials and devices for such actuators has been developed for adaptive structures. The types of actuators can be classified based on the excitation phenomena or the types of materials used.

Shape memory alloy actuators (*SMA*). Shape memory alloys are adaptive materials. They undergo a thermoelastic transformation from austenite to martensite when subjected to a temperature below the critical temperature. In the martensite state, the alloy is plastic and can be easily deformed to obtain a desired shape. When heated above the critical temperature, the martensite phase transforms into the austenite phase, and the material returns to its original shape. The ability of the material to remember its original shape gives it the name shape memory alloy. If it is once again subjected to a temperature below the critical one and no macroscopic shape changes occur, it is said to be a one-way effect. This "free recovery" process can be repeated several times, however, with the material having to be deformed each time the temperature is below the critical temperature. A two-way effect can be obtained if a close loading is applied during the temperature cycle. During this process, the loading will deform the martensite at low temperatures, the shape memory alloy will return to its original shape at high temperatures, caused by the transition to the austenite phase, and the transformation to martensite during the next cooling cycle, which will allow for the loading to deform the alloy once more. An intrinsic "two-way" effect exists in shape memory alloys, where the material has shape memory at low temperature and at high temperature. In these materials it is not necessary to apply any load to force the material to "remember" its shape. However, this effect can be obtained in both cases (with and without applied load), the effect is small and little known. Shape memory alloy actuators have been used in many automated applications. These thermally actuated applications included a shock damping valve, thermal compensation in automatic transmissions for drive shafts, and reduced noise in gearboxes. Using shape memory alloy actuators for thermal actuation offers several benefits, including high forces, large displacements, small adaptive sizes, high stress per unit

volume, and different actuation modes: linear, bending, torsion. Shape memory alloy actuators can be in the form of washers, wires, tubes, films or helical shapes. For applications involving cyclic stresses due to compressive/tensile forces, prestressed coil springs are most often used. The actuators are constrained, by the structure of the assembly, so that the alloy does not return to its original shape during heating. This produces a high stress in the actuator material, which is distributed by it to the structure, producing a stress. During the transition phase, shape memory alloys exceed a certain temperature limit, the thermal cycle produces a thermal hysteresis. These alloys exhibit premature fatigue under cyclic stress. The greater the amount of shape recovery during the thermal cycle, the shorter the operating period of the actuator. However, if a small amplitude is maintained, it increases the operating time in the normal parameters of the actuator.

Vibration damping and control using shape memory alloy actuators can be achieved using the damping hysteresis and variable stiffness actuator characteristics of shape memory alloys. These materials have high strength and high mechanical loss factors, and can be in the form of springs, for applications with passive vibration damping. The natural damping capacity of shape memory alloys can be combined with the pseudo-elastic effect that characterizes some shape memory alloys.

By inserting shape memory wires into an elastic structure, the effective stiffness of the structure can be controlled. This can influence the resonance frequency of the component and thus the resonance phenomenon can be avoided. The shape memory effect can also be used for direct vibration damping. When shape memory alloy wires are attached to the base of a cantilever beam, vibrations in the beam can be damped by producing a counterforce to these vibrations. Since the conductive energy is lost through the shape, upon heating, this method can be used for low frequency applications (2-6 Hz) to avoid excess temperature in the wires.

Piezoelectric actuators. Piezoelectric actuators, working bidirectionally, are among the most used in applications with adaptive structures. Piezoelectric materials cause an electrical charge when subjected to a mechanical stress or produce a mechanical stress when an electric field is applied to them. In the case of piezoelectric materials, the forces produced are about 0.1% for an electric field of 10 kV/cm. The stress (or strains), electric field characteristics are almost linear in the operating area, but for the saturation stress a very high electric field is required. Piezoelectric materials are actually active adaptive materials. The deformation can be positive (traction) or negative (compression) depending on the direction of the electric field. In an alternating electric field these materials will be subject to compression and tension in a cyclic fashion and will produce vibrations. The conversion also applies in this case and thus, the vibrations of a piezoelectric material will produce an alternating electric field. These materials can detect efforts, displacements, forces, pressures, or vibrations producing an electrical response. Devices based on piezoelectric actuators can detect and transmit sounds. These are called converters and are used in acoustic communication systems. The measure of the piezoelectric response to an applied electric field is a constant piezoelectric charge *d*. This measures the stress produced when an electric field is applied. The most commonly used piezoelectric constants d_{33}, d_{31}, d_h are used to compare different piezoelectric materials. The d_{33} coefficient expresses the relationship between the effort in the direction of polarization of the piezoelectric material, or along the orientation axis of the piezoelectric molecules (i.e. the direction of the electric field) and the electric field. The coefficient d_{31} describes the relationship between the effort perpendicular to the direction of the electric field and the electric field.

The electromechanical torque coefficient k is used for the electromechanical conversion. This factor expresses the conversion of stored mechanical energy into stored electrical energy. The planar torque coefficient k_p denotes the relationship between the electric field applied in the d_{33} direction, and the simultaneous mechanical reaction in the d_{31} direction. The magnitude of the torque coefficient k_t expresses the relationship between the electric field in the d_{33} direction and the mechanical reaction in the same direction. The square of the torque coefficient k_{t2} represents the ratio between the mechanical energy induced and the electrical energy obtained, which represents the efficiency of the conversion process.

The most used piezoelectric elements are in the form of discs, washers or blocks (clogs). The magnitude of the mechanical stress produced in the material depends on the thickness of the element

and the amplitude of the electric voltage applied in the direction of the thickness. These elements are used in a wide number of applications: sonic, ultrasonic transducers, fish finders, ignition devices, etc. Piezoelectric tubes provide an alternative method for producing stresses. In piezoelectric tubes, the mechanical stress depends on the length of the tube and the thickness of its wall. Such tubes can work radially or by traction/compression. Such ceramic, piezoelectric tubes are used as actuator-type elements in lithographic semiconductors, microscopy, tubular optical fibers, etc.

A large number of applications require different functional characteristics such as large displacements, large load capacity, or large frequency bandwidth. These requirements led to the development of new types of actuators. To increase the effort in piezoelectric actuators, several thin piezoelectric elements can be used, mounted inside them. In this configuration, the total displacement will be equal to the sum of the displacements in each element. Using these thin elements, allows the application of a high electric field, which leads to an increase in effort. This type of actuator (package) can generate, for displacements of 100 μm, forces equal to several tons.

The displacement capacity of piezoceramic materials, in many sonic applications, is increased by the mechanical torque of these elements with flexible metal frames. The flexural actuators, formed by piezoelectric elements and materials with flexible properties, through mechanical amplification, lead to volume modification. Actuators from composite materials have been developed so as to obtain the advantage of directional connectivity in composite structures. These include biomorphic materials, piezoelectric polymers, and the new rainbow and thunder technologies.

Biomorphic alloys, which are composed of two coupled piezoelectric materials, can be used as direct actuators, voltage generators in two-layer structures. There are two possibilities for connecting these elements. In series, the biomorphic material is constructed in such a way that the polarization of the two materials is opposite to each other. When an electric potential is applied to the two elements, regardless of polarity, one material will try to contract and the other to expand. These opposite actions will lead to obtaining the bending effect. In parallel, the polarization of the two materials is done in the same direction, but the electrode between the two layers is common, while the outer electrodes are covered by the same potential. This leads to the expansion of one material and the contraction of the other, obtaining a bending effect. However, these biomorphic elements do not have a high load capacity, and can generate displacements of approximately 1mm. These actuators have been incorporated into the construction of dot matrix printers to achieve high speeds.

The moon type actuator consists of two crescent-shaped disks, one metallic, the other piezoelectric, mounted on top of each other. Its functioning as an actuator has the effect of coupling the radial extensions and contractions of the piezoelectric disc, with the flexibility properties of the two ends of the metallic material. The device produces displacements of 30 μm and generates greater forces than the biomorphic ones.

Rainbow and thunder devices are structurally similar to biomorphic devices, both having two layers. The major difference between them is that the bi structured system in the case of rainbow and thunder is restricted. These low frequency and low force devices produce displacements between 20-50μm for frequencies below 40 Hz. However, these devices do not offer the displacements given by the biomorphic ones, but the force can be greater than the biomorphic ones and they have sufficiently large displacements to offer an alternative to the biomorphic actuators.

Another recently developed piezoelectric device for increasing displacements is the piezoelectric motor. The type of propagating wave is the surface or 'surfing' wave. The piezoelectric motor combines two fixed waves 90 degrees out of phase in time and space, and is controllable in both directions of rotation, which means elastic waves induced by the piezoelectric ring. A slip ring in contact with a wavy surface of an elastic body mounted on a piezoelectric material is driven in both directions by changing sinusoidal and cosinusoidal input voltage. These engines have the benefit of a moderate moment (not a violent one) but the duration of use is short, under the conditions of temperature variation.

Piezoelectric actuators have been intensively studied for applications with adaptive structures. An example of the application of these types of actuators is Toyota ***TEMS*** (Toyota Electronic

Modulated Suspension), which was developed to improve the maneuverability and stability of automobiles and the comfort of passengers.

Piezoelectric actuators glued or mounted in adaptive structures have also been studied for investigating surfaces. A number of experiments have been conducted with piezoelectric elements embedded in carbon fiber composites for shape control.

Electro- strictive actuators. Electro- strictive is a phenomenon observed in all dielectric materials. When an electric field is applied along a dielectric material, the dipoles self-align with the field. This process induces an internal effort and the material changes its dimensions. If the electric field is removed, the dipoles reorient and the material returns to its original dimensions. If the direction of the electric field is reversed, the dipoles align with it again and an effort is induced. Because the effort $\boldsymbol{S}$ is proportional to the square of the electric field E, ($S = ME^2$), S is always positive (the material is always under tension) independent of the polarity of the applied electric field. To obtain a bidirectional (tension/compression) effect for electro- strictive materials, a polarized electric field is usually used.

These materials are evaluated according to mechanical properties, which include internal stresses produced by an applied electric voltage (which is similar to the constant piezoelectric voltage given by the relationship $d = dS/dE$), force generation capacity, degree of hysteresis, dielectric constant k , the dissipation factor d, the operating temperature t. The dielectric constant is a measure of the charge capacity of the electrostrictive element. The higher this value, the higher the electric potential can be applied along the material before it fails, or the current of the material The dissipation factor or dielectric loss is a measure of the conductivity losses through the material.

Although the electro- strictive effect is present in dielectric materials, the stress amplitude is usually small and useless. The electro- strictive effect is known to occur in a number of piezoelectric materials such as Rochelle salt, barium titanate modified ***PZT***, but the effect is always smaller compared to the piezoelectric effect. However, ***PNM*** was created specifically for high electro-strictive voltage and very low hysteresis properties. This material produces stresses that are comparable to piezoelectric ***PZT*** stresses under negligible hysteresis conditions.

Electro- strictive materials offer an important advantage for quick actions. These materials do not exhibit hysteresis and as a result are materials for high frequency, high power, and precision applications such as sonic transformers, deformable mirrors, laser generators and optical systems, piezoelectric ceramic materials. Electro- strictive materials can be used to actuate different (geometric) structures. In fact, with a few exceptions, the geometric shapes that can be used for piezoelectric materials can also be applied to electro- strictive materials.

Magneto-strictive actuators. Magneto- strictive is similar to electro- strictive, except that the conducting field is magnetic. Magneto- strictive materials have a magnetic anisotropy in their atomic structure. Dimensional changes (internal stresses) are obtained as a result of the reorientation of atomic magnetic moments, or small domains of magnetism. The more the amplitude of the magnetic field increases, the more atoms align, the magnetic saturation being obtained for the magnetic alignment of all atoms with the applied magnetic field. If this field reverses, a similar material behavior is observed. The magneto- strictive voltage is also positive.

The most well-known types of actuators made of magneto- strictive materials are of the rod or cylinder type. A typical configuration of actuators is that of active magneto- strictive elements tightly wound in the form of excitation springs. Magneto- strictive materials have been used for the development of rotary motors (direct drive). Magneto- strictive actuators were studied for helicopter propeller blades to control its vibrations, by changing the shape of the flaps. An active, vibration-isolating platform with a magneto- strictive actuator was developed to reduce the shocks sustained by the base. This system gave results for shocks, but some residual vibrations remain present in the structure. For vibration isolation, magneto- strictive actuators are used to isolate low frequencies, but digital processing limits the response time. In the actuator prototype, when a coil with 50 turns on a terfenol-D core, with an extension of 5.22μm, was fed at a current of 7[A], an effort of 0.021% was obtained. It should be noted that the voltages obtained in magneto- strictive materials are lower than

those produced in piezoelectric materials, and the hysteresis is higher than that in magnetostrictive materials.

Actuators from electrorheological materials. Rheology is the science that deals with flow and deformation problems. An electrorheological fluid (***ER***) is a fluid whose viscosity changes depending on the electrical voltage applied to the material. These materials are used for a wide range of applications, as particles dielectrics suspended in electrically non-conductive liquids. These suspended particles are between 0.1-1.0μm, uniformly distributed in the fluid.

ER fluids give very good results in the case of distributed loading. The characteristic tension of these fluids, it is possible to categorize their behavior in pre and post flow regimes. These regimes depend on the strength of the electric field and the rheological properties of the material, which can be adjusted by varying the amplitude of the electric field. These ***ER*** materials also belong to a category of "highly adaptive" materials. The yield stresses for these materials are between one and several percent.

Applications with ***ER*** actuators are divided into 4 categories: static mode (free mechanisms), variable flow control (valves), vibration damping devices (shock absorbers), and reduced modes (grabbing devices). ***ER*** fluids flowing between two chambers/cavities can be controlled by changing the viscosity of the fluid. For vibration damping, ***ER*** fluids work in reduced configurations. The reduced configuration is primary when the fluid is under reduced stress, while the fluid works under extensional or compressive stresses in the extended configuration.

The first adaptive structure using ***ER*** fluids was patented in 1990. By incorporating an ***ER*** fluid into another passive cavity of the structure, the response of the entire structure can be controlled. Using a sandwich beam with ***ER*** fluids will give the assembly the ability to adjust its stiffness and damping parameters. Adaptive beam-type structures, similar to those described previously, have the ability to change their dynamic characteristics to the variation of the stress conditions. By applying a real-time control scheme, noises and vibrations can be controlled with such composites. ***ER*** fluids can mechanically couple two surfaces, by increasing or decreasing viscosity, by applying or removing an electric field, which can even be used for clamping devices.

However, each type of material described in the previous section has a set of independent coefficients and a general set of evaluation criteria for comparing the actuator properties. Typically, the performance of an actuator is evaluated by a number of performance variables: displacement, generated force, hysteresis, response time, bandwidth, temperature, accuracy, power and weight.

Applications of adaptive structures. The field of adaptive structures is relatively new, but it enjoys wide attention due to the impact it has on the performance, safety and stability of many systems used in space, aerospace, communications, transportation, industrial and civil applications. During the last years, numerous applications with adaptive structures have been realized and demonstrated.

Applications with adaptive structures can be classified into 4 areas, in which this technology is used. The four categories are:

- Silencers;
- Vibration dampers;
- Adaptive shape control;
- Monitoring the integrity of the structure.

Silencers. Noise is a sound that causes discomfort. It is produced by irregular vibrations. The dynamic field of sound intensity perceived by the human ear is 10^7:1, it is controlled by a logarithmic scale, which has the unit of measure dB. The threshold for human perception on this scale is 0 dB.

The industrial noise source has several distinct characteristics. One is turbulence or hiss, this is distributed along the frequency band and is known as "broadband noise". Another is "narrowband noise", which concentrates most of the acoustic energy at specified frequencies. When the noise is produced by a rotary motion, a set of tones or "tonal noises" are produced. These sources of noise are numerous. For example, noises can be produced by engines, exhaust systems, ventilation systems, ventilation systems, etc.

Active noise cancellers (***ANC***-Active Noise Cancellation) have been developed to reduce, even eliminate, some of these types of noise. Active noise control has la based on the principle of

destructive interference, whereby an unwanted sound is opposed by another sound of equal amplitude and out of phase by 180 degrees. The result is the cancellation of that sound. This principle is implemented in adaptive structures to reduce noise (eg: inside cars, aircraft, etc.).

The technology for active noise control, ***ANC*** consists of sensors, signal conditioners, control system, power amplifier, and actuators. In a typical ***ANC*** system, operating in a static harmonic noise field, sounds will be sensed with an array of microphones, the signal from each microphone will be analyzed by a central processor and a digital signal processor.

Different sensors can be encountered in such applications. Sensors used in ***ANC*** systems include eddy current proximity sensors, tachometers, accelerometers, microphones, and piezoelectric sensors. Mostly proximity sensors and tachometers are used to determine the alternative characteristic of the source noise. Microphones are the most well-known sensors for monitoring indoor noises. Finally, piezoelectric actuators are used to monitor noises associated with vibrations such as those in transformers.

The most common actuator used for active sound control is a simple variable control speaker. Loudspeakers are used to cancel noises by applying a "mirror image" of that sound. Based on the previous theory, the amplitude of these noises is annihilated. A second approach to active noise control is to cancel the noise source. In these applications, the most used are speakers based on ceramic, piezoelectric and electromagnetic materials. They are mainly used to control vibrating panels. The presented applications are considered to be examples for active noise control.

Active vibration dampers. Vibrations can be the cause of material damage through fatigue stress, or can compromise the performance of precision instruments. They can also be a potential risk to human health, through the industrial noises produced, and a potential cause of damage to heavy equipment and structures. Occasional vibrations can cause disturbances and reduce the sensitivity of gyroscopes, communication antennas, etc. Due to the vibrations of the machine tools in the area, they can affect the tolerances and surface finish of the precision machines. However, the elimination of unwanted vibrations is very important for various reasons. Traditionally, vibrations are absorbed by passive methods, involving springs and dampers. Such dampers usually do not have a large enough bandwidth to damp/attenuate all vibrations.

The technology of adaptive structures can also be used for applications involving vibration damping. Active structures can create cancellation disturbances (similar to noise control) or use ceramic or piezoelectric materials and resonance modifiers to dissipate vibration energy. Active vibration control (***AVC***) differs from active noise control (***ANC***) because the vibrations that are damped by ***AVC*** are in the material structure, while the vibrations that are eliminated by ***ANC*** are in the air (sounds). However, the basic principles used in ***ANC*** can also be applied to ***AVC*** and the control hardware and software architecture is generally similar for both technologies.

The vibrations from the cutting tools negatively affect the final surface of the processed piece and limit the speed of the operations. By actively reducing the vibrations of the cutting tools, a significant improvement of the final surface was obtained.

Active shock absorbers are also used in some automobile suspensions to improve their handling and stability, as well as passenger comfort. Toyota's Electronic Modulated Suspension (***TEMS***) is based on a stability sensor and a shock adjustment device using piezoelectric sensors and actuators and an electronic control system.

Many of the cross-type elements have been studied only for a single domain of isolated active vibrations, for different loads specific to the bearings. The Boeing Corporation has developed an anti-vibration engine for aeronautical applications. Thus, the dynamic response of vibrations is reduced engine relative to the environment. A similar concept was patented by GEC-Marconi for reducing vibrations on maritime vessels. Bridgestone Corporation presents a similar concept for isolating vibrations from large machine tools such as milling machines. General Motors developed a similar concept with applicability in the automobile industry. Anti-vibration suspensions were developed by Nissan, Hitachi, and others. Robert Bosch GmbH has studied such applications for agricultural machines as well. A constant active bar length is also described in a patent, by Kaman Aerospace Corporation, which is intended not so much to reduce vibrations as to compensate and transform them

into thermal deformations for large space structures. The Singer Company describes their use for laser gyro rings.

Active vibration damping is also being studied to reduce vibrations in helicopter rotors, gearboxes, etc. By reducing the vibration level in helicopters, the pilot can fly longer and the helicopter's maneuverability and fuel consumption are greatly improved. A number of theoretical methods for reducing these vibrations are studied by positioning piezoelectric sensors and actuators along the helicopter blade to reduce vibrations at those locations and modeling the rotor/blade by finite element analysis using the mass and stiffness of the blade, the type of flexural deformations in the blades and rotor/blade torque. The simulation showed a significant reduction in vibrations. Recently, some of this theoretical research has been put into practice by Sikosky Aircraft, which works to reduce vibrations in reducers and helicopter rotors.

Another area of use of active vibration dampers is to reduce vibrations of aircraft panels. Aircraft panels increase aerodynamic resistance and implicitly fuel consumption and reduce aircraft maneuverability.

CHAPTER 2
General Information Regarding the use of Rheological Materials, Devices and Mathematical Models

2.1. Rheological materials technological comparison [22, 30, 31, 35, 104, 106, 132, 200]. Electrorheological fluids and magnetorheological suspensions are systems of particles that, under the effect of electric and magnetic fields respectively, can increase their viscosity by 2-6 orders of magnitude, passing from a liquid state to a solid state, in time intervals of the order of milliseconds [62].

Electrorheological materials. Electrorheological (***ER***) materials were discovered in 1949 by W.M. Winslow. ER materials are solutions of colloidal, polarizable particles, with dimensions of the order of 1-100 μm, in insulating solvents, with a high dielectric constant.

General characterization of *ER* materials. When applying a strong electric field, of the order of kV/m, the ER materials, in flow, change their rheological properties (viscosity, plasticity, elasticity) forming chains, in the sequence shown schematically in fig.2.1. It is found that the particles have a tendency to form chains even at low intensities of the applied electric field. As the field intensity increases, the chains are sheared harder and harder and when the particle velocity drops to zero, the chains become perpendicular to the electrode surfaces. The increase in viscosity, by up to three orders of magnitude, is due to the energy consumed for the dissociation of particle chains [36]. Flow resumes only when the applied shear stress exceeds the dynamic yield stress. From that moment on, the ER material behaves like an ordinary fluid, with constant viscosity [35]. Therefore, ER materials have different behaviors: in the pre-flow regime and in the post-flow regime. Most applications are with controllable shear behavior in the post-flow regime. Figure 2.2 shows an idealized diagram of the shear behavior of an ER material. The pre-flow regime exists only at small deformations, $\gamma < \gamma_y$. In the post-flow regime, a linear dependence of the shear stress (τ) on the strain rate (g) is observed, according to the relationship:

$$\tau = \tau y + \eta . g \qquad (2.1)$$

where ***τy*** is the dynamic flow voltage, which is strongly dependent on the applied electric field ($E1 < E2 < E3$, $\tau y1 < \tau y2 < \tau y3$); η – the plastic viscosity which is little dependent on the electric field [77]. Applications of ER materials are of two types: (i) controllable devices and (ii) adaptive structures.

Controllable devices operate with constant viscosity, following a principle of operation based on two fundamental configurations of interaction of the ER material with the electrode: 1 – with fixed electrode and 2 – with mobile electrode. These two configurations are illustrated schematically in fig.2.3. The controllable devices, based on the fixed electrode configuration, from fig.2.3(a), contain stationary electrodes, between which the ER material flows, with a certain flow, produced by a pressure gradient. In the sliding electrode configuration, the electrodes are parallel and at least one of them can move tangentially, under the effect of a shearing force of the ER material, as in fig. 2.3(b). The sliding is controlled by the speed of the sliding electrode and by the shearing force of the material, exerted between the electrodes [80].

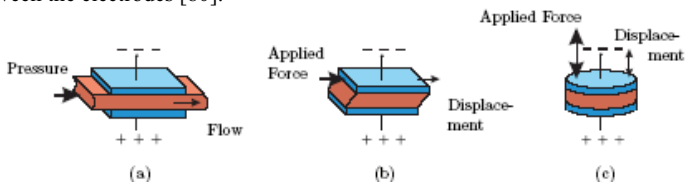

Fig.2.1. Illustration of the two fundamental configurations of interaction between the electrodes (1) and the ER or MR material (2), in controllable devices: (a) fixed electrode; (b) sliding electrode; (c) pressed electrode [80].

Adaptive structures have adjustable rheological properties due to the incorporation of at least one ***ER*** component. It works in pre-flow mode, being subjected to two types of stresses: shear or traction. According to the general definition, adaptive structures have the ability to detect external stimuli and to react so that their behavior falls within certain predetermined performance criteria. In general, the control of adaptive structures can be achieved actively by reducing the vibrations of the structure with the help of an external actuator that introduces additional energy into the system or semi-actively, by changing the stiffness and damping properties of the structure with the help of the ***ER*** component [80]. An example of an adaptive structure with semi-active control is obtained by embedding a core of ***ER*** material in an elastomer plate. The characteristics of this structure are illustrated in figure 2.2. The elastomer plate in fig. 2.2(a) has an ***ER*** core with a thickness of 1.8 mm, the outer layers being 0.46 mm. The yield strength of the material ER (τ_y) depends on the intensity of the electric field (E) according to the relationship:

$$\tau_y = aE_1 + bE_2 \qquad (2.1)$$

where a = 0.8867 and b = 0.7833 are experimentally determined constants. The usual value of the flow shear is $\gamma_y \approx 1$ %. The relationship (2.1) was represented graphically in fig. 2.2(b). Viscosity of the ***ER*** material is $\eta = 0.25$ Pas. The elastomer in which the ***ER*** core was incorporated has shear modulus G = 12 MPa and Poisson's ratio $\mu = 0.4$.

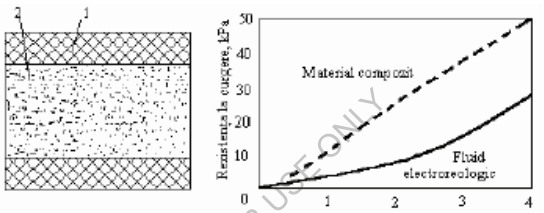

Fig.2.2. Characteristics of an adaptive ***ER*** core elastomer structure: (a) assembly scheme: 1-elastomer, 2-***ER*** material; (b) the dependence of the yield strength on the intensity of the applied electric field, in the ***ER*** material and in the composite [79, 81].

When it is bent with a deformation speed of the order of 102s-1, under the effect of a force arranged perpendicular to the layering direction, the resistance of the composite material increases with the intensity of the electric field acting on the ***ER*** core. From fig. 2.2(b) it can be seen that this increase is quasi-linear, the value of the flow resistance of the composite material being always higher than that of the ***ER*** material [81]. Due to their ability to store applied electrical energy and dissipate external mechanical energy, ***ER*** materials have been introduced into certain industrial applications that have had a particular impact in the respective fields.

Applications of *ER* materials. Within the two main categories of applications of ER materials can be found: 1 – controllable devices such as: valve, support for engines and mechanisms; brake and clutch; shock absorber, etc.; 2 – adaptive structures type: bridges, blocks, etc. Controllable valves were discovered and researched by W.M. Winslow and have a fixed electrode configuration. These valves allow control of flow and pressure loss, which can reach approx. 6.9 MPa, requiring no moving parts. Reaction times are below 1 ms. Controllable supports for motors and mechanisms have been known since 1987. A model of such a support is shown in figure 2.3. The elasticity of the support is ensured by the rubber ribs (1) and the membrane (3). The stiffness of the support is regulated by means of the inertia channel (4) which also contains the electrodes. The compliance of the assembly changes (increases) with the increase of the vibration frequency, up to 50 Hz [81]. Controllable brakes and clutches were also discovered by W.M. Winslow, remaining at the stage reached by his research, until the 80s. ***ER*** clutches have a sliding electrode configuration, which can have different geometries, with concentric cylinders or parallel discs, as shown in fig. 2.4(a), respectively (b). High speed clutches have been perfected, capable of transmitting torques of over 6 Nm. Controllable brakes have also been studied that operate at speeds of up to 4000 rpm and can develop frictional forces of up to 225 N [81].

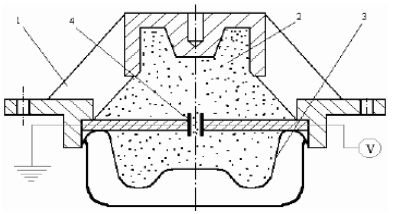

Fig.2.3. Controllable ***ER*** support configuration model, for motors or mechanisms: 1- elastic rubber rib, 2- ***ER*** material, 3- elastic membrane, 4- inertia channel [81].

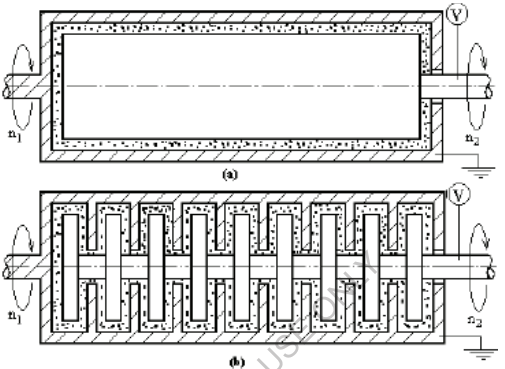

Fig.2.4. Model of controllable ***ER*** clutches: (a) with concentric cylinder; (b) with parallel discs [81].

Controllable dampers can be used in a wide range of applications due to their ability to change the ratio between speed and flow limit. In certain applications it is required that the shock absorbers can develop a wide range of controllable forces. Thus, shock absorbers were developed with concentric cylinders, multiple, which can be connected in parallel, in series or in combined ways. The speed-force variation, of the controllable device, is dependent on the way in which the connection between the hydraulic paths of the shock absorber is made. Fig.2.5 shows schematically a typical configuration of a controllable shock absorber, with concentric cylinders. It is observed that the electrodes are connected alternately, either to the ground (1) or to the high voltage source (2). The cover of the shock absorber (3) represents the outer electrode, connected to the ground. When energized, the electrodes form a set of parallel capacitors. The fluid passage channels between the electrodes can be connected in a different way than in parallel. The parallel connection ensures the largest range of controllable forces.

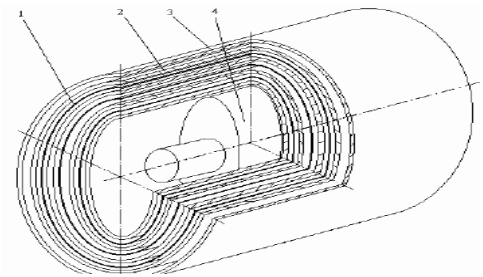

Fig.2.5. Schematic illustration of the configuration of a controllable ***ER*** damper, with concentric cylinders and passage channels connected in parallel: 1-electrodes connected to the ground, 2- electrodes connected to the high voltage source, 3-damper casing, 4-piston [95, 96].

The performance of the damper depends on: the size of the space between the electrodes; the thickness of the electrodes; the radii of the piston, shaft and shell and the length of the damper. This damper configuration ensures greater compactness, compared to classic dampers [96]. Currently, the classic controllable ***ER*** dampers, illustrated in fig.2.6, have been developed with fixed or sliding electrode configurations. In the shock absorber with fixed electrodes, from fig.2.6(a), the damping force of the piston (1) is controlled by the pressure loss in the discharge channels (3) through which the ER fluid (2) is forced to pass. Electrodes (4) are fixed plates. In the damper with sliding electrodes, illustrated in fig. 2.6(b), the damping force is controlled by changing the frictional resistance of the ER fluid, when passing through the discharge channels. In this case, the piston (1) acts as a sliding electrode. Most applications of controllable ER dampers are found in aeronautics, such as airplane landing gear or helicopter spars (where dynamic loads reach values of 2 kN, at frequencies up to 150 Hz). Other cases where it is necessary to use controllable shock absorbers, due to the very high level of vibrations, are heavy vehicles (where torsion bar type shock absorbers have been manufactured, capable of controlling torques of up to 1 kNm, at frequencies of 2 Hz) or automatic washing machines, with centrifuge.

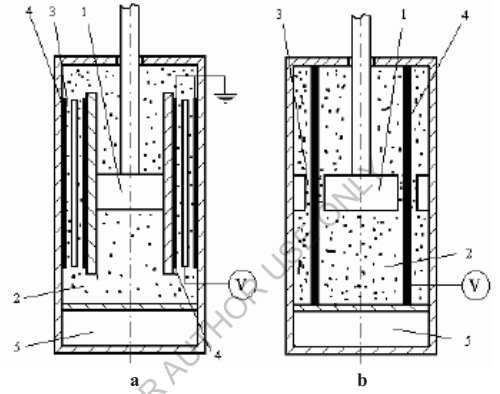

Fig.2.6. Models of controllable ***ER*** dampers, classic: (a) with fixed electrode; (b) with electrode slider: 1-piston, 2-***ER*** fluid, 3-discharge channel, 4-electrode, 5-pressure accumulator [96].

Adaptive structures are obtained by incorporating ER shock absorbers in stress concentrating areas. The role of ***ER*** materials is to control and modify the friction in the damper bearings, regulating the compliance of large constructions (blocks, bridges, etc.) in areas with high seismic activity [95].

Magnetorheological materials. Magnetorheological (***MR***) materials are stable suspensions of ultrafine ferromagnetic particles, with sizes of the order of 0.05-10 μm, in a carrier fluid, insulating medium.

General characterization of *MR* materials. When applying a magnetic field, MR materials have the ability to change their viscosity by up to six orders of magnitude, due to the formation of chains of aligned particles. The phenomenon is illustrated in fig.2.7.

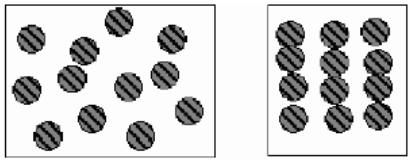

Fig.2.7. Schematic illustration of the reversible behavior of particles within ***MR*** materials: (a) layout disordered, in the absence of the external magnetic field; (b) alignment along a single direction, upon application of the field [96].

The formation of the "pearl" chains, as the rows of aligned ***MR*** particles in fig. 2.7(b) are also called, is accompanied by the modification of the rheological (elasticity, plasticity, viscosity), magnetic, electrical, thermal, acoustic, properties etc., but the main effect is the increase in apparent viscosity. When the magnetic field is removed, the particles return to the disordered state in fig. 2.7(a) [96].

There are 3 major components in the structure of an ***MR*** material: the ferromagnetic particles, the carrier fluid and the stabilizer.

a. **The dispersed ferromagnetic particles** have a spherical shape and occupy approx. 20-50% of the ***MR*** material volume. Currently, soft (remagnetizable) magnetic material powder such as iron carbonyl (FeCO) is used. An example of such powder is S-3700, obtained by the ISP company, by decomposing iron pentacarbonyl, Fe(CO)5. The chemical composition of the particles of this brand is: Fe-max 1%, C-max 0.7%, O-max 1%, N.

b. **The carrier fluid** serves as a continuous isolation medium and must have a viscosity of 0.01-1 Pa·s at 4000C. The carrier fluids currently used are: water, glycol, kerosene and synthetic or mineral (silicone) oil.

c. **The stabilizer** has the role of keeping the particles suspended in the fluid, preventing them from clumping together or settling by gravity. Stabilization is done differently, depending on the concentration of the particles: a) at low concentrations, around 10%, stabilization consists of the formation of a gel that favors dispersion and lubrication, changes viscosity and inhibits wear. An example of such a stabilizer is silica gel, formed by ultrafine and porous silica particles, which have the ability to absorb large amounts of liquid; b) at high concentrations, up to 50%, stabilization is done with surface-active, neutral or ionic substances that adhere to the surface of the particles, favoring their arrangement in finely dispersed, spatially branched structures. ***ER*** materials are obtained by grinding in ball mills, where all the components of the material, including the carrier fluid, are introduced and their fragmentation and mixing occurs under the effect of ball collisions, at speeds of the order of 2000 rpm. Regarding the influence of the intensity of the applied magnetic field on the variation of the tension with the shear rate, fig. 2.8 is presented. It is observed that the shear stress stabilizes with the increase of the shear speed but increases proportionally, depending on the square root of the intensity of the applied magnetic field [96, 104, 105].

A "good" ***MR*** material is characterized by: (i) low initial viscosity; (ii) high shear stress values at certain values of the magnetic field intensity; (iii) negligible temperature dependence and (iv) high stability.

As already mentioned, pure iron has the best ***MR*** properties. Its superiority is illustrated in fig.2.9. It is observed that the flow resistance of the pure iron MR suspension, from fig. 2.9(b) is approx. six times higher than that of the suspension based on iron oxide in fig. 2.9(a).

It should be noted that ***MR*** materials have superior properties to ***ER*** materials, from the following points of view: 1 – they have higher flow resistance, as can be seen by comparing fig.2.2 (b) with fig.2.9 (b); 2 – they have greater stability to impurities and contamination elements, which usually appear during the production and use of the material; 3 – the energy consumption is lower (the required powers, lower than 50 W, can be provided, at voltages of 12-24 V and intensities of 1-2 A, even by electric batteries).

Due to both their superiority over ***ER*** materials and their easily controllable rheological properties, ***MR*** materials are successfully used in shock and vibration control applications.

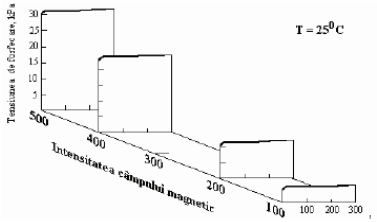

Fig.2.8. The influence of the intensity of the magnetic field on the variation of the stress depending on the shear rate, in an ***MR*** material [105].

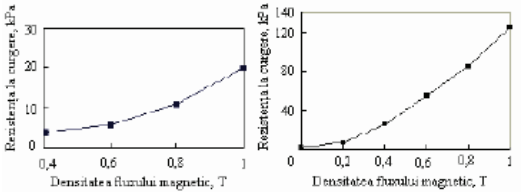

a **b**

Fig.2.9. The influence of the particle material on ***MR*** properties: (a) for iron oxide; (b) to a suspension of 40 % pure iron [105].

Applications of MR materials. The applications of ***MR*** materials can be found within the same general categories found in ***ER*** materials – controllable devices and adaptive structures. The most widespread controllable devices with ***MR*** materials are dampers. Several types of dampers with ***MR*** materials are shown schematically in fig. 2.10. The classic ***MR*** shock absorber, from fig. 2.10(a), has the disadvantage that the effect of the electromagnet (4) must cover the entire diameter of the cylinder, so a rather large region, which requires a very strong magnetic field [104]. The damper variants in fig.2.10(b) and (c) use a flow control valve which, from a functional point of view, is a controlled hydraulic resistance.

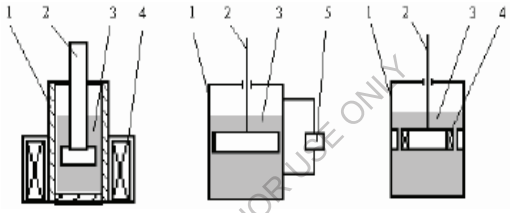

a **b** **c**

Fig.2.10. Types of dampers controllable with ***MR*** materials: (a) classic damper; (b) damper with external valve of regulation; (c) damper with built-in control valve: 1-cylinder, 2-piston, 3-***MR*** fluid, 4-electromagnetic coil, 5-flow control valve [104, 106].

The flow rate of the ***MR*** fluid (4) through the valve (5) is regulated by means of a magnetic field perpendicular to the flow direction. The flow control valve is an assembly of cylinders and coaxial rings, around the outside of which a coil of copper wire is wound. The solenoid thus formed generates a magnetic field perpendicular to the axis of the valve, which can reach, for example, an intensity of 300 kA/m, at a current of 1.2 A and a number of 1000 turns. An example of the use of ***MR*** fluid controllable devices are the dampers in the driver's seats on heavy trucks, the controllable brakes and clutches, the braking systems in car driving simulators, etc. ***MR*** fluid controllable dampers are very promising candidates for adaptive structure stiffness control systems, especially in cases with high risk of exposure to natural calamities such as large storms or earthquakes. Such a damper for anti-seismic protection, produced by Lord, is sketched in fig. 2.11. The stroke of the damper is ± 2.5 cm. The master cylinder (8) has a diameter of 3.8 cm and contains the piston (9), the pressure accumulator (3) and the ***MR*** fluid (4). The magnetic field is produced by the coil (5), placed on the piston. The power absorbed during the operation of the damper is less than 10 W. The response time of the assembly was less than 10 ms [106,132].

Using such dampers, Lord developed adaptive structures protected against vibrations and shocks, two examples being provided by fig. 2.12. This protection system is cheap, requires low maintenance and consumes little electricity. In principle, the dampers are placed in such a way that they dissipate the mechanical, shearing energy of the various successive segments of the structure. If correctly placed and tied, the shock absorbers provide protection for cable-stayed bridges, fig.2.12(a) and high-rise buildings, fig.2.12(b), even in case of large storms or a strong earthquake [132].

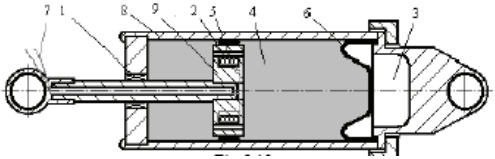

Fig.2.11. Schematic of a controllable damper with ***MR*** material: 1-bearing and seal, 2-annular hole, 3-pressure accumulator, 4-***MR*** fluid, 5- electromagnetic coil, 6- elastic diaphragm, 7-electromagnet supply wires, 8- cylinder, 9-piston [106].

A particular application of ***MR*** fluids is high precision finishing. The material to be processed is brought into contact with the ***MR*** fluid exactly in the area to be removed. When the magnetic field is applied, the ***MR*** fluid - which until then rotated together with the workpiece - suddenly increases its viscosity, which leads to the separation of a superficial layer, only in the targeted area. If the process is properly calibrated and controlled by computer, a typical machining accuracy of 50 μm is ensured for superfinishing operations [106].

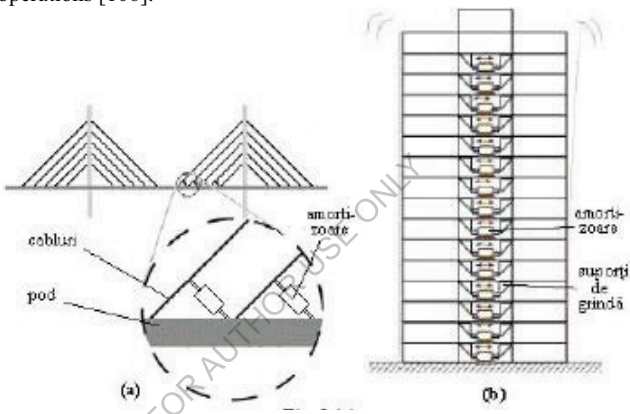

Fig.2.12. Illustration of the use of controllable shock absorbers, with ***MR*** material, in the construction of adaptive structures: (a) for bridges fixed by cables; (b) in multi-store buildings [106, 110, 111].

Within smart materials, two more "sensory" categories have recently been included - optical materials and marking particles - which, however, occupy negligible fractions of the world market. Compared to shape memory materials – which are unanimously considered the first to be used in adaptive applications, other smart materials can be considered “in their infancy” [100]. This was reflected by the space given to each of the categories of materials presented in this work.

Rheological materials - comparison - control generalities. ***MR*** materials consist of micrometric (3.8μm), magnetizable particles suspended in liquid. ***MR*** materials generally consist of a concentration of 20.40% pure iron particles suspended in a carrier fluid such as mineral or synthetic oil, water or glycol. A variety of additives similar to commercial lubricants are used to prevent gravitational settling of particles and ensure their maintenance in suspension, increase lubrication, change initial viscosity and inhibit wear (Encyclopedia of Smart Materials). The critical volume concentration (***CPVC***) defined by Lokander and Stenberg (2003) depends on the apparent density of the iron particle powder. The effect of ***MR*** materials does not increase much with the increase of this ***CPVC*** concentration. ***MR*** fluids are controllable fluids in terms of magnetic properties. MR fluids are finding more and more applications in industry. These applications include shock and vibration absorbers, semi-active dampers, brakes, different actuation systems [17, 21]. They are seriously considered as anti-seismic dampers in civil engineering. The Cedrat Technologies concern experimentally researched, for its potential buyers, such equipment, proposing for the control of the

dynamic behavior of the structures, the models presented in the figure below in three variants: with active, hybrid and semi-active control.

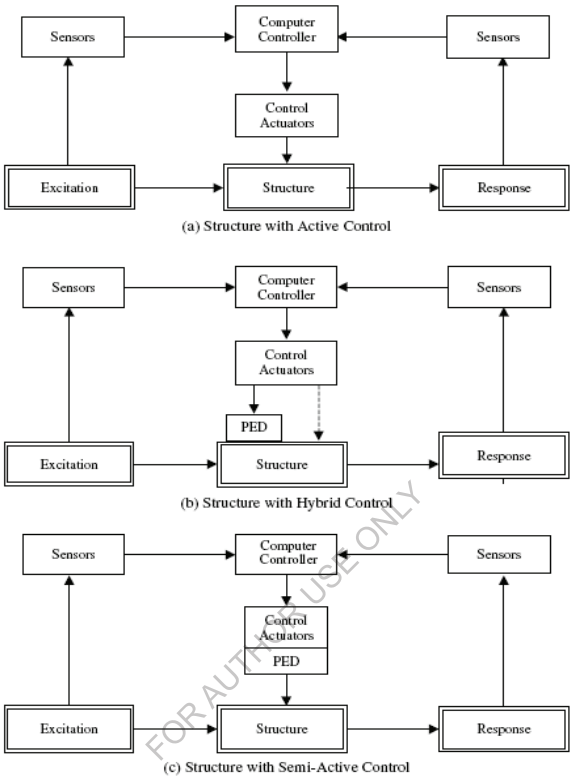

Fig.2.13. Various variants of control schemes with passive energy dissipation (PED).

MR fluids are substances that, under the controlled action of the magnetic field, change their state from a liquid to a semi-solid state in a time of the order of milliseconds. Adaptation of damping force can be done more than 500 times per second. The ***MR*** damper controller determines its tuning with each vibration thus preventing the damper action then when it is not the case. The MR substances generically called Rheonetic Fluids are specially intended for the field of vibration damping, and the coupling with the electronic control of movements takes on a new dimension.

2.2. Operating modes with rheological fluids [22, 24, 106].

The basic magnetorheological fluid operating modes are: flow operating mode, valve type; shear operation mode, brake type; operating mode by pressing; combined operating modes.

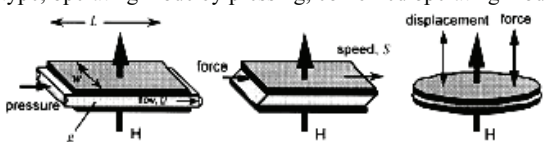

a- valve; b- sliding brake; c- brake by pressing

Fig. 2.14. Modes of operation with magnetorheological fluids (Carlson and Jolly, 2000).

In order to obtain the desired control over the damping force, it is necessary for the damper to work with a minimum volume of modified rheological fluid, determined by the contact surface:

$$V = Lwg \tag{2.2}$$

2.3. Types of magnetorheological dampers, properties and some relationships

A wide use of magneto-rheological shock absorbers is also the rotary ones, used especially as auxiliary components alongside springs. The application in figure 2.15 shows a rotary damper used in a joint of an articulated arm type robot, to reduce the vibrations generated in the manipulation process by the coupling compensation springs, a construction detail of the mounting of the electromagnet and a characteristics for the rotary movement, for various values of the damping coefficient.

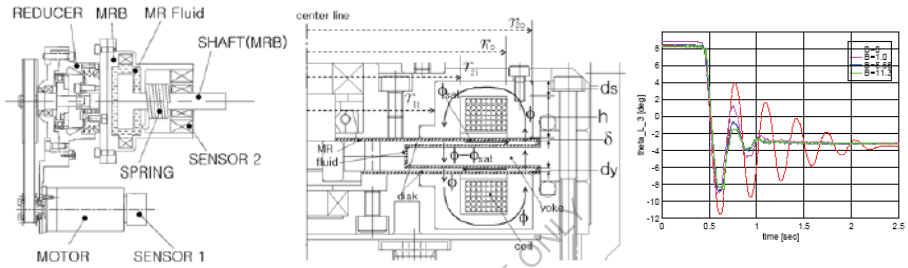

Fig.2.15. Rotation mode with AMR, constructive detail regarding the mounting of the electromagnet and the variation of the angular displacement by changing the damping coefficient

Research from other universities and institutes in the world, in particular the Seismological Research Institute of Tsukuba-shi, Ibaraki-ken in Japan, has shown that many applications in building vibration compensation techniques are made by using linear magneto-rheological damping devices based on hydraulic cylinders of special construction (fig. 2.16). From the analysis of the figures, it can be seen that the ***AMR*** works as a mechanical filter and intelligent shock absorber, through the use in its construction of springs to compensate for its own flow vibrations (mechanical filter function), as well as an ***AMR*** through the existence of the electromagnet and the flow holes (magneto-rheological damping function).

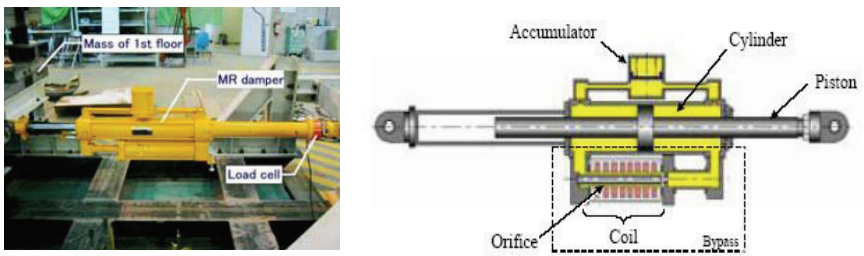

Fig.2.16. Seismic attenuation installation made at the Institute of the Seismological Research Tsukuba-shi, Ibaraki-ken, Japan and schematic diagram of researched ***AMR***.

The company ReacTec, England is one of the main companies that deals with the production of equipment and special devices for reducing vibrations both in the field of manufacturing, machines as well as in the field of civil constructions, industrial or even in the field of health, creating specific equipment to control harmful vibrations from work. The device, of the respective company, provides

on-line vibration reduction through the semi-active control of the rheological parameters. The passive isolation systems practiced in many industrial applications have as their target the reduction of a critical frequency, requiring their change if the working conditions, respectively if the unwanted frequency, changes. ReacTec automatic control technology adapts the damping devices to the specific conditions, adapting the amplitude, respectively the frequency to the required conditions, so as to finally reduce the harmful effect of vibrations.
Within the Department of Mechanics and Industrial Engineering at the University Northeastern in Boston, USA has made magnetorheological damping devices for rehabilitation exercises, as well as for prostheses, in order to balance between its various segments. These devices are rotating, concentrically designed, to increase the damping forces, as well as the adjustment range.

2.4. Mathematical models of magneto-rheological dampers (MMR) [6, 17, 20, 21, 22, 30, 51, 80]
The Bingham model simulates a relatively simplified ***MR*** damper. The model includes a Coulomb friction force f_y connected in parallel with a viscous element with coefficient c, figure 2.17. The model is simplified because it does not highlight the damping force-speed hysteresis.

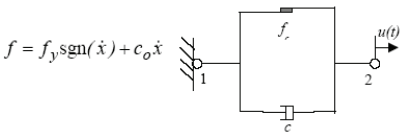

Fig.2.17. The Bingham mechanical model including a Coulomb friction force and a viscous friction force.

The Bouc-Wen model is more extensive, including the hysteresis curve. The model is represented in figure 2.18. The model is more complex and requires a closed-loop control algorithm (Dyke et al., 1998 [35, 36], Yang et al., 2002 [77], Liao and Lai, 2002 [99]).

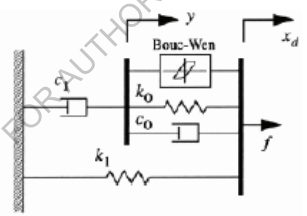

Fig.2.18. Mechanical model of the MR- damper based on the Bouc-Wen model (Dyke et al., 1998).

The equations describing the Bouc-Wen algorithm for the behavior of the magnetorheological damper can be written in the following form:

(2.3)

$$f = c_1\dot{y} + k_1(x_d - x_0)$$
$$\dot{z} = -\gamma\left|\dot{x}_d - \dot{y}\right|z\left|z\right|^{n-1} - \beta(\dot{x}_d - \dot{y})\left|z\right|^n + A(\dot{x}_d - \dot{y})$$
$$\dot{y} = \frac{1}{c_0 + c_1}\{\alpha z + c_0\dot{x}_d + k_0(x_d - y)\}$$

where $\boldsymbol{f}$ is the damping force and is described by the primary displacement variables, $\boldsymbol{x}_d$ and $\boldsymbol{y}$, and by the state variable $\boldsymbol{z}$ which also takes into account the time evolution of the force. The viscous damping parameters c0 and c1 as well as the parameter α depend on the variable magnetic field (on the coil supply voltage). Parameters $\boldsymbol{\beta}$ and $\boldsymbol{x}_0$ are constant and determined by experimental research.

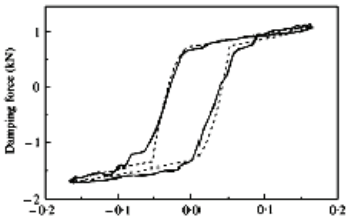

Fig.2.19. The hysteresis characteristic of the damping force- travel speed. Comparison between the experimental research (solid line) and the numerical simulation results of the Bouc-Wen model (broken line) (Choi et al., 2001).

The Li (2000 [99]) model is a model in which the ***MR*** material operates in two rheological domains: pre-flow and post-flow. It is considered that in the pre-flow domain, the deformations are viscoelastic, and in the post-flow domain, the deformations are viscoplastic. The mechanical model is presented in figure 2.20.

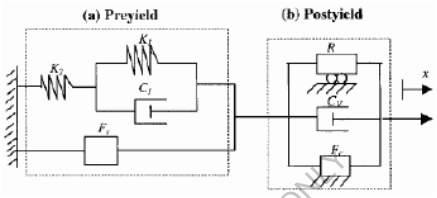

Fig.2.20. The viscoelastic-plastic model of the MR damper – according to the research of Li et al. (2000).

The equations, according to the model proposed by Li et al. are:

$$\begin{aligned} F &= F_{ve} + F_y, && |F| \le F_c, \ \text{preyield} \\ F &= C_V \dot{x} + R\ddot{x} + F_C \operatorname{sgn}(\dot{x}), && |F| > F_c, \ \text{postyield} \end{aligned} \tag{2.4}$$

where $\boldsymbol{F}_c$ is the force in the field of elastic deformation of the ***MR*** material in the shock absorber after applying the magnetic field, $\boldsymbol{C}_V$ is the viscous damping coefficient and $\boldsymbol{R}$ is the equivalent inertial mass. The viscoelastic force $\boldsymbol{F}_{ve}$ needs to be determined separately according to the theory of viscoelasticity. Li et al. (2000) made experimental tests of the dynamic properties of the damper ***MR***. The characteristics of damping force-displacement function, speed and time are presented in fig. 2.21.

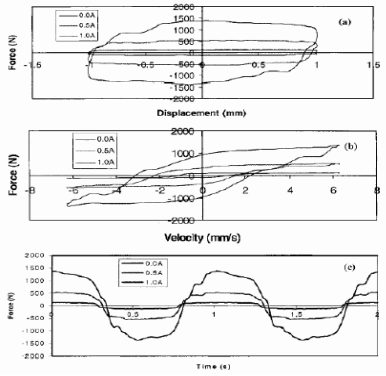

Fig.2.21. Experimental characteristics of the Li model. (a) force versus displacement, (b) force versus speed and (c) force versus time for different fields, displacement amplitude X0 = 1mm, frequency f = 1 Hz, current I = 0.5 A (Li et al., 2000).

The Oh and Onoda model. Oh and Onoda (2002) designed and built a variable MR damper to demonstrate vibration displacement in structures. The physical model and the mechanical model are presented in figures 2.22 and 2.23.

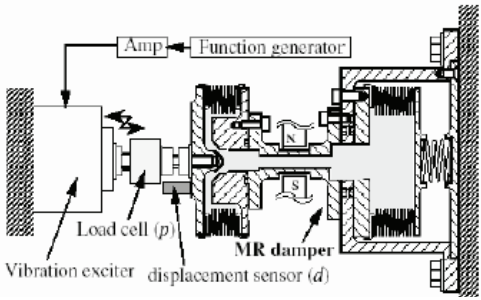

Fig.2.22. The experimental model for the dynamic tests of the MR damper (Oh and Onoda, 2002).

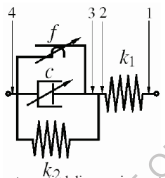

Fig.2.23. The equivalent mechanical model consisting of springs, viscous damper, and dry friction component specific to the MR damper model, Oh and Onoda (2002).

The dynamic properties were measured by applying a sinusoidal excitation force while keeping the magnetic field of intensity ***H*** constant.

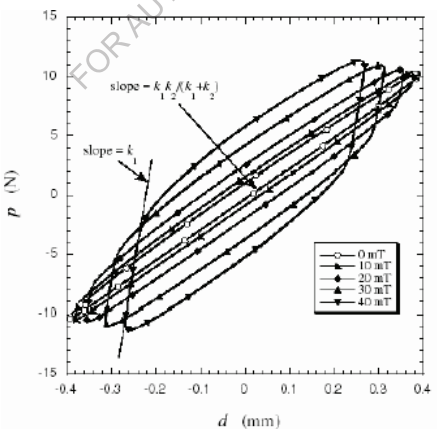

Fig.2.24. The variation characteristic of the damping force as a function of displacement in the ***MR*** damper, for different magnetic fields (Oh and Onoda, 2002).

The Choi model (2001 [30, 31]) proposes a polynomial model of degree 6 in which the damping force is expressed by the relation:

$$F_d = \sum_{i=0}^{6} a_i v^i \tag{2.5}$$

The parameters a_0 ...a_6 are defined experimentally for positive or negative accelerations and speed v raised to the power i.

The extended Bingham model. Gamota and Filisko [44] presented an extension of the Bingham model that describes the behavior of the ER in the pre-flow and post-flow state. This visco-elastic-plastic model consists of the series Bingham model with three elements of a linear solid (Zener element) shown in figure 2.25. The force in this system is given by:

$$F = \begin{cases} c_0\dot{x}_1 + f_c \cdot \operatorname{sgn}(\dot{x}_1) \\ k_1(x_2 - x_1) + c_1(\dot{x}_2 - \dot{x}_1) \\ k_2(x_3 - x_2) \end{cases} \quad , \quad |F| > f_c$$

$$F = \begin{cases} k_1(x_2 - x_1) + c_1\dot{x}_2 \\ k_2(x_3 - x_2) \end{cases} \quad , \quad |F| \le f_c \tag{2.6}$$

where the damping coefficient c_0 and the friction force fc are simulations of those in the Bingham model for the plastic viscosity, respectively for the flow state. The parameters c_1, k_1 and k_2 are associated with the elasticity properties of the fluid for the pre-flow region (Gamota and Filisko [44], Spencer et.all [176,177].

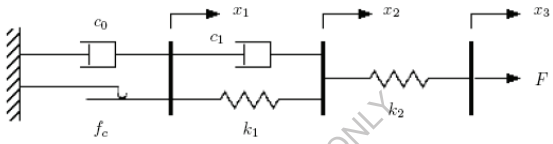

Fig.2.25. Extended Bingham model (Spencer et al. [176]).

The three-element model. Focusing on the dynamic behavior of ***AER*** and ***AMR*** Powell [150, 151] proposed an analogous mechanical model consisting of viscous damper, nonlinear spring and friction element, connected in parallel (fig. 2.26). To reproduce the force-velocity hysteresis characteristic that is confirmed experimentally (cf. fig.2.27b), the Coulomb friction force f_c is modeled by the static and dynamic coefficients fcs and f_{cd}.

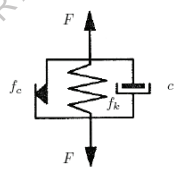

Fig.2.26. The three-element model (Powell [150, 151]).

The mathematical model is expressed in the form:

$$f_c = \begin{cases} f_{cs}\Big(1 + (f_{cd}/f_{cs}) \cdot \exp(-a\,|\dot{z}|)\Big) \cdot \tanh(e\dot{z}) \\ f_{cd}\Big(1 - \exp(-b\,|\dot{z}|)\Big) \cdot \tanh(e\dot{z}) \end{cases} \quad , \quad \begin{matrix} \dot{z} \cdot \ddot{z} \ge 0 \\ \dot{z} \cdot \ddot{z} < 0 \end{matrix} \tag{2.7}$$

where z is the displacement transmitted ***AMR*** or ***AER***, and z' and z'' the speed and acceleration. The force generated by damper is given by:

$$F = f_c + f_k + c\dot{z} \tag{2.8}$$

where $f_k = k \cdot tanh(dz)$ is the nonlinear force of the spring in the elastic zone. In this model, the model coefficients dependent on the damping parameters f_{cs}, f_{cd}, a, b, c and e as well as on the elasticity parameters d and k were established through experimental research. A comparison between behavior assumed and observed ***AER*** or ***AMR*** is shown in fig.2.27.

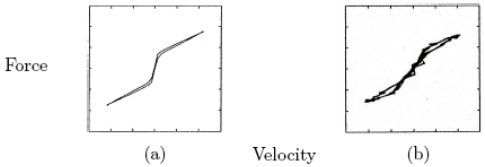

Fig.2.27. Comparison between the simulated results: (a) and those obtained experimentally; (b) Force-velocity characteristic for the model with three elements (Powell [150, 151]).

The three-element model is quite close to reality and is much easier to simulate numerically than the extended Bingham model.

The BingMax model. A model with similar components is the BingMax discrete element model presented by Makris et al.[109,110]. It consists of a Maxwell element with a Coulomb friction element, fig.2.28.

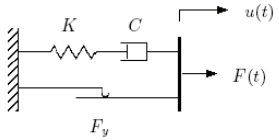

Fig.2.28. BingMax model (Makris et al. [109, 110]).

The force F(t) in this system is given by:

$$F(t) = K \int_0^t \exp\left(-\frac{t-\tau}{\lambda}\right) \dot{u}(\tau)\,\mathrm{d}\tau + F_y \cdot \mathrm{sgn}\left[\dot{u}(t)\right] \tag{2.9}$$

where $\boldsymbol{\lambda}$ is the ratio of the damping constant $\boldsymbol{C}$ and the spring stiffness $\boldsymbol{K}$, and $\boldsymbol{F}_y$ is the friction force. The equation can also be written:

$$F(t) + \lambda \cdot \frac{\mathrm{d}F(t)}{\mathrm{d}t} = C \cdot \dot{u}(t) + F_y \cdot \mathrm{sgn}[\dot{u}(t)] \tag{2.10}$$

The nonlinear visco-elastic-plastic model. The visco-elastic-plastic model presented by Kamath and Wereley [87, 88] combines two linear flow mechanisms with nonlinear functions, fig. 2.29.

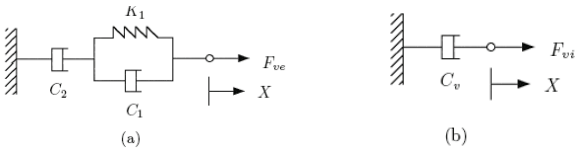

Fig.2.29. Viscoelastic-plastic model (Kamath and Wereley [87, 88]).
(a) Vasco-elastic mechanism; (b) Viscous mechanism.

In the flow region the behavior of the fluid is simulated by three elements, considering the linear behavior of the fluid (Jeffreys model). The visco-elastic force $\boldsymbol{F}_{ve}$ generated by this system is governed by:

$$F_{ve} + \frac{C_1 + C_2}{K_1} \cdot \frac{\mathrm{d}F_{ve}}{\mathrm{d}t} = C_2\dot{X} + \frac{C_1 C_2}{K_1} \cdot \ddot{X} \tag{2.11}$$

where $\boldsymbol{C}_1$, $\boldsymbol{C}_2$ and $\boldsymbol{K}_1$ are the damping and stiffness parameters, and $\boldsymbol{X}$ is the displacement transmitted to the device. In the post-flow region the response is represented by the dependence relation viscous:

$$F_{vi} = C_v \dot{X} \tag{2.12}$$

where the damping coefficient $\boldsymbol{C}_v$ is the apparent viscosity coefficient of the fluid (fig.2.30b). The form of transition from the pre-flow regime to the post-flow regime is made through a non-linear combination within the final force relationship, between the visco-elastic and viscous components $\boldsymbol{F}_{ve}$ and $\boldsymbol{F}_{vi}$:

$$F = F_{ve} S_{ve} + F_{vi} S_{vi} \tag{2.13}$$

Where:

$$S_{ve} = \frac{1}{2}\left[1 - \tanh\left(\frac{\alpha - \alpha_y}{4\varepsilon_y}\right)\right] \quad S_{vi} = \frac{1}{2}\left[1 + \tanh\left(\frac{\alpha - \alpha_y}{4\varepsilon_y}\right)\right] \tag{2.14}$$

(Kamath and Wereley [87, 88]).The block diagram of the relationship between force and displacement is presented in fig. 2.30; $\boldsymbol{L}_{ve}$ and $\boldsymbol{L}_{vi}$ are linear operators.

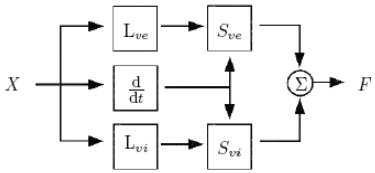

Fig.2.30. Schematic of the visco-elastic-plastic model (Kamath and Wereley [87, 88]).

Non-parametric models are based on their performance. These usually require the acquisition of experimental data regarding behavior in different tasks, under different conditions (Jung et al. 2004). The models proposed in this category are based on Chebychev polynomials (Ehrgott and Masri 1992, Gavin et al. 1996b [49, 50, 51]), on neural networks (Chang and Roschke 1998, Zhang and Roschke 1998, Wang and Liao 2001), neuro-fuzzy systems (Schurter and Roschke 2000) or on the identification technique (Jin et al. 2001, Jin et al. 2002), as an example: Ehrgott and Masri (1992) use Chebyshev polynomials for AMR modeling. Two probes were used to generate the damping force. In the first case, the damping force is a function of displacement and velocity and is described by two orthogonal Chebyshev polynomial functions. In the second case, the force is a function of speed and acceleration and is also described by Chebyshev orthogonal polynomial functions. Comparison of the experimental results are shown in fig.2.67. and shows that in the second case, the damping behavior is described more precisely. This method was extended by Clamroch and Gavin (1995), and Gavin et al. (1996b), who established that the force is not only a function of displacement and speed, but also of the electric field. The analytical results were compared with the experimental data and a satisfactory expression of the damping force was found.

$$F(x,\dot{x}) \approx \hat{F}(x,\dot{x}) = \sum_{i,j=0}^{m} C_{ij} T_i(x') T_j(\dot{x}') \quad F(x,\dot{x},E) \approx \hat{F}(x,\dot{x},E) = \sum_{i,j,k=0}^{m} C_{ijk} T_i(x') T_j(\dot{x}') T_k(E') \tag{2.15}$$

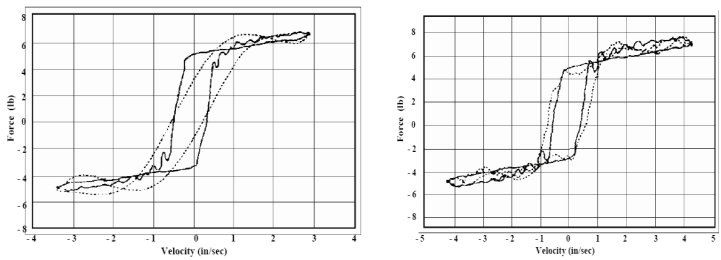

(a) force as a function of displacement and velocity; (b) force as a function of velocity and acceleration

Fig. 2.31.Comparison of experimental hysteresis and Chebycheff characteristic.

Neural network models reproduce the nonlinear behavior of ***AMR*** much more precisely. These systems emulate the properties of the nervous system and are composed of neurons, which are the component elements, and synapses, which represent the connections between them. Connections can be adjusted by learning the algorithm to more accurately reproduce the behavior of the system (Pacific Northwest National Laboratory and Batelle Memorial Institute 1997.) This involves using experimental input and output data or data from mathematical simulation of the system, which will be modeled . Chang and Roschke (1998) propose a multilayer network (***MLP***) for modeling ***AMR***. ***MLP*** networks are some of the most common types of networks, which have the particularity of using only one non-linear function. The network consists of 6 input neurons, one output neuron and 12 neurons in the hidden layer. Zhang and Roschke (1998) proposed two neural networks for ***AMR***. The first predicts the damping force when the tension is known, and refers to the inverse model. It consists of 8 input neurons, one output neuron and 5 neurons in the hidden layer. Another proposed model predicts the tension, when the damping force is known. It refers to the inverse model and consists of 4 input neurons, one output, and 10 neurons in the hidden layer. Gauss-Newton learning algorithm based on Levenberg-Marquardt learning algorithm and OBS strategy were used for both models. Wang and Liao (2001) proposed a neural network for direct identification of ***AMR***. This model consists of a neural network in which the output is linked to the input layer. This model has three layers with 15 input neurons, one output neuron and 15 neurons in the hidden layer.

Neuro-fuzzy models are other models that emulate the dynamic behavior of ***AMR***. In these new models neural networks are used to adjust the fuzzy logic parameters. Fuzzy logic incorporates knowledge about the system into a controller, using various functions that use vague concepts such as: free, strong, weak, moderate, etc. The desired output size is determined based on the input fuzzy information, just like the decision of the human brain. The neuro-fuzzy model proposed by Schurter and Roschke (2000) for small ***AMR***s uses neural networks to train functions that simulate the relationships between inputs: damper displacement, velocity, voltage signal and output: damping force. A nero-fuzzy application is the Adaptive Neuro-Fuzzy Inference System (***ANFIS***) from the Matlab Fuzzy Logic Toolbox, which is used to determine the parameters needed to model the damper. This application uses a learning algorithm combined with backpropagation gradient and the least squares method. Learning and data validation were generated using the phenomenological model proposed by Spencer Jr. et al. (1997 [176, 177]).

Often the non-parametric models are much more complicated and difficult to achieve due to the very large number of experimental determinations for the exact establishment of the necessary parameters, so the less precise parametric modeling is preferable, if the required precision is not very high.

2.6. Control laws of AMR [16, 17, 30, 31, 93, 106, 131, 150, 151, 160, 161, 194, 195, 200]

AMR is a non-linear device, which is why it is necessary to develop a control algorithm that ensures all the advantages determined by its characteristics. Several control strategies were researched by Jung et al. (2004), among which we can mention: optimal control, which assumes a mathematical model as precise as possible and an intelligent control. The performances of the different proposed control systems were simulated in the works of Dyke and Spencer Jr. (1997 [35] Jansen and Dyke (2000 [36]), by using a single AMR, and Jansen and Dyke (1999), in the implementation of ***AMR*** multiple A synthesis of research is presented by Jung et al. (2004.)

Optimal control [36]. A very interesting proposed algorithm for ***AMR*** control, called closed optimal control, was developed by Dyke et al. (1996a,b [36]). This is the most used algorithm for ***AMR*** (Jung et al. 2004.) This strategy consists of a bang-bang (on-off) controller, which causes the damper to generate a required control force, which is then determined by an active controller ideal, fig. 2.32. The feedback link is used to produce the required force, fc, which is ultimately determined by a linear optimal controller, $\boldsymbol{K}_c(s)$, based on the structural measurements, $\boldsymbol{y}$, and the measured force, $\boldsymbol{f}$.

$$f_c = \mathcal{L}^{-1}\left\{-\mathbf{K_c}(s)\mathcal{L}\left(\begin{bmatrix}\mathbf{y}\\ f\end{bmatrix}\right)\right\} \tag{2.16}$$

where: $\boldsymbol{L}\{.\}$ is the Laplace transform. The linear controller is obtained by using the ***H₂/LQG*** strategy. The strategy consists in keeping the tension constant, if the force generated by the damper, $\boldsymbol{f}$, is equal to the required force $\boldsymbol{f}_c$. When the amplitude of the force f is smaller than the amplitude of the force fc and both forces have the same sign, the applied voltage is set to the maximum value to increase the damping force and to bring it as close as possible to the necessary one. This algorithm, for selecting the applied voltage, is represented in fig. 2.32. and described by equation 2.16.

$$v = v_{\max} H\{(f_c - f)f\} \tag{2.17}$$

where $\boldsymbol{v}_{\max}$ is the maximum voltage associated with the saturation of the magnetic field of the ***AMR***, and $\boldsymbol{H}(.)$ is the Heaviside step function. The performance of the closed optimal control algorithm was evaluated by numerical simulation (Dyke et al. 1996b) and experimentally by (Dyke et al. 1996a).

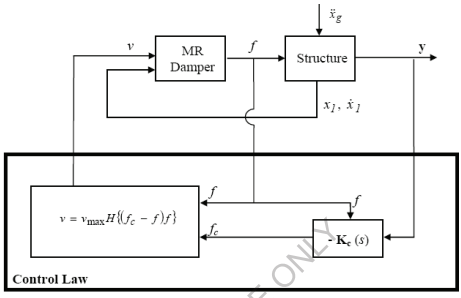

Fig.2.32. Block diagram of the optimal control algorithm (Dyke et al. 1996a,b [36]).

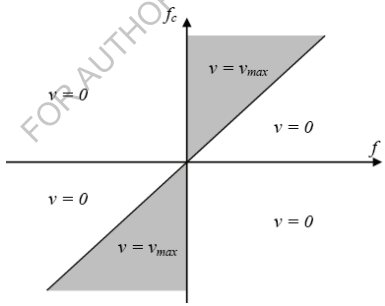

Fig.2.33. Graphic representation of the closed optimal control algorithm (Clipped-Optimal Control Algorithm) (Dyke et al. 1996a,b [36]).

The performance of this algorithm for several dampers was verified experimentally by Yi et al. (1998) and Yi et al. (2001), Jansen and Dyke (1999), and Dyke (1998.) The performance of this algorithm for multiple dampers was verified by numerical simulation on a sexapod structure equipped with 4 ***AMR***s by sinusoidal signal excitation close to the first two eigenmodes of vibration of the structure Yi et al. (1998). It was found that the optimal closed controller was good, reducing the response of the structure. ***AMR*** in combination with the control algorithm has also been applied to the reduction of cable vibrations in suspension bridges subjected to the action of wind. Numerical simulation was developed by Johnson et al. (2000, 2001). And the experiments led by Christenson (2001) and Christenson et al. (2001, 2002) confirmed these results. Other interesting research includes shifting the vibration spectrum in coupled structures and controlling the lateral torsional response of irregular structures compared to others (Christenson 2001, Christenson and Spencer Jr. 1999, Christenson et

al. 1999, 2000). Another algorithm proposed by Chang and Zhou (2002) and Zhou et al. (2002) consists of a linear quadratic regulator (***LQR***) for optimal damping force determination and an inverse neural network for voltage calculation necessary to produce this force. This inverse neural network uses the data obtained from the phenomenological model developed by Spencer et al. (1997.).
Another control strategy proposed for use with ***AMR*** was developed based on Lyapunov stability theory. In the description by Yi et al. (2001), the first step consists in choosing the Lyapunov function that is appropriate to the state of the analyzed system. The success of this strategy in reducing the response of the structure was demonstrated analytically by Dyke and Spencer (1997), Jansen and Dyke (1999, 2000), and experimentally by Yi et al. (2001). The work of McClamroch and Gavin (1995), also based on the Lyapunov theory, proposes a bang-bang control strategy. The total vibrational energy (kinetic and potential) of the structure is represented by a Lyapunov function. The goal of this strategy was to reduce the rate of energy transmitted to the structure. Thus, the derivative of the Lyapunov function used to describe the vibrational energy was minimized.

Intelligent Control [18]. Another model based on the control strategy has been successfully applied in vibration reduction. It ensures the real control of the structure (Sreenatha and Pradhan 2002.) The non-linear behavior and complexity of the system determined the creation of sophisticated, computerized, often impractical models to be used in the development of control strategies. Intelligent, control-based technology has become an alternative to real systems. Three broad categories of intelligent control algorithms have been proposed for use with AMR: neural network control, neuro-fuzzy control, and fuzzy logic control. Shiraishi et al. (2002) proposed an adaptive neural network to control the structural model of the graph equipped with a magnetorheological damper. The control strategy consists of a structural identification network and a control network. When entering the network for identification, the control system takes into account the changes in the ***AMR*** characteristics as well as the structure. The shock absorber was placed between the ground floor and the first floor. The identification and control network was used to identify the displacement of the first floor at each time step, based on the last 5 values of the displacement of the ground floor, the first floor and the current control. Dalei and Jianqiang (2002), used an adaptive control strategy based on neural networks for ***AMR*** control based on isolated structures. This composed two networks: the control neural network (neural network control ***NNC***), for determining the control voltage and the neural network identification (***NNI***), for estimating the controller error on the reaction path. Each network has three layers with 5 x 11 x 1 nodes. The 4th term reaction algorithm was used to support the two neural networks. The numerical simulation showed that this strategy is more useful compared to the neural network controller without the term to the power of 4. In the category of neural control is the work of Ni et al. (2002), which proposes two neural networks for controlling the vibrations of suspended cables using ***AMR***. Both algorithms use incomplete output observations, the first one is intended for the complete model and has two functions: controller and observer (fig. 2.70). Off-line learning has been refined so that the controller emulates the force that can be achieved with a fully state-controlled ***LQG*** controller.

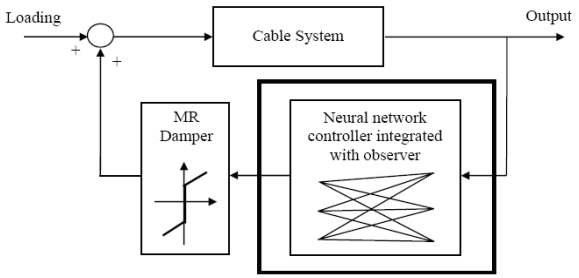

Fig.2.34. Neural network controller for the full-order model (Ni et al. 2002).

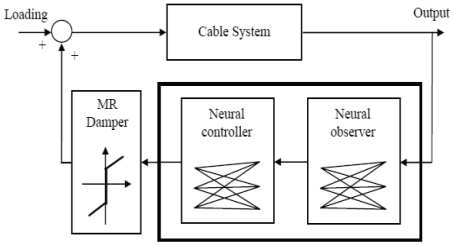

Fig.2.35. Neural network controller for reduced-order model (Ni et al. 2002) .

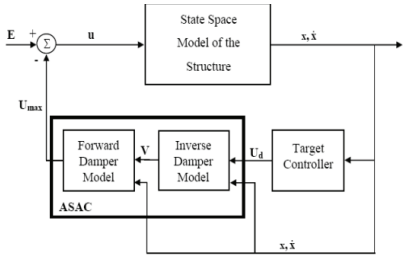

Fig.2.36. Block diagram for feedback control target including controller (Schurter and Roschke 2001) .

The second algorithm was designed to reduce the order of the model and includes an observation network with summation to the control network. The off-line learning used for the controller is similar (fig.2.36.) The analytical results showed that the performances of the two neural controllers were comparable to the ***LQG*** controller with full state observation. Xu et al. (2003) also proposed the use of neural networks for ***AMR*** control. The strategy consists of four layers, reaction with neural network and Levenberg-Marquardt algorithm for solving the time delay. Numerical simulation showed that this model is superior to the traditional method of temporal analysis of the unfolding of the elasto-plastic phenomenon. A different research was done by Schurter and Roschke (2001a,b) who developed neuro-fuzzy controllers. This technique consists of 5 steps. The first is to establish the target controller, in this case it is the controller on the feedback path, proportional to the fourth order inertia, ***LQR***. The second step contains the integration of the target controller with the system model and damper. To convert the required force into the actual force control, a semi-active ***ASAC*** converter was introduced. It includes an inverse damper model that calculates the required voltage ***V*** that can produce the desired force and a forward model for predicting the applied force. For this study, the inverse model was the modified version of the Bingham model, and the neuro-fuzzy model was proposed for the forward model.

An intelligent control strategy that does not require algorithm learning and does not require much acquired data is **the fuzzy controller**. This category of controllers is based on fuzzy logic, which uses intuitive understanding of the system's behavior to determine the controller's action, fig. 2.37. This strategy has been successfully applied with active control components (Casciati et al. 1994a,b,c, Casciati and Yao 1994, Furuta et al. 1994, Iiba et al. 1994, Goto et al. 1994, Yamada et al. 1994, Yeh et al. 1994, Fujitani et al. 1995, Aldawod et al. 1997, Battaini et al. 1997, 1998, Mitsui et al. 2002), where the fuzzy algorithm was used to determine the required force control using some components of semi-active control, (Nagarajaiah 1994, Sun and Goto 1994, Kelly 1997, Symans and Kelly 1999), where the algorithm was converted into voltage or current applied to the component so that its mechanical properties are modified.

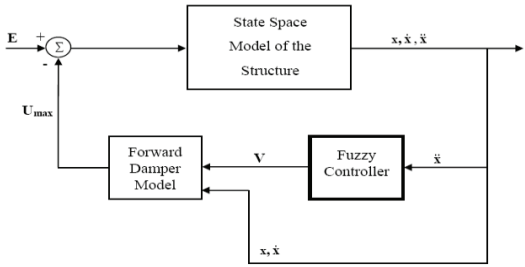

Fig.2.37. Block diagram of the feedback loop system containing the fuzzy controller (Schurter and Roschke 2001).

CHAPTER 3
General Information Regarding the Dynamic Behavior in Robotics

3.1. Mathematical models of the dynamic behavior of RI

To be able to realize the full range of manipulation applications, a robot must be able to touch any point in its workspace with an arbitrary orientation of the hand. For this reason, the three variables (***x, y, z***), or (***θ, Φ, r***) that define the position of the hand are not sufficient to describe its orientation. Three additional variables are needed, usually of rotation, defined as: ***roll***, ***pitch*** and ***yaw***, names taken from navigation (RPY system). To understand the meaning of these notions, extend the arm, with the wrist horizontal and the fingers together (fig. 3.1). The hand is rotated from the position with the opening of the palm down to that with the opening of the palm up, keeping all this time fingers pointing in the same direction. This movement is that of roll Now, with your fore arm outstretched, without twisting your wrist, the direction is changed by pointing it up and down. This movement is the pitch. Finally, with fingers glued and outstretched and without rolling or pitching movements, orient the fingers as much as possible far to the right, then to the left. This is the drift movement. These independent movements constitute degrees of freedom, but it must be mentioned that there is no freedom at the joints unlimited movement. For example, the drift capacity a of the human wrist is about 60 degrees. So there are certain combinations of hand position and orientation impossible to achieve in humans. The same will be true for robots. In applications robotized, the entire position configuration is defined as configuration three-dimensional and of the orientation of the gripper (requiring therefore for full definition six numerical values). A set of configurations, introduced by the robot's training (learning) action, together with the speed regime information, constitute the motion database for a robot application. Gripper configurations are specified relative to a coordinate system attached to the workpiece. The position of the piece (and therefore the attached coordinate syst em) is variable, known at any time, relative to another coordinate system (ex. Reference system, the base of the robot). It is necessary to solve the following problem: given a configuration A, known in relation to a coordinate system B, and given the location of system B in relation to another coordinate system C, to find the location of point A measured in coordinate system C (fig. 3.2) [10,11,14,15,26,27,28]. It is assumed that system B is only translated relative to C, not rotated, so the two systems have parallel coordinate axes. It follows that position A is described by the vector:

$$A_B = [x_B,\ y_B,\ z_B]^T \qquad (3.1)$$

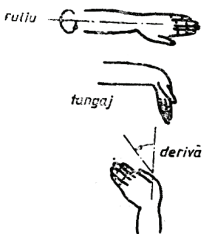

Fig.3.1. Elementary types of movements

The subscript B indicates that the variables are measured relative to the system of coordinates B. The origin of coordinate system B is known relative to system C:

$$B_C = [x_C,\ y_C,\ z_C]^T \qquad (3.2)$$

Then A in relation to C is given by:

$$A_C = A_B + B_C = [x_B + x_C,\ y_B + y_C, z_B + z_C]^T \qquad (3.3)$$

In this way, vector addition provides the solution to such problems, provided there is no rotation.
Let us now consider the problem of rotation: let there be two rectangular coordinate systems OXYZ and OUVW, whose origins coincide. The OXYZ coordinate system is fixed, being considered the reference system. The OUVW system rotates with respect to the reference system. Let $[i_x, j_y, k_z]$ and $[i_u, j_v, k_w]$ be the unit vectors along the coordinate axes of the OXYZ and OUVW systems respectively.
A point ***P*** can be represented by its coordinates with respect to both coordinate systems. For simplicity, let's consider the point P fixed with respect to the OUVW system. The vector results:
$p_{uvw} = [p_u\ ,\ p_v\ ,\ p_w\ ]^T$ and $p_{xyz} = [p_x\ ,\ p_y\ ,p_z\ ]^T$ (3.4)

which represent the same point ***P***, respectively in relation to the OXYZ and OUVW systems. Using a transformation matrix A, of size 3x3, we will transform puvw's coordinates into coordinates expressed with respect to the OXYZ system, after the OUVW system has been rotated:

$$p_{xyz} = A^* p_{uvw} \tag{3.5}$$

According to the definition of a vector:

$$p_{uvw} = p_u i_u + p_v j_v + p_w k_w \tag{3.6}$$

where p_u , p_v , p_w represent components of the vector puvw along the O_u, O_v and O_w axes, using the definition of the scalar product gives the components of p_{xyz}:

$$\begin{aligned} p_x &= i_x\, p = i_x\, i_u p_u + i_x\, j_v p_v + i_x\, k_w p_w \\ p_y &= j_y\, p = j_y\, i_u p_u + j_y\, j_v p_v + j_y\, k_w p_w \\ p_z &= k_z\, p = k_z\, i_u p_u + k_z\, j_v p_v + k_z\, k_w p_w \end{aligned} \tag{3.7}$$

or, in a matrix expression (3.8):

$$\begin{bmatrix} p_x \\ p_y \\ p_z \end{bmatrix} = \begin{bmatrix} i_x i_u & i_x j_v & i_x k_w \\ j_y i_u & j_y j_v & j_y k_w \\ k_z i_u & k_z j_v & k_z k_w \end{bmatrix} \begin{bmatrix} p_u \\ p_v \\ p_w \end{bmatrix} \tag{3.8}$$

$$A = \begin{bmatrix} i_x i_u & i_x j_v & i_x k_w \\ j_y i_u & j_y j_v & j_y k_w \\ k_z i_u & k_z j_v & k_z k_w \end{bmatrix} \tag{3.9}$$

The transformation A is called orthogonal, and since the vectors in the vector products are unitary, this transformation is also orthonormal. If the OUVW system rotates through an angle $\propto$ around the OX axis, then:

$$p_{xyz} = R_{x,\propto} p_{uvw} , \tag{3.10}$$

$R_{x,\propto}$ being called the rotation matrix around the OX axis with the angle $\propto$, and

$$R_{x,\alpha} = \begin{bmatrix} i_x i_u & i_x j_v & i_x k_w \\ j_y i_u & j_y j_v & j_y k_w \\ k_z i_u & k_z j_v & k_z k_w \end{bmatrix} = \begin{bmatrix} \mathbf{1} & 0 & 0 \\ 0 & \cos\alpha & -\sin\alpha \\ 0 & \sin\alpha & \cos\alpha \end{bmatrix} \tag{3.11}$$

Similarly, for the rotation with the angle β around the OY axis and with the angle φ around the OZ axis (3.12).

$$Ry,\beta = \begin{bmatrix} \cos\beta & 0 & \sin\beta \\ 0 & 1 & 0 \\ -\sin\beta & 0 & \cos\beta \end{bmatrix} \quad ; \quad Rz,\varphi = \begin{bmatrix} \cos\varphi & -\sin\varphi & 0 \\ \sin\varphi & \cos\varphi & 0 \\ 0 & 0 & 1 \end{bmatrix} \tag{3.12}$$

where $\boldsymbol{R}_{x,\propto}$, $\boldsymbol{R}_{x,\beta}$ and $\boldsymbol{R}_{x,\varphi}$ are the basic rotation matrices. The fourth component $\boldsymbol{w}$ of the homogeneous coordinates can be considered as a scale factor. In robotics applications $\boldsymbol{w}$=1. A homogeneous transformation matrix is a 4x4 matrix that transforms a vector expressed in homogeneous coordinates

from one coordinate system to another. In a homogeneous transformation matrix, partitioning (3.13) can be considered.

$$T = \begin{bmatrix} R_{3x3} & p_{3x1} \\ f_{1x3} & 1 \end{bmatrix} \tag{3.13}$$

where: $\boldsymbol{R}_{3x3}$- is the rotation matrix; $\boldsymbol{p}_{3x1}$- translation matrix; $\boldsymbol{f}_{1x3}$- perspective transformation.

3.2.Forward kinematics (*FK*). To describe the translations and rotations between the arms, the Denavit-Hartenberg method is used. This consists of a matrix method of establishing a coordinate system for each arm of an articulated chain. The D-H representation leads to a 4x4 homogeneous transformation matrix, which represents the coordinate system of each arm in the joint, compared to the system of the previous arm. Thus, a point attached to the gripper can be expressed in the coordinates of the robot base. In the axis of its articulation, for each arm an orthonormal Cartesian coordinate system (x_i, y_i, z_i,) can be established, with i =1, 2,3, ., n (n- number of degrees of freedom) and, in addition the base coordinate system. Since a rotation joint has only one degree of freedom, each coordinate frame (x_i, y_i, z_i,) of the robot arm corresponds to joint ($\boldsymbol{i}$+1), and is attached to arm $\boldsymbol{i}$ [29,83,84,85]. Each coordinate system is established based on three rules: the z_{i-1} axis is along the movement axis of joint *i*; the xi axis is normal to the z_{i-1} axis; the y-axis completes the rectangular coordinate system. The D-H representation of a rigid arm depends on four geometric parameters that completely describe any rotational or prismatic joint: $\boldsymbol{\theta}_i$ – the angle of the joint from the x_i-axis to the x_{i-1} axis, measured around the z_i-axis 1; $\boldsymbol{d}_i$ – the distance from the origin of the *i*-1 coordinate frame to the intersection of the $\boldsymbol{z}_{i-1}$ axis with the x_i axis, measured along the z_{i-1} axis; $\boldsymbol{a}_i$ – the distance from the intersection of the $\boldsymbol{z}_{i-1}$ axis with the xi axis to the origin of the *i* system, measured along the $\boldsymbol{x}_i$ axis; $\boldsymbol{\alpha}_i$ – the angle made by the z_{i-1} axis with the z_i axis, by rotating around the x_i axis. The previously described parameters $\boldsymbol{\alpha}_i$, $\boldsymbol{d}_i$, $\boldsymbol{a}_i$ represent the rotational torque parameters and remain constant for a robot, and $\boldsymbol{\theta}_i$ represents the joint variable or the internal coordinate i. For a translational couple, $\boldsymbol{d}_i$ is the joint variable, and the rest of the parameters are constant. Once the D-H coordinate system is established, a homogeneous transformation matrix can be obtained that relates the *i* coordinate frame to the *i*-1 coordinate frame. A vector $\boldsymbol{r}_i$ expressed in the $\boldsymbol{i}$ coordinate system can be expressed as $\boldsymbol{r}_{i-1}$ in the *i*-1 coordinate system performing the following successive transformations: rotation around the $\boldsymbol{z}_{i-1}$ axis by an angle $\boldsymbol{\theta}_i$ to align the $\boldsymbol{x}_{i-1}$ axis with the $\boldsymbol{x}_i$ axis (the $\boldsymbol{x}_{i-1}$ axis is parallel to the $\boldsymbol{x}_i$ axis); translation along the $\boldsymbol{z}_{i-1}$ axis by a distance $\boldsymbol{d}_i$ to make the $\boldsymbol{x}_{i-1}$ and $\boldsymbol{x}_i$ axes coincide; translation along the $\boldsymbol{x}_i$ axis by a distance $\boldsymbol{a}_i$ to make the two origins coincide; rotation around the $\boldsymbol{x}_i$ axis by an angle $\boldsymbol{\alpha}_i$ to make the two coordinate systems coincide. Each of these four operations can be expressed by a basic homogeneous rotation/translation matrix, and the product of the four basic transformation matrices gives a composite homogeneous transformation matrix $\boldsymbol{A}^{\boldsymbol{i}}_{\boldsymbol{i-1}}$, called the D-H transformation matrix for adjacent coordinate systems. So:

$$\mathrm{A}^{i}_{i-1} = T_{z,\theta}T_{z,d}T_{z,a}T_{z,\alpha} = \begin{bmatrix} c\theta_i & -c\alpha_i s\theta_i & s\alpha_i s\theta_i & a_i c\theta_i \\ s\theta_i & c\alpha_i c\theta_i & -s\alpha_i c\theta_i & a_i s\theta_i \\ 0 & s\alpha_i & c\alpha_i & d_i \\ 0 & 0 & 0 & 1 \end{bmatrix} \tag{3.14}$$

where $c\boldsymbol{\theta}_i = \cos\boldsymbol{\theta}_i$, and the is $\boldsymbol{d}_i$, α_i, $\boldsymbol{a}_i$ are constants and $\boldsymbol{\theta}_i$ is the variable of the kinematic rotation. For a prismatic couple $\boldsymbol{A}^{\boldsymbol{i}}_{\boldsymbol{i-1}}$ becomes:

$$\mathrm{A}^{i}_{i-1} = \begin{bmatrix} 1 & 0 & 0 & 0 \\ 0 & c\alpha_i & -s\alpha_i & 0 \\ 0 & s\alpha_i & c\alpha_i & d_i \\ 0 & 0 & 0 & 1 \end{bmatrix} \tag{3.15}$$

3.3.Inverse kinematics. Given the position and orientation of the gripper of a T^6_0 robot it must we obtain the vector of angles in the joints $\boldsymbol{\theta} = (\boldsymbol{\theta}_1, ..., \boldsymbol{\theta}_6)^T$ so that the gripper is positioned

and oriented according to the application. The calculation of the angles in the applications is done geometrically, the matrix of the arm being given. The calculation is done in two stages: the position vector from the base to the wrist is calculated and the first three angles in the joints are obtained: θ_1, θ_2, θ_3; the last two (three) angles: θ_4, θ_5,(θ_6) are obtained using both the previously calculated values for θ_1, θ_2, θ_3 and the orientation submatrices T^i_0, where i = 4, 5, 6. In general, the inverse kinematics problem can be solved by different methods: the inverse transformation (calculation of the inverse matrix); dual matrices (introduced by Denavit in 1956); quaternian algebra and dual vectors; iterative; geometric approaches (of the type introduced by Lee and Zigler in 1984). It is advisable to find a closed-form arm solution for the manipulator. Fortunately, most commercial robots are characterized by one of the following sufficient conditions, which make a closed-form arm solution possible: a) three consecutive joint axes that intersect; b) three consecutive axes of joints parallel to each other. In order to solve the inverse kinematics problem of the robot, more attention is paid to the geometric approach. In these approaches, based on the local coordinate system, attached Sci segments and the geometry of the human arm, different configurations of a robot of this type can be identified, with the help of three configuration indicators (shoulder, elbow and wrist) - the first two being associated with the solution of the first three joints and the last indicator of joints 5 and 6. These three indicators of arm configurations are pre-specified to find the inverse solution, which is obtained in two steps: the position vector from the shoulder to the wrist is obtained. This vector is used to obtain the solutions $q_i = \upsilon_i$ of each of the first three joints i (i = 2,3,4), by analyzing the projections of the position vector on the planes (x_{i-1}, y_{i-1}) and the second, the angles of the last two joints are obtained using the angles calculated in step 1 for the first three joints, and projecting the segments also on the x_{i-1}, y_{i-1} planes. The dual relative velocity vectors of the couple i in relation to the system of i-1 coordinates, containing the relative linear velocity and the following form: [3,12,37,43,46,47,141,142,143, 144,178,179,180,181,182,183,184].

$$\dot{S}(i)=\begin{pmatrix}\omega^{i}_{i,i-1}\\ \cdots\cdots\cdots\\ v^{i}_{i,i-1}\end{pmatrix}\quad \dot{S}_1=\begin{pmatrix}\omega^{1}_{1,0}\\ v^{1}_{1,0}\end{pmatrix}=\begin{pmatrix}0\\0\\\dot{q}_1\\\cdots\cdots\\0\\0\\0\end{pmatrix}\quad \dot{S}_2=\begin{pmatrix}\omega^{2}_{2,1}\\ v^{2}_{2,1}\end{pmatrix}=\begin{pmatrix}\dot{q}_2\\0\\0\\\cdots\cdots\\0\\0\\0\end{pmatrix}$$

$$\dot{S}_3=\begin{pmatrix}\omega^{3}_{3,2}\\ v^{3}_{3,2}\end{pmatrix}=\begin{pmatrix}\dot{q}_3\\0\\0\\\cdots\cdots\\0\\0\\0\end{pmatrix}\qquad \dot{S}_4=\begin{pmatrix}\omega^{3}_{4,3}\\ v^{3}_{4,3}\end{pmatrix}=\begin{pmatrix}\dot{q}_4\\0\\0\\\cdots\cdots\\0\\0\\0\end{pmatrix} \tag{3.16}$$

where $\omega^{i}_{i-1,I}$ represents the relative angular velocity, and $v^{i}_{i,i-1}$ represents the relative linear velocity.

3.4.Matrix model of velocities, accelerations, forces and moments. The P-Q torsor method uses the Newton-Euler equations. The disadvantage of isolating bodies with the additional introduction of connection forces was eliminated by introducing incidence and transfer matrices [81,82,83,84,85]. The method presents the advantage of using matrix-vector equations with the possibility of easy implementation the mathematical model on the computer. The graph associated with an articulated structure represents the block scheme of links with a well-defined meaning, which characterizes a certain manipulation structure. Within a graph, bodies are represented by circles and

couples by chains. The generation direction of the graphs is established by convention - from the element to the slide and from the element to the rotation coupler.

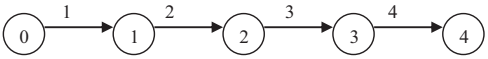

Fig.3.2. The graph associated with the Arm type robot structure

Incidence and transfer matrices eliminate the inconvenience of methods that use the mathematical model Newton-Euler, namely ensures the introduction of the sign with which the forces and moments from the links would have been written on the incident bodies. Body-couple incidence matrices will be denoted by (***G***) and couple-body matrices by (***Z***). Determining the bodies-couples type of incidence matrix requires first to determine on a tabular basis the links between the various bodies in compliance with the convention made, for the generation of the graph associated with the handling structure. The table below was determined based on the graph associated with the structure. The table associated with the structure will be of the following form:

Bodies\Joints	**1**	**2**	**3**	**4**
Corpul i_{k-}	0	1	2	3
Corpul i_{k+}	1	2	3	4

Body ***0*** represents the frame of the handling structure or the body considered fixed. The elements $G_{i,k}$ of the bodies-couples incidence matrix include the elements: -1 if side ***k*** leaves node ***i***; +1 if side ***k*** enters from node ***i***; 0 if side ***k*** is not connected to node ***i***; (in the graph, the side represents the couples, and the nodes represent the bodies).

$$[\Gamma]=\begin{bmatrix}[G_1] & [G_1^{\otimes}]\\ [G] & [G^{\otimes}]\end{bmatrix} \tag{3.17}$$

where: G_1 - is the matrix partition corresponding to the bat and includes one line and n columns, where n represents the number of moving bodies of the manipulation structure; G^*_1- is the matrix partition corresponding to the bat and includes the couples that form the closed or open accounts of the structure - the matrix partition includes a line and ***n -k =c*** columns, where ***k*** is the total number of couples, and *c* is the number of couples sectioned in order to obtain the graph tree; ***G*** - is the matrix partition that includes ***n*** lines and ***n*** columns corresponding to the movable bodies of the structure manipulation; G^* - is the matrix partition that includes ***n*** lines and ***c*** columns corresponding to the ***n*** mobile bodies and sectional couplings. The determination of the elements of the couple-body incidence matrix is carried out by traversing the graph associated with the analyzed structure, from the body to the base. We assume the existence of an articulated system with n moving bodies and ***k*** couplings, where ***k >n***, so with ***c*** cycles. In order to obtain the graph tree associated with the manipulation structure, we will proceed to the sectioning of ***c*** couples. We denote the intersected couples by ***k****. The body ***i*** is connected to the rest of the articulated structure by means of the couplings, k_1, k_2, k_1*, according to the portion of the graph in fig.3.3.

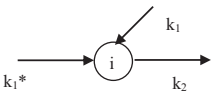

Fig.3.3. Part of the graph associated with the structure

where: $\boldsymbol{k}_1$ - is the side entering the node; $\boldsymbol{k}_2$ - is the side coming out of the node; $\boldsymbol{k}_1$* - is the side sectioned in the goal of obtaining the graph tree. In fig. 3.4, which represents the forces and reactions acting on body $\boldsymbol{i}$, were made the following notations: $\boldsymbol{r}_{gi}$ - the position vector of the center of gravity of body $\boldsymbol{i}$; $\boldsymbol{g}_i$ - position of the center of gravity of body $\boldsymbol{i}$; $\boldsymbol{N}_{k1}$ - the reaction in the $\boldsymbol{k}_1$ couple; $\boldsymbol{M}_{k1}$ - moment in $\boldsymbol{k}_1$ coupling; $\boldsymbol{N}_{k2}$ - the negative reaction from the $\boldsymbol{k}_2$ couple (according to the meaning in the graph); $\boldsymbol{M}_{k2}$ - the negative moment in the $\boldsymbol{k}_2$ coupling; $\boldsymbol{N}_{k1}$* - the reaction from the sectioned couple $\boldsymbol{k}_1$*; $\boldsymbol{M}_{k1}$* - the moment in the sectional coupling $\boldsymbol{k}_1$*; $\boldsymbol{b}_{k1}$ - the vector of the reaction arm in the $\boldsymbol{k}_1$ coupling; $\boldsymbol{b}_{k2}$ - the vector of the reaction arm in the $\boldsymbol{k}_2$ coupling; $\boldsymbol{b}_{k1}$* - the vector of the reaction arm from the $\boldsymbol{k}_1$* coupling; $\mathfrak{F}$ - vector of resisting forces in the center of gravity of body $\boldsymbol{i}$; $\mathfrak{R}$ - the vector of resisting moments applied in the center of gravity of the body $\boldsymbol{i}$. Approaching the mathematical model of dynamic behavior involves approaching the kinematic analysis of position, speed and acceleration, as well as the matrix-vector determination of the force arms, as well as the tensors of inertia and kinetic moments. The method uses the Newton-Euler formalism, but without isolating the component bodies of the structure, so without the express introduction of the connecting forces.

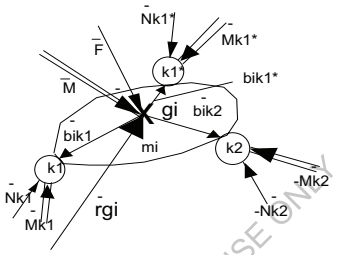

Fig.3.4. The arrangement of forces on a hypothetical body of the structure

The proper software platform ROBO-PVAFM was designed in LabVIEW software by using the following general matrix model that contents velocities, accelerations, forces and moments.
For the analyze of the robot's positions was used the following matrix 3x3 equation:

$$r_i^0 = r_1^0 + D_1^0 r_2^1 + D_2^0 r_3^2 + \cdots + D_{i-1}^0 r_i^{i-1} \tag{3.18}$$

$$D_1^0 = \begin{bmatrix} c1 & -s1 & 0 \\ s1 & c1 & 0 \\ 0 & 0 & 1 \end{bmatrix}, c1 = \cos(\varphi_{01} + \rho_1)$$

where: $\boldsymbol{r}_1^0$is the absolute position vector of the $\boldsymbol{i}$ joint; $\boldsymbol{r}_i^{i-1}$is the relative position vector from the $\boldsymbol{i}$ joint to $\boldsymbol{i}$-1 joint; $\boldsymbol{D}_{i-1}^0$ is the transfer matrix from the Cartesian system $\boldsymbol{i}$-1 to Cartesian base system; $\boldsymbol{\varphi}_{ij}$- angular at home position between $\boldsymbol{i}$ and $\boldsymbol{j}$ systems. For the analyze of the velocities was used 6x6 matrix equation by using the dual vectors that content the angular and linear velocities:

$$\begin{pmatrix} \omega_{i,0}^i \\ v_{i,0}^i \end{pmatrix} = T_{i-1}^i T_{i-2}^{i-1} \ldots . T_1^2 \begin{pmatrix} \omega_{1,0}^1 \\ v_{1,0}^1 \end{pmatrix} + T_{i-1}^i T_{i-2}^{i-1} \ldots . T_2^3 \begin{pmatrix} \omega_{2,1}^2 \\ v_{2,1}^2 \end{pmatrix} + \cdots + \begin{pmatrix} \omega_{i,i-1}^i \\ v_{i,i-1}^i \end{pmatrix} \tag{3.19}$$

$$\begin{pmatrix} \omega_{i,0}^0 \\ v_{i,0}^0 \end{pmatrix} = \begin{bmatrix} D_i^0 & 0 \\ 0 & D_i^0 \end{bmatrix} \begin{pmatrix} \omega_{i,0}^i \\ v_{i,0}^i \end{pmatrix}$$

$$T_{i-1}^i = \begin{bmatrix} D_{i-1}^i & 0 \\ -D_{i-1}^i r_i^{i-1} & D_{i-1}^i \end{bmatrix}$$

$$D_i^0 = D_1^0 D_2^1 \dots D_{i-1}^{i-2} D_i^{i-1}$$

where: $\begin{pmatrix} \omega_{i,0}^i \\ v_{i,0}^i \end{pmatrix}$ – dual absolute angular and linear velocity vector of the ***i*** joint versus ***i*** Cartesian system; $\begin{pmatrix} \omega_{i,0}^0 \\ v_{i,0}^0 \end{pmatrix}$- dual absolute velocity angular and linear vector of the *i* joint versus Cartesian base system; $\boldsymbol{T}_{i\text{-}1}{}^{i}$- matrix transfer 6x6 from ***i***-1 to ***i*** Cartesian system; $\begin{pmatrix} \omega_{i,i-1}^i \\ v_{i,i-1}^i \end{pmatrix}$- dual relative angular and linear velocity vector between ***i*** and ***i***-1 joints versus ***i*** Cartesian system.

For the analyze of accelerations was used the 6x6 matrix equation:

$$\begin{pmatrix} \varepsilon_{i,0}^i \\ a_{i,0}^i \end{pmatrix} = T_{i-1}^i T_{i-2}^{i-1} \dots . T_1^2 \left(\ddot{S}(1)\right) + T_{i-1}^i T_{i-2}^{i-1} \dots . T_2^3 \left(S\ddot{(}2)\right) + \cdots + \left(\ddot{S}(i)\right) \tag{3.20}$$

$$\begin{pmatrix} \varepsilon_{i,0}^0 \\ a_{i,0}^0 \end{pmatrix} = \begin{bmatrix} D_i^0 & 0 \\ 0 & D_i^0 \end{bmatrix} \begin{pmatrix} \varepsilon_{i,0}^i \\ a_{i,0}^i \end{pmatrix}$$

$$\left(S\ddot{(}i)\right) = \begin{pmatrix} (\varepsilon_{i,i-1}^i) + \widehat{[\omega}_{i-1,0}^i](\omega_{i,i-1}^i) \\ (a_{i,i-1}^i) + \widehat{[\omega}_{i-1,0}^i]^2 \left(r_i^{i-1}\right) + 2\widehat{[\omega}_{i-1,0}^i](v_{i,i-1}^i) \end{pmatrix}$$

where: $\begin{pmatrix} \varepsilon_{i,0}^i \\ a_{i,0}^i \end{pmatrix}$-dual absolute angular and linear acceleration vector of the ***i*** joint versus the ***i*** Cartesian system; $\begin{pmatrix} \varepsilon_{i,0}^0 \\ a_{i,0}^0 \end{pmatrix}$- dual absolute angular and linear acceleration vector of the ***i*** joint versus Cartesian base system; $(\varepsilon_{i,i-1}^i)$ -angular relative acceleration between ***i*** and ***i***-1 joints; $(a_{i,i-1}^i)$- linear relative acceleration between ***i*** and ***i***-1 joints; $\widehat{[\omega}_{i-1,0}^i]$- angular absolute velocity antisymmetric vector of the ***i***-1 joint vs. ***i*** Cartesian system; $\widehat{[\omega}_{i-1,0}^i]^2 \left(r_i^{i-1}\right)$- centrifuge- centripetal acceleration; $2\widehat{[\omega}_{i-1,0}^i](v_{i,i-1}^i)$- Coriolis acceleration; $\left(S\ddot{(}i)\right)$- dual relative acceleration matrix.

For the forces analyze was used the matrix equation:

$$(P) = [z_u]\{(F^0) - [m_u](a_{gi,0}^0)\} \tag{3.21}$$

$$[z_u] = \begin{bmatrix} \begin{bmatrix} 1 & 0 & 0 \\ 0 & 1 & 0 \\ 0 & 0 & 1 \end{bmatrix} G_{11} & \dots & \begin{bmatrix} 1 & 0 & 0 \\ 0 & 1 & 0 \\ 0 & 0 & 1 \end{bmatrix} G_{1i} \\ \vdots & \ddots & \vdots \\ \begin{bmatrix} 1 & 0 & 0 \\ 0 & 1 & 0 \\ 0 & 0 & 1 \end{bmatrix} G_{i1} & \dots & \begin{bmatrix} 1 & 0 & 0 \\ 0 & 1 & 0 \\ 0 & 0 & 1 \end{bmatrix} G_{ii} \end{bmatrix}$$

$$[m_u] = \begin{bmatrix} \begin{bmatrix} 1 & 0 & 0 \\ 0 & 1 & 0 \\ 0 & 0 & 1 \end{bmatrix} m_1 & \dots & [0] \\ \vdots & \ddots & \vdots \\ [0] & \dots & \begin{bmatrix} 1 & 0 & 0 \\ 0 & 1 & 0 \\ 0 & 0 & 1 \end{bmatrix} m_i \end{bmatrix}$$

$$(F^0) = \begin{pmatrix} [D_1^0](F_1^1) \\ \vdots \\ [D_i^0](F_i^i) \end{pmatrix}$$

$$\left(a_{gi,0}^0\right) = \begin{pmatrix} [D_1^0](a_{g1,1}^1) \\ \vdots \\ [D_i^0](a_{gi,1}^i) \end{pmatrix}$$

where: ($\boldsymbol{P}^0$)- is the matrix of active force, reduced to the base Cartesian system; [z_u]- unitary joints-bodies matrix; ($\boldsymbol{F}^0$)- matrix of resistive forces reduced to the base; ($\boldsymbol{F}_i^i$)- matrix of resistive forces reduced to $\boldsymbol{i}$ Cartesian system; [$\boldsymbol{m}_u$]- unitary matrix of mass obtained by multiplying $\boldsymbol{m}_i$ by unitary matrix for the space; ($\boldsymbol{a}^0_{gi,0}$)- absolute linear acceleration matrix for the centre of gravity $\boldsymbol{g}_i$ reduced to the base Cartesian system; $\boldsymbol{G}_{i,j}$- is current value from the incidence body- joints matrix $\boldsymbol{G}$ obtained by using the associated graph to the robot's structure.
For the moments analyze was used the equation:

$$(Q) = [z_u]\{(M^0) - \left(\dot{K}_{gi,0}^0\right) + [\widehat{B}][(P^0)\} \tag{3.22}$$

$$(M^0) = \begin{pmatrix} [D_1^0](M_1^1) \\ \vdots \\ [D_i^0](M_i^i) \end{pmatrix}$$

$$\left[\hat{B}\right] = \begin{bmatrix} [\hat{b}_{11}^0]G_{11} & \dots & [\hat{b}_{1i}^0]G_{1i} \\ \vdots & \ddots & \vdots \\ [\hat{b}_{i1}^0]G_{i1} & \dots & [\hat{b}_{ii}^0]G_{ii} \end{bmatrix}$$

$$\left[\hat{b}_{11}^0\right] = \begin{bmatrix} 0 & -b_{11z}^0 & b_{11y}^0 \\ b_{11z}^0 & 0 & -b_{11x}^0 \\ -b_{11y}^0 & b_{11x}^0 & 0 \end{bmatrix}$$

$$\left(b_{i,k}^0\right) = (r_k^0) - \left(r_{gi}^0\right)$$

$$\left(\dot{K}_{gi}^0\right) = \begin{pmatrix} [D_1^0]\left(\dot{K}_{g1,0}^1\right) \\ \vdots \\ [D_i^0]\left(\dot{K}_{gi,0}^i\right) \end{pmatrix}$$

$$\left(\dot{K}_{gi,0}^i\right) = [J_{gi}^i](\varepsilon_{i,i-1}^i) + \widehat{[\omega}_{i-1,0}^i][J_{gi}^i](\omega_{i,i-1}^i)$$

$$[J_{gi}^i] = \begin{bmatrix} \frac{m(B^2+C^2)}{3} + m(b^2+c^2) + m(Bb+Cc) & -\left(\frac{mAB}{4} + \frac{mAb}{2} + \frac{mBc}{2} + mab\right) & -\left(\frac{mAC}{4} + \frac{mAc}{2} + \frac{mCc}{2} + mac\right) \\ -\left(\frac{mAB}{4} + \frac{mAb}{2} + \frac{mBc}{2} + mab\right) & \frac{m(A^2+C^2)}{3} + m(c^2+a^2) + m(Cc+Aa) & -\left(\frac{mBC}{4} + \frac{mBc}{2} + \frac{mCb}{2} + mbc\right) \\ -\left(\frac{mAC}{4} + \frac{mAc}{2} + \frac{mCc}{2} + mac\right) & -\left(\frac{mBC}{4} + \frac{mBc}{2} + \frac{mCb}{2} + mbc\right) & \frac{m(B^2+A^2)}{3} + m(a^2+b^2) + m(Aa+Bb) \end{bmatrix}$$

where: ($\boldsymbol{Q}$)- matrix of the active moments in a joints; ($\boldsymbol{M}^0$)- matrix of the resistant moments in all joints; - [$\widehat{\boldsymbol{B}}$]anti-symmetric matrix of force's arm; ($\boldsymbol{P}^0$)- matrix for active forces; $(K_{gi}^{\prime 0})$ - matrix of the variation of the kinetic moment reduced to the base Cartesian system; $\left(\dot{\boldsymbol{K}}_{gi}^0\right)$- matrix of the variation of the kinetic moment of the g_i centre of gravity reduced to base Cartesian system ($\dot{\boldsymbol{K}}_{gi}^i$))- matrix of the variation of the kinetic moment of the g_i centre of gravity reduced to $\boldsymbol{i}$ Cartesian system; $\left(\boldsymbol{b}_{i,k}^0\right)$- absolute matrix vector force's arm from $\boldsymbol{g}_i$ center of gravity to the $\boldsymbol{k}$ joint; [$\boldsymbol{J}_{gi}^i$]- inertial tensor of the $\boldsymbol{i}$ body.

CHAPTER 4
State of Art of Theoretical and Experimental Research

4.1.Analysis of the use of magnetorheological dampers in the RI technique. Following the analysis of the current stage of the use of magnetorheological devices, it was found that the rheological technique is very little applied for the purpose of reducing vibrations in robotic production processes, and not at all in the construction of robots and peri-robotic components. This determined the approach of such a theme within the work, a topic that is strictly topical considering that robot structures work in environments with very wide frequency spectra, alongside different machine tools, which generate disruptive forces that are difficult to control, and which, finally, it determines inaccuracies of the movement of the end-effector RI. From the articles studied, it emerged that the technique of applying rheological damping in mechanical applications is strictly up-to-date, the magnetorheological devices ensuring, relatively easily, the interface between the mechanical system to be optimized and the electronic control. This has determined that many manufacturing companies of precision mechanical components also address these aspects, making damping components of this type, both for rotational movement and for translational movement. In addition, numerous companies and research in the field have revealed the fact that by applying optimal or newer, intelligent control laws, they succeeded in compensating or moving unfavorable frequencies in the attenuation field, thus obtaining a vibration-free behavior. The research carried out has not sufficiently used the advantages offered by these intelligent types of vibration behavior optimization methods, attenuation methods that ensure a wider range of attenuation, and adaptive vibration control. The field of dynamic behavior was also insufficiently developed, as well as its coverage with control and optimization methods and parameters. In this paper, these problems were also addressed, developing the field of global dynamic behavior, with new parameters among which we can mention: the global dynamic compliance ***GDC***, the global dynamic coefficient of viscous damping ***VGDDC***, the equivalent global dynamic coefficient of viscous damping ***VGDDEC***, local dynamic viscous damping coefficient ***VLDDC***, etc. These dynamic parameters are the most suggestive when analyzing the global and local dynamic behavior, ensuring the obtaining of information either for the entire structure of the robot or for each individual module, thus being able to determine the component with the most unfavorable vibration behavior. Since these parameters are dynamic parameters, they are not constant, specifying the various influences on the behavior of environmental factors, disruptive forces, acceleration regimes, loads and movement configuration, information strictly necessary for the implementation of intelligent damping. With the help of these parameters, it will be easier to follow the way in which the magnetorheological dampers determine the change in the dynamic performances and implicitly the frequency spectrum. The current researchers analyzed in the work revealed the fact that Fourier analysis was not used to determine the frequency spectrum and its optimization, most of the researches being limited to the analysis of the index characteristics and less of the frequency ones. For this reason, the paper addressed the design and development of a proprietary Fourier analyzer, with the help of LabVIEW virtual instrumentation. In order to determine the parts of the motion program, more vulnerable or with a frequency spectrum that overlaps, in the low harmonics, the mechanical working frequencies of the serviced machine, the assisted tracing of the Fourier spectrum for the robotic structure in motion was approached. Also, for the analysis of how the structure is balanced, the Fourier analysis was approached with and without the magnetorheological damper, in both directions of motion, in order to determine the influences on the spectrum of the direction of motion, of possible pauses in the progress of a movement, as well as for determining its online optimization.

4.2. Critical analysis of the mathematical models addressed. The mathematical models approached were both parametric and non-parametric models, very general, all researchers starting from the premise of the closeness of the model to real behavior. In the addressed bibliographic research, the comparison between the theoretical models and the real behavior was carried out by the assisted tracing of some characteristics and their comparison with the experimentally acquired ones

(Bingham, Carlson, Bouc-Wen, Powell, [6, 17, 20, 21, 22, 30 , 51, 80]). Thus: the Bingham model simulates a relatively simplified ***MR*** damper; the Bouc-Wen model is more extensive, including the hysteresis curve; the model is more complex and requires a closed-loop control algorithm (Dyke et al., 1998 [35, 36], Yang et al., 2002 [77], Liao and Lai, 2002 [99]); the Li model (2000 [99]) is a model in which the ***MR*** material operates in two rheological domains: pre-flow and post-flow, but a model that uses constant coefficients of viscous damping, generalized forces with linear evolution, inconsistent with the experimental research carried out in the work; the Oh and Onoda (2002) model was designed and made to demonstrate the displacement of vibrations in structures; this is an equivalent model based on springs, viscous friction and dry friction, a model that does not highlight hysteresis; the Choi model (2001 [30, 31]) proposes a polynomial model of degree 6, which also does not highlight the hysteresis; the extended Bingham model was made by Gamota and Filisko [44] and represents an extension of the Bingham model that describes the behavior of the ER in the pre-flow and post-flow state; the model highlights the presence of hysteresis, but it is not accurate enough compared to the real behavior, because it uses constant coefficients, which precisely control the areas of the damping force-travel speed characteristic and presents the biggest errors compared to the real ones; the model is even more complicated to approach through numerical simulation; the model with three Powell elements [150, 151], does not sufficiently highlight the hysteresis, it being numerically controlled only by the static and dynamic coefficients introduced; the BingMax model is a BingMax discrete element model presented by Makris et al.[109,110], a model that is complicated to transpose into a numerical simulation model; the non-linear visco-elastic-plastic model presented by Kamath and Wereley [87, 88] combines two linear flow mechanisms with non-linear functions, both models are excessively theorized without being close to the real functioning, as found by comparing the characteristics; the Bi-viscous model (Stanway et al. [185, 186]) linearized model by introducing the two slopes for the elastic function and the viscous function, but does not highlight the hysteresis; non-parametric models are based on their performance; these, usually, require the acquisition of experimental data regarding behavior in different tasks, under different conditions (Jung et al. 2004); the models proposed in this category are based on Chebychev polynomials (Ehrgott and Masri 1992, Gavin et al. 1996b [49, 50, 51]), on neural networks (Chang and Roschke 1998, Zhang and Roschke 1998, Wang and Liao 2001), on neuro-fuzzy systems (Schurter and Roschke 2000) or on the identification technique (Jin et al. 2001, Jin et al. 2002), as an example: Ehrgott and Masri (1992) use Chebyshev polynomials for ***AMR*** modeling; these models are unusable in the numerical simulation technique; neural network models reproduce the nonlinear behavior of ***AMR*** much more precisely; these systems emulate the properties of the nervous system and are composed of neurons and synapses; connections can be adjusted by learning the algorithm to more accurately reproduce the behavior of the system (Pacific Northwest National Laboratory and Batelle Memorial Institute 1997); Schurter and Roschke (2000) neuro-fuzzy models are other models that emulate the dynamic behavior of AMR; in these new models, neural networks are used to adjust the fuzzy logic parameters; fuzzy logic incorporates knowledge about the system into a controller, using various functions that use vague concepts such as: free, strong, weak, moderate, etc.; the desired output size is determined based on the input fuzzy information, like the decision of the human brain; learning and data validation were generated using the phenomenological model proposed by Spencer Jr. et al. (1997 [179, 180]). From the research of the current stage it results that there were no complex modeling approaches accompanied by numerical simulations, which highlight as clear as possible the differences between the real and the theoretical model and to allow an easier approach to compensate for any inadvertences. Equipped with these aspects, the paper addressed numerical simulation, accompanied by data acquisition, with the help of LabVIEW virtual instrumentation, as well as model research, simultaneously with experimental research, and the introduction of curve parametrization. Many of the models approached by various researchers do not take the phenomenon of hysteresis present in the real behavior (Bingham, [6]) or are far from the real model (Parker, Powell [152]), as are the values and the allure of the characteristics. Due to this fact, the own approach sought that the mathematical model could be compared with the real one, by comparing the specific characteristics, followed by its completion. It was found that the closest model to the real one is the modified Bouc-

Wen model. It was taken over in our own research and completed with new equations, with several parameters with the help of which, following the simulation and validation of the model, to create a mathematical model as real as possible, with the help of which, later, to approach the research on the model , research much cheaper and with immediate results. Through research on the model, it was possible to establish the 19 new parameters introduced, in such a way that, by adjusting these parameters, the agreement between the model and the experimental damper is achieved, with the minimization of the errors between them. From the comparative analysis of the approached mathematical model and the modified Bouc-Wen model, it was found that there are differences in the hysteresis area, in the beginning and end areas of the action of the damping force, as well as on the slopes both in compression and in expansion, reason for which the mathematical model approached was completed with new equations and coefficients, which control these parts of the characteristic, as well as the introduction of the parameterization of the characteristic in such a way that through theoretical research through numerical simulation it is determined how the coefficients of the mathematical model influence the parameters of the parameterized curve damping force- travel speed. In addition, it was found that the hysteresis curve is not identical for each frequency in the spectrum, it moves its peaks depending on the frequency, which is why the proposed model also took over these inadvertences by introducing a frequency-dependent hysteresis coefficient, coefficient expressed by a periodic function as the sum of sinusoids. In order to personalize the mathematical model and identify all its coefficients, the numerical simulation and analysis of the influence of all the coefficients of the model on the damper characteristic parameters were approached. Thus, it was possible to draw conclusions regarding the way in which the various coefficients of the mathematical model influence the dynamic behavior, and therefore implicitly, the parameters of the damping force-travel speed characteristic, making their identification relatively easy and obviously validating the mathematical model with an error below 1%.

4.3. Analysis of how to optimize industrial robots. Optimizing the dynamic behavior of the RI involves several directions of action, among which the following can be mentioned: shape optimization taking into account the dynamic response of the RI structure both through theoretical research and through research assisted with data acquisition; optimization of the servo drive with the convenient choice of the components necessary to obtain a response in accordance with the performance criteria imposed, as well as with the respective application; optimization of controllers and programming languages; optimization through analysis and assisted synthesis, with the convenient choice of mechatronic components; optimization of dynamic and vibratory behavior through the convenient choice of mechatronic components, working regimes (speed characteristics, simultaneous or successive movements, etc.), or through the introduction of intelligent or non-intelligent compensating elements, which ensure active or passive control of stiffness, global dynamic compliance, global depreciation coefficient, etc. From the analysis of the way in which the various researches in the field presented the optimization of the dynamic behavior of the robotic structures, the following results emerged: (i) ***AMR***s were not implemented in the robotic structures, although these shock absorbers ensure vibration control in a very wide frequency range, known to be the fact that the attenuation of vibrations obviously increases the precision and accuracy of movement on the trajectory, this being a permanent desire of the builders and users of industrial robots; (ii) there was no clear and precise methodology regarding the way of research and implementation, with the establishment the opportunities and the place of application of the damper, not having researched the global and local dynamic behavior, and not having introduced the new qualitative assessment parameters of the dynamic behavior, according to those proposed by this book; (iii) there was no virtual instrumentation with the help of which to determine the value of the parameters according to the theoretical model with the real one, the comparison being made only through experimental research and on the model, much more expensive and without the possibility of introducing, relatively easily, the possible model corrections.

4.4. Analysis of how the theoretical research is validated by the experimental one. The experimental research addressed in this work revealed the fact that most of the mathematical models addressed are highly theorized, and the differences compared to the real behavior is more than 15% (Carlson, Parker, Powell, Choi, Bingham, etc. models), which is why it was approached the model that resulted in the smallest error, of about 5% between the real and the simulated behavior, this being the modified Bouc-Wen model. From the comparative analysis of the characteristics determined experimentally with those obtained by numerical simulation, it was found that there are large differences at the ends of the characteristic and the slope of the characteristic depending on the frequency, which is why new equations were introduced depending on the intensity of the current absorbed by the damper coils, for all coefficients of the mathematical model, equations of the third degree. It was tried to introduce equations of the fourth degree, but the introduced effect was quite similar to those of the third degree. Thus, it was possible to approach the damping force-travel speed characteristics exactly at the limit points of the characteristic, as well as at the inflection points. After completing the mathematical model and parametrizing the curves, we moved on to the stage of identifying the coefficients. This stage aimed at reducing the modeling error, ensuring a cumulative error of at most 1%, as can be seen from the comparison of the real characteristics with the simulated ones. This stage consisted in the analysis of the way in which each coefficient of the mathematical model influences the parameters of the damping force-travel speed characteristic and the choice of these coefficients in such a way that the simulated characteristics come as close as possible to the real ones. In the analysis of the research of the current stage, it was found that there was no clear methodology regarding the approach to the theoretical and experimental research of such complex models, nor did the approached models allow a broader approach, with multiple possibilities of adjustment, which is why the proposed model and validated within the thesis included the modified Bouc-Wen model, completed with four more equations of the third degree and a periodic relation for the hysteresis coefficient. After identifying the coefficients and validating the model, the error obtained was below 1%.

4.5. Directions and research addressed in the work. Among the priority directions that were addressed within the work, and that resulted, as a result of the bibliographic research carried out, are:

• the approach of simultaneous model and experimental research, in order to identify the coefficients and validate the mathematical model;

• completion of the modified Bouc-Wen type mathematical model, which after comparison with the own experimental results proved to be the closest to reality, with new equations, with more parameters, such as the model adjustment operation, in order to put agree with the real model, to be as simple as possible and with as few errors as possible;

• the introduction of new parameters in the technique of optimizing the dynamic behavior of the RI and researching the influence of these parameters, depending on the modification of the parameters of the magnetorheological damper. Among these new parameters can be mentioned: global dynamic coefficient of viscous damping ***VGDDC***, equivalent global dynamic coefficient of viscous damping ***VGDDEC***, local dynamic coefficient of viscous damping ***VLDDC***, global dynamic factor of viscous damping, local and global dynamic compliance;

• the research approach related to the comparison between these parameters, in the operation of the RI, with or without magnetorheological damping, with movement in both directions, in order highlighting the degree of imbalance of the robot's arms, as well as determining the global and local behavior with highlighting the place of implementation of the magnetorheological dampers;

• performing some experimental determinations regarding the damping force, depending on the intensity of the magnetic field, in off-line and on-line mode, as well as the experimental determination of the additional damping factor and its variation depending on the frequency and the intensity of the current supplying the coils shock absorber;

• online research of the total dynamic coefficient of viscous damping ***VGDDTC***, and of the mode of action on the transfer of frequencies within the Fourier spectrum;

• determination of the Fourier spectrum for movement in both directions in order to determine the degree of imbalance;

• comparative determination of the Fourier spectrum in the excitation variants of the base of the robot structure with magnetorheological damper, with air damper and without damper, in order to highlight the comparative effect of ***AMR*** on the Fourier spectrum;

• theoretical research of vibrations through the design and theoretical research of numerical simulation results of various complex types of periodic vibrations;

• creating a virtual instrument for generating acceleration signals with at least 10 own frequencies within the Fourier spectrum, in order to approximate the acceleration signals acquired by accelerometers as realistically as possible;

• the research of vibration controllers, highlighting the various passive, semi-active, active, adaptive and intelligent types;

• researching the kinematic and dynamic behavior with highlighting the specific characteristics and modeling them with our own LabVIEW instrumentation;

• determination of own matrix-vector relations, for the analysis and assisted synthesis of robotic structures, in order to ensure the absorption of the effect of damping forces when intelligent dampers are introduced into the ***RI*** structure;

• theoretical case study for the linear magneto-rheological damper addressed in the research and highlighting the influence of the loss gradient between the chambers and the $\boldsymbol{PD}_2$ type control law, on the dynamic behavior;

• assisted experimental research of global dynamic compliance;

• experimental determination of the global depreciation factor through research with data acquisition and application of the radical method from 2;

• experimental determination of the damping energy;

• theoretical research with the help of LabVIEW virtual instrumentation and elementary transfer functions of shock absorbers and complex mechanical systems of shock absorbers and springs;

• designing LabVIEW virtual tools for generating complex automation block schemes with multiple reactions, various corrections, regulators and control laws;

• the approach of an own mathematical model for the researched linear magneto-rheological damper and the design of LabVIEW virtual instrumentation for theoretical and experimental research with data acquisition;

• parametrization of the characteristics of damping force – vs. velocity, for the purpose of theoretical research on the model and validation of the model;

• identifying the coefficients of the model and adjusting the equations in order to obtain a modeling error of maximum 1%;

• designing, making and using an intelligent magneto-rheological damping structure;

• the approach of own methods for optimizing the local and global dynamic behavior for industrial robots.

CHAPTER 5
Research and Theoretical Contributions in the Technique of Applying Intelligent Absorbers to Industrial Robots

5.1. Assisted theoretical research of vibrations. Uncontrolled vibrations, oscillations, contortions, bending, etc. are major problems of assemblies in large space structures, space robotics or other space systems (antennas, telescopes, etc.). Spatial structures are usually of low weight and high flexibility. The lack of rigidity, the low weight, and the absence of aerodynamic resistance make it difficult to dampen vibrations, oscillations, bending, twisting, etc., once caused. These vibrations, oscillations and other such elastic deformations are generated by the work equipment, by the operation with such structures (positioning guidance systems, micro-asteroids, micro-vibrations due to thermal cycles of the structure, etc.). Next, an ***AVC*** (advance vibration control) application is presented for an articulated arm robot structure, which uses an active system with electro or magnetorheological dampers to control and reduce vibrations. The numerical modeling and simulation was carried out taking into account the technical characteristics and the existing model in the laboratory. The numerical simulation was carried out with the help of a proprietary LabVIEW virtual tool. Fig. 5.1 shows the index characteristics determined based on the block diagram in fig. 5.2. The presented characteristics (fig. 5.1) are determined by the $\boldsymbol{PT}_1$ type controller and by the $\boldsymbol{PT}_2$ mobile element, in the variant of an unstable operation due to the too high amplification factor on the reaction path. By introducing electro or magnetorheological damping, through an internal feedback loop (fig. 5.2), it is observed that the operation passes into the stable range (fig. 5.1).

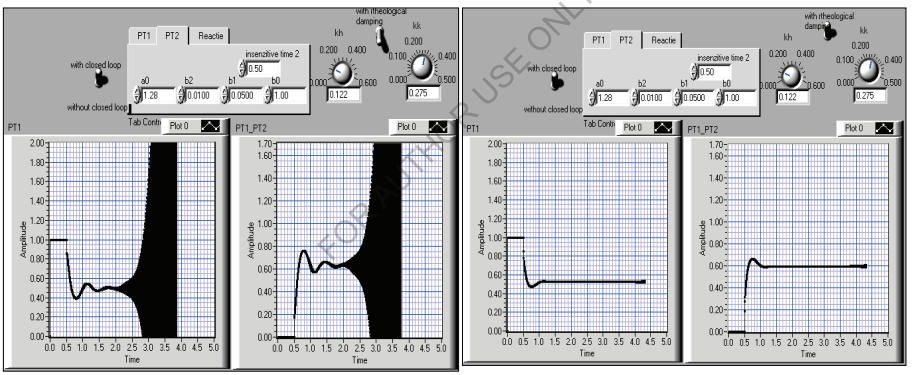

Fig. 5.1. Mechanical vibrations of the rotation module: **a**- unstable operation due to the high amplification factor on the reaction path; **b**- stable operation after the introduction of magneto-rheological damping.

The degree of bending depends on a number of factors such as: the dimensions of the structure, the physical properties (Young's modulus, stiffness, flow coefficient of the material, etc.), the distribution of actuators, and the type of applied load. Actuators can also be mounted on or inside the structure for multi-layer composite structures. Deformation sensors or movements are used to detect surface deformations, and the measured quantity is used by the control system to command different actuators to achieve the desired shape control effect. Deformable mirrors are used in many applications, such as laser beam steering, generation of various excitation frequencies, distortion curve correction for thermal distortions, and due to their own weight in large, high-precision systems, to correct for thermal and atmospheric distortions in telescopes high power, etc.

Today, there is a high interest in the use of adaptive structure technologies in the aerospace and defense sectors, for the adaptive control of the shape of airplane wings, helicopter rotors and propellers, thrusters, missile stabilizers, etc. Through the adaptive control of the shape of airplanes, the aim is to reduce aerodynamic resistance and improve fuel consumption and speed. Adaptive shape control has also been studied for rocket stabilizers. Composite structures are intensively studied for their use in the construction of airplanes in the future. The use of composite structures offers the advantage of the possibility of mounting actuators and sensors both inside and on their surface. However, many studies have been done regarding the manufacture of systems for testing, systems that have built-in sensors and actuators. Adaptive covers for airplanes are also intensively studied for the possibility of implementing some antennas in them. Once the sensor and actuator are embedded in such a shell, adaptive shape control and correction will also be necessary factors for performance adjustment. It should be noted that the need for shape control in large spatial structures is a consequence of the lack of rigidity of the structure, due to the reduced weight, flexibility and design used in these structures. Apart from those mentioned above, the almost zero weight, the lack of aerodynamic resistance, and the exposure of the structures to thermal cycles make it necessary to use some adaptive structures. However, achieving the desired shape and precision of the structure makes the necessary operations difficult. In these conditions, adaptive shape control is a solution for maintaining performance and consequently considerable research is being carried out in this regard.

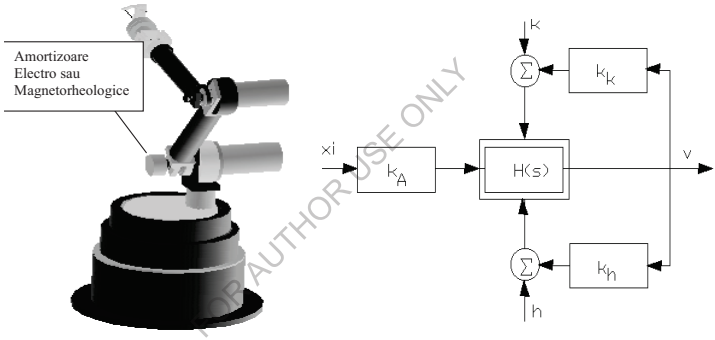

Fig.5.1. Articulated arm type robot with electro or magnetorheological dampers in couplers and the block diagram of such a module

The large spatial structures are made up of subassemblies of resistance beams covered with panels. The elastic deformations in these structures can be minimized by ensuring the rigidity of the components, which can be obtained by creating a network of sensors and actuators. Active beams are proposed for their use in couplings and in points with loads similar to bearings, in order to obtain precision and correction of the structure. The control of the shape of the panels or reflective segments on the surface can be obtained using a distribution strategy of sensors and actuators, and an adaptive control system, for which it is strictly necessary to approach the simulation of the complex acceleration signal, with at least the first ten own frequencies. To highlight the Fourier spectrum and the acceleration index characteristic, the LabVIEW virtual tool was created for the generation of complex sinusoidal signals that include 10 harmonics with various amplitudes, frequencies and phases, fig. 5.2. The complex acceleration signal is necessary in the simulation process of the damper excited with continuous periodic signals. The instrument has the possibility of adjusting the position of the harmonics in the spectrum, as well as the amplitudes and phases, so that the simulated excitation acceleration signal is identical to the real signal.

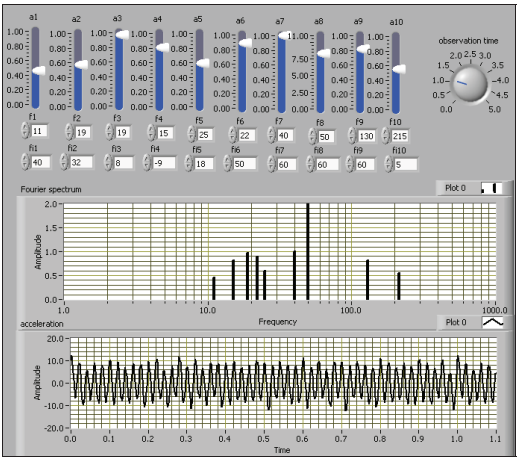

Fig.5.2. The front panel of the LabVIEW virtual instrument for the generation of complex acceleration signals depending on the parameters determined from the Fourier spectrum.

5.2. Vibration controller research. Simulation with the help of LabVIEW's own instrumentation of various types of controllers.

Vibration controllers. In general, vibration controllers can be classified into four categories: passive, active, adaptive and intelligent controllers.

Passive vibration controllers. Passive vibration absorbers have been used in many applications where vibration absorbing materials distribute the energy from vibration sources. The most used vibration sensors are: polyurethane foam, rubber, shock absorbers and piezoelectric materials. Passive vibration control methods are easy to implement and favorable vibration reductions can be obtained, which, however, are dependent on the system and the vibration frequency. Any change in the dynamics of the installation requires changing the passive vibration sensors with others, of other sizes and other characteristics. In fig.5.3 you can follow a virtual tool for choosing a certain type of passive vibration sensor, by mounting it in parallel or in series, or by changing the parameters of the sensor with another one with greater rigidity.

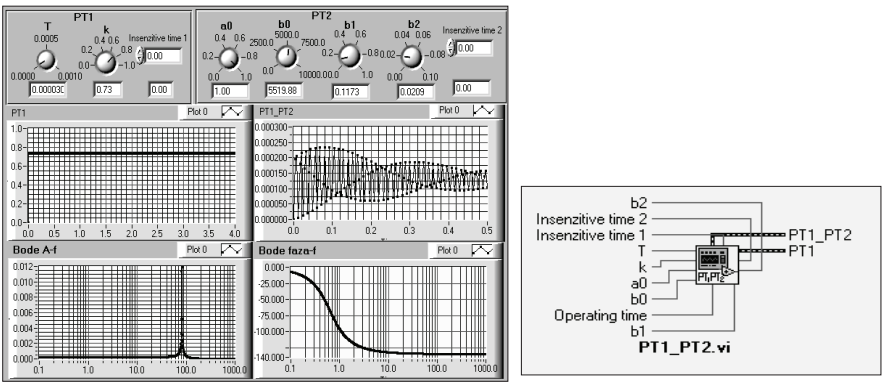

Fig.5.3.The real and frequency response of a passive damper and the icon of the program.

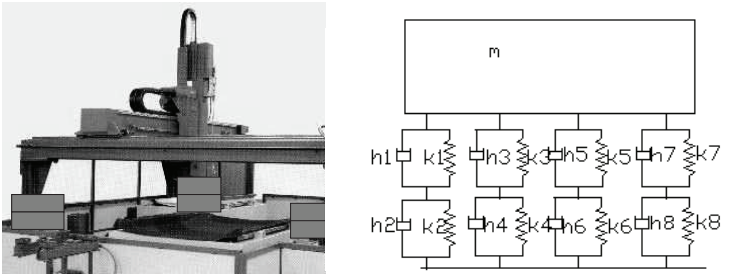

Fig.5.4. Gantry type machine on passive vibration sensors - variant 1 and equivalent mechanical diagram.

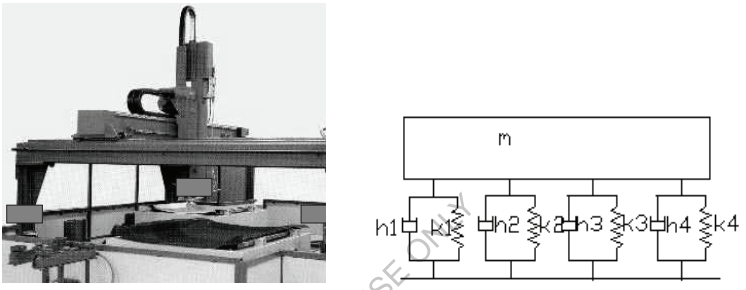

Fig.5.5. Gantry type machine on passive vibration sensors - version 2 and equivalent mechanical diagram.

Depending on the damping variant, based on the presented simulation program, the frequency spectrum can be determined and, depending on the disruptive vibration spectrum, one of the variants can be chosen, respectively with vibrashock type elements mounted two by two, respectively with elements of vibrashock type mounted singly, having 30% less rigidity than the previous case. From the calculations performed, based on the equivalent mechanical scheme, it follows that the equivalent stiffness for the first variant, if all the vibrashock elements are identical, is:

$\boldsymbol{k}_{echiv} = 2\boldsymbol{k}_i$, and for the second option: $\boldsymbol{k}_{echiv} = 4\boldsymbol{k}_i$.

If the stiffness $\boldsymbol{k}_i$ in the second option is lower by 30%, it still results in a higher resonance frequency as can be seen in fig. 5.6, which means that this variant can be used for wider frequency domains, the damping variant working as a low-pass filter with a higher bandwidth [0-110Hz], compared to the previous case of [0-80Hz].

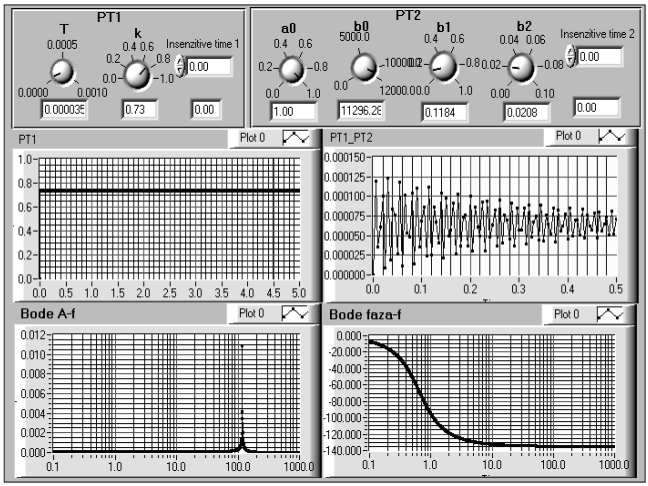

Fig.5.6. The real and frequency response of the passive vibration sensor- option 2.

Active vibration controls. Active controllers are controllers that use active components whose parameters cannot be changed online. The most common active controller is the proportional-integral-derivative (***PID***) controller whose proportional, derivative and integral constants can be determined based on its mitigating effect on the investigated technical installation (fig. 5.7a). In the problems related to active vibration control, controllers using other techniques were also observed. Fanson and Caughey used a technique based on the root locus method and used the feedback loop in a cantilever beam system (fig. 5.7b). Preumont, Dufour and Malekian used the reaction from the local force, the continuous signal being applied to piezoelectric actuators (fig. 5.8a). Baz and Poh designed an active controller for the control of structural vibrations of a flexible beam, using a modified method of spatial modal control, to select the optimal locations for arranging and determining the excitation voltage of the piezoelectric actuators (fig. 5.8b). The design methods of active controllers require knowledge from various fields such as linear and non-linear automation, mechanics, vibrations, modal analysis, vector analysis, etc., and a mathematical model as accurate as possible to the real one. The disadvantage of active controllers is that they do not cover too wide a range of vibrations, so that, in the case of a substantial change in the vibration spectrum of the structure subject to optimization, the redesign of the controller is necessary.

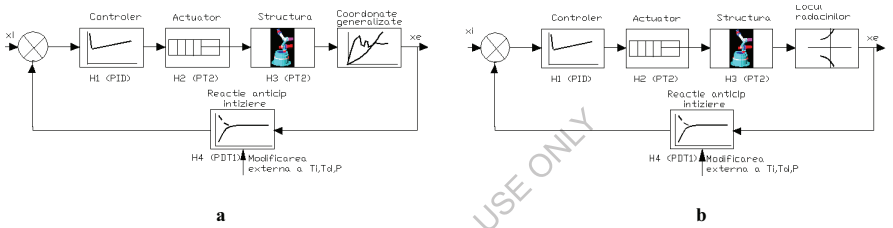

Fig.5.7. Vibration reduction scheme with active ***PID*** controller and reaction **a**: according to indicial characteristics of space and speed; **b**: according to the roots locus.

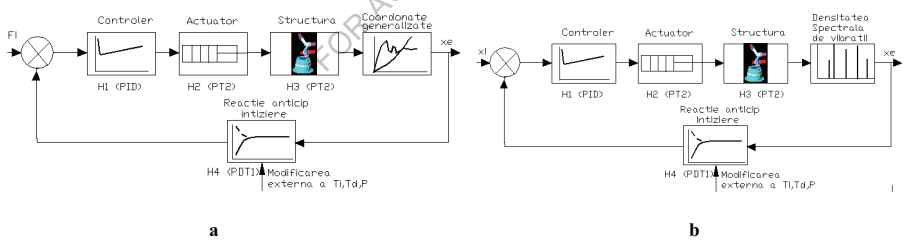

Fig.5.8. Vibration reduction scheme with active ***PID*** controller **a**: of disturbing forces and reaction according to the indicial characteristics of speed and space; **b**: reaction according to the Fourier frequency spectrum.

Adaptive vibration controllers. Adaptive controllers are controllers whose parameters can be modified online. A typical approach of the adaptive vibration controller consists in feeding an error signal through a special filter and applying the resulting signal to the technical installation. The filter coefficients are automatically adjusted by an adaptive algorithm in order to obtain the most favorable vibration reductions. The most widespread adaptive algorithm is the least squares (***LMS***) algorithm. Elliott, Stothers and Nelson presented an algorithm for adapting the coefficients of a string of finite impulse response (***FIR***) filters whose outputs were linearly coupled to another string of error detector points in order to minimize the mean square error signals. Eriksson, Allie, and Greiner investigated the use of adaptive finite impulse response (***IIR***) filters. Baumann studied the potential of an adaptive feedback loop approach in vibration damping. Adaptive vibration controllers are recommended when the parameters of the technical installation are not known or when there are inaccuracies in the system.

The parameters of the adaptive controllers are modified online to obtain the best performance. Adaptive algorithms based on ***FIR*** or ***IIR*** filters are limited to linear control.

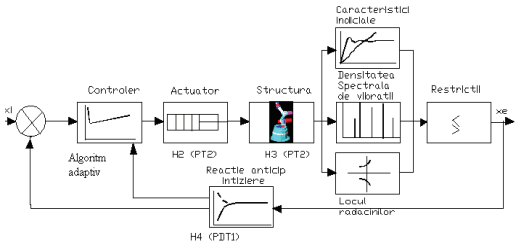

Fig.5.9. Vibration reduction scheme with adaptive controller, on-line regulation of reaction after restrictions and control method.

Intelligent vibration controls. One of the definitions of intelligent controllers formulated by Mayhan and Washington is: "An intelligent controller is one that supports different inputs, disturbances, parameter changes and noises by using a specific methodology". A big disadvantage of intelligent controllers is the large amount of calculations required to develop such a controller, something that can cause problems in real applications. Snyder and Tanaka presented a design using a feedback controller based on a neural network. Their results showed that the controller almost completely eliminated the vibrations even if the excitation frequency changed during the operation. Intelligent vibration controllers contain adaptive and self-learning features in control systems and provide solutions for non-linear applications with inputs and outputs. The results of both simulations and real-time experiments have shown that these controllers are, for problems with nonlinear vibrations, more efficient, more robust and less sensitive to disturbances than traditional adaptive controllers.

CMAC* (Cerebellar Model Articulation Controller) neural networks**. The first ***CMAC neural network was approached by Albus to approximate the information processing characteristics of the human brain. Later, Miller developed a practical implementation of the ***CMAC*** neural network in real-time control applications. The ***CMAC*** neural network can learn non-linear relationships from a wide range of functions and generally converges the results in a small number of iterations. ***CMAC*** represents a neural network with associative memory in which each input leads to a subset whose values are summed to form the outputs. For the bidirectional case, the loads within a generalized zone are updated after each control cycle according to the optimization equation of the type:

$$w_{i,j}(k+1) = w_{i,j}(k) + \frac{\beta(u(k) - p(k))}{(2c+1)^2} \tag{5.1}$$

where: $\boldsymbol{u}$(k) is the input at time $\boldsymbol{k}$, $\boldsymbol{p}$(k)- the probability of ***CMAC*** at time $\boldsymbol{k}$, $\boldsymbol{\beta}$- the ratio of learning, $\boldsymbol{c}$- the generalized size, $\boldsymbol{w_{i,j}(k)}$, $\boldsymbol{w_{i,j}(k+1)}$- the loads on line $\boldsymbol{i}$ and column $\boldsymbol{j}$ at moments $\boldsymbol{k}$ and $\boldsymbol{k}$+1. The ***CMAC*** probability, $\boldsymbol{p}$(k) is determined with the relation:

$$p(k) = \sum_{i=-c}^{c} \sum_{j=-c}^{c} w_{i,j}(k) \tag{5.2}$$

Among the advantages of using ***CMAC*** neural networks, the following can be mentioned: the speed of convergence is high, so the calculation time is small, the number of training cycles is small, it requires few calculations to make corrections compared to other neural networks that include complex principles and non-linear functions. The ***CMAC*** neural network consumes a relatively small

amount of memory and is not sensitive to disturbances. ***CMAC*** neural networks can be used with good results in the ***BMS*** (Biological Motor System) structure. In ***BMS*** the command signal for each muscle is a function of several variables. It includes the reaction signals from the sensors that measure the position, speed, acceleration of the hand, stretching of the muscles, tension in the tendons, tactile sensations from the various points of the "skin". Entries are directed to a memory location. The command output includes the sum of the contents of the selected memory location (figs. 5.10-5.13).

The large-scale use in the near future of intelligent materials and structures in the construction of ***RI*** ensures the optimal conditions in order to obtain extreme precision, stability and optimal control, priority requirements for the use of ***RI*** as active elements in the technique of technological processing, priority direction of current research in this field. The use of ***RI*** as a processing system can be possible in a short time through the rapid implementation of the requirements expressed in this chapter, requirements that essentially express that an ***RI*** can be used to carry out various active technological operations, only under the conditions of ensuring an intelligent control of its operation (figs.5.10.-5.13.). An example of the simulation of the ***CMAC*** application is presented in figs.5.12.- 5.13.

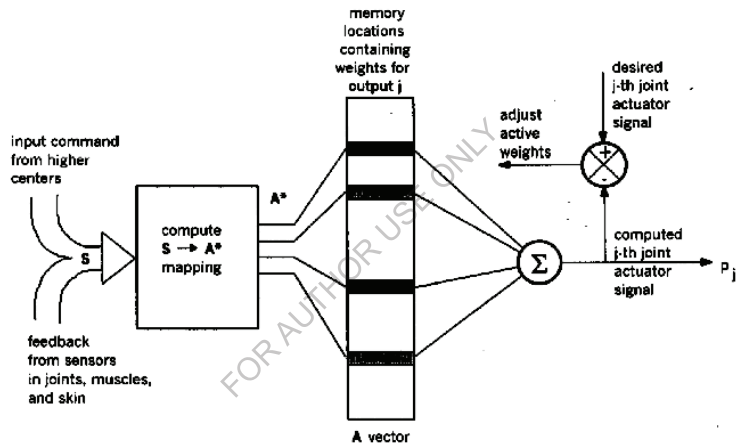

Fig.5.10. Block diagram of a ***CMAC*** network for controlling an actuator in a joint of the ***RI***.

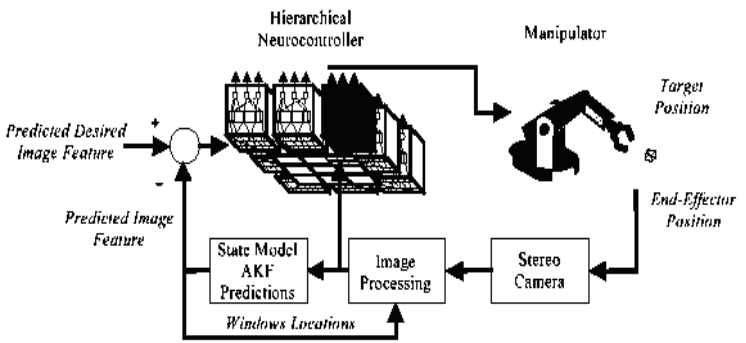

Fig.5.11. The visual servo actuation principle based on ***CMAC*** hierarchical neural networks.

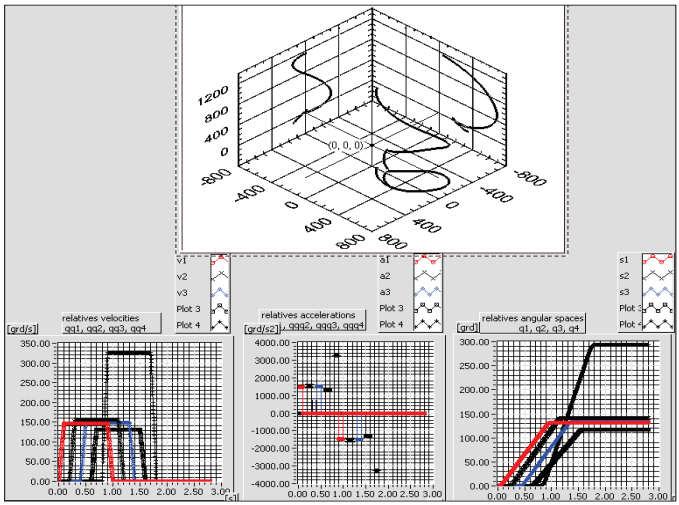

Fig.5.12. Dual camera operating mode providing position feedback in a complex ***RI*** motion using LabVIEW virtual instrumentation.

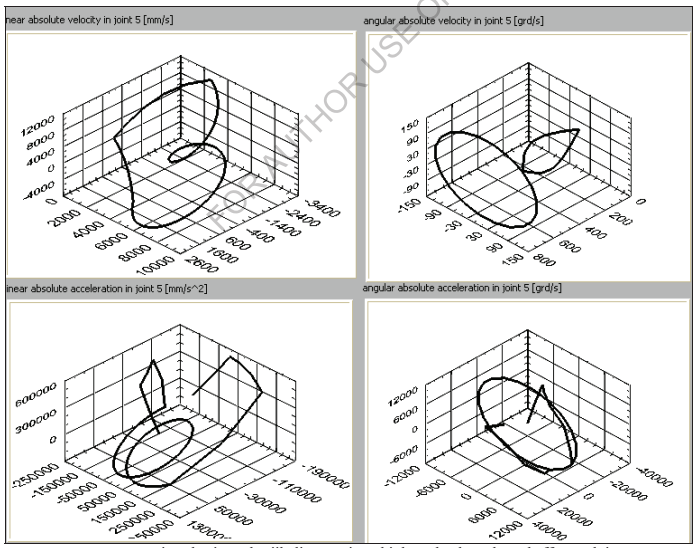

Fig.5.13. Absolute linear and angular velocities and accelerations of the end effector of the simulated articulated arm type robot.

5.3. Theoretical contributions regarding the kinematic and dynamic behavior of industrial robots - case study on the didactic experimentally researched robot structure. Through the numerical simulation with the help of LabVIEW virtual instrumentation, it was possible to determine some characteristics in real coordinates, with the aim of choosing the various parameters of the speed characteristics, to obtain the necessary trajectory of the end effector. The virtual instrumentation

includes programs for the assisted research of various types of robots and can also be used in the research of various other mechanical applications. The created virtual instrument is strictly necessary for the theoretical research of the acceleration signal, after applying the magneto-rheological damper, or an air damper. Assisted kinematic analyze usually used to choose the best solution in one robotics application. Generality, the optimization work means finding the best solution for one problem under given circumstances. The optimization step is typically obtained through the use of mathematical models. Mathematical model of optimization means that the problem at hand is formalized in a stringent mathematical way and the best solution, under the given circumstances, is found by using mathematical algorithms and the assisted research. In general, optimization phase involves imposing an objective function, constraints caused by the construction of the systems, performance and an iterative algorithm for calculating getting convergence solutions. Usually, aided research use iterative algorithms for tracking obtain convergence solutions. When it comes to *design optimization*, Papalambros et al. gives the following definition in [1]: "Informally, but rigorously, we can say that design optimization involves: the selection of a set of variables to describe the design alternatives; the selection of an objective (criterion), expressed in terms of the design variables, which we seek to minimize or maximize; the determination of a set of constraints, expressed in terms of the design variables, which must be satisfied by an desirable or acceptable design; the determination of a set of values for the design variables, which minimize (or maximize) the objective, while satisfying all the constraints." In any cases of optimization work, the required steps are: establishing all desirable or combination of acceptable- desirable and needed optimizing ways; define the optimization functions conformity with the needed results; establishing the objective function's values and constraints violation; establishing the optimization mathematical iterative algorithm; define detailed system parameters model; make the simulation procedure and obtain the results characteristics; comparing the results with the required performances and adjust, iteratively, the objective functions to be optimal function and finally to touch the imposed target. Many design methods, which are applicable to robot design, exist in academic literature. Since the design of robots begins with dimensioning its various links to meet performance specifications, most of them stress the kinematic layout and its optimization. The concept of manipulability was introduced by Yoshikawa [228] as a means to measure the ability of robotic mechanisms in positioning and orienting end effecters. Asada [229] introduced the generalized inertia ellipsoid as a tool to measure the capability of changing the velocity of the end effecter. Furthermore, Graettinger and Krogh [230] developed the acceleration radius like a global generalization of the point wise local measures of dynamic responsiveness proposed by other researchers such as Yoshikawa [228]. The acceleration radius is a uniform lower bound on the magnitude of the acceleration that can be achieved at the end effecter from any state (joint position and velocity) in the operating region. Furthermore, Bowling presents in [231] a thorough analysis of robotic manipulator dynamic performance. Ma and Angeles [232] showed how the architecture of a manipulator is optimized under dynamic isotropy conditions. In recent years, Angeles show one forward methods which focus on the kineto- static optimization of manipulators [233]. The minimization of the condition number of the Jacobian has been put forward by others [234], but Angeles introduced the *characteristic length*, which prevents the evaluation of any version of the condition number. In [235], was introduced the concept of *homogeneous space* in order to relieve the designer from the concept of characteristic length. Other kinematic performance measures used by industrial manufacturers that affect the shape of the workspace is the so called *stroke*. The stroke is defined as the offset between maximum reach and minimum reach of the end effecter of a robot.

The simulation of a robot system in RobotStudio software employs, the real robot program, the virtual controller and the configuration file that are identical to the real one. Other simulation products like WorkspaceLt [228], RoboticSimulation [237], NI-Robotics [238], RoboNaut [239], SimRobot [240], Open Dynamics Engine [241], Bullet Physics [242], NVidia PhysX [243] or DART [244], RoKiSim[245] or Gazebo [246].

In the paper [227-263] authors show, by using the special software like RoboAnalyzer, Robotech, V-Rep, RoKiSim, Ros, WorkspaceLt, RoboticSimulation, NI-Robotics, RoboNaut, SimRobot, Gazepo, some characteristics and solve direct and inverse kinematics problem and also the direct and inverse dynamic problem, but without show the mathematical matrix model and without show how could be influenced the forces and moments variation by different velocity variation or to have the possibility to choose the parameters of the trapezoidal velocity characteristics to obtain the minimum variation of the forces and moments between some studied cases like shown in the paper. After were analyzed state of art in the field of kinematics of robot, the papers [227-263] we can do the following conclusion that justify the proper research: many of the researchers not used the mathematical matrix form like will be described in this paper; the assisted solutions for kinematic behavior analyze not used the general definition of the trapezoidal characteristics with the different origin of time for each movement, the acceleration and deceleration time, the velocity constant values established by using the imposed space movement in each joints; the proper assisted kinematic analyze have the possibility to change on-line different parameters like constant velocity, the time parameters, to study how could be influenced the velocity variation with the final goal to obtain one minimum of variation; the optimization process, to choose the best solution of the movement type, contents one proper algorithm using the pounder theory. In the proper assisted research were used some virtual instruments what were established by transpose the proper mathematical matrix form of the robots kinematics in to the LabVIEW programs. The proper LabVIEW instrumentation have some modules of clusters what assured to accomplish the proposed goals. One module contents the times parameters of the trapezoidal velocities characteristics for the movements in each joints, like the time to the common origin, the acceleration time, the deceleration time, the time of the movement cycle, the value of the constant velocity. With this module will be possible to show all different analyzed cases of the movements. The module that contents the 3D characteristics show some important results like the validation of the mathematical matrix form of the position and the transfer matrices between the Cartesian systems, the variation of the velocities vectors in the space to see the variation of the module and the angular position vs. base Cartesian systems of these vectors. Comparative with other research and other used software, this research and the created instrumentation offer the possibility to change some kinematic or functional- constructive parameters and to see the changes of characteristics. By applying this matrix method and the virtual instrumentation, will be easily established what will be the best solution of the movements, the best constructive parameters of robot's bodies, the best solution of the velocities variation values, to obtain one good results of the dynamic behavior with minimum variation of the moments in all joints. Kinematics analyse contents analyse of the positions, velocities and accelerations in all robot's joints. The paper shown some results of this analyse for the following robots types: Gun, Arm, Scale, Cartesian and Double Portal. The general matrix equations for position, velocity and acceleration analyse are [264-267]:

$$\left(r_i^0\right) = \left(r_{i-1}^0\right) + \left[D_{i-1}^0\right]\left(r_i^{i-1}\right) \tag{5.3}$$

$$\begin{pmatrix} \left(\omega_{i,0}^i\right) \\ \left(v_{i,0}^i\right) \end{pmatrix} = \left[T_{i-1}^i\right] \begin{pmatrix} \left(\omega_{i-1,0}^{i-1}\right) \\ \left(v_{i-1,0}^{i-1}\right) \end{pmatrix} + \begin{pmatrix} \left(\omega_{i,i-1}^i\right) \\ \left(v_{i-1,i}^i\right) \end{pmatrix}$$

$$\begin{pmatrix} \left(\omega_{i,0}^0\right) \\ \left(v_{i,0}^0\right) \end{pmatrix} = \begin{bmatrix} [D_i^0] & [0] \\ [0] & [D_i^0] \end{bmatrix} \begin{pmatrix} \left(\omega_{i,0}^i\right) \\ \left(v_{i,0}^i\right) \end{pmatrix}$$

$$\begin{pmatrix} \left(\varepsilon_{i,0}^i\right) \\ \left(a_{i,0}^i\right) \end{pmatrix} = \left[T_{i-1}^i\right] \begin{pmatrix} \left(\varepsilon_{i-1,0}^{i-1}\right) \\ \left(a_{i-1,0}^{i-1}\right) \end{pmatrix} + (S''(i))$$

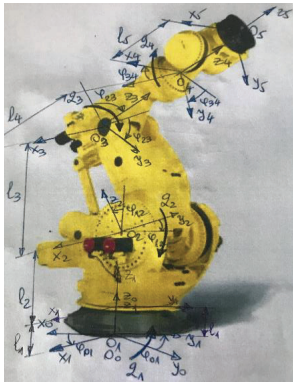

Fig.5.14. The arm type studied robot

$$(S''(i)) = \begin{pmatrix} (\varepsilon^i_{i,i-1}) + (\widehat{\omega}^i_{i-1,0})(\omega^i_{i,i-1}) \\ (a^i_{i,i-1}) + (\widehat{\omega}^i_{i-1,0})^2(r^i_{i,i-1}) + 2(\widehat{\omega}^i_{i-1,0})(v^i_{i,i-1}) \end{pmatrix}$$

$$\begin{pmatrix} (\varepsilon^0_{i,0}) \\ (a^0_{i,0}) \end{pmatrix} = \begin{bmatrix} [D^0_i] & [0] \\ [0] & [D^0_i] \end{bmatrix} \begin{pmatrix} (\varepsilon^i_{i,0}) \\ (a^i_{i,0}) \end{pmatrix}$$

$$(a_{gi,0})^0 = \begin{pmatrix} [D^0_1](a^1_{g1,0}) \\ [D^0_2](a^2_{g2,0}) \\ [D^0_3](a^3_{g3,0}) \\ [D^0_4](a^4_{g4,0}) \\ \dots \end{pmatrix}$$

$$[T^i_{i-1}] = \begin{bmatrix} [D^i_{i-1}] & 0 \\ -[D^i_{i-1}][\tilde{r}^{i-1}_i] & [D^i_{i-1}] \end{bmatrix} \tag{5.4}$$

$$(r^0_5) = (r^0_1) + [D^0_1](r^1_2) + [D^0_1][D^1_2](r^2_3) + [D^0_1][D^1_2][D^2_3](r^3_4) + [D^0_1][D^1_2][D^2_3][D^3_4](r^4_5)$$

- for the velocities:

$$\begin{pmatrix} (\omega^5_{5,0}) \\ (v^5_{5,0}) \end{pmatrix} = [T^5_4][T^4_3][T^3_2][T^2_1] \begin{pmatrix} (\omega^1_{1,0}) \\ (v^1_{1,0}) \end{pmatrix} + [T^5_4][T^4_3][T^3_2] \begin{pmatrix} (\omega^2_{2,1}) \\ (v^2_{2,1}) \end{pmatrix} + [T^5_4][T^4_3] \begin{pmatrix} (\omega^3_{3,2}) \\ (v^3_{3,2}) \end{pmatrix} + [T^5_4] \begin{pmatrix} (\omega^4_{4,3}) \\ (v^4_{4,3}) \end{pmatrix} + \begin{pmatrix} (\omega^5_{5,4}) \\ (v^5_{5,4}) \end{pmatrix}$$

$$\begin{pmatrix} (\omega^0_{5,0}) \\ (v^0_{5,0}) \end{pmatrix} = \begin{bmatrix} [D^0_5] & [0] \\ [0] & [D^0_5] \end{bmatrix} \begin{pmatrix} (\omega^5_{5,0}) \\ (v^5_{5,0}) \end{pmatrix}$$

$$[D^0_5] = [D^0_1][D^1_2][D^2_3][D^3_4][D^4_5]$$

$$[T^5_4] = \begin{bmatrix} [D^5_4] & 0 \\ -[D^5_4][\tilde{r}^4_5] & [D^5_4] \end{bmatrix}$$

$$\begin{pmatrix} (\varepsilon^5_{5,0}) \\ (a^5_{5,0}) \end{pmatrix} = [T^5_4][T^4_3][T^3_2][T^2_1] \begin{pmatrix} (\varepsilon^1_{1,0}) \\ (a^1_{1,0}) \end{pmatrix} + [T^5_4][T^4_3][T^3_2](S''(2)) + [T^5_4][T^4_3](S''(3)) + [T^5_4](S''(4)) + (S''(5))$$

$$(S''(5)) = \begin{pmatrix} (\varepsilon^5_{5,4}) + (\widehat{\omega}^5_{4,0})(\omega^5_{5,4}) \\ (a^5_{5,4}) + (\widehat{\omega}^5_{4,0})^2(r^5_{5,4}) + 2(\widehat{\omega}^5_{4,0})(v^5_{5,4}) \end{pmatrix}$$

where: $\boldsymbol{r}_i{}^0$is the absolute position vector of the ***i*** joint; $\boldsymbol{r}_i{}^{i-1}$is the relative position vector from the ***i*** joint to ***i***-1 joint; $\boldsymbol{D}_{i-1}{}^0$ is the transfer matrix from the Cartesian system ***i***-1 to Cartesian base system; $\boldsymbol{\varphi}_{ij}$-angular at home position between ***i*** and ***j*** systems; $\begin{pmatrix} \boldsymbol{\omega}^i_{i,0} \\ \boldsymbol{v}^i_{i,0} \end{pmatrix}$ – dual absolute angular and linear velocity vector of the ***i*** joint versus ***i*** Cartesian system; $\begin{pmatrix} \boldsymbol{\omega}^0_{i,0} \\ \boldsymbol{v}^0_{i,0} \end{pmatrix}$- dual absolute velocity angular and linear vector of the *i* joint versus Cartesian base system; $\boldsymbol{T}_{i-1}{}^i$- matrix transfer 6x6 from ***i***-1 to ***i*** Cartesian system; $\begin{pmatrix} \omega^i_{i,i-1} \\ \boldsymbol{v}^i_{i,i-1} \end{pmatrix}$- dual relative angular and linear velocity vector between ***i*** and ***i***-1 joints versus ***i***

Cartesian system; $\begin{pmatrix}\boldsymbol{\varepsilon}_{i,0}^{i}\\ \boldsymbol{a}_{i,0}^{i}\end{pmatrix}$ -dual absolute angular and linear acceleration vector of the ***i*** joint versus the ***i*** Cartesian system; $\begin{pmatrix}\boldsymbol{\varepsilon}_{i,0}^{0}\\ \boldsymbol{a}_{i,0}^{0}\end{pmatrix}$- dual absolute angular and linear acceleration vector of the ***i*** joint versus Cartesian base system; $(\boldsymbol{\varepsilon}_{i,i-1}^{i})$ -angular relative acceleration between ***i*** and ***i***-1 joints; $(\boldsymbol{a}_{i,i-1}^{i})$- linear relative acceleration between ***i*** and ***i***-1 joints; $[\widehat{\boldsymbol{\omega}}_{i-1,0}^{i}]$- angular absolute velocity antisymmetric vector of the ***i***-1 joint vs. ***i*** Cartesian system; $[\widehat{\boldsymbol{\omega}}_{i-1,0}^{i}]^{2}(\boldsymbol{r}_{i}^{i-1})$- centrifuged- centripetal acceleration; $2[\widehat{\boldsymbol{\omega}}_{i-1,0}^{i}](\boldsymbol{v}_{i,i-1}^{i})$- Coriolis acceleration; $(\boldsymbol{S}\ddot{(\iota)})$- dual relative acceleration matrix.

For the forces analyze was used the following mathematic matrix model:

$$(P) = [z_u]\{(F^0) - [m_u](a_{gi,0}^0)\} \tag{5.5}$$

$$[z_u] = \begin{bmatrix} \begin{bmatrix}1&0&0\\0&1&0\\0&0&1\end{bmatrix}G_{11} & \dots & \begin{bmatrix}1&0&0\\0&1&0\\0&0&1\end{bmatrix}G_{14} \\ \vdots & \ddots & \vdots \\ \begin{bmatrix}1&0&0\\0&1&0\\0&0&1\end{bmatrix}G_{41} & \dots & \begin{bmatrix}1&0&0\\0&1&0\\0&0&1\end{bmatrix}G_{44} \end{bmatrix}$$

$$[m_u] = \begin{bmatrix} \begin{bmatrix}1&0&0\\0&1&0\\0&0&1\end{bmatrix}m_1 & \dots & [0] \\ \vdots & \ddots & \vdots \\ [0] & \dots & \begin{bmatrix}1&0&0\\0&1&0\\0&0&1\end{bmatrix}m_4 \end{bmatrix}$$

$$(F^0) = \begin{pmatrix}[D_1^0](F_1^1)\\ \vdots \\ [D_i^0](F_4^4)\end{pmatrix}$$

$$(a_{gi,0}^0) = \begin{pmatrix}[D_1^0](a_{g1,1}^1)\\ \vdots \\ [D_i^0](a_{g4,1}^4)\end{pmatrix}$$

where: $(\boldsymbol{P}^0)$- is the matrix of active force, reduced to the base Cartesian system; $[z_u]$- unitary joints-bodies matrix; $(\boldsymbol{F}^0)$- matrix of resistive forces reduced to the base; $(\boldsymbol{F}_i^i)$- matrix of resistive forces reduced to ***i*** Cartesian system; $[\boldsymbol{m}_u]$- unitary matrix of mass obtained by multiplying $\boldsymbol{m}_i$ by unitary matrix for the space; $(\boldsymbol{a}^0{}_{g4,0})$- absolute linear acceleration matrix for the centre of gravity $\boldsymbol{g}_4$ reduced to the base Cartesian system; $\boldsymbol{G}_{i,j}$- is current value from the incidence body- joints matrix ***G*** obtained by using the associated graph to the robot's structure.

For the moments analyze was used the equation:

$$(Q) = [z_u]\{(M^0) - (\dot{K}_{gi,0}^0) + [\widehat{B}][(P^0)\} \tag{5.6}$$

$$(M^0) = \begin{pmatrix}[D_1^0](M_1^1)\\ \vdots \\ [D_i^0](M_4^4)\end{pmatrix}$$

$$[\hat{B}] = \begin{bmatrix}[\hat{b}_{11}^0]G_{11} & \dots & [\hat{b}_{1i}^0]G_{14} \\ \vdots & \ddots & \vdots \\ [\hat{b}_{i1}^0]G_{41} & \dots & [\hat{b}_{44}^0]G_{44}\end{bmatrix}$$

$$[\hat{b}_{11}^0] = \begin{bmatrix} 0 & -b_{11z}^0 & b_{11y}^0 \\ b_{11z}^0 & 0 & -b_{11x}^0 \\ -b_{11y}^0 & b_{11x}^0 & 0 \end{bmatrix}$$

$$(b_{i,k}^0) = (r_k^0) - (r_{gi}^0)$$

$$(\dot{K}_{gi}^0) = \begin{pmatrix} [D_1^0](\dot{K}_{g1,0}^1) \\ \vdots \\ [D_4^0](\dot{K}_{g4,0}^4) \end{pmatrix}$$

$$(\dot{K}_{g4,0}^4) = [J_{g4}^4](\varepsilon_{4,3}^4) + \widehat{[\omega}_{3,0}^4][J_{g4}^4](\omega_{4,3}^4)$$

$$[J_{gi}^i] = \begin{bmatrix} \frac{m(B^2+C^2)}{3} + m(b^2+c^2) + m(Bb+Cc) & -(\frac{mAB}{4} + \frac{mAb}{2} + \frac{mBc}{2} + mab) & -(\frac{mAC}{4} + \frac{mAc}{2} + \frac{mCc}{2} + mac) \\ -(\frac{mAB}{4} + \frac{mAb}{2} + \frac{mBc}{2} + mab) & \frac{m(A^2+C^2)}{3} + m(c^2+a^2) + m(Cc+Aa) & -(\frac{mBC}{4} + \frac{mBc}{2} + \frac{mCb}{2} + mbc) \\ -(\frac{mAC}{4} + \frac{mAc}{2} + \frac{mCc}{2} + mac) & -(\frac{mBC}{4} + \frac{mBc}{2} + \frac{mCb}{2} + mbc) & \frac{m(B^2+A^2)}{3} + m(a^2+b^2) + m(Aa+Bb) \end{bmatrix}$$

where: (***Q***)- matrix of the active moments in a joints; (***M***^{0})- matrix of the resistant moments in all joints; - $[\widehat{\boldsymbol{B}}]$anti-symmetric matrix of force's arm; (***P***^{0})- matrix for active forces; $(K_{gi}^{\prime 0})$ - matrix of the variation of the kinetic moment reduced to the base Cartesian system; $(\dot{\boldsymbol{K}}_{g4}^0)$- matrix of the variation of the kinetic moment of the $\boldsymbol{g}_4$ centre of gravity reduced to base Cartesian system; $(\dot{\boldsymbol{K}}_{g4}^4)$)- matrix of the variation of the kinetic moment of the $\boldsymbol{g}_4$ centre of gravity reduced to **4** Cartesian system; $(\boldsymbol{b}_{i,k}^0)$- absolute matrix vector force's arm from $\boldsymbol{g}_i$ center of gravity to the ***k*** joint; $[\boldsymbol{J}_{g4}^4]$- inertial tensor of the **4** body.

Following the analysis of the current state of research in the field of dynamic behavior of robots we can make the following observations: (i) many of the current research has used simplified mathematical models and the results have not been conclusive; (ii) much of the research has focused on robot components and less on the whole; (iii) in the modeling of the dynamic behavior were not used matrices of incidence bodies-joints and joints-bodies, as well as graphs associated to the structures to take into account the principle of action and reaction in establishing the equations of dynamic behavior; (iv) many of the current studies have not highlighted the analysis of positions, speeds, accelerations, forces and moments for each joint of the structure. In this way, information related to the centripetal, tangential and Coriolis forces used in the dimensioning of the various organology components in each joint could not be provided; (v) the research did not reveal differences in dynamic behavior for the up or down movement of the robot, as well as between the movement with object and without the object to be manipulated in the mechanical hand; (vi) much research has focused only on simulating motion in 3D space, or solving Forward Kinematics (***FK***) and Inverse Kinematics (***IK***); (vii) it was not highlighted how the inertia tensors are modified due to the change of the dimensions of the robot bodies, as well as the influence of their modification on the dynamic behavior of the robot; (viii) the kinematic and dynamic modifications for the simultaneous or successive movements in each joint as well as the simultaneous-successive combined movements obtained by modifying the parameters of the pseudo-trapezoidal speed characteristics in the joints, were not highlighted; (ix) how the mass of each body of the robot's structure influences the dynamic behavior of the structure has not been analyzed; (x) many of the researches have analyzed the dynamic behavior using specialized software for certain types of robots without being able to define another structure through the program, by defining the type of joint: rotation or translation or by defining the axis of movement by rotation or translation.

The interactive proper platform (***ROBO-PVAFM***) for analysis of forward kinematics (***FK***) and inverse dynamics (***ID***) uses LabVIEW software **14**.0. This project was created for the complex analysis of various types of robots including: articulated Arm, Scara, Cartesian and Double Portal.

The personal contributions introduced through the design and realization of the interactive platform (ROBO-PVAFM) aimed at completing the existing software with new modules to solve the reported deficiencies. The component modules of the platform's ensure a high degree of generality in the use for analysis of various types of robots, by completing the input data to define, as accurately as possible, the robot structure from the kinematic and dynamic point of view. The input data concerning the type of each module and body- joints and joints- body matrix offers the generality to design robot in concordance with his application. The software platform has the possibility to graphically represent 3D and 2D the variations vs. time of positions, velocities, accelerations, forces, moments as well as the variations of the positions of these vectors in space in all joints, with the possibility of framing these variations in precision-stability cones.

The platform ***ROBO-PVAFM*** was designed by using the complex mathematical model for positions, velocities, accelerations, forces and moments.

The software platform comprises the following components: ***(a)*** - the input data module in the form of clusters that: (i) define the parameters of the characteristics of space, speed, acceleration, Jerk for the movements in all joints; (ii) the dimensions of each body and its material for the purpose of calculating the masses; (iii) direction and type rotation or translation of axes of movement in each joints; ***(b)*** 2D and 3D characteristics for: (i) displacements, linear and angular velocities, linear and angular accelerations, forces, variation of kinetic moments and absolute moments in all joints; (ii) the modules of the displacement vectors, velocities, accelerations, forces and moments as well as the angular position of these vectors versus the basic plane; ***(c)*** the joints and gravity centers positions matrix; ***(d)*** column matrices of the G and Z bodies-joints and joints- bodies; ***(e)*** graph associated to the robot structure; ***(f)*** the button to select the movement with or without the object in the hand, see fig.5.15. The types of robots that could be studied with this platform we can see on the fig.5.16.

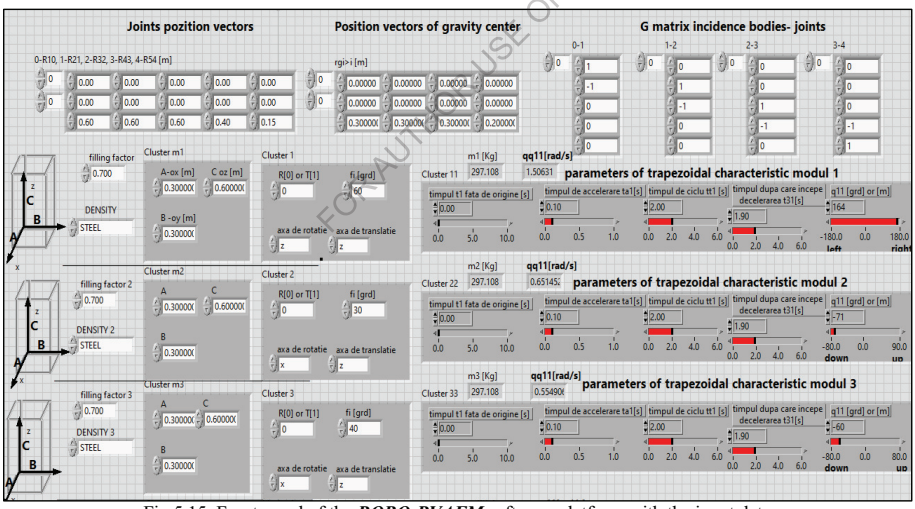

Fig.5.15. Front panel of the ***ROBO-PVAFM*** software platform with the input data.

The assisted research show what is the differences between some robots types and offers the possibility to calculate some mechanical parts by using the forces, moments, accelerations, velocities in all robot's joints, see Tables I-X. The positions analyze show haw will be changed the space trajectory in some different types of the movements- simultaneously, successive or complex.

After was analyzed the results we can do the following remarks: (i) the platform could be used to determine the singular points in the space by show the space trajectory in some different cases of the movements: simultaneously, successive, or complex; (ii) the program has the possibility to declare for each joint the axis of movement, the direction, the arrangement of the joint from the element to the slide, or from the element to the rotation torque or vice versa; (iii) by highlighting the variation

of the projections of the position vectors on each axis, the maximum variation can be determined and which is the axis with the maximum variation; (iv) by representing the variation in space of the position's module vector, the spatial variation of the angle versus base, as well as the variation of the position vector in space, will be possible to determine the case what could be influenced the dynamic behavior, see Tables I and II; (v) the results of the variation of the projections of the linear velocities on axes and the variation of the velocity module, the variation of angle versus base and the space trajectory of the velocity could be used to minimize these variations with the important influence to the dynamic behavior, see the Tables III and IV; (vi) in order to minimize the variation of the forces on each axis, the diminution of the variation of the acceleration projections, of the variation of their modules, as well as of the reduction of the angular variation of the acceleration vectors are priority directions of analysis, see Tables V and VI; (vii) in order to improve the dynamic behavior of robots, an important direction is to reduce the variation of the projections of forces on the axes, the variation of their modules, as well as the variation in space, with diminishing as much as possible the change of direction of these variations; the most unfavorable variations are present in Arm type robot and Scara robot, see Tables VII and VIII; (viii) the variations of moments are approximately the same for the analyzed robots, except the Arm type robot; moment analysis with this program offers designers the opportunity to use the values of moment variations for the mechanical parts calculations and to reduce these variations by resizing various bodies or by modifying the Cartesian system from the base, depending on the application, or by modifying the servo drive in various axes for framing Jerk variation within a maximum of 5 times the maximum speed, see Tables IX and X; (ix) the variation of the angle of the moment vector in space determines a cone of precision- stability on the minimization of which depends the optimal operation, from the dynamic point of view of the respective robot, depending on the desired application; in the case of the analyzed robots, with the adopted angular space differences, in the conditions of maintaining the movement on each axis within 2 s, the double portal robot has the biggest variation, respectively 70 [grd] compared to 50 [grd] Scale, 20 [grd] Arm si 12 [grd] Cartesian; (x) the largest variation of the moment vector module at the end-effector is at the Arm type robot 4000 [Nm], compared to the other studied robots, respectively Cartesian 40 [Nm], Scara 350 [Nm] and Double Portal 20 [Nm], under the conditions of comparable speeds and accelerations on each servo-controlled axe; the articulated Arm type robot was simulated in the conditions of simultaneous movement; in the successive movements, the maximal variation is 3000 [Nm].

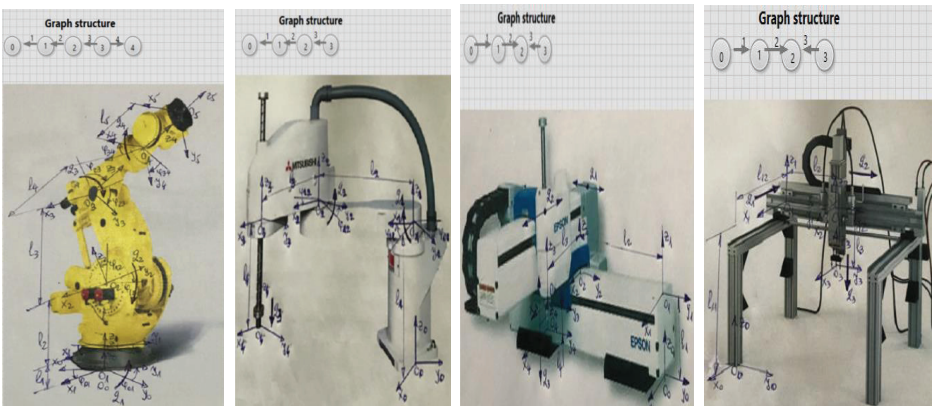

a b c d

Fig.5.16. Types of robots that could be used by OLROBOT software platform: a- Arm type robot; b- SCARA type robot; c- Cartesian type robot; d- Double Portal type robot.

TABLE I. PROIECTIONS OF THE POZITIONS VECTORS IN ALL AXES

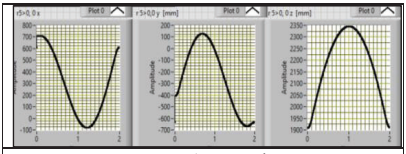

a- Arm type robot

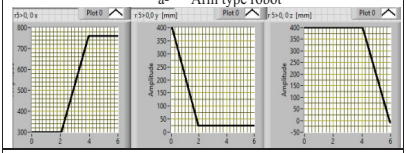

b- Cartesian robot type

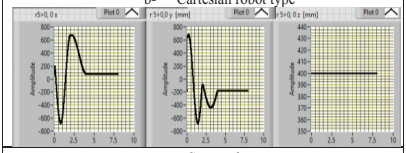

c- Scara robot type

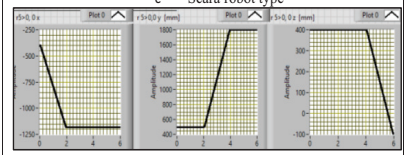

d- Double Portal robot type

TABLE II. SPACE POZITION VECTORS, MODULES AND SPACE ANGLES

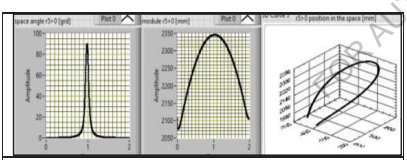

a- Arm type robot

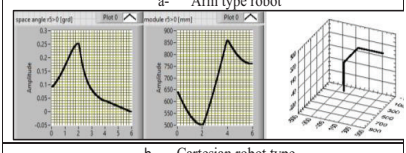

b- Cartesian robot type

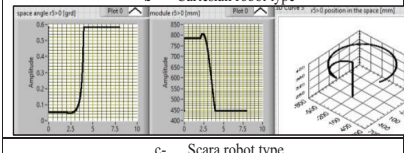

c- Scara robot type

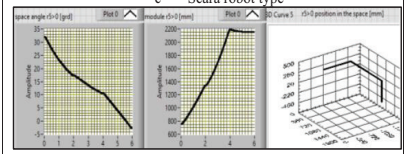

d- Double Portal robot type

TABLE III. PROJECTIONS OF THE LINEAR VELOCITIES VECTORS

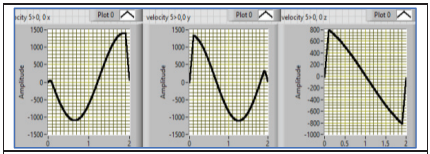

a- Arm type robot

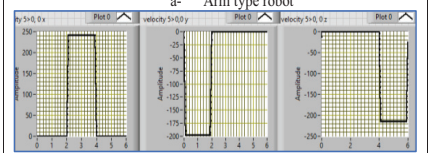

b- Cartesian type robot

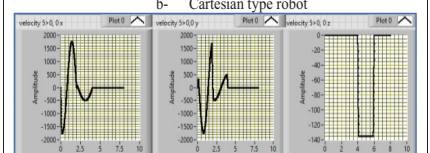

c- Scara type robot

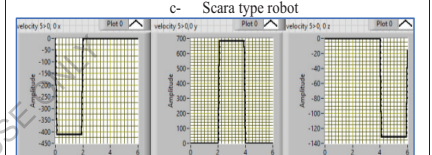

d- Double Portal robot type

TABLE IV. SPACE VELOCITY VECTORS, MODULES AND SPACE ANGL

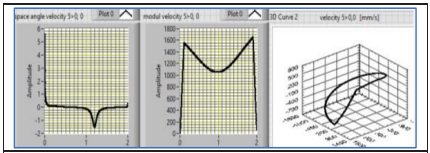

a- Arm type robot

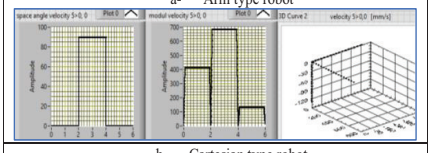

b- Cartesian type robot

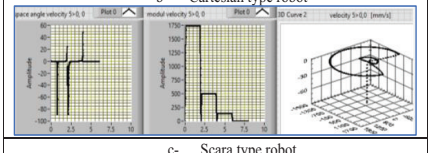

c- Scara type robot

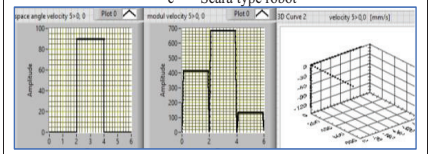

d- Double Portal robot type

TABLE V. PROJECTIONS OF THE LINEAR ACCELERATIONS VECTORS

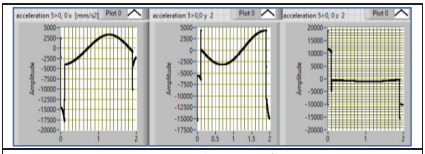

a- Arm type robot

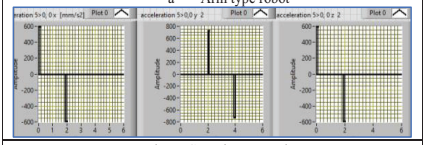

b- Cartesian type robot

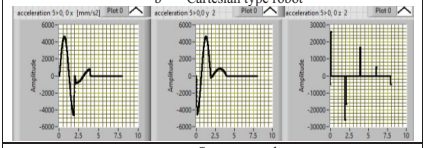

c- Scara type robot

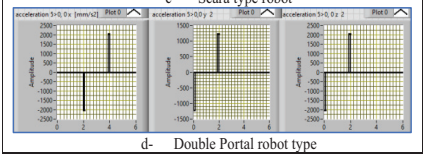

d- Double Portal robot type

TABLE VI. SPACE ACCELERATIONS VECTORS, MODULES AND SPACE ANGLES

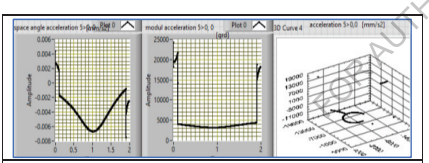

a- Arm type robot

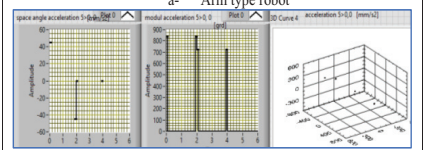

b- Cartesian type robot

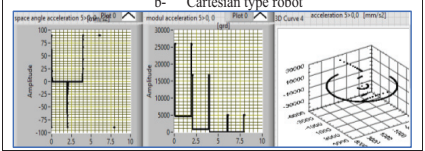

c- Scara type robot

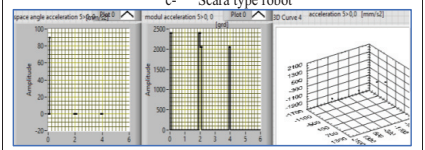

d- Double Portal robot type

TABLE VII. PROJECTIONS OF THE END-EFFECTERS FORCES VECTORS

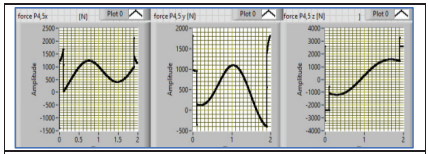

a- Arm type robot

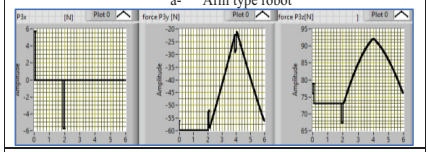

b- Cartesian type robot

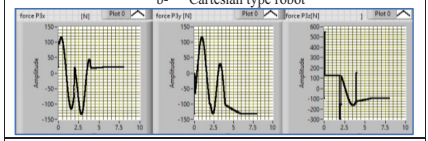

c- Scara type robot

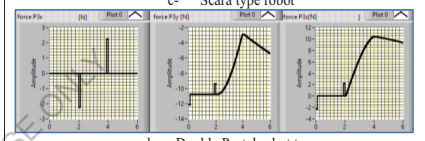

d- Double Portal robot type

TABLE VIII. SPACE END-EFFECTERS FORCES VECTORS, MODULES AN SPACE ANGLES

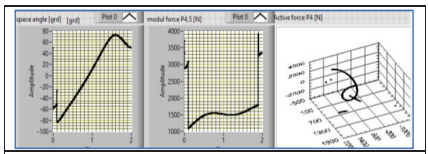

a- Arm type robot

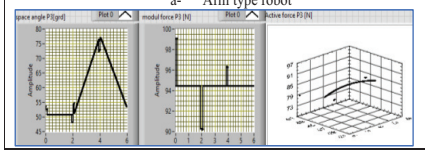

b- Cartesian type robot

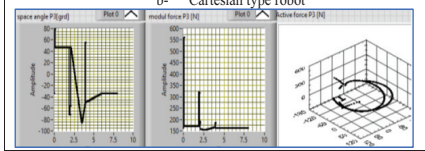

c- Scara type robot

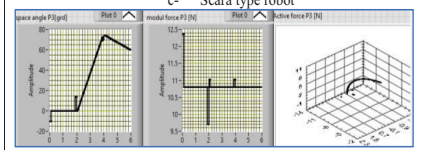

d- Double Portal robot type

TABLE IX. PROJECTIONS OF THE END-EFFECTERS MOMENTS VECTOR

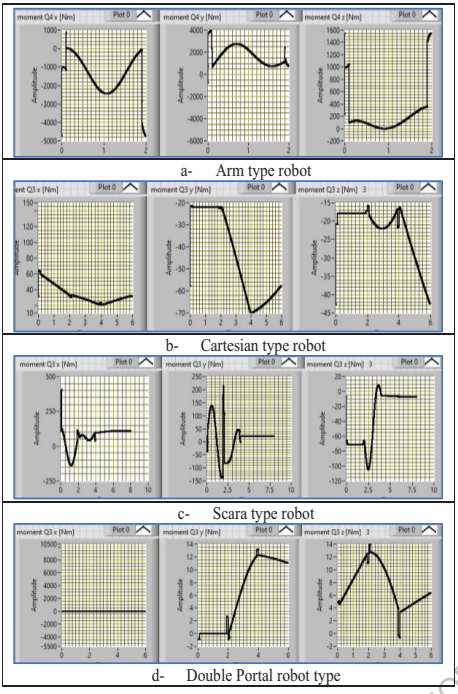

a- Arm type robot

b- Cartesian type robot

c- Scara type robot

d- Double Portal robot type

TABLE X. SPACE END-EFFECTERS MOMENTS VECTORS, MODULES AND SPACE ANGLES

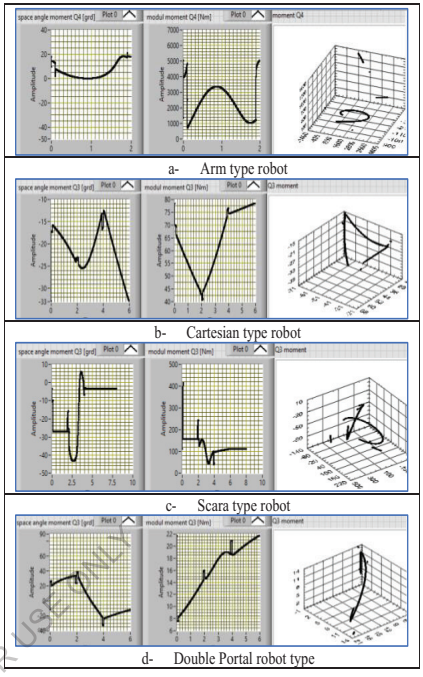

a- Arm type robot

b- Cartesian type robot

c- Scara type robot

d- Double Portal robot type

NR. OF STUDIED CASE	TYPE OF MOVEMENT	TRAPEZOIDAL CHARACTERISTICS OF RELATIVE VELOCITIES IN ALL FOUR ROBOT'S JOINTS
1	0-2-4-6	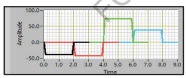
2	0-0-0-0	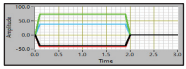
3	0-0.1-0.2-0.3	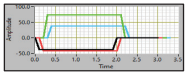
4	0-3-6-9	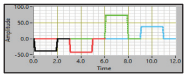
5	0-2-0-2	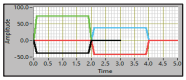
6	2-0-2-0	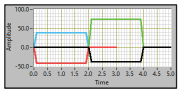
7	2-2-0-0	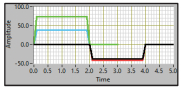
8	0-0-2-2	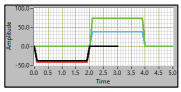
9	0-1.9-3.9-5.9	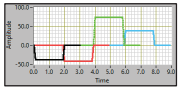
10	0-1-3-5	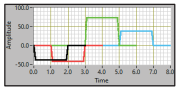

Fig.5.17. The type of the movements in all robot's joints that were studied

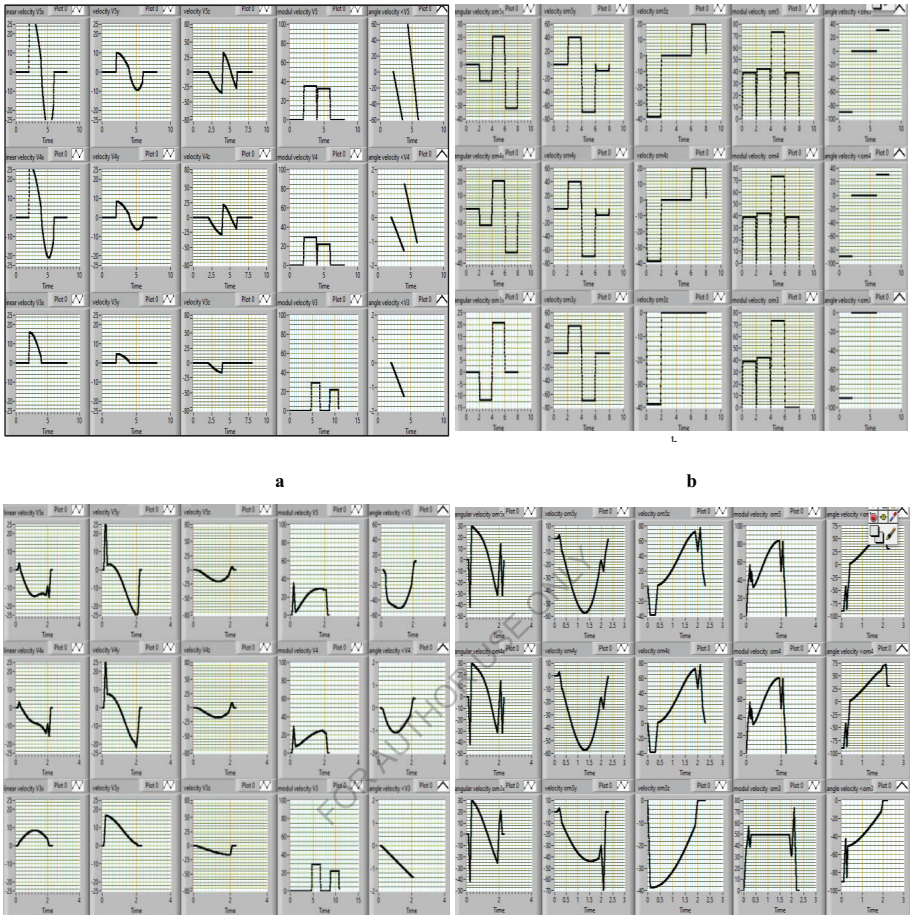

Fig.5.18. Front panel with the results of simulation for absolute velocities from 3,4 and 5 robot's joints; a- linear velocities characteristics for the successive movements in each robot's joints (0-2-4-6); b- angular velocities characteristics for the successive movements in each robot's joints (0-2-4-6); c- linear velocities characteristics for the successive and simultaneously movements in each robot's joints (0-0.1-0.2-0.3); d- angular velocities characteristics for the successive and simultaneously movements in each robot's joints (0-0.1-0.2-0.3).

The pounder for each robot's joint was calculate in function of the influence of current joint to the others. In analyze of the arm type robot, for the joints number 3, 4 and 5 were established the following maximal pounders: $\boldsymbol{p}_3$-300 (important influence of joint nr.3); $\boldsymbol{p}_4$-200 (influence only joint nr.2); $\boldsymbol{p}_5$-100 (influence only end effecter). In fig.5.18(a,b) are the simulation results of the linear and angular absolute velocities in all axes, reduced to the robot's base. In table XI are the ranges of all velocities components, necessary to see the minimum value of each of them. The pounder theory consist in calculate the powder of each optimization criteria and after that the sum of these powders.

TABLE XI- the minimal values of the linear and angular velocities in the 5, 4, and 3 robot's joints.

	v5x	v5y	v5z	Mod[v5]	>v5	v4x	v4y	v4z	Mod[v4]	>v4	v3x	v3y	v3z	Mod[v3]	>v3
0-2-4-6	50	**20**	53	35	120	45	18	48	30	4	18	**5**	20	**30**	1.5
0-0-0-0	**10**	28	25	**30**	58	14	32	22	26	**1**	8	18	20	**30**	**1.3**
0-0.1-0.2-0.3	20	50	**22**	35	**50**	15	46	22	30	1.5	8	18	**16**	**30**	1.4
0-3-6-9	55	**20**	55	38	120	45	**16**	50	30	3	16	**5**	**16**	**30**	1.5
0-2-0-2	38	50	45	38	120	26	35	21	25	2	18	**5**	20	**30**	1.4
2-0-2-0	38	55	55	38	125	28	53	50	30	2.5	**1**	18	22	**30**	1.4
2-2-0-0	20	39	**22**	35	60	**10**	34	**20**	**22**	**1**	8	18	17	**30**	1.4
0-0-2-2	33	**55**	**55**	35	120	28	42	55	30	2.6	8	16	**16**	**30**	1.4
0-1.9-3.9-5.9	60	**20**	60	35	130	50	**16**	50	30	2.8	16	6	20	**30**	1.4
0-1-3-5	60	35	62	35	155	44	30	50	30	155	12	12	15	18	80

	ω5x	ω5y	ω5z	Mod(ω5)	>ω5x	ω4x	ω4y	ω4z	Mod(ω4)	>ω4x	ω3x	ω3y	ω3z	Mod(ω3)	>ω3x
0-2-4-6	**50**	110	60	**75**	118	60	110	60	**75**	118	35	110	40	75	90
0-0-0-0	74	58	70	85	58	70	57	72	85	58	55	45	38	**50**	40
0-0.1-0.2-0.3	70	62	110	85	165	70	60	110	85	165	70	72	38	70	90
0-3-6-9	55	110	60	**75**	120	55	110	60	**75**	120	**32**	110	38	75	90
0-2-0-2	125	108	**38**	84	**16**	120	108	**38**	90	**18**	80	110	38	85	28
2-0-2-0	115	**33**	140	85	130	120	**33**	140	85	125	110	82	7	84	**5**
2-2-0-0	125	98	120	84	95	125	95	105	83	100	125	**27**	38	75	42
0-0-2-2	115	90	120	84	120	115	90	120	83	110	80	100	38	75	42
0-1.9-3.9-5.9	**50**	110	60	**75**	120	**32**	110	60	**75**	120	**32**	110	38	75	90
0-1-3-5	55	110	60	**75**	120	55	110	60	75	120	55	110	38	75	90

TABLE XII- the maximal values determined by using the pounder theory.

	v5x	v5y	v5z	Mod[v5]	>v5	v4x	v4y	v4z	Mod[v4]	>v4	v3x	v3y	v3z	Mod[v3]	>v3	
pounder	100					200					300					
0-2-4-6	20	100	41.50943396	85.71428571	41.66666667	44.44444444	178.2397671	192000	146.6666667	50	16.66666667	300	240	180	16.66666667	
0-0-0-0	100	71.42857143	88	100	86.20689655	142.8571429	100	88000	169.2307692	200	37.5	83.33333333	240	180	300	
0-0.1-0.2-0.3	50	40	100	85.71428571	100	133.3333333	69.56521739	88000	146.6666667	133.3333333	37.5	83.33333333	300	180	278.5714286	
0-3-6-9	18.18181818	100	40	78.94736842	41.66666667	44.44444444	200	200000	146.6666667	66.66666667	18.75	300	300	180	260	
0-2-0-2	26.31578947	40	48.88888889	78.94736842	41.66666667	76.92307692	91.42857143	84000	176	100	16.66666667	300	240	180	278.5714286	
2-0-2-0	26.31578947	36.36363636	40	78.94736842	40	71.42857143	60.37735849	200000	146.6666667	80	300	83.33333333	218.1818182	180	278.5714286	
2-2-0-0	50	51.28205128	100	85.71428571	83.33333333	200	94.11764706	80000	200	200	37.5	83.33333333	282.3529412	180	278.5714286	
0-0-2-2	30.3030303	36.3636364	40	85.7142857	41.6666667	71.4285714	76.1904762	220000	146.666667	76.9230769	37.5	93.75	300	180	278.571429	
0-1.9-3.9-5.9	16.66666667	100	36.66666667	85.71428571	38.46153846	40	200	200000	146.6666667	71.42857143	18.75	250	240	180	278.5714286	
0-1-3-5	16.66666667	57.14285714	35.48387097	85.71428571	32.25806452	45.45454545	106.6666667	200000	146.6666667	1.290322581	25	125	320	300	4.875	

	ω5x	ω5y	ω5z	Mod(ω5)	>ω5x	ω4x	ω4y	ω4z	Mod(ω4)	>ω4x	ω3x	ω3y	ω3z	Mod(ω3)	>ω3x	Total
0-2-4-6	100	100	63.33333333	100	13.55932203	54.25728814	60	126.6666667	200	30.50847458	274.2857143	73.63636364	52.5	200	16.66666667	194926.5
0-0-0-0	67.56756757	71.42857143	54.28571429	88.23529412	27.5862069	110.3448276	115.7894737	105.5555556	176.4705882	62.06896552	174.5454545	180	55.26315789	300	37.5	91525.2
0-0.1-0.2-0.3	71.42857143	40	54.54545455	88.23529412	9.696969697	38.78787879	110	69.69696969	176.4705882	21.81818182	137.1428571	112.5	55.26315789	214.2857143	16.66666667	90933.95
0-3-6-9	90.90909091	100	63.33333333	100	13.33333333	53.33333333	60	126.6666667	200	30	300	73.63636364	55.26315789	200	16.66666667	203278.5
0-2-0-2	40	40	100	89.28571429	100	400	61.11111111	200	166.6666667	200	120	73.63636364	55.26315789	176.4705882	33.57142857	87571.41
2-0-2-0	43.47826087	36.36363636	27.14285714	88.23529412	12.30769231	49.23076923	200	54.28571429	176.4705882	20.83333333	87.27272727	98.78048781	300	178.5714286	300	203321.1
2-2-0-0	40	51.28205128	31.66666667	89.28571429	16.84210526	67.36842105	69.47368421	72.38095238	180.7228916	36	76.8	300	55.26315789	200	33.71428571	83249
0-0-2-2	43.47826087	36.36363636	31.66666667	89.28571429	13.33333333	53.33333333	73.33333333	63.33333333	180.7228916	32.72727273	120	81	55.26315789	200	35.71428571	222604.6
0-1.9-3.9-5.9	100	100	63.33333333	100	13.33333333	53.33333333	60	126.6666667	200	30	300	73.63636364	55.26315789	200	16.66666667	203195.2

The sum of all current pounder is calculate with relation:

$$p_{nr.case} = \sum_{1}^{15} p_{3,4,5} \frac{p_{min/case}}{p_{crt/case}} \qquad (5.7)$$

After was applied the pounder theory will be obtained the results shown in the table XII. After were analyzed all simulation results and was applied the pounder theory we can do the following remarks: (i) the best solution to obtain the minimum variation of the velocities in all robot's joints is the case ***0-0-2-2*** that mince the simultaneously and successive two by two, the movement in the first and second joints and, the third and fourth robot's joints after 2 seconds; (ii) the optimization algorithm and pounder theory could be applied in many other assisted research were after was applied the multi objective function, if the results is zero; (iii) by using the LabVIEW instrumentation will be possible to research many other influences in the velocities variation like the dimensions of bodies and the parameters of the trapezoidal characteristics.

5.4. The approach of an own mathematical model of the magneto rheological damper in accordance with the experimental results. From the critical analysis of the current state, it emerged that the mathematical models approached do not ensure the reduction of modeling errors compared to the real results, which is why a mathematical model was proposed in which, compared to those used until now, they introduce non-linearities such as polynomials of degree 3, for each of the parameters present in the mathematical model. The most complex mathematical model, the modified Bouc-Wen model, was chosen. Thus, the proposed and researched model will be completed with 4 more polynomial equations of the 3rd degree and with an equation that takes into account the Fourier spectrum when the robot structure is excited. The model will have several parameters, with the help of which the modeling will be much closer to reality. Approaching such a more complex mathematical model also involves more elaborate numerical simulation programs that are difficult to design without a simulation instrumentation such as LabVIEW virtual instrumentation. Thus, compared to the models in the current stage, with a maximum of 18 variable parameters, the new mathematical model has 19 new parameters. It is of the form:

$$
\begin{aligned}
&f = c_0(x'-y') + k_0(x-y) + k_1(x-x_0) + \alpha z \\
&y' = \frac{1}{c_0 + c_1}[\alpha z + c_0 x' + k_0(x-y)] \\
&z' = -\gamma|x'-y'|z|z|^{n-1} - \beta(x'-y')|z|^n + \delta(x'-y') \\
&\alpha(i) = \alpha_3 i^3 + \alpha_2 i^2 + \alpha_1 i + \alpha_0 \\
&c_0(i) = c_{03} i^3 + c_{02} i^2 + c_{01} i + c_{00} \\
&c_1(i) = c_{13} i^3 + c_{12} i^2 + c_{11} i + c_{10} \\
&k_0(i) = k_{03} i^3 + k_{02} i^2 + k_{01} i + k_{00} \\
&\delta = \sum \delta_{0i} \sin(2\pi \upsilon_i + \varphi_i)
\end{aligned}
\tag{5.8}
$$

where: f is the damping force [N]; x and y are the variable displacements, primary and secondary [m]; z is the internal variable of *AMR* [m]; k_0 , k_1 are the non-linear internal stiffnesses of the ***AMR***, [N/m] depending on the intensity of the electric current [A]; c_0 and c_1 are the internal viscous friction parameters of ***AMR*** [Ns/m]; α is the internal parameter with non-linear evolution, dependent on the intensity of the electric current, respectively on the magnetic field; the β parameter characterizes the amplification value of the damping force vs. speed; x_0 is the displacement disturbance [m]; δ is the hysteresis parameter; δ_{0i} is the hysteresis parameter related to each frequency in the spectrum; υ_i is the frequency from the Fourier spectrum; φ_i is the phase corresponding to each frequency in the spectrum. This mathematical model was the basis for the design of the LabVIEW virtual tool for numerical simulation. In order to determine the way in which the various coefficients of the mathematical model influence the allure of the damper characteristics, the design of a virtual comparative numerical simulation tool was also approached. The numerical simulation of the mathematical model consisted in the assisted determination of the time-dependent variation characteristics of the damping force, the displacement, the speed and the attenuation energy. From these characteristics, the most important characteristics of ***AMR*** were determined, through soft

modeling, namely the characteristics of damping force vs. speed and damping force vs. displacement. In order to determine the way in which the various coefficients influence these characteristics, was studied the parameterization of the characteristic damping force vs. speed.

5.5. Parameterization of damping force characteristics vs. speed. The parameterization aimed to introduce some variables for each area of the allure of the damping force vs. speed. Thus, as can be seen in fig.5.19.: the parameter p_1 represents the inclination of the characteristic in the expansion phase; p_2 the slope of the characteristic in the compression phase; p_3 the slope of the characteristic at the peak of the hysteresis curve; p_4 the maximum size of the hysteresis at the minimum speed; p_5 hysteresis size at maximum speed; p_6 coordinate y of the quasi-linear allure of the characteristic; p_7 maximum coordinate y of the characteristic; p_8 maximum abscissa of the characteristic; p_9 abscissa of the hysteresis peak. By changing the values of all the coefficients and comparing the characteristics, it will be possible to determine how the various parameters are influenced by the changes in the coefficients of the mathematical model and to try to adjust the characteristic force vs. speed of movement, so that the allure of the characteristic approaches the experimentally determined characteristic.

5.6. Identification of the damper parameters by comparing the theoretical results with the experimental ones and validating the mathematical model. Identifying how the parameters of the damping force characteristic vs. the speed of movement are influenced by the coefficients of the mathematical model that was made by comparing the ***AMR*** characteristics for various values of the coefficients and the subsequent establishment of the way in which they modify the parameters p_1-p_9.

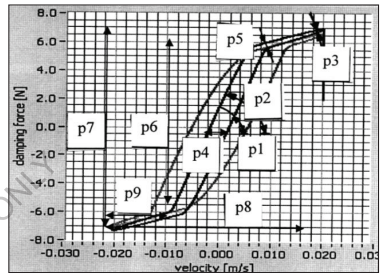

Fig.5.19. Parametrized damping force vs. speed characteristic of the damper

Following the numerical simulation, fig.5.20-5.26, the following conclusions can be highlighted: change in the intensity of the electric current determines the change in parameters p_1, p_2, p_6, p_7; the change in the displacement disturbance x_a determines the change in the parameters p_3, p_5; the change of the internal coefficient γ determines the change of the parameters p_3, p_5; the change the vibration amplitude x determines the change in parameters p_7, p_8, p_9; the modification of the global stiffness k_1 determines the modification of the parameters p_3, p_4, p_5, p_7; the modification of the amplification of the damping force β determines the modification of the parameters p_3, p_6, p_7; the modification of the hysteresis term δ determines the modification of the parameters p_1, p_2, p_3, p_4, p_5, p_9; the change of the internal coefficient of the second order α_2 determines the change of the parameters p_3, p_6, p_7; the change of the internal coefficient of the first order α_1 determines the change of the parameters p_3, p_6, p_7, p_9; the change in the second-order viscous damping coefficient c_{02} determines the change the parameter p_3.

By comparing the real characteristics with the simulated ones, it can be seen that the characteristics in fig.5.25 are the closest to those obtained experimentally. Based on the data included as input data in the front panel of the virtual simulation device, the values of all the parameters of the proposed model are determined, which represents the experimentally validated mathematical model for the researched application, under the conditions presented in the experimental research. Actual versus simulated characteristics for damping force vs. speed, after the identification operation of the coefficients, based on the numerical simulation, are presented in fig. 5.26.

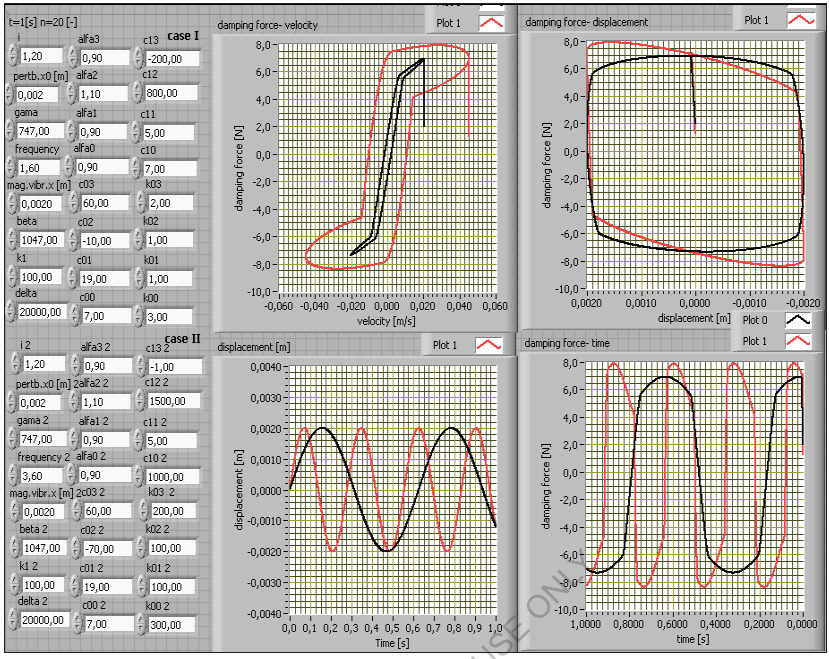

Fig.5.20. ***AMR*** characteristics obtained by simulation after changing $\boldsymbol{v}$, $\boldsymbol{k}_{00}$, $\boldsymbol{k}_{01}$, $\boldsymbol{k}_{02}$, $\boldsymbol{c}_{02}$, $\boldsymbol{c}_{10}$, $\boldsymbol{c}_{12}$, $\boldsymbol{c}_{13}$.

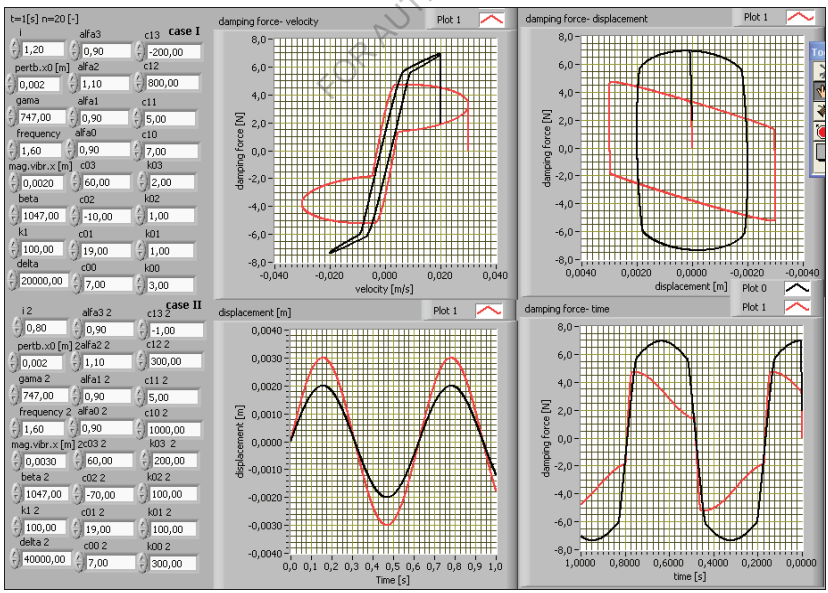

Fig.5.21. ***AMR*** characteristics obtained by simulation after changing k_{00} , k_{01} , k_{02} , k_{03} , c_{02} , c_{10} , c_{12} , c_{13} , i , x , δ.

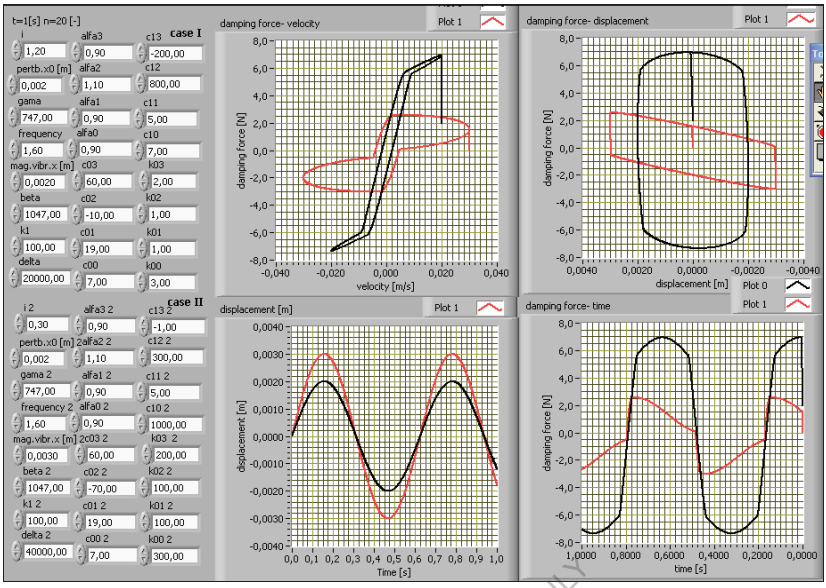

Fig.5.22. ***AMR*** characteristics obtained by simulation after changing k_{00}, k_{01}, k_{02}, k_{03}, c_{02}, c_{10}, c_{12}, c_{13}, i, x, δ.

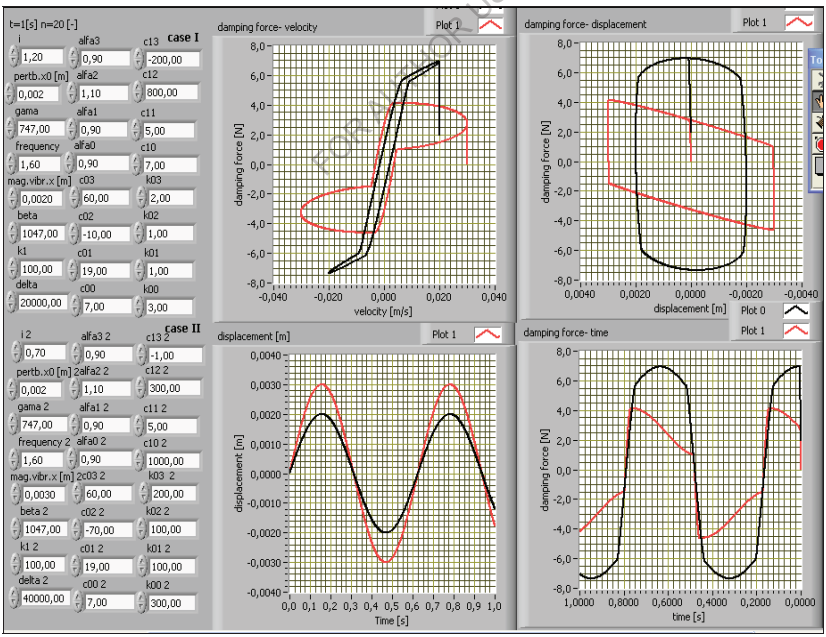

Fig.5.23. ***AMR*** characteristics obtained by simulation after changing k_{00}, k_{01}, k_{02}, k_{03}, c_{02}, c_{10}, c_{12}, c_{13}, i, x, δ.

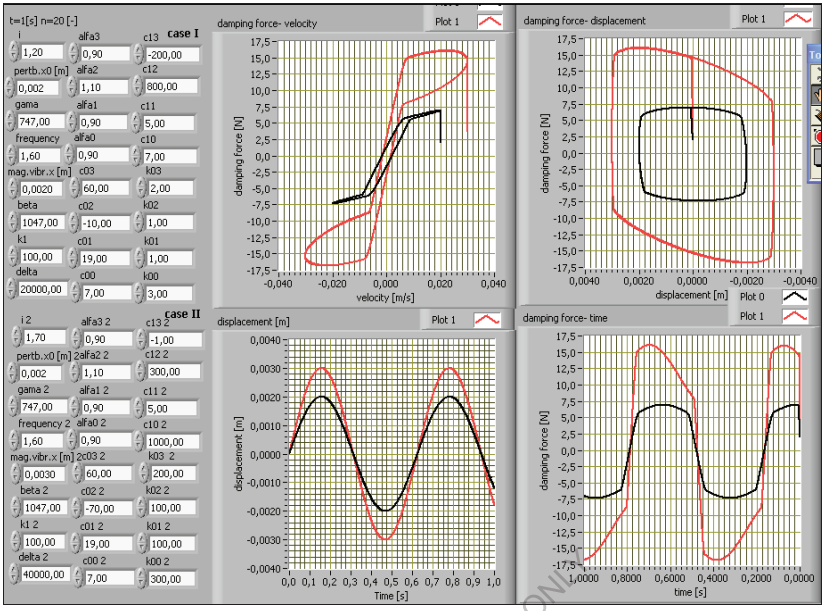

Fig.5.24. ***AMR*** characteristics obtained by simulation after changing k_{00} , k_{01} , k_{02} , k_{03} , c_{02} , c_{10} , c_{12} , c_{13} , i , x , δ.

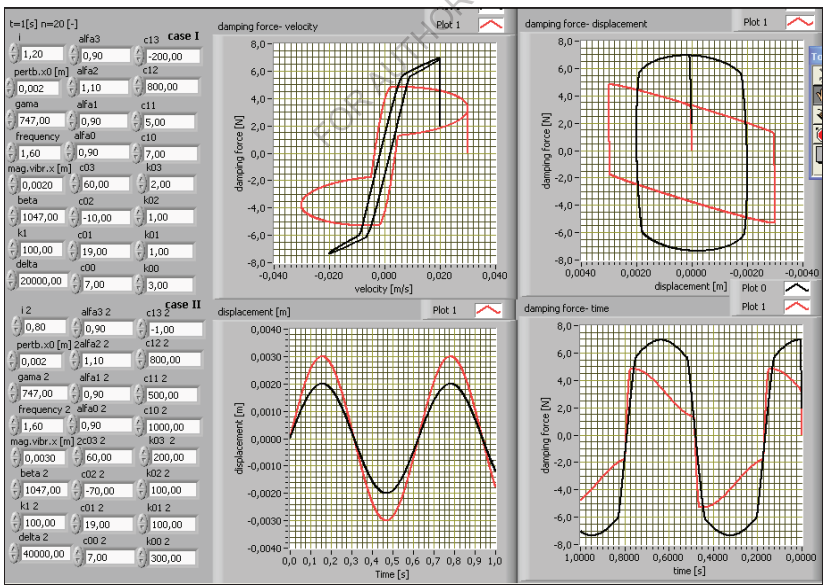

Fig.5.25. ***AMR*** characteristics obtained by simulation after changing k_{00} , k_{01} , k_{02} , k_{03} , c_{02} , c_{10} , c_{11} , c_{13} , i , x , δ.

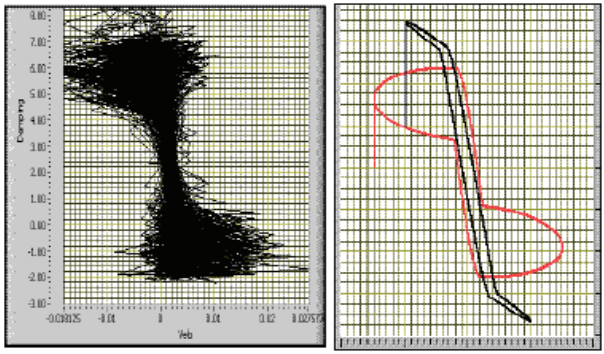

Fig.5.26. The real and simulated comparative characteristics for damping force vs. speed for i=0.8A.

The validated mathematical model for AMR used is:

$$
\begin{aligned}
&f = c_0(x'-y') + k_0(0.003-y) + 100(x-0.002) + \alpha z \\
&y' = \frac{1}{c_0+c_1}[\alpha z + c_0 x' + k_0(0.003-y)] \\
&z' = -747|x'-y'|z|z|^{n-1} - 1047(x'-y')|z|^n + 40000(x'-y') \\
&\alpha(i) = 0.9i^3 + 1.1i^2 + 0.9i + 0.9 \\
&c_0(i) = 60i^3 - 70i^2 + 19i + 7 \\
&c_1(i) = -i^3 + 300i^2 + 5i + 1000 \\
&k_0(i) = 200i^3 + 100i^2 + 100i + 300 \\
&\delta = 50\sin(10\pi + 0.21) + 1.1\sin(18\pi + 0.31) + \\
&+ 1.4\sin(30\pi + 0.62)
\end{aligned}
\tag{5.9}
$$

The comparative error obtained after the identification of the coefficients and the validation of the mathematical model is below 1%, as can be seen from the comparison of the damping force-vs. speed characteristics, fig.5.26. The mathematical model of the damping force can be used after validation in the complex, matrix-vector model of the force-moment torsion of the dynamic behavior of the robots, which will also include the effect of the damping force of the ***AMR***. It can be expressed in the final form:

$$
\left(\frac{F}{M}\right) = [[z_u][z_u]]\left[\left(\frac{F_R + f(i)}{M_R}\right) - [diag(m_i)][J^0_{gi}]\left(\frac{(a^0_{gi})}{(\varepsilon(i)) - [\hat{\omega}^0_{i-1,0}](\omega(i))}\right) - \left(\frac{(0)}{[\hat{B}][z_u][(F_R + f(i)) - [diag(m_i)](a^0_{gi})}\right)\right] \tag{5.10}
$$

CHAPTER 6
Assisted Experimental Research of Magnetorheological Dampers Applied to Robotic Structures

The experimental research was carried out following two major objectives: the first objective was the determination and validation of an original mathematical model, as close as possible to reality for the magnetorheological damper, in order to use this model, in the future, within the matrix-vector expression of the torque-modement torsion in couples and a second highlighting the optimization of the dynamic behavior of a didactic robot, after the application of ***AMR***. In order to obtain a mathematical model as close as possible to the real functioning, the modified Bouc-Wen type mathematical model was approached, a more complex model, considered as such, due to ensuring minimal errors between the simulated and experimental characteristics (about 1%), which was completed with four additional equations with 19 new coefficients. This approach allowed a better approximation of the simulated characteristics compared to the real ones. For the second objective, new parameters of the dynamic behavior were introduced with the help of which the analysis of how the introduction of ***AMR*** in the structure of industrial robots ensures the optimization of the dynamic behavior was carried out. The research was carried out in the Research Laboratory of the Dynamic Behavior of Industrial Robots, within the Faculty of IIR, Politehnica University of Bucharest. In the research, an articulated arm type teaching robot and an own ***AMR*** magnetorheological damper, mounted between the base and the end effector, specific equipment for researching the behavior of structures to vibrations, as well as the acquisition board, the own LabVIEW instrumentation, were used for the theoretical and experimental research.

6.1. Experimental research methodology. The experimental research methodology includes assisted research with data acquisition and numerical simulation. The research methods used will have to ensure the achievement of the following objectives:

• establishing a new mathematical model, as close as possible to the real functioning of such a magnetorheological damper;
• completion of the matrix-vector mathematical model for the force-moment torsor with the terms that can ensure its online control;
• experimental determination of some operating characteristics of the magnetorheological damper, characteristics to be compared with those obtained by numerical simulation;
• obtaining some operating characteristics of the magnetorheological damper through numerical simulation and the parameterization of these curves in order to facilitate the validation of the model and the identification of all coefficients;
• theoretical research through numerical simulation with the establishment of the influence of the coefficients of the mathematical model on the allure of the operating characteristics of the AMR and the establishment of the dependence of the parameters of the curves, compared to the modified coefficients of the mathematical model;
• establishing, by online modification of the values of all the coefficients of the mathematical model, the various dependencies, in order to approximate as accurately as possible the real behavior compared to the simulated one;
• comparing the characteristics of the damping force - the speed of movement of the linear damper rod, with the determination of possible inadvertences and the establishment of compensation methods and completion of the model.

In order to achieve the above-mentioned objectives, in addition to the specific experimental stands, the own LabVIEW virtual instrumentation was used both for experimental research and for theoretical research, as well as the acquisition board, the signal conditioner, specific vibration research equipment that is described below. As a working procedure, a line for generating a periodic excitation force with certain frequencies was used, applied to the base of the structure of the didactic robot and the acquisition of data on five simultaneous channels. The excitation force was applied to the basic module of the used didactic robot, on which the magnetorheological damper was mounted,

between the base and the end effector. The acquisition of experimental data consisted of: simultaneous five-channel determination of accelerations, forces, displacements and speeds. Thus, the following were determined: the acceleration at the base module; acceleration at the end-effector; excitation force; damping force and displacement of the end-effector. To determine the excitation force, the resistive measurement method was used, which consists in measuring the voltage drop on a sunt type resistance, followed by the calibration of the measurement, by comparing the determined values with the force measured with a dynamometer. Accelerations at the base and end-effector were experimentally determined using two accelerometers, an own amplification module connected to the accelerometers, connector, acquisition board and virtual data acquisition instrumentation. The damping force was measured with the help of an inductive transducer, connected to the Hottinger bridge and respectively to the connector and the acquisition board.

6.2. Scheduling of experimental determinations and the used stands. The preliminary experimental determinations aimed at: firstly, determining the dynamic behavior of the robot in several variants, namely: with magnetorheological damper, with air damper, or without damper and secondly, the validation of the approached mathematical model, with the identification of all coefficients. The experimental research consisted in: determining the variation of the global transfer function (***GTF***) depending on the frequency of ***AMR***; determining the variation of the global dynamic compliance depending on the ***GDC*** vs.frequency; determining the variation of global dynamic transmissibility ***Tr*** according to frequency; determining the variation of the damping force depending on the speed; determining the variation of the damping force depending on the frequency; determination of the variation of the excitation force depending on the frequency; determining the displacement according to the frequency; determining the variation of the acceleration of the module from the base as a function of time; determining the variation of the acceleration of the module from the base depending on the frequency; determining the variation of the acceleration of the end-effector as a function of time; determining the variation of the end-effector acceleration depending on the frequency; determining the variation of the global dynamic viscous damping coefficient ***VGDDC***; determination of the total dynamic coefficient of viscous damping ***VGDDTC***.

The mathematical models of the functions that have been determined are:

$$GTF = \frac{FFT(x(j\omega))}{FFT(F_{am}(j\omega))}; GDC = \frac{FFT(x(j\omega))}{FFT(F_{ex}(j\omega))}; Tr = \frac{FFT(a_2(j\omega))}{FFT(a_1(j\omega))}. \quad (6.1)$$

where: $\boldsymbol{x}$ is the displacement of the damper rod [m]; $\boldsymbol{F}_{am}$ - damping force [N]; $\boldsymbol{F}_{ex}$- excitation force [N]; $\boldsymbol{a}_2$- acceleration of the end-effector [m/s^2]; $\boldsymbol{a}_1$- acceleration of the module from the base [m/s^2]. Many of these determinations were made through the use of software components, based on the acquired data. Mathematically, global dynamic compliance can also be determined as a ratio of energy variation:

$$GDC = \frac{1}{k(j\omega)} = \frac{\int_0^T x(t)e^{-j\omega t}dt}{\int_0^T F_s(t)e^{-j\omega t}dt} = \frac{FFT(x)}{FFT(F)} = \frac{E_x(j\omega)}{E_F(j\omega)} \quad (6.2)$$

For the presented determinations, the experimental stand shown in fig. 6.1 and 6.2 was used.

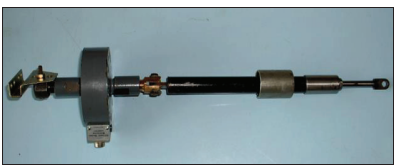

Fig.6.1. The inductive force transducer with the didactical magnetorheological damper.

Fig.6.2. Experimental didactical stand for the assisted research of the damper parameters.

The experimental stand consisted of the following components:
• articulated arm teaching robot made in the research laboratory a dynamic behavior DIRI-RSP-IIR-UPB;
• electrodynamic exciter type 11075, RFT Germany;
• connector type CB-68 LP, fig.5.3, National Instruments, USA;
• acquisition board type PCI 6221 M, National Instruments USA;
• frequency generator type POF-1, KABID Poland;
• amplifier for frequency generator type LV 102, MMF Germany;
• personal computer, Taiwan;
• inductive displacement transducer type 16.1 IAUC Romania;
• Hottinger bridge type KWS/T-5, Germany;
• calibrated resistance for determining the excitation force;
• self-built magnetorheological shock absorber;
• LabVIEW software version 14.0;
• proper LabVIEW virtual instrumentation, specific to assisted research with data acquisition and for numerical simulation.

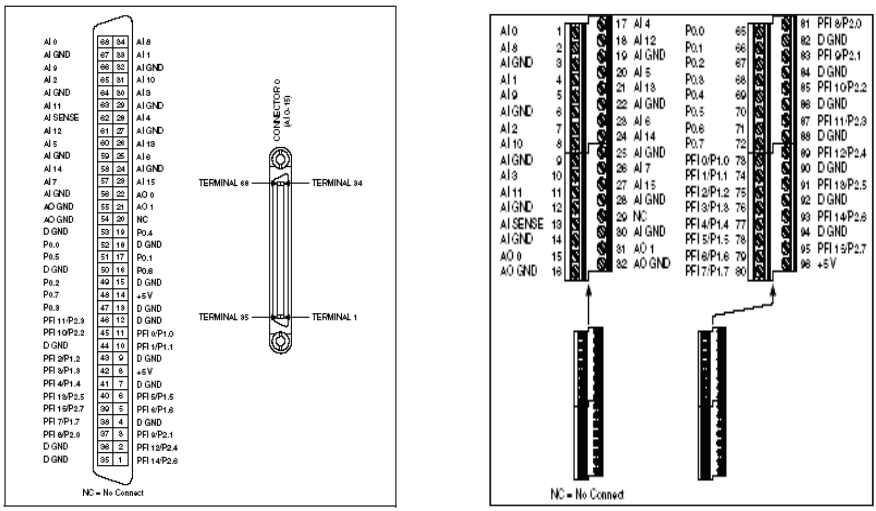

Fig.6.3. Acquisition board connector type CB68 LP from National Instruments, USA.

The created virtual instrumentation is specialized for the research of dynamic behavior, and ensure low costs and a short time for the research activity. The assisted theoretical research was carried out using a LabVIEW virtual tool with the help of which it was aimed to obtain, based on the own mathematical model for the magnetorheological damper, some specific characteristics: force vs. speed, force vs. displacement; damping force and travel speed vs. time; damping energy vs. time. The implementation of magnetorheological shock absorbers in the structure of the robots was carried out in order to attenuate vibrations with certain frequencies and amplitudes, which can determine the instability of the movement. For this purpose, these vibrations are either attenuated, or they are transferred to a higher frequency domain, as will be seen by analyzing the results of the experimental research. The experimental research was carried out on a didactic arm type robot with U profile of the arms and consisted in the excitation at the base of the robot structure, with a periodic force, of variable frequency and the simultaneous determination on five acquisition channels, of the excitation force, of the damping force, the displacement of the end effector, the acceleration at the base and at the end effector.

6.3. The proper used LabVIEW virtual instrumentation. LabVIEW virtual instrumentation, designed for assisted experimental research, is presented in figures 6.4-6.8, and for theoretical research in figures 6.9-6.10. The virtual tool for assisted research with data acquisition includes, see fig. 6.5, several modules: the data entry mode regarding the digital control of the movement, task/channels in – MyDigitalOut Task0, the command line, lines – dev 1/port0/line0 , where dev 1 is the device for the used PCI 6224M acquisition card, port0line0, is the port and the command line digital, mode for entering task/channels acquisition data in 2, DAQ Assistant 20, mode for entering data related to active ports, in centesimal, button regarding the stop motion command, mode for averaging acquired data, averaging type – linear, etc. The tasks of ordering, purchasing and connecting the transducers are presented in fig. 6.10-6.12.

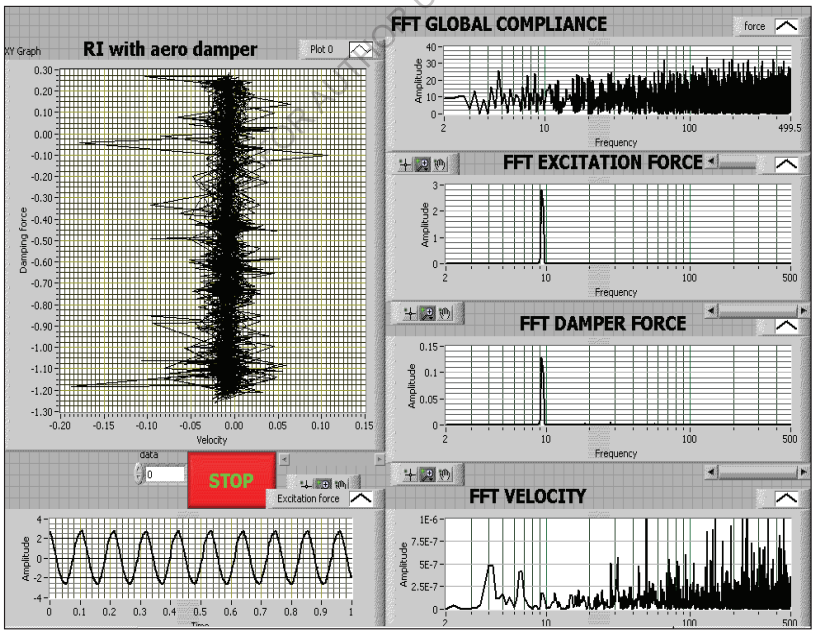

Fig.6.4. The front panel of the LabVIEW virtual instrument for determination
real characteristics: damping force vs. speed, excitation force vs. time, and a
frequency characteristics: speed, damping force, excitation force, global dynamic compliance vs. frequency.

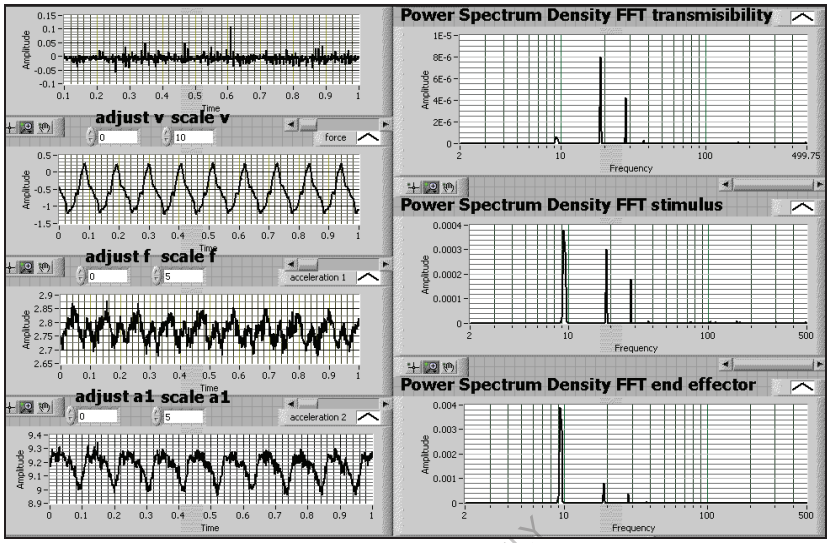

Fig.6.5. The front panel of the LabVIEW virtual instrument for determining real characteristics: angular velocity. damping force, base acceleration, end effector acceleration vs. time, and frequency characteristics: end effector power spectral density, base power spectral density, transmissibility vs. frequency.

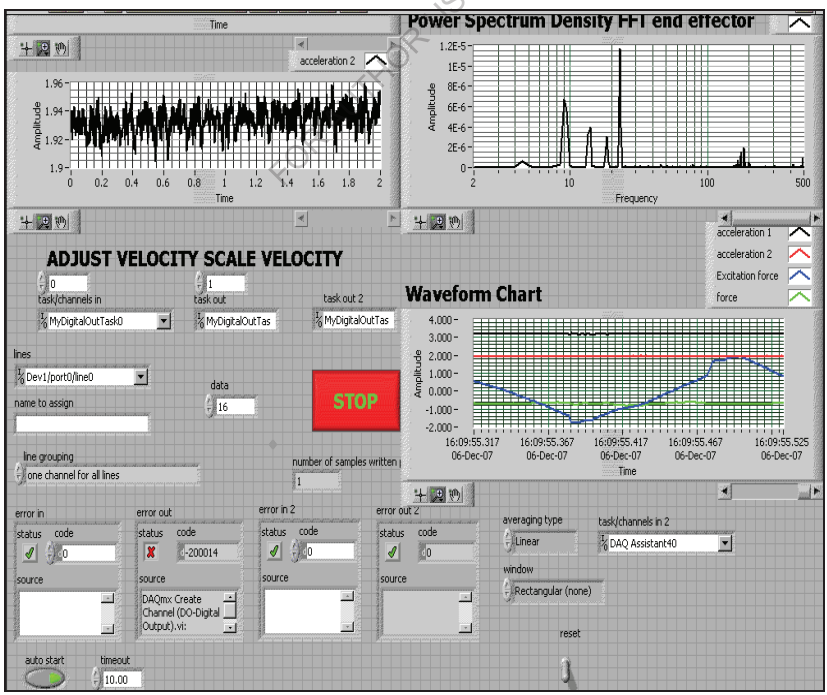

Fig.6.6. The front panel of the LabVIEW virtual instrument for simultaneous five-channel determination of real characteristics: excitation force, damping force, angular velocity, base and end effector acceleration, vs. time.

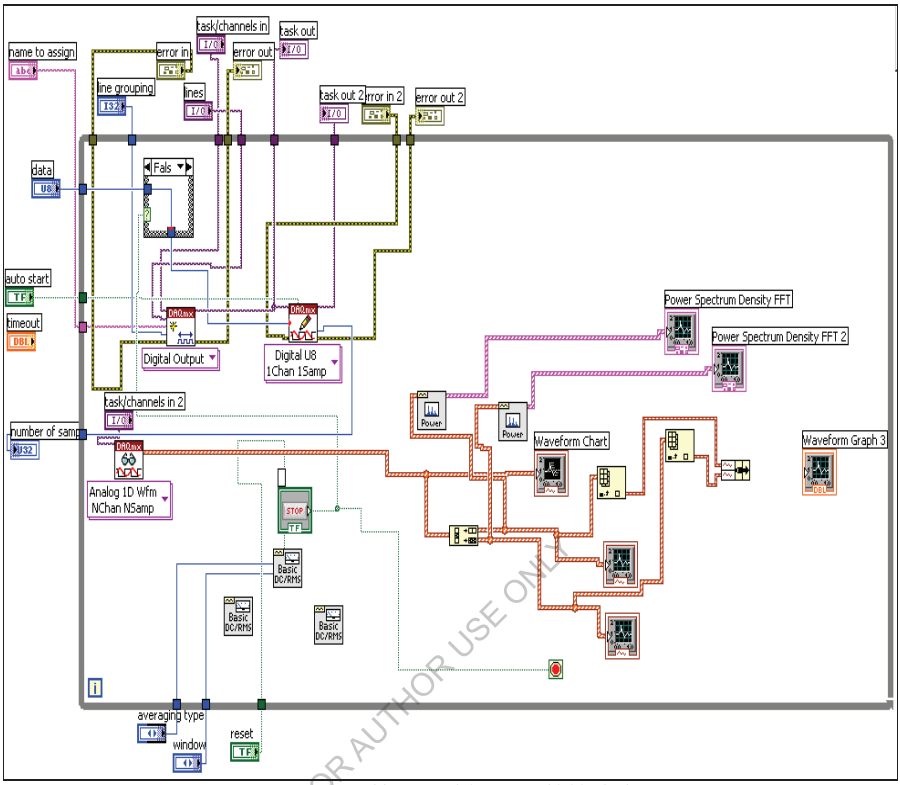

Fig.6.7. Block schema of the virtual acquisition LabView instrument for 5 simultaneously channels.

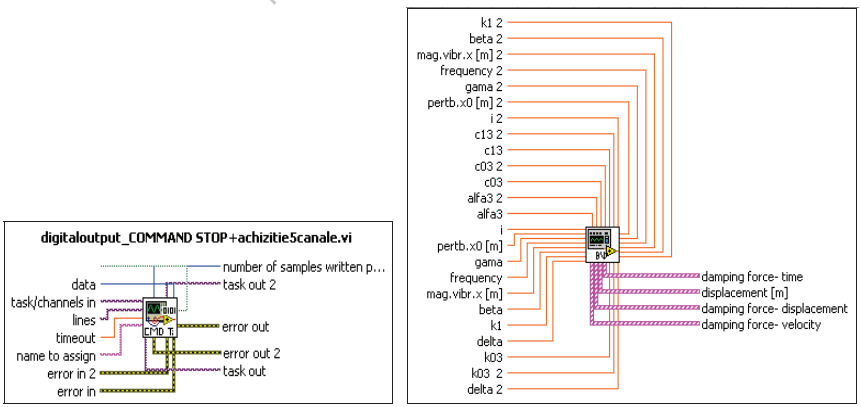

Fig.6.8. Icons of the LabView VI-s for the data acquisition and theoretical research.

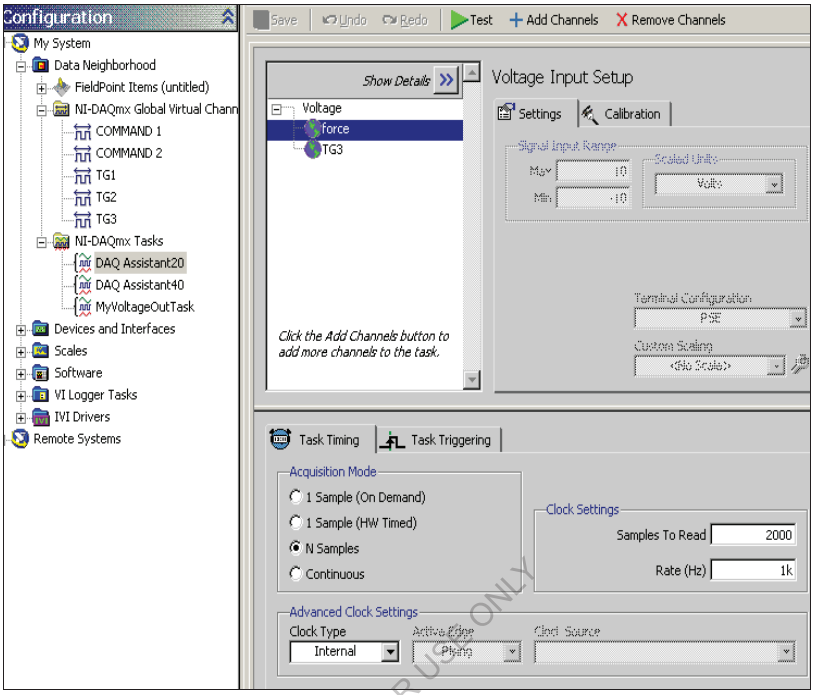

Fig.6.9. DAQ Assistant 20 acquisition task including acquisition on two simultaneous channels for force and angular velocity.

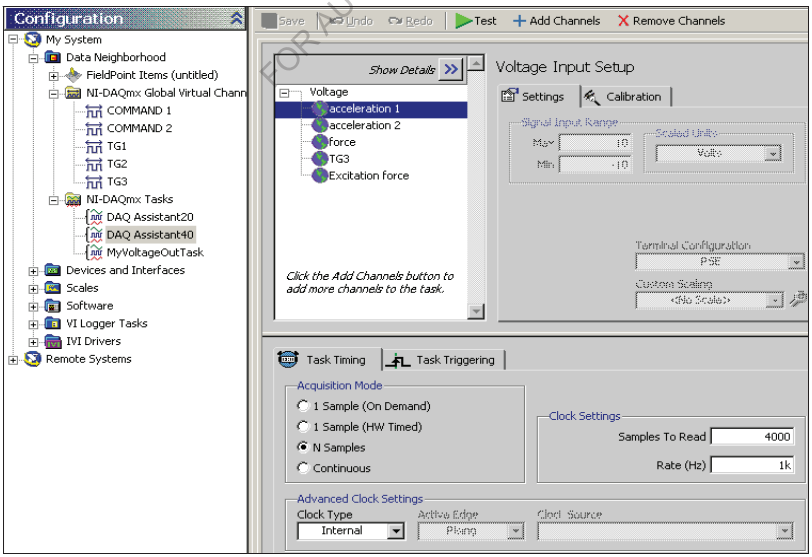

Fig.6.10. DAQ Assistant 40 acquisition task including acquisition on five simultaneous channels for acceleration on the robot base, acceleration on the end-effecter, excitation force, damper force and angular velocity.

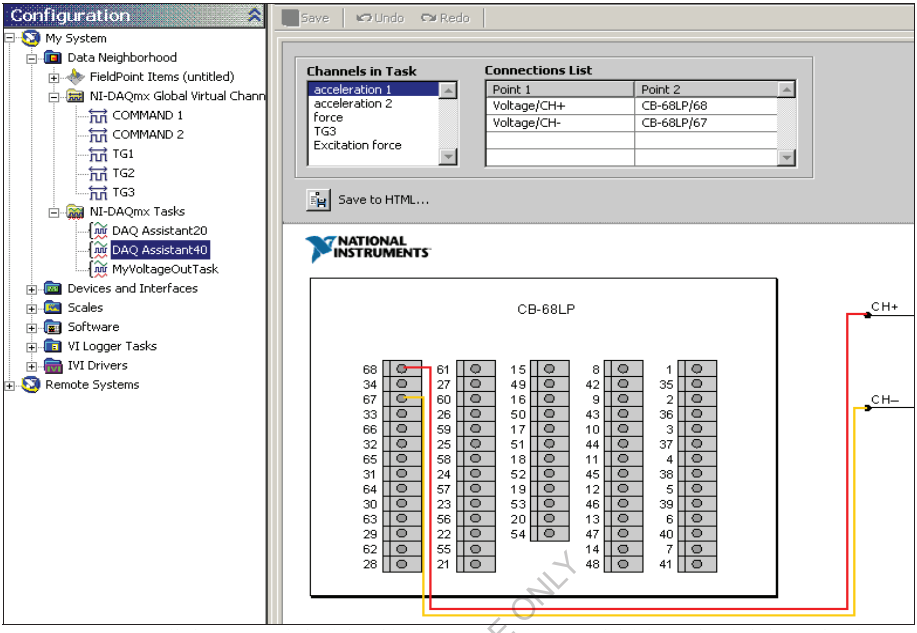

Fig.6.11. Connections to the connector of the acquisition board for the acquisition of the acceleration signal at the base of the robot.

The new mathematical model for the matrix-vector relation of the ***F-M*** force-moment column matrix, for ***RI***, with magnetorheological damper, will be of the form:

$$\begin{pmatrix} F^0 \\ M^0 \end{pmatrix} = \begin{bmatrix} z_u & 0 \\ 0 & z_u \end{bmatrix} \cdot \begin{pmatrix} D_i^0 (F_R^i + f(i)) \\ D_i^0 M_R^i \end{pmatrix} - diag \begin{bmatrix} sign \dfrac{v_u^i}{|v_u^i|} m_{u_i} & sign \dfrac{\omega_u^i}{|\omega_u^i|} J_{g_i} \end{bmatrix} \cdot \left[D_i^0 \right] \begin{pmatrix} \left(a_{i,0}^i\right) + \left[\widehat{\omega}_{i,0}^i\right]^2 \left(r_{g_i}^i\right) \\ \left(\varepsilon_{i,i-1}^i\right) + \left[\omega_{i-1,0}^i\right] \left(\omega_{i,i-1}^i\right) \end{pmatrix} +$$

$$+ \begin{bmatrix} z_u & 0 \\ 0 & z_u \end{bmatrix} \cdot \begin{pmatrix} (0) \\ \left[G_{i,k}\right] \left(\hat{b}_{i,k}\right) \left(\left(D_i^0 (F_R^i + f(i))\right) - diag \left[sign \dfrac{v_u^i}{|v_u^i|} m_{u_i} \right] \cdot \left[D_i^0\right] \left(a_{i,0}^i\right) + \left[\widehat{\omega}_{i,0}^i\right]^2 \left(r_{g_i}^i\right) \right) \end{pmatrix} \cdot \tag{6.3}$$

where ***f***(i) is the magnetorheological damping force.

The virtual tools developed for the research of the dynamic behavior of the elements and a systems by using transfer functions are shown in figs. 6.12...6.14.

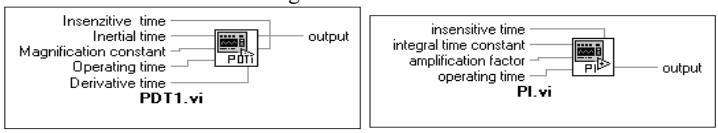

Fig.6.12. LabView icons for the virtual instrumentation of ***PDT***1 and ***PI*** transfer functions.

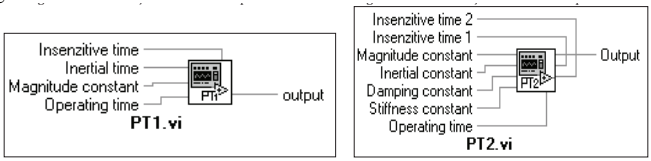

Fig.6.13. LabView icons for the virtual instrumentation of ***PT***1 and ***PT***2 transfer functions.

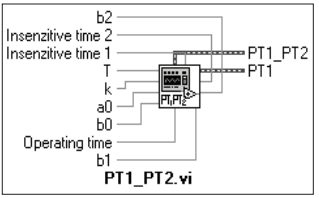

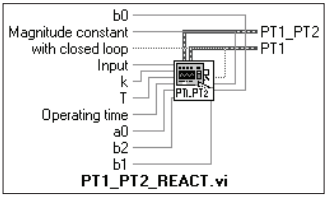

Fig.6.14. LabView icons for the virtual instrumentation for systems ***PT***1_***PT***2 and ***PT***1_***PT***2_***REACT*** transfer functions.

CHAPTER 7
Contributions and Experimental Research in the Technique of Using Intelligent Magnetorheological Dampers in Optimizing the Dynamic Behavior of RI

7.1. The intelligent damper concept and the intelligent damping structure. An intelligent shock absorber is part of a function within an intelligent system. In the in this case, the intelligent shock absorber ensures, instead of the actuator that introduces an active force, a damping force in accordance with the variable voltage with which the coils are supplied the shock absorber. This voltage is determined by the accelerometer mounted on the end-effector, depending on the vibrations of this module during operation, voltage vibrations, which then are transformed and applied by means of a 3-stage amplifier, at the level of the coils magnetorheological damper. Thus, the voltage oscillations, directly proportional to those of acceleration of the end-effector, are transformed at the level of the intelligent shock absorber oscillations of the damping force, see fig.7.1.

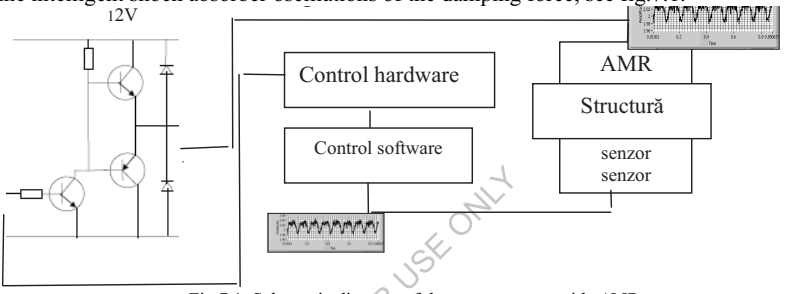

Fig.7.1. Schematic diagram of the smart system with ***AMR.***

Thus, the acceleration oscillations are transformed into voltage oscillations applied on the basis of the first amplification stage of the ***AMR***, 0.8-2[V], amplifier which is on the power path, (feeding with the voltage of 12[V]) of the ***AMR***. The results of using the intelligent structure with ***AMR*** can be seen in fig.7.2.

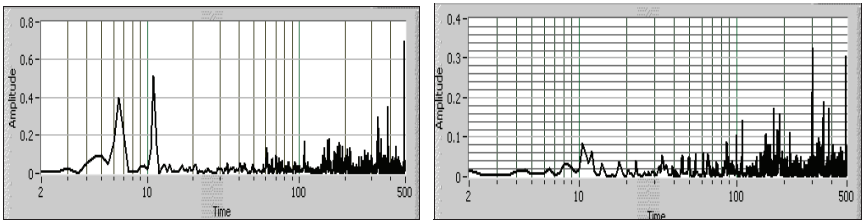

Fig.7.2. Fourier spectrum in the classical version and in the intelligent structure version.

The structure presented in fig.7.1. represents an intelligent structure for mitigating vibrations with ***AMR***. The vibration spectrum is determined by means of the data acquisition line that includes accelerometer type SN 30711 IMI, SUA, amplifier with a stage of amplifier, CB68 NI USA connector, PCI 6224M NI USA acquisition board, input port and own LabVIEW virtual acquisition tool. This spectrum from the sensor is then transformed through an amplifier and applied to the ***AMR***, through the same LabVIEW virtual instrument and another amplifier with three stages of amplification, the last stage controlling the power stage of the ***AMR*** (the 12[V] circuit of supply of ***AMR*** electromagnets). From the analysis of the preliminary results regarding the use of the intelligent vibration attenuation structure, it can be observed that by applying the signal taken from the accelerometers, the low frequency resonances are attenuated, fig.7.2, leaving the high frequency ones

which are less attenuated, due to the voltage oscillations, of low amplitude, which does not sensitize the base of the transistor in the first power stage. To mitigate the high-frequency vibrations, it is necessary to use a more complex amplifier that amplifies the high-frequency oscillating voltage up to the limit of the opening voltage of the transistor in the first amplification stage.

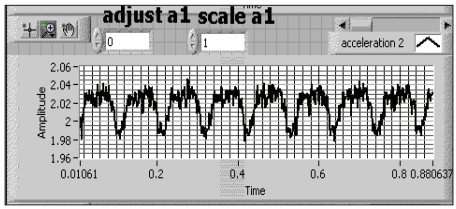

Fig.7.3. The signal of acceleration that will be amplifier and input on the smart damper.

7.2. Experimental determination of global dynamic compliance (*DGC*) and global dynamic viscous damping coefficient (*VGDDC*) and the introduction of intelligent magneto-rheological dampers (*AMRI*) in the *RI* structure. ***GDC*** global dynamic compliance is one of the most important parameters of the dynamic behavior of industrial robots. In robotic manufacturing systems, it is necessary to know the vibratory behavior of the robot, the global dynamic coefficient of viscous damping, ***VGDDC***, of the structure and how the variation of the acceleration of the robot modules influences the damped mechanical vibrations of the ***RI*** structure, in order to bypass the resonance frequencies in the Fourier spectrum.

The presented method of ***GDC***- assisted research of the robot with and without magnetorheological damper is a method that uses LabVIEW virtual instrumentation version 14.0 complete, both for theoretical research and for data acquisition. In this way, it is very easy to compare the theoretical and real behavior and to adjust the mathematical model that was the basis of the numerical simulation.

Vibration damping systems, as well as shock absorbers, are used to move vibrations within the Fourier spectrum. Anti-vibration isolation systems are usually passive and are used to reduce vibrations in the range of certain frequencies. But, often, in many robotic applications, the excitation forces vary in a very wide frequency range, and vibration dampers fail to reduce them throughout this range. In semi-active vibration damping systems, the stiffness and damping coefficient can be changed during movement. By changing the rigidity of the support of the damping system, the position of the poles of the vibrating system can be changed in order to avoid resonances.

On-line control aims to monitor the critical points of the structure and to know the frequency response of the system. This adaptive anti-vibration isolation system can change the operating conditions in accordance with the dominant load, regarding the anti-vibration isolation capacity compared to passive systems. Thus, forces with unwanted frequencies within the Fourier spectrum are reduced in different loading situations and a much wider frequency range is covered, in which they are active. Magnetorheological fluids are part of the class of smart materials, where the flow properties are quickly modified by applying a magnetic field. These changes are proportional to the intensity of the applied electric or magnetic field and are reversible in a time of the order of milliseconds. These fluids quickly pass from the fluid state to the semi-fluid, or semi-solid state, after the application of the magnetic field. These materials are relatively simple to apply and represent an interface between the control electronics and the mechanical system for moving the vibrations of the robot structure (Choi and Lee, 2001).

The determination of the proper vibration modes of the structure was applied to know the resonance frequencies. The frequency spectrum includes the amplitude-frequency and phase-frequency characteristics of the mechanical structure. The analysis of the frequency characteristics is very important for understanding the dynamic performance of the body-couple system of the robot structure.

If the dynamic impact with a periodic force at the base of the robot structure is $\boldsymbol{F}_s(t)$, and the response displacement of the tool center point, ***TCP*** is $\boldsymbol{x}(t)$, then the ***GDC*** of the ***TCP*** is defined by relation (7.1), where $EF(j\omega)$ and $Ex(j\omega)$ are the complex energy spectrum of the impact force, at the base of the robot structure, and respectively the response displacement of the ***TCP***.

Global dynamic compliance, ***GDC*** will be:

$$\frac{1}{k(j\omega)} = \frac{\int_0^T x(t)e^{-j\omega t}dt}{\int_0^T F_s(t)e^{-j\omega t}dt} = \frac{FFT(x)}{FFT(F)} = \frac{E_x(j\omega)}{E_F(j\omega)} \tag{7.1}$$

The ***GDC*** amplitude is calculated with the relation:

$$\frac{1}{k(\omega)} = \sqrt{(\mathrm{Re}\{\frac{1}{k(j\omega)}\})^2 + (\mathrm{Im}\{\frac{1}{k(j\omega)}\})^2} \tag{7.2}$$

The viscous global dynamic damper coefficient ***VGDDC***, ***c*** without magnetorheological damping, for each resonance frequency, is determined with the relation:

$$c_i = 2\xi_i \frac{k_i(\omega)}{\nu_{n_i}} \tag{7.3}$$

where ν_{ni} is the natural frequency.

The damping factor for each resonant frequency, ξ_i is determined from the Fourier spectrum by relation:

$$\xi_i = \frac{\nu_{i1} - \nu_{i2}}{2\nu_{iR}} \tag{7.4}$$

where ν_{1i} and ν_{2i} are the frequencies obtained by method 2 [2] for each resonance frequency. The equivalent global dynamic coefficient of viscous damping, which is obtained with the relation:

$$c_{eq} = \frac{E}{\pi\omega x^2} \tag{7.5}$$

where: ***E*** is the damping energy in one cycle, [Nm]; $\boldsymbol{\omega}$ - response pulsation of the robot arm [rad/s]; ***x***- displacement for each resonant frequency, [m]. The damping energy is determined with the relation:

$$E = \int_0^{2\pi/\omega} F(t)x'(t)dt \tag{7.6}$$

where: ***F***(t) is the variable damping force determined experimentally through data acquisition, [N]; ***x***'(t) – speed of movement of the arm determined by the derivation of the movement characteristic, [m/s].The total global dynamic coefficient, after applying ***AMR*** is:

$$c_f = c + c_{eq} \tag{7.7}$$

The results can be seen in tables 7.1-7.6., and the 3D characteristics of ***VGDDC*** and ***VGDDEC*** in fig.7.4-7.7. It can be noted that by increasing the intensity of the supply current of the damper coils, the ***VGDDEC*** increase is obtained for each resonance in the Fourier spectrum. Through a command law by points or according to a predefined mathematical curve for the control voltage of the ***AMR***, depending on the Fourier experimental spectrum, the Fourier vibration spectrum can be obtained as desired. The assisted research of the global dynamic compliance ***GDC***, of the viscous global dynamic damper coefficient ***VGDDC***, of the viscous global dynamic damper equivalent coefficient ***VGDDEC*** as well as the influence of the parameters of the magnetorheological damper ***AMR*** on the dynamic behavior as a whole, paves the way for the optimization of the Fourier spectrum for the entire frequency spectrum. By applying intelligent magnetorheological dampers, it will be possible, relatively easily, to move the resonance frequencies in the attenuation band, by activating the damper coils with different intensities depending on the amplitude of the vibrations determined by the accelerometers.

TABLE 7.1. Global dynamic compliance of the researched robot structure (***GDC***) [cm/daN].

	rezonance frequencies											
	50	65	70	80	90	100	110	120	130	160	170	180	200
csi	0.4	0.307692	0.285714	0.25	0.222222	0.2	0.181818	0.166667	0.153846	0.125	0.117647	0.111111	0.1
	0.6	0.6	0.6	0.01	0.5	0.01	0.01	1.2	0.1	0.5	0.8	0.5	0.01
	0.18	0.2	0.4	0.01	0.1	0.01	0.65	0.01	0.01	0.1	0.25	0.1	0.01
	0.2	0.2	0.6	0.25	0.01	0.1	0.1	0.2	0.18	0.01	0.01	0.01	1.2
1/k	0.01	0.01	0.7	0.01	0.1	0.1	0.1	0.01	0.11	0.1	0.2	0.2	0.05
	0.01	0.01	0.8	0.1	0.1	0.2	0.2	0.01	0.4	0.01	0.25	0.25	0.15
	0.01	0.01	0.25	0.01	0.05	0.1	0.1	0.01	0.1	0.2	0.01	0.2	0.45
	0.01	0.01	0.1	0.01	0.1	0.25	0.25	0.01	0.25	0.4	0.4	0.4	1.2

TABLE 7.2. Global dynamic stiffness of the researched robot structure (***GDR***) [daN/cm].

	1.666667	1.666667	1.666667	100	2	100	100	0.833333	10	2	1.25	2	100
	5.555556	5	2.5	100	10	100	1.538462	100	100	10	4	10	100
	5	5	1.666667	4	100	10	10	5	5.555556	100	100	100	0.833333
k	100	100	1.428571	100	10	10	10	100	9.090909	10	5	5	20
	100	100	1.25	10	10	5	5	100	2.5	100	4	4	6.666667
	100	100	4	100	20	10	10	100	10	5	100	5	2.222222
	100	100	10	100	10	4	4	100	4	2.5	2.5	2.5	0.833333

TABLE 7.3. Viscous Global Dynamic Damping Coefficient (***VGDDC***) [Ns/m].

	0.026667	0.015779	0.013605	0.625	0.009877	0.4	0.330579	0.002315	0.023669	0.003125	0.00173	0.002469	0.1
	0.088889	0.047337	0.020408	0.625	0.049383	0.4	0.005086	0.277778	0.236686	0.015625	0.005536	0.012346	0.1
	0.08	0.047337	0.013605	0.025	0.493827	0.04	0.033058	0.013889	0.013149	0.15625	0.138408	0.123457	0.000833
c	1.6	0.946746	0.011662	0.625	0.049383	0.04	0.033058	0.277778	0.021517	0.015625	0.00692	0.006173	0.02
	1.6	0.946746	0.010204	0.0625	0.049383	0.02	0.016529	0.277778	0.005917	0.15625	0.005536	0.004938	0.006667
	1.6	0.946746	0.032653	0.625	0.098765	0.04	0.033058	0.277778	0.023669	0.007813	0.138408	0.006173	0.002222
	1.6	0.946746	0.081633	0.625	0.049383	0.016	0.013223	0.277778	0.009467	0.003906	0.00346	0.003086	0.000833

TABLE 7.4. The viscous global dynamic damping coefficient (***VGDDTC***) [Ns/m] when ***i***=0 [A].

	50	65	70	80	90	100	110	120	130	160	170	180	200
	1683.6667	2014.7791	2125.6054	2960	2567.8765	3180	3333.5785	3227.3148	3469.6686	4115.125	4335.7301	4558.4691	5100
	1745.8889	2046.3373	2132.4082	2960	2607.3827	3180	3008.0858	3502.7778	3682.6864	4127.625	4339.5363	4568.3457	5100
c+c_equiv.	1737	2046.3373	2125.6054	2360	3051.8272	2820	3036.0579	3238.8889	3459.1492	4268.25	4472.4083	4679.4568	5000.8333
[Ns/m]	3257	2945.7456	2123.6618	2960	2607.3827	2820	3036.0579	3502.7778	3467.5169	4127.625	4340.9204	4562.1728	5020
i=0	3257	2945.7456	2122.2041	2397.5	2607.3827	2800	3019.5289	3502.7778	3451.9172	4268.25	4339.5363	4560.9383	5006.6667
	3257	2945.7456	2144.6531	2960	2656.7654	2820	3036.0579	3502.7778	3469.6686	4119.8125	4472.4083	4562.1728	5002.2222
	3257	2945.7456	2193.6327	2960	2607.3827	2796	3016.2231	3502.7778	3455.4675	4115.9063	4337.4602	4559.0864	5000.8333

TABLE 7.5. The viscous global dynamic damping total coefficient (***VGDDTC***) [Ns/m] when ***i***=0.3 [A].

	2606.667	2932.779	3041.605	3877	3484.877	4098	4251.579	4146.315	4390.669	5041.125	5262.73	5487.469	6032
	2668.889	2964.337	3048.408	3877	3524.383	4098	3926.086	4421.778	4603.686	5053.625	5266.536	5497.346	6032
c+c_equiv	2660	2964.337	3041.605	3277	3968.827	3738	3954.058	4157.889	4380.149	5194.25	5399.408	5608.457	5932.833
[Ns/m]	4180	3863.746	3039.662	3877	3524.383	3738	3954.058	4421.778	4388.517	5053.625	5267.92	5491.173	5952
i=0.3	4180	3863.746	3038.204	3314.5	3524.383	3718	3937.529	4421.778	4372.917	5194.25	5266.536	5489.938	5938.667
	4180	3863.746	3060.653	3877	3573.765	3738	3954.058	4421.778	4390.669	5045.813	5399.408	5491.173	5934.222
	4180	3863.746	3109.633	3877	3524.383	3714	3934.223	4421.778	4376.467	5041.906	5264.46	5488.086	5932.833

TABLE 7.6. The viscous global dynamic damping equivalent coefficient (***VGDDEC***), [Ns/m] vs.intensity [A] and freq.

c_equiv	i=0 [A]	1657	1999	2112	2335	2558	2780	3003	3225	3446	4112	4334	4556	5000
	i=0.3 [A]	2580	2917	3028	3252	3475	3698	3921	4144	4367	5038	5261	5485	5932
	i=0.45 [A]	2377	2411	2443	2473	2503	2533	2563	2593	2623	2714	2744	2775	2836

7.3. Assisted experimental research in order to validate the proposed mathematical model and the AMR effect on the dynamic behavior of the RI. Experimental research in order to validate the model mathematically proposed consisted in experimental determination of strength characteristics vs. speed and comparison them with the strength characteristics vs. speed determined by numerical simulation. In a first phase, the comparison performed between features obtained experimentally and those generated by the mathematical modified Bouc-Wen model taken from research bibliography of the current state.

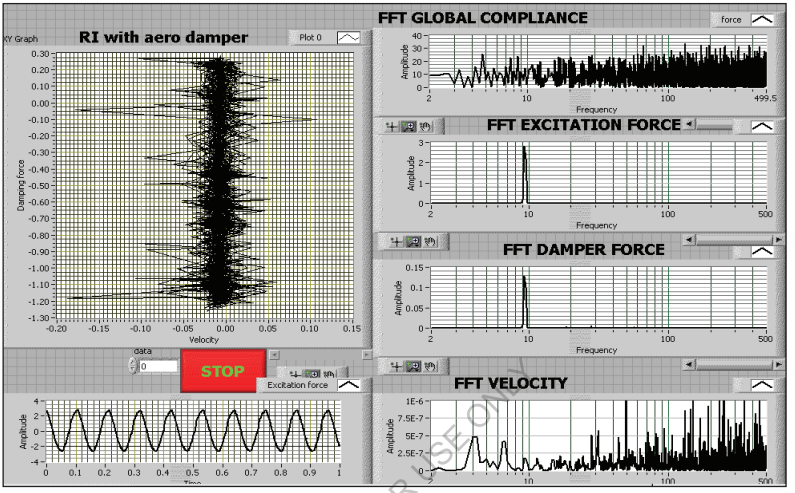

Fig.7.4. The real characteristics force vs. speed, excitation force vs. time and the Fourier spectra vs. speed, damping force, excitation force and global compliance for the case of using an air damper for the excitation frequency of 10Hz.

It was observed that these characteristics are very different, which led to the approach of a mathematical model more elaborated and completed with four additional equations and an equation that takes into account the Fourier spectrum. In this case, the proposed mathematical model has an additional 19 new parameters, which made the identification activity difficult. By using the LabVIEW virtual equipment for simulation, as well as the parametrization of the force vs. speed characteristics of the shock absorber, it was possible to identify the coefficients, which would ultimately lead to obtaining comparative force vs. speed characteristics that would fall within an error of maximum 1%, compared to the real characteristics. For the assisted determination of the coefficients of the mathematical model, the parameterization of the force vs. speed characteristics was carried out, so that through the assisted numerical simulation, the way in which the various coefficients of the mathematical model influence the various parameters of the characteristic and obviously the exact establishment of their values to be determined leads to obtaining characteristics as close as possible to the real ones. The simulated characteristics for ***AMR***, very close to the real characteristics, were obtained following the research on the model, for various values of the coefficients of the proposed model. So that, based on the successive comparison of the various characteristics obtained by simulation, with those obtained experimentally, in the end, an approximation of them was obtained shown in fig. 7.40. The mathematical model for ***AMR*** used in the experimental research and validated by the comparative method is presented in subchapter 7.5. The real force-velocity characteristics, determined experimentally for the researched didactic robot, on which the air shock absorber and the magnetorheological shock absorber ***AMR*** were mounted, are presented in fig. 7.9-7.31.

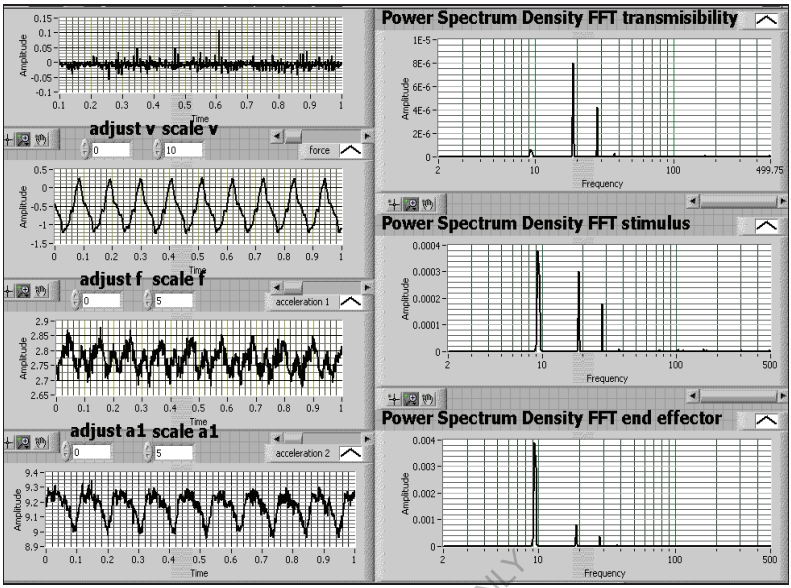

Fig.7.5. The real characteristics of damping force, excitation force, base acceleration and end-effector acceleration vs. time and the Fourier spectra for the base, end-effector and transmissibility for the case of using an air damper for an excitation frequency of 10Hz.

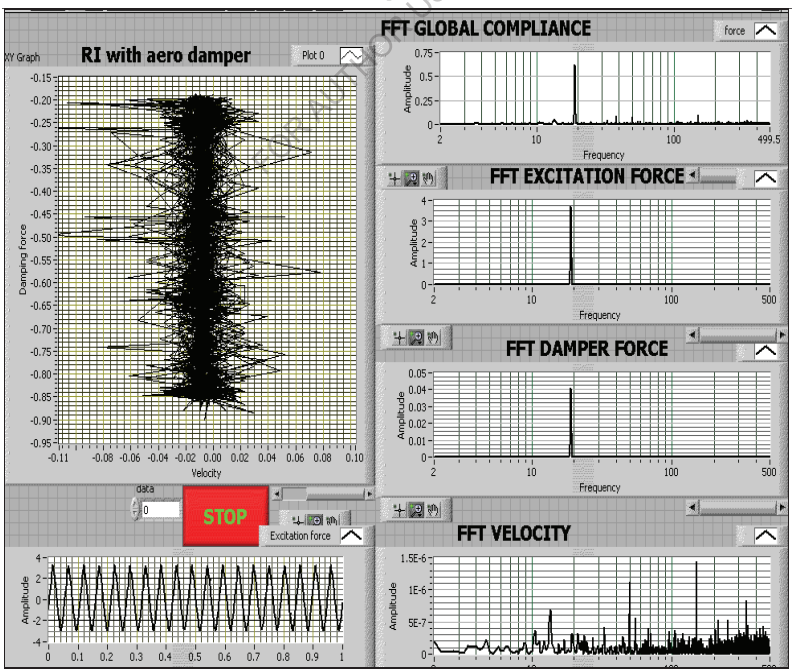

Fig.7.6. The real characteristics force vs. speed, excitation force vs. time and the Fourier spectra for speed, damping force, excitation force and global compliance for the case of using an air damper for the excitation frequency of 20Hz.

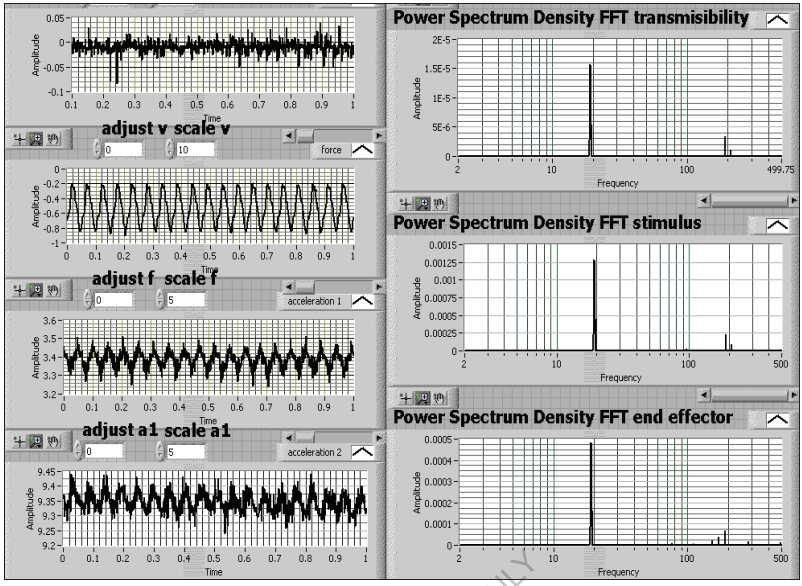

Fig.7.7. The real characteristics of damping force, excitation force, base acceleration and end-effector acceleration vs. time and the Fourier spectra for the base, end-effector and transmissibility for the case of using an air damper for an excitation frequency of 20Hz.

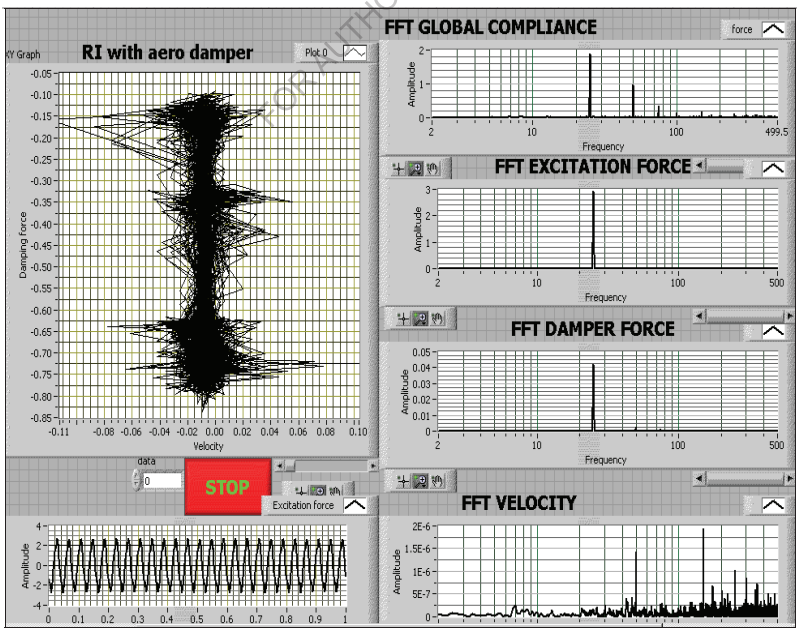

Fig.7.8. The real characteristics force vs. speed, excitation force vs. time and the Fourier spectra for speed, damping force, excitation force and global compliance for the case of using an air damper for the excitation frequency of 25Hz.

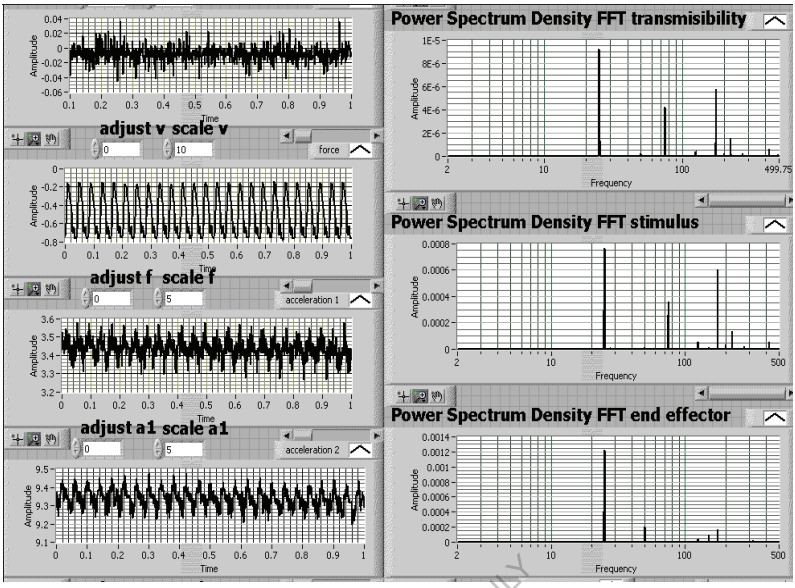

Fig.7.9. The real characteristics of damping force, excitation force, base acceleration and end-effector acceleration vs. time and the Fourier spectra for the base, end-effector and transmissibility for the case of using an air damper for the excitation frequency of 25Hz.

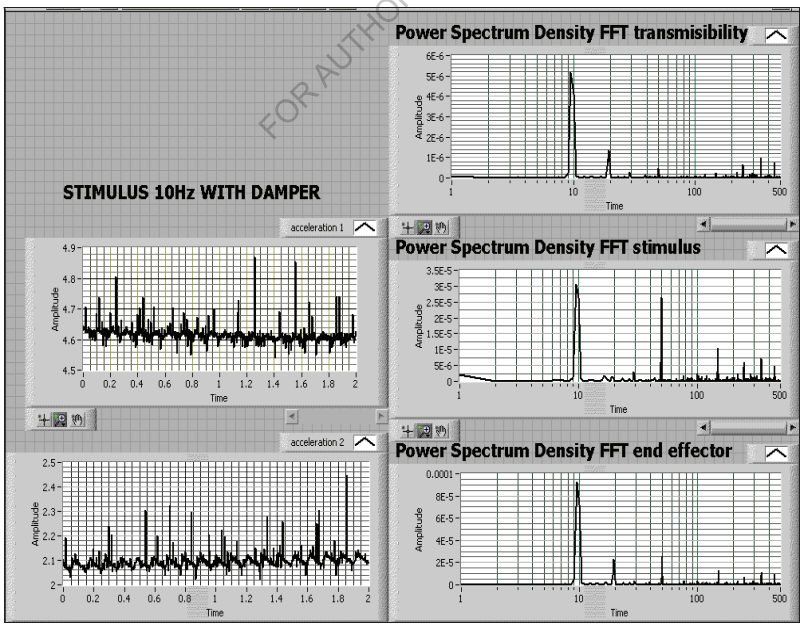

Fig.7.10. The real acceleration characteristics of the base and end-effector vs. time and the Fourier spectra for the base, end-effector and transmissibility in the case of ***AMR*** and excitation with a frequency of 10Hz.

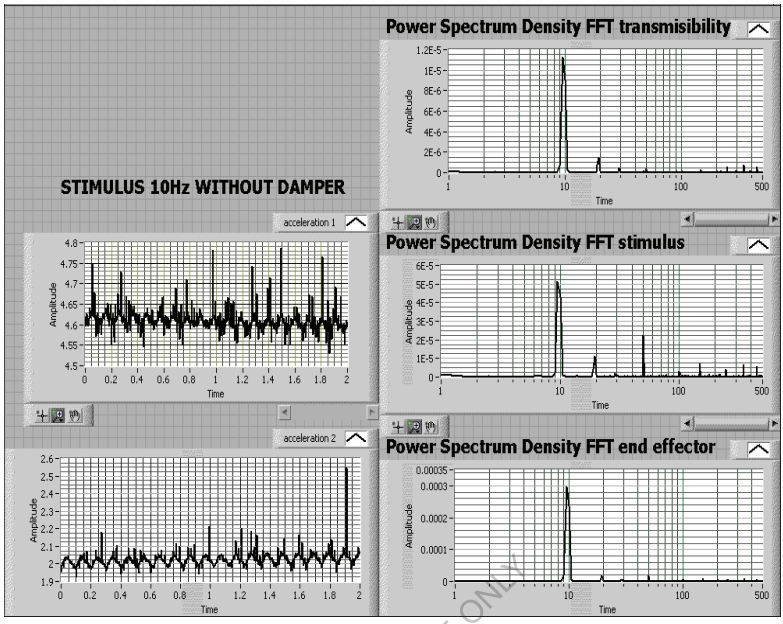

Fig.7.11. The real acceleration characteristics of the base and end-effector vs. time and the Fourier spectra for the base, end-effector and transmissibility in the case without a damper and excitation with a frequency of 10Hz.

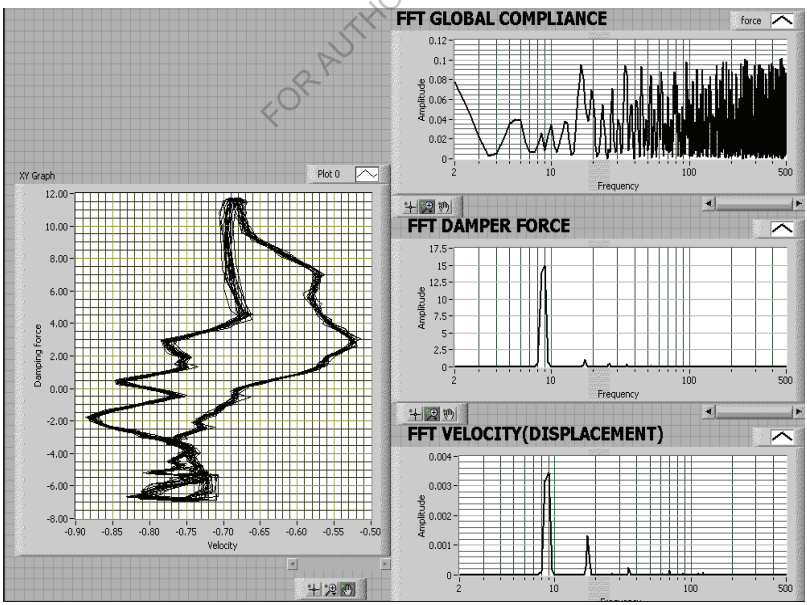

Fig.7.12. The real force vs. speed characteristics and the Fourier spectra for speed, damping force and ***CDG*** for the case with ***AMR*** and an excitation with a frequency of 9Hz.

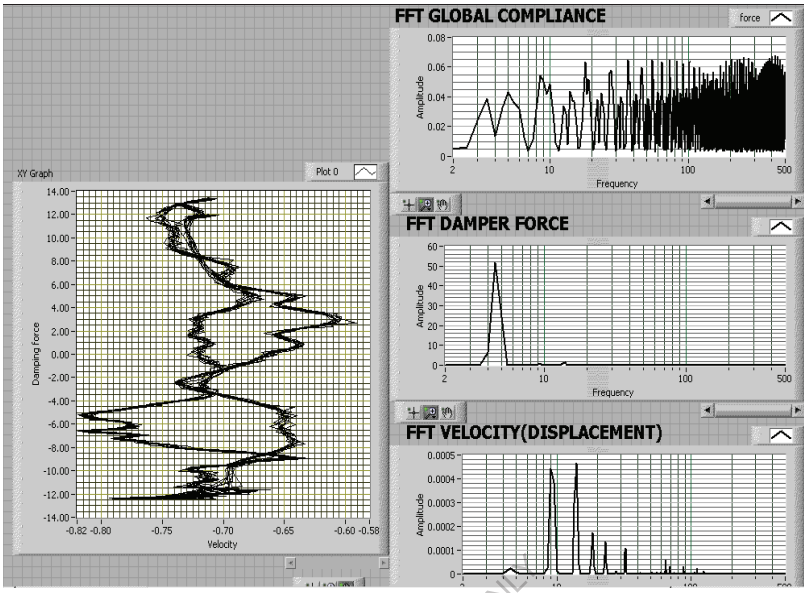

Fig.7.13. The real force vs. speed characteristics but the Fourier spectra for speed, damping force and ***CDG*** for the case with ***AMR*** and an excitation with a frequency of 5Hz.

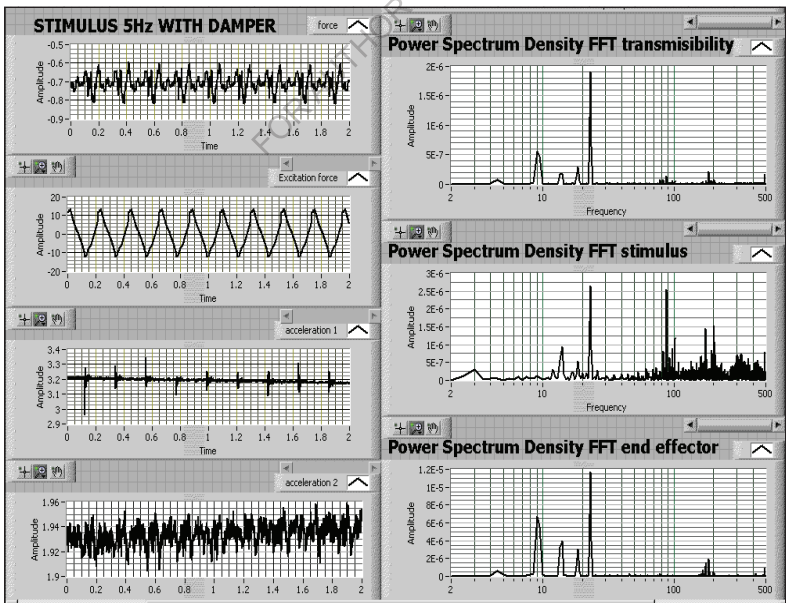

Fig.7.14. The real characteristics of damping force, excitation force, base and end-effector acceleration vs. time and the Fourier spectra for the base, end-effector and transmissibility for the case with AMR and excitation with a frequency of 5Hz.

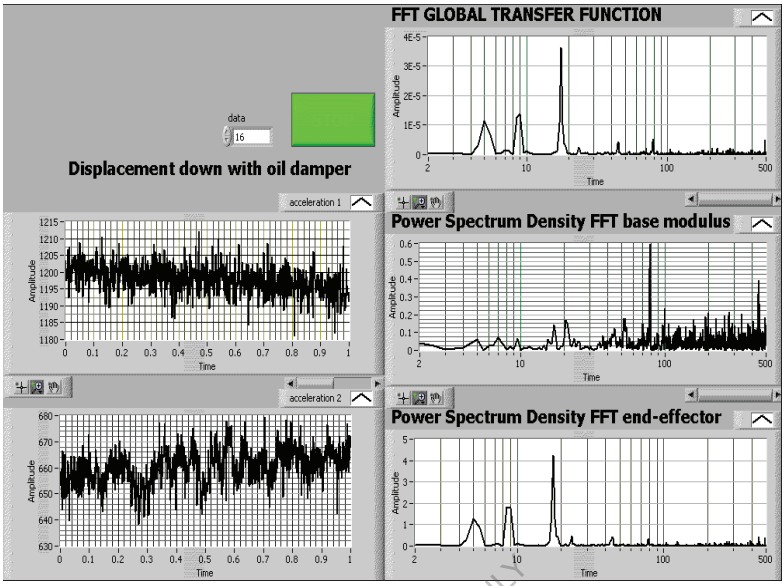

Fig.7.15. Actual base and end-effector acceleration characteristics and Fourier spectra for the base, end-effector and ***FTG*** global transfer function for the downward ***AMR*** arm movement.

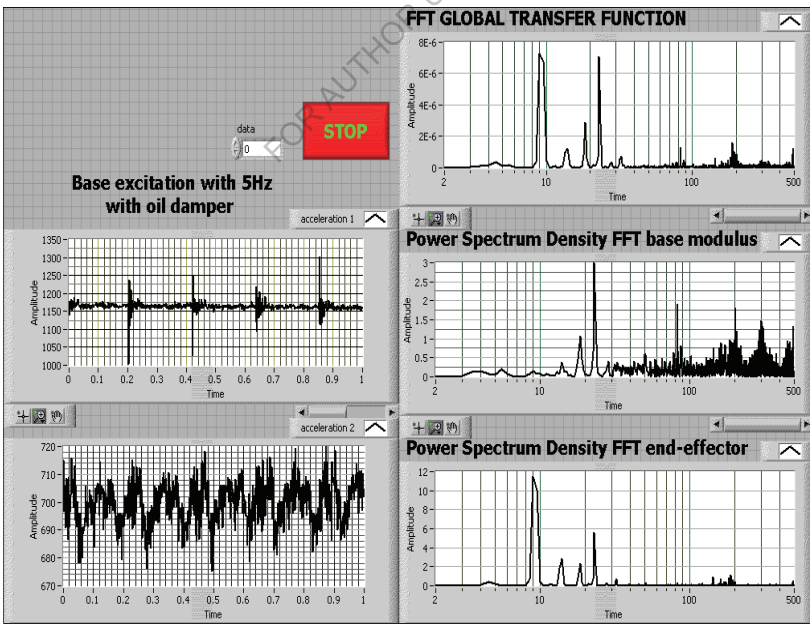

Fig.7.16. The real characteristics of the base and end-effector acceleration vs. time and the Fourier spectra for the base, end-effector and ***FTG*** for the robot with ***AMR*** and 5Hz base excitation.

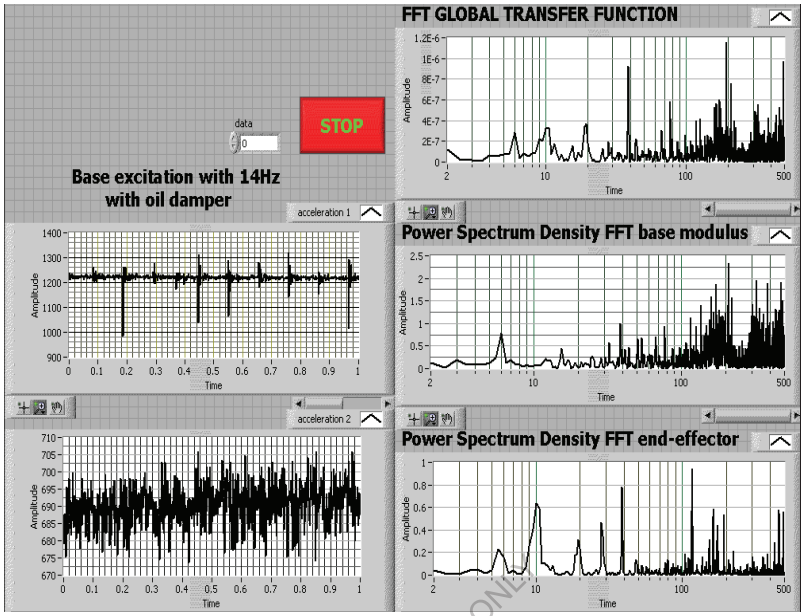

Fig.7.17. The real characteristics of the base and end-effector acceleration vs. time and the Fourier spectra for the base, end-effector and ***FTG*** for the robot with ***AMR*** and 14Hz base excitation.

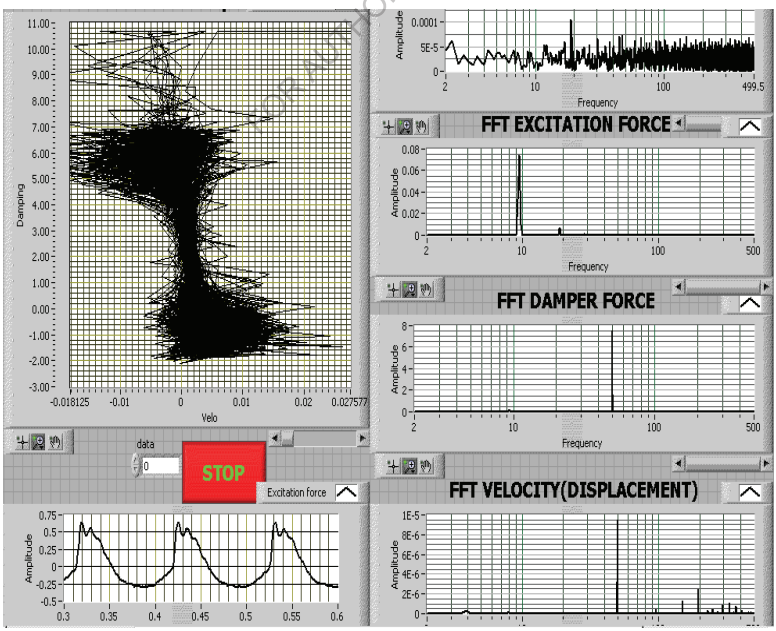

Fig.7.18. Actual damping force-vs. speed characteristics for ***RI*** with ***AMR*** with 9 Hz base excitation.

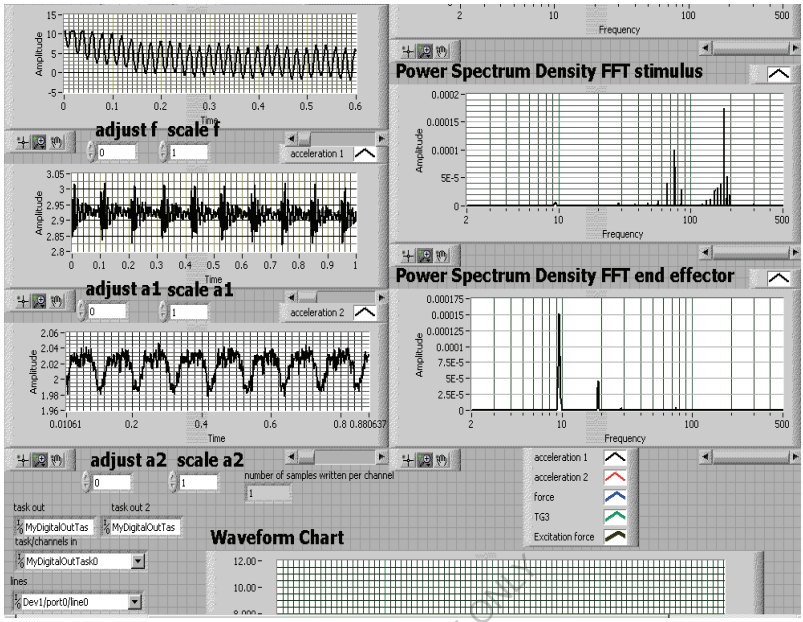

Fig.7.19. The real base and end-effector acceleration characteristics and the base and end-effector frequency spectra for ***RI*** with ***AMR*** with 9Hz base excitation.

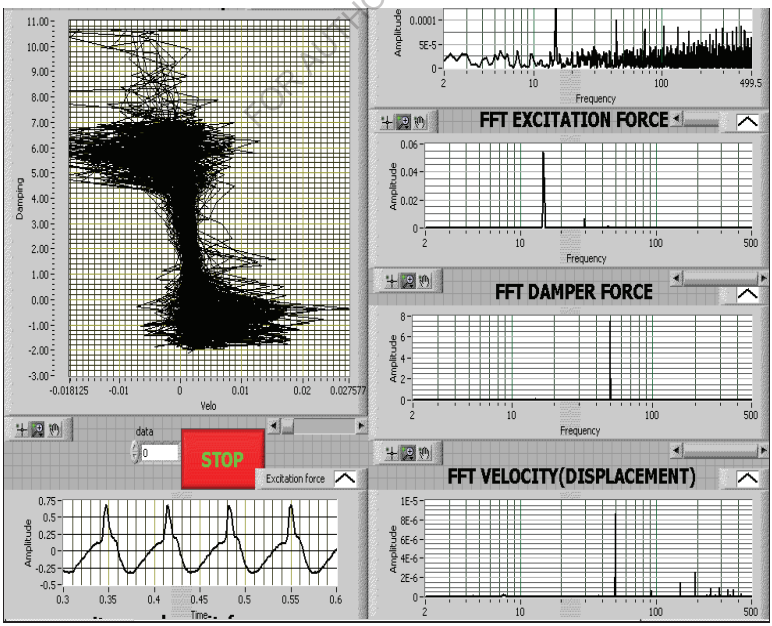

Fig.7.20. Actual damping force-vs. speed characteristics for ***RI*** with ***AMR*** with 17Hz base excitation.

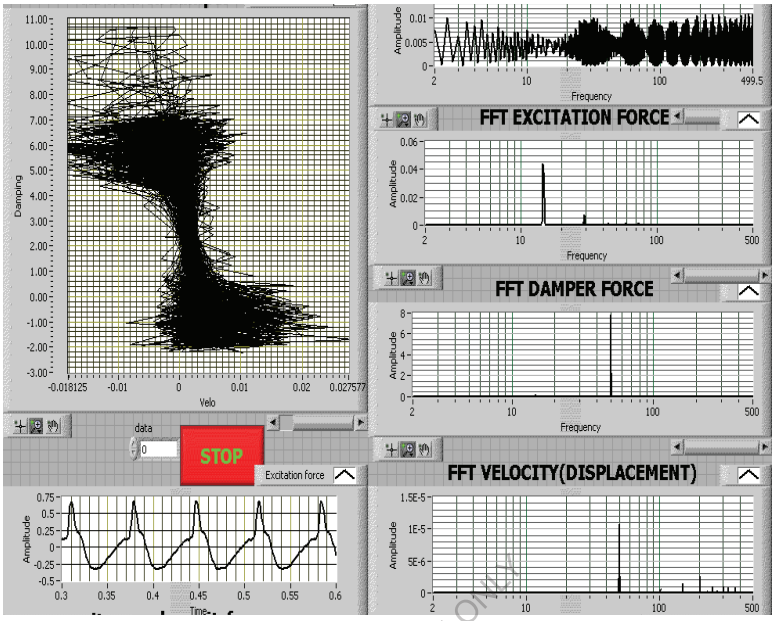

Fig.7.21. Actual damping force-vs. speed characteristics for ***RI*** with ***AMR*** with 15Hz base excitation.

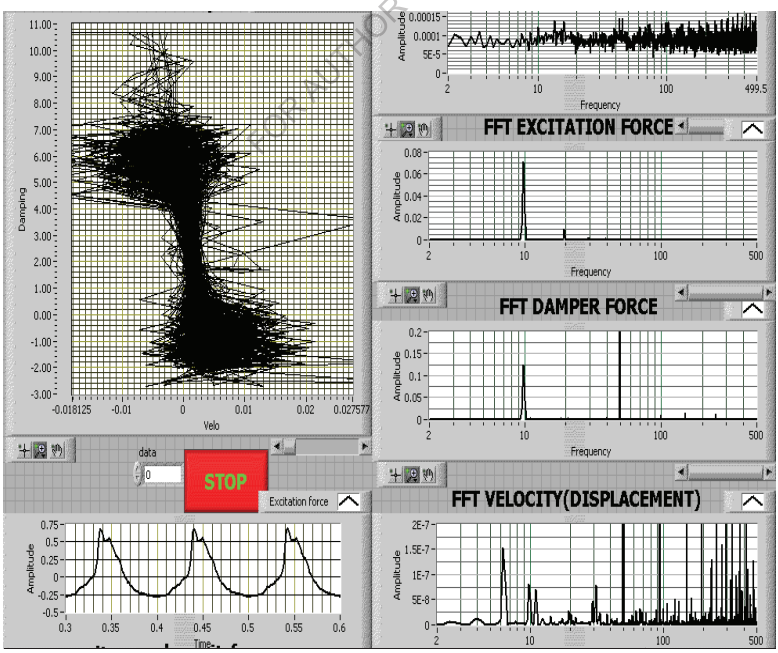

Fig.7.22. Actual damping force-vs. speed characteristics for ***RI*** with ***AMR*** with 10Hz base excitation.

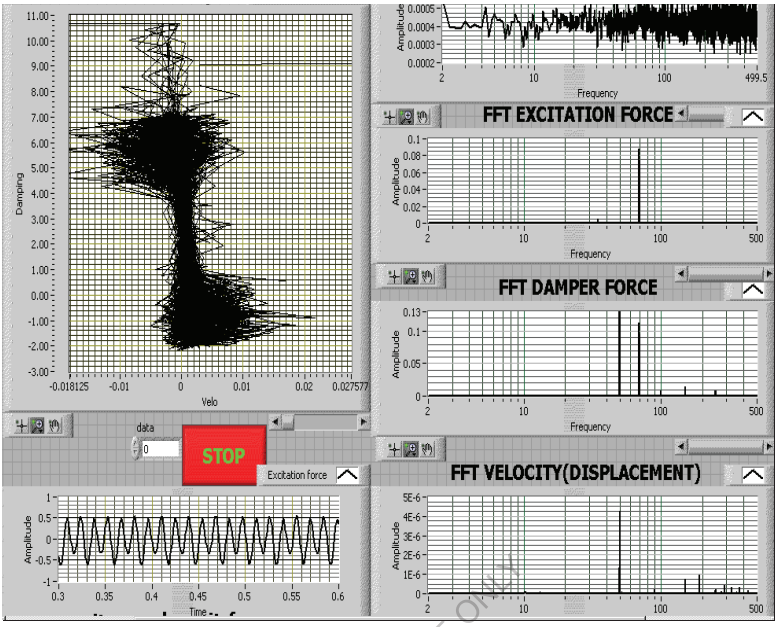

Fig.7.23. Actual damping force-vs. speed characteristics for ***RI*** with ***AMR*** with 70Hz base excitation.

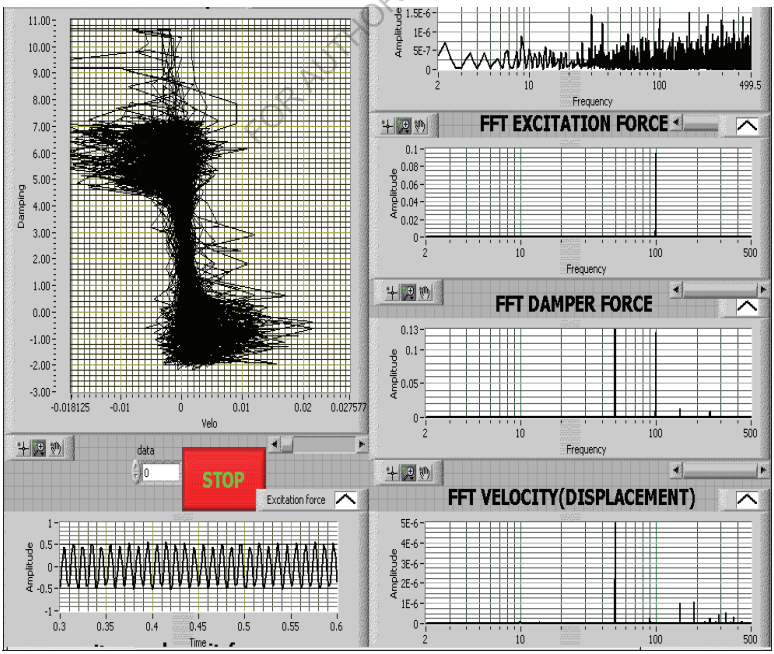

Fig.7.24. Actual damping force-vs. speed characteristics for ***RI*** with ***AMR*** with 100Hz base excitation.

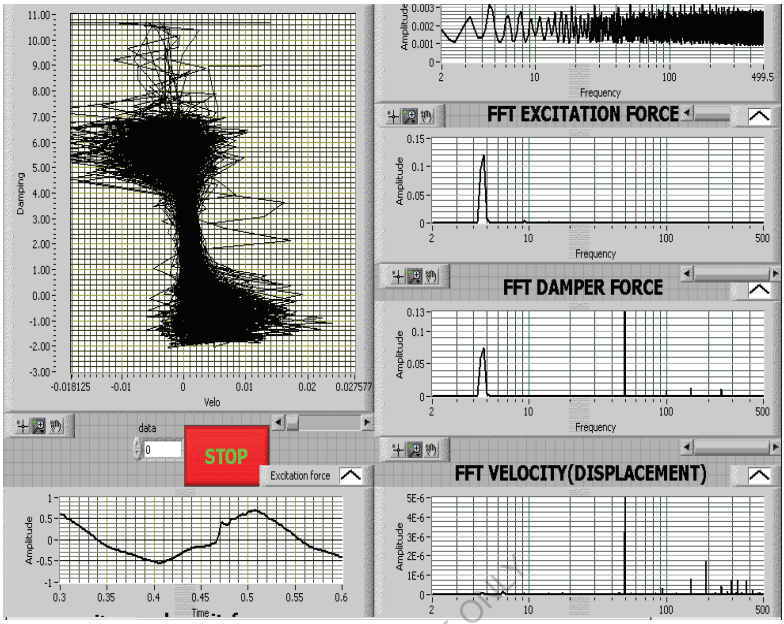

Fig.7.25. Actual damping force-vs. speed characteristics for ***RI*** with *AMR* with 5Hz base excitation.

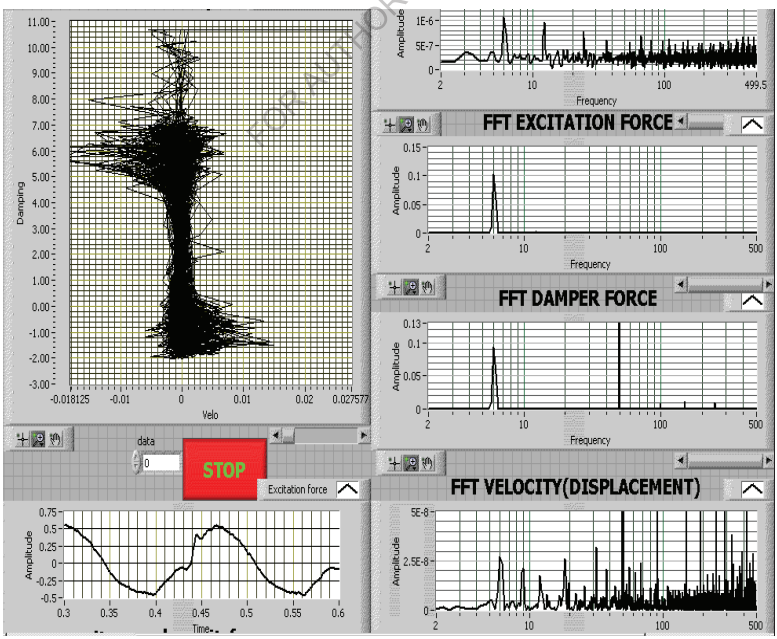

Fig.7.26. Actual damping force-vs. speed characteristics for ***RI*** with ***AMR*** with 6Hz base excitation.

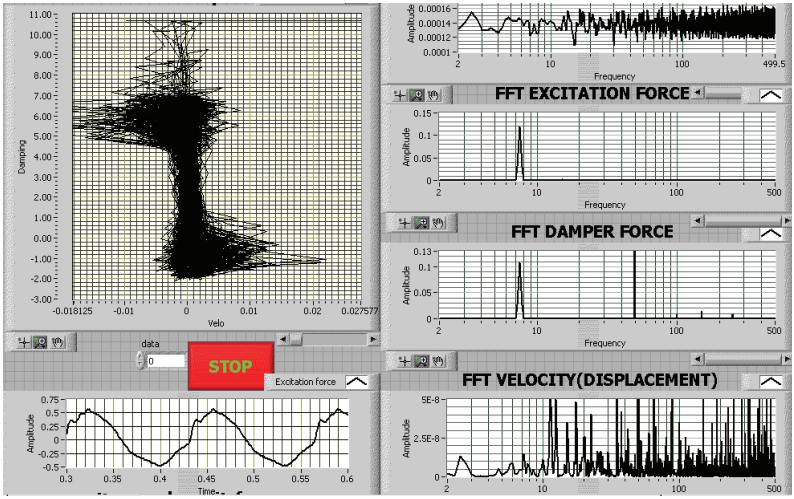

Fig.7.31. Caracteristicile reale forta de amortizare- viteza de deplasare pentru RI

Fig.7.27. Actual damping force-vs. speed characteristics for ***RI*** with ***AMR*** with 8Hz base excitation.

7.4. Synthesizing some results of specific AMR characteristics such as damping force-velocity, damping force-displacement, speed and displacement as a function of time obtained in the experimental research. Following the analysis of the real and frequency characteristics, determined experimentally for the vibration damping of the researched teaching structure, in the version with magnetorheological damper, with air damper and without damper, the data summarized in tables 7.7-7.9 resulted. They contain information on transmissibility ***TR***, global dynamic compliance ***GDC***, damping force, damping energy, etc.

TABLE 7.7. Variation of global dynamic transmissibility and compliance in motion with air damper.

in miscarea cu amortizor cu aer (achizitie pe 5 canale simultane)

Frecventa de excitatie [Hz]	Tip amortizor	Transmisibilitatea frecventa/amplitudine [Hz]/[mm/daN] [v] /[A]	Complianta Dinamica Globala frecventa/amplitudine [Hz]/[mm/daN] [v] /[A]	Forta de amortizare [daN] [v] /[A]	Forta de amortizare - viteza de deplasare [$F_{min-max}$]/ [$v_{min-max}$]
10	Amortizor cu aer	10/0.5 10^{-6}; 19/8 10^{-6}; 28/4 10^{-6}	4/20; 7/19; 8/19; 12/18; 14/18; 18/18; 19/18; 20/19; 21/19; 25/18; 28/19; 32/17	9/0.12; 18/0.01; 28/0.01	-1.3 la 0.2/ -0.05 la 0.05 (1.5/0.1) **15**
20	-''-	20/1.5 10^{-5}; 190/3 10^{-6}; 210/1 10^{-6}	20/0.6; 28/0.14; 40/0.14; 150/0.15	20/0.04	-0.9 la -0.2/ -0.04 la 0.04 (0.7/0.08) **8.75**
25	-''-	25/9 10^{-6}; 75/4 10^{-6}; 130/0.5 10^{-6}; 180/5 10^{-6}; 220/1.5 10^{-6}; 420/0.5 10^{-6}	25/1.8; 50/1; 75/0.4; 100/0.2; 150/0.2; 250/0.1	25/0.04; 50/0.002; 75/0.001	-0.8 la -0.1/ -0.04 la 0.02 (0.7/0.06) **11.66**
30	-''-	30/1 10^{-6}; 88/7 10^{-6}; 120/1.4 10^{-6}; 180/3.8 10^{-6}; 200/9 10^{-6}; 220/1.2 10^{-6}	21/0.1; 30/1; 50/0.4; 80/0.1; 88/0.25; 120/0.1; 150/0.3; 250/0.1	30/0.07; 88/0.005	-1 la -0.15/ -0.06 la 0.04 (0.85/0.1) **8.5**
35	-''-	38/1 10^{-6}; 90/7 10^{-6}; 130/1.4 10^{-6}; 190/3.8 10^{-6}; 210/8 10^{-6}; 240/1.2 10^{-6}	35/4.2; 50/0.5; 70/2; 80/0.1; 100/2; 140/1; 150/0.5; 180/0.5; 250/0.5	35/0.05; 70/0.025; 100/0.05	-0.9 la -0.05/ -0.05 la 0.03 (0.85/0.08) **10.625**
50	-''-	50/1.2 10^{-5}; 150/0.00025 10^{-6}; 200/5 10^{-6}; 250/0.002 10^{-6}	4/120; 7/150; 12/120; 15/120; 18/110; 22/140; 26/130; 30/100; 32/110; 34/110; 40/180; 45/120; 50/120; 52/120; 55/150; 60/140; 63/110; 70/150; 80/90; 85/110; 90/180; 95/110; 100/160; 110/160; 120/150; 130/90; 140/150; 150/150; 200/150	50/0.08;	-1 la 0/ -0.05 la 0.04 (1/0.09) **11.11**
60	-''-	60/0.8 10^{-6}; 180/3.8 10^{-6}	4/0.02; 50/0.05; 60/0.18; 150/0.05; 170/0.04; 230/0.03; 250/0.05; 400/0.05	60/0.014	-0.8 la -0.25/ -0.04 la 0.04 (0.55/0.08)

					6.875
70	-‘’-	70/2.8 10^{-5}; 150/1 10^{-6}; 200/2.5 10^{-5}; 400/1 10^{-6}	25/0.02; 30/0.02; 32/0.03; 40/0.01; 50/0.15; 58/0.03; 68/0.02; 70/0.01; 150/0.08; 250/0.07; 350/0.07	70/0.0035	-0.66 la -0.36/ -0.05 la 0.04 (0.3/0.09) **3.33**
80	-‘’-	40/0.2 10^{-6}; 80/3.5 10^{-6}; 120/0.4 10^{-6}; 160/0.5 10^{-6}; 190/0.55 10^{-6}; 220/0.1 10^{-6}	4/0.01; 20/0.01; 32/0.01; 50/0.13; 90/0.01; 100/0.01; 120/0.04; 150/0.075; 220/0.06; 250/0.07; 280/0.02; 320/0.075; 350/0.025; 400/0.06	40/0.00025; 80/0.001; 120/0.00025	-0.62 la -0.42/ -0.04 la 0.04 (0.2/0.08) **2.5**
90	-‘’-	90/5.5 10^{-6}; 180/0.8 10^{-6}; 220/0.2 10^{-6}	3/0.005; 5/0.005; 8/0.005; 11/0.005; 13/0.005; 15/0.005; 18/0.018; 30/0.01; 43/0.01; 50/0.05; 53/0.005; 80/0.008; 100/0.005; 160/0.04; 200/0.01; 220/0.01; 250/0.03; 280/0.015; 320/0.01; 400/0.03	45/0.0002; 90/5 10^{-5}; 100/2.5 10^{-5}; 120/2.5 10^{-5}; 180/2.5 10^{-5}; 200/1 10^{-5}; 300/1 10^{-5}	-0.58 la -0.42/ -0.04 la 0.04 (0.16/0.08) **2**
100	-‘’-	100/5 10^{-7}; 120/1 10^{-7}; 200/2.3 10^{-6}; 300/1 10^{-7}; 400/1 10^{-7}; 450/2 10^{-7};	3/0.01; 50/0.12; 60/0.01; 70/0.01; 80/0.01; 90/0.01; 100/0.01; 110/0.01; 130/0.015; 200/0.02; 250/0.05; 270/0.02; 300/0.03; 320/0.01; 350/0.05; 400/0.03; 450/0.04	12/1.25 10^{-5}; 15/2.5 10^{-5}; 50/2 10^{-5}; 100/8 10^{-5} ; 110/2 10^{-5}; 150/1 10^{-5}; 200/1 10^{-5}; 300/1.8 10^{-5}; 400/1 10^{-5};	-0.62 la -0.38/ -0.05 la 0.04 (0.24/0.09) **2.66**
150	-‘’-	72/0.8 10^{-7}; 95/0.8 10^{-7}; 150/2.2 10^{-7}; 170/0.2 10^{-7}; 180/1.5 10^{-7}; 220/0.5 10^{-7}; 250/0.2 10^{-7}; 270/0.6 10^{-7}; 300/0.5 10^{-7}; 420/5.8 10^{-7};	4/0.01; 5.5/0.01; 15/0.015; 18/0.012; 28/0.01; 30/0.015; 38/0.008; 50/0.05; 100/0.01; 120/0.012; 130/0.015; 150/0.04; 170/0.01; 180/0.01; 190/0.01; 230/0.015; 250/0.03; 260/0.015; 300/0.015; 350/0.025; 360/0.018; 400/0.01; 420/0.045;	4.8/0.5 10^{-5}; 5.5/0.8 10^{-5}; 13/0.2 10^{-5}; 72/1.3 10^{-5}; 98/0.5 10^{-5}; 100/1.8 10^{-5}; 150/2.5 10^{-5}; 160/0.6 10^{-5}; 200/0.6 10^{-5} 250/0.1 10^{-5}; 300/1.8 10^{-5}; 370/0.1 10^{-5}; 400/0.5 10^{-5};	-0.56 la -0.46/ -0.05 la 0.03 (0.1/0.08) **1.25**
200	-‘’-	190/6 10^{-6}	50/0.06; 150/0.04; 230/0.01; 250/0.03; 270/0.025; 330/0.018; 350/0.02; 420/0.018; 450/0.03;	12/0.00025; 100/0.00001; 300/0.00001;	-0.57 la -0.45/-0.05 la 0.04 (0.12/0.09) **1.33**
300	-‘’-	4/5 10^{-8}; 100/3 10^{-8}; 180/4 10^{-8}; 190/2 10^{-8}; 200/2 10^{-8}; 270/3.5 10^{-8}; 290/4 10^{-8}; 300/2 10^{-8}; 370/2 10^{-8}; 400/3 10^{-8}; 450/1.7 10^{-7}	50/0.15; 150/0.1; 220/0.02; 250/0.1; 320/0.02; 350/0.08; 450/0.08;	15/8 10^{-5}; 100/2 10^{-5}; 150/1 10^{-5}; 200/1 10^{-5}; 300/1.8 10^{-5}; 400/0.5 10^{-5};	-0.56 la -0.46/ -0.05 la 0.04 (0.1/0.09) **1.11**
400	-‘’-	45/4 10^{-8}; 100/3 10^{-8}; 180/3.5 10^{-8}; 300/4 10^{-8}; 350/2 10^{-8}; 400/4 10^{-8}; 450/2 10^{-8};	3/0.04; 50/0.2; 130/0.05; 150/0.15; 220/0.02; 250/0.05; 320/0.01; 330/0.02; 360/0.04; 430/0.05;	6/5 10^{-6}; 13/1.5 10^{-6}; 100/2.5 10^{-6}; 110/2.3 10^{-5}; 150/8 10^{-6}; 210/1 10^{-5}; 320/1.5 10^{-5}; 400/3 10^{-6}	-0.55 la -0.47/ -0.04 la 0.03 (0.08/0.07) **1.14**
500	-‘’-	25/2 10^{-8}; 50/3 10^{-8}; 100/2 10^{-8}; 180/2 10^{-8}; 200/2 10^{-8}; 300/3 10^{-8}; 320/3 10^{-8}; 400/5 10^{-8}; 500/2 10^{-7};	50/0.13; 120/0.03; 150/0.075; 220/0.03; 240/0.04; 280/0.03; 350/0.03; 400/0.02; 450/0.02; 490/0.03;	100/2 10^{-6}; 110/1.8 10^{-5}; 150/5 10^{-6}; 210/7 10^{-6}; 250/1 10^{-6}; 310/1.8 10^{-5}; 350/1 10^{-6}; 400/2 10^{-6}; 480/1 10^{-6};	-0.55 la -0.47/ -0.04 la 0.03 (0.08/0.07) **1.14**

TABLE 7.8. Transmissibility between base and end effector with base excitation in the version with/without damper.

Tip amortizor utilizat	Frecventa de excitatie [Hz]	Transmisibilitate		Tip amortizor utilizat	Transmisibilitate	
		Frecventa spectru [Hz]	Amplitudine din spectru [-]		Frecventa spectru [Hz]	Amplitudine din spectru [-]
AMR	10	10	$3.5\ 10^{-6}$	fara AMR	10	$5.5\ 10^{-6}$
		20	$2.8\ 10^{-6}$		20	$4.5\ 10^{-6}$
		30	$0.2\ 10^{-6}$		30	$0.3\ 10^{-6}$
		50	$0.15\ 10^{-6}$		50	$0.2\ 10^{-6}$
		130	$0.15\ 10^{-6}$		130	$0.2\ 10^{-6}$
		220	$0.8\ 10^{-6}$		220	$0.8\ 10^{-6}$
		320	$0.9\ 10^{-6}$		320	$0.9\ 10^{-6}$
		420	$0.8\ 10^{-6}$		420	$0.8\ 10^{-6}$
AMR	14	14	$3.8\ 10^{-6}$	Aero	6.5	$1.1\ 10^{-5}$
		20	$6.5\ 10^{-6}$		15	$0.25\ 10^{-5}$
		180	$0.5\ 10^{-6}$		20	$1.5\ 10^{-5}$
		220	$0.1\ 10^{-6}$		26	$0.18\ 10^{-5}$
		340	$0.2\ 10^{-6}$		50	$0.18\ 10^{-5}$

TABLE 7.9. Global dynamic compliance in the version with/without damper.

Frecventa de excitatie [Hz]	Tip de amortizor	Complianta dinamica globala		Tip de amortizor	Complianta dinamica globala	
		Frecventa din spectru [Hz]	Amplitudine [mm/N]		Frecventa din spectru [Hz]	Amplitudine [mm/N]
7	AMR	6.5	0.55	Fara amortizor	2	1.2
		14	0.65		8	0.98
		20	0.05		14	0.8
		38	0.18		21	0.9
		42	0.1		32	1.1
		50	0.8		40	0.9
		55	0.1		41	0.98
		61	0.18		52	0.4
		150	0.1		100	0.5
10	AMR	10	0.6	Fara amortizor	5	1
		20	0.2		11	0.75
		30	0.32		15	0.25
		40	0.52		18	0.37
		60	0.4		25	1.25
		70	0.08		30	0.6
		80	0.3		40	0.55
		90	0.32		45	1.25
		110	0.33		55	0.85
		130	0.28		60	0.5
		140	0.18		62	0.5
		150	0.15		72	1.4
		160	0.22		80	0.4
		180	0.25		90	1.25
		200	0.2		100	0.6
		220	0.28		110	0.35
14	AMR	10	0.02	Cu amortizor cu aer	6.5	0.05
		33	0.01		14	0.025
		45	0.01		20	0.005
		95	0.072		50	0.1
		180	0.06		100	0.1
		200	0.03		160	0.1
		220	0.02		200	0.02
20	AMR	12	0.04	Cu amortizor cu aer	5	0.1
		19	0.02		7	0.03
		21	0.04		9	0.04
		35	0.02		12	0.11
		48	0.07		18	0.12
		57	0.03		22	0.13
		70	0.02		28	0.12
		73	0.04		30	0.08
		80	0.04		33	0.09
		98	0.05		40	0.09
		110	0.02		50	0.09

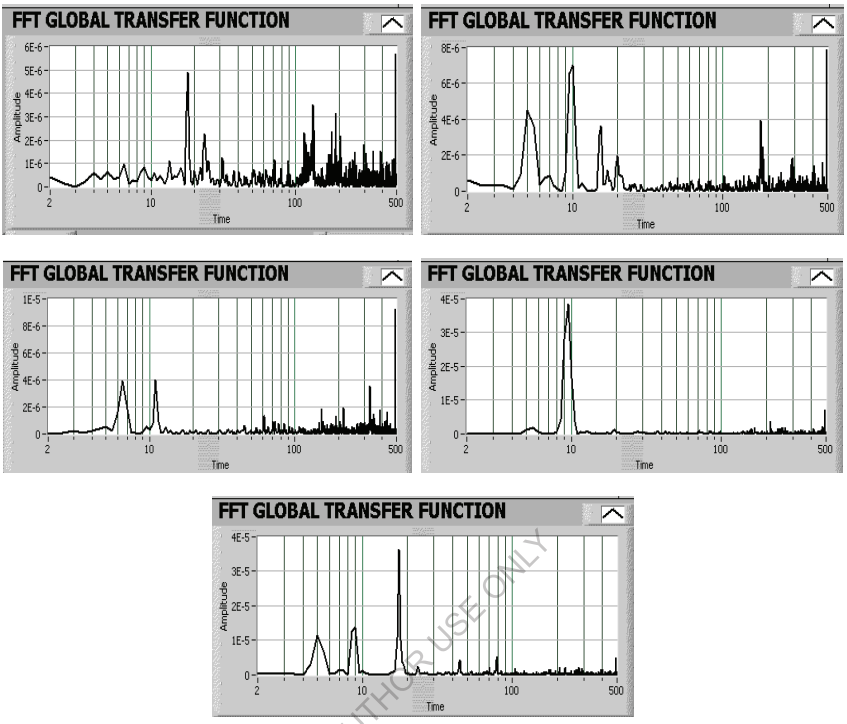

Fig.7.28. The Fourier spectrum for various cases:
a- upward movement with ***AMR***, b- upward movement with damper
c- upward movement without damper, d- downward movement without damper,
e- downward movement with ***AMR***.

After analyzing the results of the experimental research, the following conclusions can be highlighted:
- ***GDC***, for the operation of the robot structure with ***AMR***, is reduced and transferred to higher frequencies by more than 6-8 Hz;
- global dynamic transmissibility ***GDT*** is reduced by more than 35% at frequencies between 10-100Hz when using AMR, compared to the case without shock absorber and by about 20% compared to the case with air shock absorber;
- by using ***AMR***, compared to the case of moving the arm with an air damper or without a damper, the transfer of the first three resonance frequencies, from the Fourier spectrum, to higher frequencies was observed (compare the characteristics of fig. 7.28.a,b,c,d ,e), respectively 1,6,11 Hz for the upward movement without damping, 5,10,16 Hz in the upward movement with air damper, 15, 18, 24 Hz upward movement with ***AMR***, 1.5, 9 Hz in the downward movement without damping and 5,9,18 Hz in the downward movement with ***AMR***;
- due to the imbalance of the arm, the Fourier spectrum is different in up and down movement, the unbalanced force of gravity acting as a shock absorber. In this case, for the upward and downward movement, for the same damping option, the upward movement frequencies are higher than the downward movement ones, respectively 1,6,11 Hz compared to 1,5,9 Hz in the movement without damping and respectively 15,18,24 Hz compared to 5,9,18 Hz in the movement with AMR (fig.7.28.a,b,c,d,e);

- the global dynamic transmissibility ***GDT*** is higher in the area of low frequencies, frequencies comparable to the resonant frequency of the structure of 14 Hz, at excitations of 10, 20 Hz, see table 7.8;
- the transmissibility between the base and end-effector, at a base excitation of 10 Hz with ***AMR*** is much reduced compared to the case without damping, respectively 3.5 10^{-6} compared to 5.5 10^{-6} at the first frequency in the spectrum of 10 Hz and 2.8 10^{-6} compared to 4.510^{-6} at the spectrum frequency of 20 Hz, see table 7.8;
- the transmissibility is approximately the same for excitations in the field of higher frequencies, above 35 Hz (the working frequency range of the didactic robot);
- global dynamic compliance ***GDC*** is higher in the range of low excitation frequencies, for example 10 Hz, for example 20mm/N corresponding to a frequency of 4 Hz in the spectrum, compared to 0.2 for a frequency in the spectrum of 20 Hz, at an excitation of 20 Hz, see table 7.9;
- the global dynamic compliance is maximum at an excitation of 10 Hz, which means that the structure of the robot has a mechanical resonance close to 10 Hz, which is located at 14 Hz;
- the damping force is maximum for the case with air damper at 9 Hz;
- from the analysis of the variation ratio of the damping force against the speed, the damping energy can be determined; the energy coefficient calculated as the previously mentioned ratio is maximum at 10 Hz-15; then it is located at the values of: 11.66 at 25 Hz; 11.11 at 50 Hz; 10.62 at 35 Hz; 8.75 at 20 Hz; 8.5 at 30 Hz.

7.5. Analysis of experimental research results for the purpose of intelligent dynamic optimization. The research resulted in the following conclusions, which lead to the optimization of the dynamic behavior of the robotic structures and the assurance of the future application of these structures in the modern intelligent manufacturing technique.
Among the results of the research, the following stand out:
• the experimental research carried out used a series of LabVIEW virtual tools original, made specifically for such research. Among them stand out: ***VI*** virtual instrument, for data acquisition on 5 simultaneous channels; ***VI*** for the theoretical simulation of ***AMR***; own Fourier analyzer for both theoretical and applied research; ***VI***s for simulating mechanical and electronic corrections; ***VI***s for simulating complex servo systems with various laws of control and multiple reactions of position and speed;
• the approach of own mathematical models in order to determine the parameters dynamic behavior, newly introduced in theoretical research;
• approaching new parameters regarding behavior and behavior optimization dynamics of robotic structures;
• creating a matrix-vector mathematical model regarding the force-moment torsion;
• the conception and use of an intelligent system for optimizing the vibration behavior a robotic structures using AMR;
• the experimental determination of the new parameters of the dynamic behavior, the parameters used for the first time to analyze the dynamic compliance of industrial robots: ***GDC*** global dynamic compliance; the viscous dynamic damping coefficient ***VGDDC***;
• the use for the first time in the experimental research of the dynamic behavior of ***RI*** of the "radical of 2" method aimed at the experimental determination of the damping factor and respectively of the damping coefficient for each resonant frequency within the Fourier spectrum;
• determining the global dynamic damping coefficient ***GDDC*** for ***RI*** structures;
• the use of an own mathematical model for determining the damping force a ***AMR***, experimentally validated model within a maximum error of 1%;
• research with the determination of the variation of global dynamic transmissibility ***GDT*** and global dynamic compliance ***GDC*** in the movement of the ***RI*** arm with shock absorber and without or with air shock absorber;

• parameterization of ***AMR*** characteristics force vs. speed and the use of these parameters in the technique of online establishment of the value of the identification coefficients between the theoretical model and the real one;
• by applying magnetorheological dampers in intelligent damping systems the attenuation of low-frequency vibrations, unfavorable vibrations for ensuring extreme precision, and the transfer of the entire Fourier spectrum to higher frequencies by about 20Hz were achieved;
• by applying ***AMR*** to a didactic research structure, it was achieved, for the first time, the realization of an intelligent vibration attenuation structure, a system that uses a magnetorheological damper operated online by means of an electronic interface and an acquisition board;
• the transfer of vibrations to a higher domain was significant, which is why it can be considered that the research has achieved its goal, namely the intelligent optimization of the dynamic behavior of a robotic structure, optimization carried out online, through the transformation, transfer and amplification of oscillations of acceleration, determined at the end-effector and the application of this signal in the form of oscillating voltage at the level of the ***AMR*** coils;
• the realization and preliminary research of an intelligent mitigation structure opens the horizon for the development of intelligent self-control systems of the dynamic behavior of complex automation structures that include robots, manipulators, peri-robotic systems, transport-transfer systems and complex manufacturing systems;
• the approach of intelligent attenuation systems will determine the obtaining of a Fourier spectrum that bypasses the unfavorable frequencies in the dynamic manufacturing system.

Among the future research directions, we can mention:

- In the future, this concept, of the intelligent amortization structure, will develop, system which will be applied in each joint of a robotic structure, so that the answer in frequency for each module to be optimized, thus ensuring the optimization the entire structure;
- In the future, the research of rotating magnetorheological shock absorbers will be approached and can be used and implemented more easily in the constructive structure of the ***RI*** and in the systems intelligent depreciation;
- Future development of new parameters of dynamic behavior, parameters that allow an immediate intervention on the matrix-vector mathematical models regarding the dynamic behavior of industrial robots;
- In the future, the structure of intelligent systems will include neural networks and neuro-fuzzy, so that the degree of integration of artificial intelligence, in the structure of intelligent systems, increases.

REFERENCES

[1] Agapie, A., Giuclea, M., Fagarasan, F., Dediu, H., *Genetic Algorithms: Theoretical Aspects and Applications*, Romanian Journal of Information Science and Technology, **1**, 1, 1998.
[2] Akella P. and Cutkosky, M., "Contact Transition Control with Semiactive Fingertips", *IEEE Transactions on Robotics and Automation*, Vol. 11, No 6, 1995, pp. 859-867.
[3] Angeles, J., Fundamentals of Robotic Mechanical Systems Theory, Methods and Algorithms, Springer-Verlag, New York, 1997.
[4] Anonymous: Provisional product information Rheobay TP AI 3565 and Rheobay TP AI 3566. Bayer AG, Leverkusen,1994.
[5] Anonymous: RheAct -Der hochdynamische rheo-elektrische Actuator. Carl Schenck AG, Darmstadt, 1998.
[6] Back´e, W.; Fees, G.; Murrenhof, H.: Innovative Fluidtechnik — Hochdynamischer Servoantrieb mit elektrorheologischen Fl¨ussigkeiten. ¨Olhydraulik und Pneumatik (o+p), **41** (1997) 11/12.
[7] Bar-Cohen Y., Mavroidis C., Bouzit M., Pfeiffer C. and Dolgin B., "Remote Mechanical Mirroring using Controlled Stiffness and Actuators (MEMICA)", Rutgers Docket Number 99-0056 A US and International PCT patent application has been filed by Rutgers University in September 2000d.
[8] Bar-Cohen Y., Mavroidis, C., Pfeiffer C., Culbert C. and Magruder D., "Haptic Interfaces",
Chapter in *Automation, Miniature Robotics and Sensors for Non-Destructive Testing and Evaluation*, Y. Bar-Cohen Editor, The American Society for Nondestructive Testing, Inc. (ASNT), pp. 461-468, 2000c.
[9] Bar-Cohen Y., Pfeiffer C., Mavroidis C. and Dolgin B., "MEMICA: a Concept for Reflecting
Remote-Manipulator Forces", *NASA Tech Briefs*, Vol. 24, No. 2, pp. 7a-7b, 2000a. Biorobotics Laboratory, Harvard University, http://hrl.harvard.edu/hrsl/research/parris.html.
[10] Bouzit M., Popescu G., Burdea G., and Boian R., "The Rutgers Master II-ND Force Feedback
Glove", Proceedings of IEEE VR 2002 Haptics Symposium, pp. 145-152, Orlando FL,
March 2002.Haptics Laboratory, Center for Intelligent Machines, McGill University,
http://www.cim.mcgill.ca/~haptic/devices/pantograph.html .
[11] Bird, B.; Armstrong, R.; Hassager, O.: Dynamics of polymeric liquids. J. Wiley and Sons, New York, 1987.
[12] Block, H.; Kelly, J. P.: Electro-rheology. Journal of Physics D: Applied Physics, **21** (1988), 1661-1677.
[13] Bonnecaze, R. T.; Brady, J. F.: Dynamic simulation of an electrorheological fluid. Journal of Chemical Physics, 96 (1992), 2183-2202.
[14] Bonnecaze, R. T.; Brady, J. F.: Yield stresses in electrorheological fluids. Journal of Rheology, **36** (1992), 73-115.
[15] Böse H., Berkemeier J. and Trendler A., "Haptic System Based on Electrorheological Fluid,"
Proceedings of the ACTUATOR 2000 Conference, 19-21 June 2000, Bremen GERMANY.
[16] B¨ose, H.: Private communication. October 1998.
[17] Böse H., Berkemeier J. and Trendler A., "Haptic System Based on Electrorheological Fluid," *Proceedings of the ACTUATOR 2000 Conference,* 19-21 June 2000, Bremen GERMANY.
[18] Brokate, M.; Sprekels, J.: Hysteresis and Phase Transitions. Springer-Verlag, New York, 1996.
[19] Burton, S. A.: Design and analysis of an electrorheological damper for seismic protection of structures. MS Thesis, University of Notre Dame, IN, 1996.
[20] Burton, S. A.; Makris, N.; Konstantopoulos, I.; Antsaklis, P. J.: Modeling the response of ER damper: phenomenology and emulation. Journal of Engineering Mechanics, **122** (1996), 897-906.
[21] Butz, T., Stryk, O. *Modelling and Simulation of Rheological Devices*, Sonderforshungsbereich 438: Tehnische Universitat Munchen, Universitat Augsburg, Preprint **SFB-438-**9911, 1999.
[22]Carlson, J. D.; Spencer Jr., B. F.: Magneto-rheological fluid dampers: scalability and design issues for application to dynamic hazard mitigation. In *Proceedings of the 2nd International Workshop on Structural Control,* Hong Kong,18-21 December 1996, 99-109.
[23] Marco Ceccarelli, Fabio Pugliese, Chiara Lanni, Joao Carlos Mendes Carvalho, CaPaMan (Cassino Parallel Manipulator), "A Sensored Earthquake Simulator", Proceedings of the 1999 IEEE/RSJ International Conference on Intelligent Robots and Systems, 1999, pp 1501-1506.
[24] Ciobanasu, R., Review on CAD robot design and simulation software, Bul. Inst. Pol. Iasi, Tomul L (LIV), Fasc. 6A, 2004 pp. 333-338.
[25] C.-M. Chew, G.-S. Hong and W. Zhou, Series damper actuator for force/torque control, *US Patent Provisional Application*. Application No.: 60/469,825.
[26] Clavel, R., "Delta: a fast robot with parallel geometry", Proceedings of 18th International Symposium on Industrial Robots, Lausanne, 1988.
[27] Cleary, K., Brooks, T., "Kinematics analysis of a novel 6 DOF parallel manipulator",
Proceedings of the IEEE International Conference on Robotics and Automation, 1993.
[28] Coiffet, P., La robotique. Principes et applications, Hermès, 1992.
[29] Conrad H., "Properties and Design of Electrorheological Suspensions," *MRS Bulletin*, Vol. 23, No. 8, August 1998, pp. 35-42.
[30] Choi S. B., "Control of ER Devices," *International Journal of Modern Physics B,* Vol. 13, No. 14-16, 1999, pp.2160-2167.

[31] Choi, Y.; Sprecher, A. F.; Conrad, H.: Vibration characteristics of a composite beam containing an electrorheological fluid. Journal of Intelligent Material Systems and Structures, **1** (1990), 91-104.
[32] Dasgupta, B., Mruthyunjaya, T.S., "A Newton-Euler formulation for the inverse dynamics of the Stewart platform manipulator", Mechanism and Machine Theory, 34, 1998.
[33]B. Dasgupta, T.S. Mruthyunjaya, "The Stewart Platform Manipulator: A Review", Mech. Machine Theor. , Vol. 35 , No. 1, 2000, pp. 15–40.
[34] Denavit, J., Hartenberg, R., "A kinematic notation for lower-pair mechanisms based on matrices", ASME Journal of Applied Mechanics, 1955.
[35] Dyke, S. J.; Spencer Jr., B. F.; Sain, M. K.; Carlson, J. D.: On the efficacy of magnetorheological dampers for seismic response reduction. 1997 ASME Design Engineering Technical Conferences, Sacramento, CA, 14-17 September 1997.
[36] Dyke, S.J., Spencer, B.F., Sain, M.K., Carlson, J.D., *Application of Magnetorheological Dampers to Seismically Excited Structures*, Proceedings of the 17th International Modal Analysis Conference, Kissimmee, Florida, pp. 8-11, 1999.
[37] Dymola (2003): *Dynamic Modeling Laboratory*.- Available at http://www.dynasim.se/
[38] J. Drosdol and F. Panik , "The Daimler-Benz Driving Simulator", A tool for vehicle development , February 25 – March 1 , 1985 . SAE Technical Paper Series.
[39] Ehrgott, R. C.; Masri, S. F.: Modeling the oscillatory dynamic behavior of electrorheological materials in shear.Smart Materials and Structures, **1** (1992), 275-285.
[40] Elmqvist H., Mattsson S. E., Otter M. (1999): *Modelica - A Language for Physical System Modeling, Visualization and Interaction.* – The 1999 IEEE Symposium on Computer – Aided Control System Design, CACSD'99, Hawaii, August 22-27
[41] Engelmann, B.; Hiptmair, R.; Hoppe, R. H. W.; Mazurkevitch, G.: Numerical simulation of electrorheological fluids based on an extended Bingham model. Preprint SFB-438-9902, Sonderforschungsbereich 438, Technische Universit¨at M¨unchen – Universit¨at Augsburg, 1999. World Wide Web: http://www-lit.mathematik.tu-muenchen.de/veroeff/html/SFB/992.76001.html.
[42] S. D. Eppinger and W. P. Seering, Three dynamic problems in robot force control, in *IEEE Int. Conf. on Robotics and Automation (ICRA)* (IEEE Press, 1989), pp. 392-397.
[43] A. Fattah and G. Kasaei, "Kinematics and Dynamics of a Parallel Manipulator With New Architecture", Robotica, Vol. 18, 2000, pp. 535-543
[44] Gamota, D. R.; Filisko, F. E.: Dynamic mechanical studies of electrorheological materials: Moderate frequencies. Journal of Rheology, 35 (1991), 399-425.
[45] A. Fattah and M. Oghbaei, "Singular Configuration and Workspace a Parallel Manipulator With New Architecture", in Proc. ASME Design Engineering Technical Conf.,Baltimore , MD, Sept. 10-13, 2000, DETC2000/MECH-14 100.
[46] Feng Gao, Weimin Li, Xianchao Zhao, Zhenlin Jin, Hui Zhao, "New Kinematics Structures For 2-, 3-, 4-, and 5-DOF Parallel Manipulator Designs", PERGAMON, Mechanism and Machine Theory 37, 2002, pp. 1395–1411
[47] C. Gosselin, Angeles, "Singularity Analysis of Closed Loop Kinematic Chains", IEEE Transaction on Robotics and Automation, Vol.6, No.3, 1990, pp. 281-290
[48] Gast, A. P.; Zukoski, C. F.: Electrorheological fluids as colloidal suspensions. Advances in Colloid and Interface Science, **30** (1989), 153-202.
[49] Gavin, H. P.; Hanson, R. D.; Filisko, F. E.: Electrorheological dampers, Part I: Analysis and design. Journal of Applied Mechanics, **63** (1996), 669-675.
[50] Gavin, H. P.; Hanson, R. D.; Filisko, F. E.: Electrorheological dampers, Part I: Testing and modeling. Journal of Applied Mechanics, **63** (1996), 676-682.
[51] Gavin HP., "Control of Seismically-Excited Vibration Using ER Materials and Lyapunov Methods", *IEEE Transactions and Automatics Control*, Vol. 9, No. 1, pp. 27-36, 2001.
[52] Gawrysiak M. (2002): *Stages of mechatronic design accordingto R. Isermann*. - Proc. Workshop on Mechatronic Design, Cracow, pp. 7–156.
[53] Gh. Ghita, Contributions to study of semi-active vibration control systems with applications to vibration isolation and earthquake protection, PhD Thesis, University "Politehnica" Bucharest, 2003.
[54] M. Giuclea, T. Sireteanu, D. Stancioiu, C. W. Stammers, *Modeling of magneto-rheological damper behavior by genetic algorithms based inverse method,* Proc. Ro. Acad. Series A, **5**, 1, 2004, pp.55-63.
[55] Gosselin, C., Angeles, J., "The optimum kinematics design of spherical three-degree-of-freedom parallel manipulator", ASME Journal of Mech. Trans. and Automat. in Design, 111, 2 (1989).
[56] Gosselin, C., Gagné, M., "Dynamic models for spherical parallel manipulators", IEEE Int. Conference on Robotics and Automation, Milan, 1995.
[57] Goldberg, D.E. *Genetic Algorithms in Search, Optimization and Machine Learning*, Addison-Wesley, Reading, MA, 1989.
[58] Hashimoto, H., Y. Kunii, F. Harashima, V.I. Utkin, and S.V. Grakumov (1993). Obstacle Advoidance control of multi degree of freedom manipulator using electrostatic potential field and sliding mode. *J. Robot Soc. Jpn.,* vol. 11, no. 8, pp. 1220-1228.
[59] Ha´c, A.: Optimal linear preview control of active vehicle suspension. Vehicle System Dynamics, 21 (1992), 167-195.

[60] Hayward, V., Choksi, J. Lanvin, G. Ramstein, C. 1994. Design And Multi-Objective Optimization Of A Linkage For A Haptic Interface. In Advances in Robot Kinematics.
[61] Hartsock, D. L.; Nowak, R. F.; Chaundy, G. J.: ER fluid requirements for automotive devices. Journal of Rheology, **35** (1991), 1305-1326.
[62] A.L. Helinski , "Dynamic and Kinematics Study of Stewart Platform Using Newton-Euler Techniques", Research report 13479, tank Automotive Command , January 1990.
[63] Hervé J-M., Sparacino, F., "Star. A New Concept in Robotics", Proceedings of the Third International Workshop on Advances in Robot Kinematics, Ferrara, 1992.
[64] Human Machine Interface Laboratory, Center for Advanced Information Processing, Rutgers University, http://www.caip.rutgers.edu/vrlab/ .
[65] Human-Machine Interaction Subarea, Real World Active Intelligence Area, Department of Computer-Controlled Mechanical Systems, Osaka University, Japan http://wwwdyna.mech.eng.osaka-u.ac.jp/welcome-e.html
[66] Hurmuzlu Y., Ephanov A., and Stoianovici D. (1998) " Effect of a Pneumatically Driven Haptic Interface on the Perceptional Capabilities of Human Operators ",Presence, MIT Press, Vol. 7, No. 3 pp. 290-307.
[67] Husty, M.L., "An algorithm for solving the direct kinematics of the Stewart-Gough platforms", Mechanism and Machine Theory, 31, 4, 1996.
[68] Hoppe, R. H. W.; Mazurkevitch, G.; Rettig, U.; von Stryk, O.: Modeling, simulation and control of electrorheological fluid devices. In Bungartz, H.-J. et al., editors: *Lectures on Applied Mathematics,* pages 251-276.
[69] Immersion Corporation, Cyberforce, http://www.immersion.com/products/3d/interaction/cyberforce.shtml .
[70] Immersion Corporation, CyberGrasp, http://www.immersion.com/products/3d/interaction/cybergrasp.shtml .
[71] Intelligent Mechanical and Manufacturing Systems Research, Department of Mechanical, Materials and Manufacturing, Engineering, University of Newcastle Tyn http://www.ncl.ac.uk/mmmeng/research/pmt/tactile.html .
[72] Innocenti, C., Parenti-Castelli, V., "Echelon form solution of direct kinematics for general fully-parallel spherical wrist", Mechanism and Machine Theory, 28, 4, 1993.
[73] Ivanescu, M., V. Stoian, A (1995). Variable Structure Controller for a Tentacle Manipulator. Proceedings of the 1995 IEEE International Conference on Robotics and Automation, Nagoya, Japan, May 21-27, vol. 3, pp. 3155-3160, ISBN: 0-7803-1967-2.
[74] Ivanescu, M., (2001). Moving target interception for walking robot by fuzzy controller. Proceedings of the Fourth International Conference on Climbing and Walking Robotics (CLAWAR 2001), pp. 363-376.
[75] Y. Yamada, K. Suita, K. Imai, H. Ikeda, and N. Sugimoto, "Human-robot contact in the safeguarding space," *IEEE/ASME Transactions on Mechatronics*, vol. 2., no. 4, pp.230-236,1997.
[76] S. Yun, S. Kang, M. Kim, S,-S. Yoon, "Input Preshaping Control of the safe arm with Mrbased Passive Compliant Joints," *In Proceedings of International Conference on Robotics and Automation*, pp. 2788-2793, 2004.
[77] G. Yang, B. F. Spencer, Jr., J. D. Carlson, M. K. Sain, *Large-scale MR fluid dampers: modeling, and dynamic performance conside-rations*, Report CMS 99-00234.
[78] D. Jeon, C. Park and A. Park, Vibration suppression by controlling an MR damper. *International Journal of Modern Physics B* **13**, pp. 2221-2228 (1999).
[79] Jolly, M. R.; Bender, J. W.; Carlson, J. D.: Properties and applications of commercial magnetorheological fluids. SPIE 5th Annual Int. Symposium on Smart Structures and Materials, San Diego, CA, 15 March 1998.
[80] Jolly, M. R.; Carlson, J. D.; Mu˜noz, B. C.: A model of the behaviour of magnetorheological materials. Smart Materials and Structures, 5 (1996), 607-614.
[81] Jolly, M.R., Bender, J.W., Carlson, J.D., *Properties and Applications of Commercial Magnetorheological Fluids*.
[82] S. A. Joshi and L. W. A. "Comparison Study of Two 3-DOF Parallel Manipualtors : One With Three and the Other With Four Supporting Legs", IEEE Transactions on Robotics and Automation , Vol. 19. No. 2, April 2003.
[83] Khatib., O, (1986). Real-time Obstacle Avoidance for Manipulators and Mobile Robots. Int. J. Robot. Res., vol. 5, no. 1, pp. 90-98.
[84] Kamath, G. M.; Hurt, M. K.; Wereley, N. M.: Analysis and testing of Bingham plastic behavior in semi-active electrorheological fluid dampers. Smart Materials and Structures, **5** (1996), 576-590.
[85] Kamath, G. M.; Wereley, N. M.: System identification of ER fluid dampers using a nonlinear mechanisms-based model. 1996 SPIE Conference on Smart Materials and Structures, Paper No. SPIE-2717-46, San Diego, CA, 25-29 February 1996.
[86] Kamath, G. M.; Wereley, N. M.: A nonlinear viscoelastic-plastic model for electrorheological fluids. Smart Materials and Structures, **6** (1997), 351-359.
[87] Kamath, G. M.; Wereley, N. M.: System identification of electrorheological fluid-based dampers using a nonlinear viscoelastic-plastic phenomenological model. 35th Aerospace Sciences Meeting, Paper No. AIAA-97-0359, Reno, NV, 6-9 January 1997.
[88] Kamath, G. M.; Wereley, N. M.; Jolly, M. R.: Analysis and testing of a model-scale magnetorheological fluid helicopter lag mode damper. American Helicopter Society 53rd Annual Forum, Virginia Beach, 29 April - 1 May 1997, 1325-1335.
[89] Keil, S. Beanspruchungsermittung mit Dehnungsmeβstreifen Zwingenberg a.d. Bergstaβe: CUNEUS, 1995.

[90] Kenaley G. L. and Cutkosky M. R., "Electrorheological Fluid-Based Robotic Fingers With Tactile Sensing,"*Proceedings of the 1989 IEEE International Conference on Robotics and Automation,* Scottsdale AR, pp. 132-136.
[91] J.-H. Kim and J.-H. Oh, Design and analysis of rotary MR damper using permanent magnet. in *2nd IFAC Conference on Mechatronic Systems* (Berkeley, USA, Dec. 9-11, 2002), pp.899-903.
[92] M. Kim, S.-S. Yoon, S. Kang, S.-J. Kim, Y.-H. Kim, H.-S. Yim, C.-D. Lee, I.-T. Yeo, "Safe arm design for service robot," *In Proceedings of The Second IARP -IEEE/RAS Joint Workshop on Technical Challenge for Dependable Robots in Human Environments*, pp. 88-95, 2002.
[93] Kikuchi T., Furusho J., Oda K., "Development of Isokinetic Exercise Machine Using ER Brake," *Proceedings -IEEE International Conference on Robotics and Automation*, Vol. 1, 2003, pp. 214-219.
[94] Khanicheh A., Muto A., Triantafyllou C., Weinberg B., Astrakas L., Tzika A., and Mavroidis C., "MR Compatible ERF Driven Hand Rehabilitation Device", *Proceedings of the 9th IEEE International Conference on Rehabilitation Robotics* (ICORR 2005), June 28 - July 1, 2005, Chicago, IL.
[95] Klingenberg, D. J.; van Swol, F.; Zukoski, C. F.: Dynamic simulation of electrorheological suspensions. Journal of Chemical Physics, 91 (1989), 7888-7895.
[96] Koyanagi K., Furusho J., Ryu U. Inoue A., "Development of Rehabilitation System for the Upper Limbs in a NEDO Project," *Proceedings - IEEE International Conference on Robotics and Automation*, Vol. 3, 2003, pp. 4016-4022.
[97] Koslik, B.; Rill, G.; von Stryk, O.; Zampieri, D. E.: Active suspension design for a tractor by optimal control methods. Preprint SFB-438-9801, Sonderforschungsbereich 438, Technische Universit¨at M¨unchen – Universit¨at Augsburg,1999. World Wide Web:
http://www-lit.mathematik.tu-muenchen.de/veroeff/html/SFB/982.49003.html.
[98]Kane, T.R., Levinson, D.A. Dynamics, Theory and Applications, Mc Graw-Hill, New
York, 1985.
[99] Li, Y-W., Wang, J-S., Wang, L-P., Liu, X-J., "Inverse dynamics and simulation of a 3-DOF spatial parallel manipulator", Proceedings of the IEEE International Conference on Robotics & Automation, Taipei, Taiwan, 2003.
[100] Lampe, D., Materials database on commercially available electro- and magnetorheological fluids. Institut f¨ur Luft- und Raumfahrttechnik, Technische Universit¨at Dresden, 1997. World Wide Web: http://www.tu-dresden.de/mw/ilr/lampe/HAUENG.HTM.
[101] Lampe, D.; Thess, A.; Dotzauer, C.: MRF clutch — Design considerations and performance. In *Proceedings of the Actuator 98*, Bremen, 17-19 June 1998.
[102] Latombe J.C., (1991). Robot Motion Planning Kluwer Academic Publishers, Boston.
[103] K. F. Laurin-Kovitz, J. E. Colgate, and S. D. R.Carnes, "Design of components for programmable passive impedance," *Proc. of the IEEE International Conference on Robotics and Automation*, pp. 1476-1481, 1991.
[104] Li, J.; Jin, D.; Zhang, X.; Zhang, J.; Gruver, W. A.: An electrorheological fluid damper for robots. In *Proceedings of the 1995 IEEE International Conference on Robotics and Automation*, Vol. 3, Nagoya, Japan, 21-27 May 1995, 2631-2636.
[105] H.-O. Lim and K. Tanie, "Human safety mechanisms of human-friendly robots: passive viscoelastic trunk and passively movable base," *International Journal of Robotics Research*, vol. 19, no. 4, pp. 307-335, 2000.
[106] Lord Corporation: Rheonetic MagnetoRheological (MR) Fluid Technology. Cary, NC, 1997. World Wide Web: http://www.mrfluid.com
[107] Lord Corporation, "Magnetorheological fluid MRF-132LD", Product Bulletin, 1999.
(http://www.mrfluid.com)
[108] Luecke, G.R., and Chai, Y.H., "Contact Sensation in the Synthetic Environment Using the ISU Force Reflecting Exoskeleton," IEEE Virtual Reality Annual Symposium (VRIAS'97), pg.
192-198, March 3-5, 1997, Albuquerque, NM.
[109] Makris, N.; Burton, S. A.; Hill, D.; Jordan, M.: Analysis and design of ER damper for seismic protection of structures. Journal of Engineering Mechanics, **122** (1996), 1003-1011.
[110] Makris, N.; Burton, S. A.; Taylor, D. P.: Electrorheological damper with annular ducts for seismic protection applications. Smart Materials and Structures, **5** (1996), 551-564.
[111] N. Mandal and S. Payandeh, Force control strategies for compliant and stiff contact: an experimental study, in *IEEE Int. Conf. on Systems, Man, and Cybernetics* (IEEE Press, 1994),pp. 1285-1290.
[112] Masoud, S.A., A.A. Masoud, (2000). Constrained motion control using vector potential fields, IEEE Trans. On Systems, Man and Cybernetics, part A, 30, pp. 251-272.
[113] Mavroidis C., Pfeiffer C. and Bar-Cohen Y., "Controlled Compliance Haptic Interface Using Electro-Rheological Fluids," *Proceedings of the 2000 SPIE Conference on Electro-Active Polymer Actuators and Devices (EAPAD 2000),* Newport Beach, CA, March 5-9, 2000a,Vol. 3987, pp. 300-310.
[114] Mavroidis C., Pfeiffer C., Celestino J. and Bar-Cohen Y., "Design and Modeling of an Electro- Rheological Fluid Based Haptic Interface," *Proceedings of the 2000 ASME Mechanisms and Robotics Conference,* Baltimore MD, September 10-13, 2000b, Paper DETC2000/MECH- 14121.
[115] Mavroidis C., Pfeiffer C., Lennon J., Paljic A., Celestino J., and Bar-Cohen Y., "Modeling and Design of an Electro-Rheological Fluid Based Haptic System for Tele-Operation of Space Robots," *Proceedings of the ROBOTICS 2000 Conference: The 4 th International Conference and Exposition/Demonstration on Robotics for Challenging Situations and Environments*, February 27-March 2, 2000c, Albuquerque, NM, pp. 174-180.

[116] Mavroidis C., Bar-Cohen Y. and Bouzit M., "Chapter 19: Haptic Interfaces Using Electrorheological Fluids", Invited Chapter in *Electroactive Polymer (EAP) Actuators as Artificial Muscles: Reality, Potentials and Challenges*, Y. Bar-Cohen Editor, SPIE Optical Engineering Press, February 2001, pp. 567-594.
[117] J.P. Merlet, "Parallel Manipulators, Part I: Theory, Design, Kinematics, Dynamics And Control", Technical Report no. 646, INRIA, France.
[118] Mohri, A., X. D Yang and A. Yamamoto, (1995). Collision free trajectory planning for manipulator using potential function. Proceedings 1995 IEEE International Conference on Robotics and Automation, pp. 3069-3074.
[119] Monkman G. J., "Electrorheological Tactile Display", *Presence*, MIT Press, Vol. 1, No. 2, 1992.
[120] Morasso, P.G., V. Sanguineti and T. Tsuji, (1993). A Dynamical Model for the Generator of Curved Trajectories, in Proceedings International Conference on Artificial Neural Networks, pp. 115-118.
[121] T. Morita and S. Sugano, "Development of one- D.O.F. robot arm equipped with mechanical impedance adjuster," *Proc. of the IEEE/RSJ International Conference on Intelligent Robots and Systems*, pp. 407-412, 1995.
[122] Moroni, G., Carrino, L., Ceccarelli, M., Anamateros, E., Robotized Filament Winding manufacturing: Some Experiences, Proceedings RAAD'97, Cassino, Italy: June 26-28, 1997, Edited by Marco Ceccarelli, pp.535-546.
[123] Miller, K., "Experimental verification of modelling of Delta robot dynamics by application of Hamilton principle", Proceedings of the IEEE International Conference on Robotics and Automation, 1995.
[124] Merlet, J-P. (2000), Parallel robots, Kluwer Academic Publishers.
[125] Monkman G. J., "Electrorheological Tactile Display", *Presence*, MIT Press, Vol. 1, No. 2, 1992.
[126] Mrozek Z. (2003): *Computer aided design of mechatronics system*. - Int. J. Appl. Math. Comput. Sci., 2003, Vol. 13, No. 2, 255–267
[127] Mrozek Z. (2002): *Methodology of using UML in mechatronic design.*
[128] Mrozek B., Mrozek Z. (2001): *MATLAB 6, User's Guide.*
[129] Mrozek Z. (2002): *Computer-aided design of mechatronic systems*. - Sci. Fasc., Cracow Univ. Of Technol., Series:Electrical and Computer Eng., No. 1.
[130] Nakano M., Minagawa S., and Hagino K., "PMW Flow Rate Control of ER Valve and its Application to ER Actuator Control*" International Journal of Modern Physics B*, Vol. 13, No. 14-16, 1999, pp. 2168-2175.
[131] Nikitczuk J., Weinberg B., Mavroidis C., "Rehabilitative Knee Orthosis Driven by Electro-Rheological Fluid Based Actuators," *Proceedings of the 2005 IEEE International Conference of Robotics and Automation*, Barcelona, Spain, April 18 – 22, 2005.
[132] M. Okada, Y. Nakamura, and S. Ban, "Design of Programmable Passive Compliance Shoulder Mechanism," *Proc. Of the IEEE International Conference on Robotics and Automation*, pp.348-353, 2001.
[133] Serban Olaru, Adrian Olaru, *Contribution of the modeling and simulation of the rheological dampers,* DECOM2007, Turcia, 2007.
[134] Olaru Serban , Oprean Aurel, Olaru Adrian, *Assisted research of the rheological dampers with LabVIEW instrumentation,* The 1st European DAAAM International Young Researchers´ and Scientists´ Conference, 24-27th October 2007, University of Zadar, Zadar, Croatia, 2007.
[135] Olaru, A., Olaru, S. *Research Of The Industrial Robot Dynamic Behavior With Labview Instrumentation*, OPTIROB Proceedings, Romania, 2007.
[136] Oprean Aurel, Olaru Serban, Olaru Adrian. *Some Contributions Of The Modeling And Simulation Of The Magnetorheological Dampers*, OPTIROB Proceedings, Romania, 2007.
[137] Adrian Olaru, Paune Danut, Adrian Ghionea, Serban Olaru, Peli Alexandru *Research with LabVIEW instrumentation of the robot trajectory errors,* OPTIROB Proceedings, Romania, 2007.
[138] Adrian Olaru, Serban Olaru, *Assisted optimization of the electro-hydraulic servo driving with LabVIEW instrumentation,* The 6th Iranian Aerospace Society Conference- Feb. 2007-K.N.Toosi University of Technology, Teheran, Iran, 2007.
[139] Olaru Adrian, Olaru Serban, *Assisted dynamic behavior optimization of the robots elements and systems with the virtual instrumentation*, 15th Annual (International) Mechanical Engineering Conference May 2007, Amirkabir University of Technology, Tehran, Iran, 2007.
[140] Oprean Aurel**,** Olaru Serban, Olaru Adrian, *Some contributions on the magnetorheological damper assisted research ,* OPROTEH2007, Bacau, Romania, 2007.
[141] Serban Olaru, Adrian Olaru, *Assisted research of the Bouc-Wen damper new mathematical model with LabVIEW instrumentation,* AERO2008, Teheran, Iran, 2008.
[142] Olaru, A. & Olaru, S. **-***Research of the global dynamic compliance and the viscose global dynamic damper coefficient of the industrial robot-* The 17th INTERNATIONAL DAAAM SYMPOSIUM "Intelligent Manufacturing & Automation: Focus on Mechatronics & Robotics" 08-11th November 2006, Viena, Austria.
[143] Olaru Adrian, Olaru Serban**-** *Research of the industrial robot fourier spectrum with LabVIEW instrumentation* - First Regional Conference of Mechanical Engineering Islamic Azad University, Majlessi New Town Branch December 13th, 2006.
[144] Adrian Olaru *-Assisted research of the industrial robots global dynamic compliance with LabVIEW instrumentation-* Proceedings of the 15th International Conference on Manufacturing Systems – ICMaS Published by Editura Academiei Romane, University POLITEHNICA of Bucharest, Machine and Manufacturing Systems Department Bucharest, Romania, 26 - 27 October, 2006.

[145] Olaru, A. *Assisted research with virtual LabVIEW instrumentation of the industrial robots vibration behavior,* Acta Mechannica Slovaca, Vishe Ruzbachy, Slovacia 2004.
[146] Olaru A., Olaru S., Peli Al., Paune D. 3D complex trajectory by using the robots and perirobots components, 9th International Conference on Automation/ Robotics in Theory and Practice, Slovakia 2008, p.431-444.
[147] Oppermann, G.; Penners, G.; Schulze, M.; Marquardt, G.; Flindt, R.; Naumann, T. H.: Applications of electroviscous fluids as movement sensor control devices in active vibration dampers. In Carlson, J. D., editor: *Proceedings of the International Conference on Electrorheological Fluids,* Raleigh, NC, February 1989, 287-299.
[148] Parenti-Castelli, V., Di Gregorio, R., "A new algorithm based on two extra-sensors for real-time computation of the actual configuration of generalized Stewart-Gough manipulator",Journal of Mechanical Design, 122, 2000.
[149] Pang, L., Kamath, G.M., Werely, N.M., Analysis and Testing of a Linear Stroke Magnetorheological Damper, AIAA/ASME/AHS *Adaptive Structure Forum*, Long Beach CA, Paper no 98-2040, **CP9803**, Part 4, 1998.
[150] Peschel, M.J., Roschke, P.N., *Neuro-Fuzzy Model of a Large Magnetorheological Damper*, Proceedings Texas Section- ASCE, Spring Meeting San-Antonio, 2001.
[151] Petek, N. K.: An electronically controlled shock absorber using electrorheological fluid. Society of Automotive Engineers Technical Paper Series, Paper No. 920275, 1992.
[152] Powell, J. A.: Modelling the oscillatory response of an electrorheological fluid. Smart Materials and Structures, **3** (1994), 416-438.
[153] Powell J. A., "ERF as a Means of Vibration Suppression," *Proceedings of the International Conference on Vibration and Noise,* April 25-27, 1995, pp. 1-8.
[154] G. A. Pratt and M. M. Williamson, Series elastic actuators, in *IEEE Int. Conf. on Intelligent Robots and Systems (IROS)* (IEEE Press, 1995), pp. 399-406.
[155] Rettig U. and Von Stryk O., "Numerical Optimal Control Strategies for Semi-Active Vehicle Suspension With ERF Dampers" In: K.-H. Hoffmann, R.H.W. Hoppe, V. Schulz (eds.): *Fast Solution of Discretized Optimization Problems* ISNM Vol. 138 (Birkhauser Verlag 2001) pp. 221-241.
[156] D. W. Robison and J. E. Pratt, Series elastic actuator development for a biomimetic walking robot. in *IEEE/ASME Conf. on Advanced Intelligent Mechatronics* (1999).
[157] Ruocco, S. R. Robots Sensors and Transducers. Halsted Press John Wiley Sons, New York – Toronto, 1988.
[158] Ruocco, S. R. The design of a 3-D vision sensor 3- Ruocco, S. R. The design of a 3-D vision sensor suitable for robot multi-sensor feedback. Preccding 6th International Conference on Robot Vision and Sensory Control, 1986
[159] Ruocco, S. R. The design of a 3-D vision sensor Robots Sensors and Transducers. Halsted Press John Wiley Sons, New York – Toronto, 1988.
[160] Sakaguchi M. and Furusho J., " Force Display System Using Particle-Type Electrorheological Fluids," *Proceedings of the 1998 IEEE International Conference on Robotics and Automation,* Leuven, Belgium, May 1998, pp. 2586-2590.
[161] Sakaguchi M., Furusho J., Genda E., "Basic Study on Rehabilitation Training System Using ER Actuators,"*Proceedings of the IEEE International Conference on Systems, Man and Cybernetics*, Vol. 1, 1999, pp. I-135 - I-140.
[162] Sakaguchi M. and Furusho J., " Force Display System Using Particle-Type Electrorheological Fluids," *Proceedings of the 1998 IEEE International Conference on Robotics and Automation,* Leuven, Belgium, May 1998a, pp. 2586-2590.
[163] Sakaguchi M. and Furusho J., "Development of ER Actuators and Their Applications to Force Display Systems," *Proceedings of the 1998 IEEE Virtual Reality Annual International Symposium (VRAIS)*, Atlanta, GA, 1998b, pp. 66-70.
[164] Sarcos Inc., http://www.sarcos.com .
[165]Sensable Technologies, The Phantom, http://www.sensable.com/haptics/products/phantom.html
[166] Sherman KP, Ward JW, Sherman VY, Mohsen AMMA "Surgical Trainee Assessment using a VE Knee Arthroscopy Training System (VE-KATS): Experimental Results", . Proceedings of Medicine Meets Virtual Reality 2001, pages 465-470. IOS Press, 2001
[167] Simulation and Visualisation Research Group, Department of Computer Science, The University of Hull, UK, http://www2.dcs.hull.ac.uk/simmod/index.htm.
[168] Systems Laboratory, Southern Methodist University, http://cyborg.seas.smu.edu/syslab/PHI/MasterArm.html.
[169] N.C. Singer, and W.P. Seering, "Preshaping Command Inputs to Reduce System Vibration,"*ASME Journal of Dynamic Systems, Measurement and Control*, Vol.112, pp. 76-82, 1990.
[170] Sireteanu, T., Stancioiu, D., Ghita, GH., Stammers, C.W., *Semi-active vibration control by use ofmagnetorheological dampers*, Proceedings of the Romanian Academy, **1**, 2, pp. 195-199, 2000.
[171] Sireteanu, T., Stancioiu, D., Stammers, C.W., *Modelling of Magnetorheological Fluid Dampers*, Proceedings of theRomanian Academy, **2**, 3, pp. 105-113. 2001.
[172] Sireteanu, T., Ghita, G., Giuclea, M., Stammers, C.W., *Use of genetic algorithms and semi-active fuzzy control to optimize the model and dynamic response of vibration isolation systems with magnetorheological dampers*, Second International ICSC Symposium on Fuzzy Logic and Applications, 2001.
[173] T. Sireteanu, G. Ghita, M. Giuclea, C. W. Stammers,*Use of genetic algorithms and semi-active fuzyy control to optimize the model and dynamic response of vibration isolation systems with magnetorheological dampers,* **CIMA 2001** International ICSC Congress on COMPUTATIONAL INTELLIGENCE: METHODS AND APPLICATION, University of Wales, Bangor, U.K., 19th - 22th June 2001, Paper no.1713-154 on CD ROM- Proc.;

[174] Smart Technology Limited, http://www.smarttec.co.uk/erf.htm
[175] Bar-Cohen Y., Mavroidis C., Bouzit M., Dolgin B., Harm D., Kopchok G., White R., "Virtual Reality Robotic Operation Simulations Using MEMICA Haptic System," *SmartSystems 2000: The International Conference for Smart Systems and Robotics for Medicine and Space Applications* , September 6 to 8, 2000b, Houston, Texas.
[176] D. Stancioiu, T. Sireteanu, Gh. Ghita, Simona Gheorghe*, Analytical model of magneto-rheological damper,* **SISOM'01,** The Annual Symposium of the Institute of Solid Mechanics, Bucharest, 24- 25 May, 2001, p.239 - 244.
[177] Solonon, S. Sensor and control System in -Manufacturing. McGraw- Hill
[178] Society of Automotive Engineers, "Human tolerance to impact conditions as related to motor vehicle design-SAE J885 Jul86," *SAE Handbook (SAE Information Report)*, vol.3, pp. 34.464- 34.481, 1999.
[179] Spencer Jr., B. F.: Recent trends in vibration control in the U.S.A. In *Proceedings of the 3rd International Conference on Motion and Vibration Control,* Vol. 2, Chiba, Japan, 1-6 September 1996, K1-K6.
[180] Spencer Jr., B. F.; Dyke, S. J.; Sain, M. K.; Carlson, J. D.: Phenomenological model of a magnetorheological damper. Journal of Engineering Mechanics, **123** (1997), 230-238.
[181] Staicu, St., Aplicatii ale calculului matriceal in mecanica solidelor, Edit. Académie Roumaine, Bucharest, 1986.
[182] Staicu, St., Mecanica teoretica, Edit. Didactica & Pedagogica, Bucharest, 1998.
[183] Staicu, St., "Modèle dynamique en robotique", Scientific Bulletin, Series D, Mechanical Engineering, University „Politehnica"of Bucharest, 61, 3-4, 1999.
[184] Staicu, St., "Méthodes matricielles en dynamique des mécanismes", Scientific Bulletin, Series D, Mechanical Engineering, University „ Politehnica "of Bucharest, 62, 3, 2000.
[185] Staicu, St., Zhang, D., Rugescu, R., "Dynamic Modelling of a 3-DOF Parallel Manipulator Using Recursive Matrix Relations", Robotica, Cambridge University Press, Volume 24, 1, 2006, pp. 125-130.
[186] Staicu, St., Carp-Ciocardia, D.C., "Dynamic analysis of Clavel's Delta parallel robot", Proceedings of the IEEE International Conference on Robotics & Automation, Taipei, Taiwan, 2003, pp. 4116-4121.
[187] Stanway, R.; Sproston, J. L.; Stevens, N. G.: Nonlinear modelling of an electro-rheological vibration damper. Journal of Electrostatics, **20** (1987), 167-184.
[188] Stanway, R.; Sproston, J. L.; El-Wahed, A. K.: Applications of electro-rheological fluids in vibration control: a survey. Smart Materials and Structures, **5** (1996), 464-482.
[189] Stoer, J.; Bulirsch, R.: Introduction to Numerical Analysis. 2nd edition, Springer, Berlin, 1993.
[190] Stewart, D., "A Platform with Six Degrees of Freedom", Proc. Inst. Mech. Eng., 1, 15, 180, 1965.
[191] Stroe, I., Eftimie, E., Frincu, F. "Binary there-dimensional matrix sensor with detection tensometer" Preccding 12th International Conference Mittweida 1996, pp. 273-278.
[192] Shetty D., Kolk R. (1998): *Mechatronic System Design,* PWS Publications/Brooke Cole, Boston,USA
[193] Schlemer L., Alptekin S. (1998): *Team based product Development in Mechatronics Design Class,* ASME Presentations, 1998-WA/DE-193.
[194] S. Sugano, S. Tsuto and I. Kato, Force control of the robot finger joint equipped with mechanical compliance adjuster, in *IEEE Int. Conf. on Intelligent Robots and Systems (IROS)*(IEEE Press, 1992), pp. 2005-2012.
[195] Sundar, S. and Z. Shiller (1995). Time-optimal Obstacle Avoidance, Proceedings 1995 IEEE International Conference on Robotics and Automation, pp. 3075-3080.
[196] Taylor P. M., Hosseini-Sianaki A. and Varley C. J., "Surface Feedback for Virtual Environment Systems Using Electrorheological Fluids," *International Journal of Modern Physics B,* Vol. 10, No. 23 & 24, 1996, pp. 3011-3018.
[197] Taylor P. M., Hosseini-Sianaki A. and Varley C. J., "An Electrorheological Fluid-based Tactile Array for Virtual Environments," *Proceedings of the 1996 IEEE International Conference on Robotics and Automation,* Minneapolis, MN, April 1996a, pp. 18-23.
[198] Takegaki, M. and S. Arimoto (1981). A new feedback method for dynamic control of manipulators.
[199] N. Takesue, J. Furusho and Y. Kiyota, Analytic and experimental study on fast response Mrfluid actuator. in *IEEE Int. Conf. on Robotics and Automation (ICRA)* (IEEE Press, 2003), pp. 202-207.
[200] N. Takesue, H. Asaoka, J. Lin, M. Sakaguchi, G. Zhang and J. Furusho, Development and experiments of actuator using MR fluid, in,.26th Annual Conference of the IEEE Industrial Electronics *(IECON*) (IEEE Press, 2000), pp. 1838 – 1843.
[201] Tempea et al., I., Above Spatial Mechanisms Modeling and Kinematics Analysis aided CATIA SOLUTIONS, The Eight IFToMM International Symposium on Theory of Machines and Mechanisms Bucharest, ROMANIA, August 28 - September 1, 2001, Vol. II pp.177-182.
[202] Thompson :An active sustension with optimal linear state feedback. Vehicle System Dynamics, vol.5, pp.187- 203, 1976.
[203] Tremblay, A., Baron, L., "Geometrical Synthesis of Parallel Manipulators of Star–Like Topology with a Genetic Algorithm", IEEE International Conference on Robotics and Automation, Detroit, Michigan, 1999.
[204] Tsai, L-W., Robot analysis: the mechanics of serial and parallel manipulator, John Wiley & Sons, Inc., 1999.
[205] Tsai, L-W., Stamper, R., "A parallel manipulator with only translational degrees of freedom", ASME Design Engineering Technical conferences, Irvine, CA, 1996.
[206] Uhl T., Bojko T., Mrozek Z., Petko M., Szwabowski W., Korendo Z. and Bogacz M.(1999): *Selected problems of mechatronic design*.
[207] Uhl T., ´Sliwa Z. (1996): *Selected topics in CAD/CAM systems and their applications*.

[208] Uhl T. (2002): *A system of computer-aided mechatronic design*
[209] Uhl T., Bojko T., Mrozek Z. and Szwabowski W. (2000): *Rapid prototyping of mechatronic systems*. - J. Theoret. Appl. Mech., Vol. 38, No.3, pp. 655–668.
[210] Virtual Reality Laboratory, University of Tsukuba, Japan, http://intron.kz.tsukuba.ac.jp/vrlab_web/wearablemaster/wearablemaster_e.html.
[211] D. Vischer and O. Khatib, Design and development of high-performance rorque-controlled joints, *IEEE Transactions on Robotics and Automation* **11**.(4), (1995).
[212] Vitrani M., Nikitczuk J., Morel G. and Mavroidis C., "Torque Control of Electro-Rheological Fluidic Actuators for Haptic Vehicular Instruments Control," *Proceedings of the 2004 IEEE International Conference of Robotics and Automation,* New Orleans, LA, April 26 – May 1, 2004.
[213] Dan Zahng and Clement M. Gosselin , "Kinetostatic Modeling of N-DOF Parallel Mechanism With a Passive Constraining Leg and Prismatic Actuators", Journal of Mechanical Design, Vol. 123, 2001
[214] Zinn M., Khatib O., Roth B. and Salisbury, J.K.. A New Actuation Approach for Human Friendly Robot Design, in *Int. Symp. on Experimental Robotics* (Italy, 2002).
[215] W. Zhou, C.-M. Chew and G.-S. Hong, Force control characteristics of series damper actuator, *Internal Report of Control and Mechatronics Lab.*, Dept. of Mechanical Engineering, National Univ. of Singapore (2002).
[216] I. D. Walker, "Impact configurations and measures for kinematically redundant and multiple armed robot systems," *IEEE Trans. Robotics and Automation*, vol. 10, no. 5, pp. 670-683, 1994.
[217] Wang, J., Gosselin, C., "Representation of the Singularity Loci of a Special Class of Spherical 3-dof Parallel Manipulator with Revolute Actuators", CCToM Symposium on Mechanisms, Machines and Mechatronics, Saint-Hubert (Montréal), 2001.
[218] Wellman, P.S., Peine, W.J., and Howe, R.D., "Mechanical Design and Control of a High-Bandwidth Shape Memory Alloy Tactile Display," proceedings of the International Symposium of Experimental Robotics, Barcelona, Spain, June 1997.
[219] Williams II R.L., North D., Murphy M., Berlin J., and Krier M., "Kinesthetic Force/Moment Feedback via Active Exoskeleton", Proceedings of the Image Society Conference, Scottsdale, AZ, August 2-7, 1998.
[220] Wood D., "Editorial: Tactile Displays: Present and Future," *Displays-Technology and Applications*, Vol. 18, No. 3, 1998, pp. 125-128.
[221] Weiss, W. D.; Duclos, T. G.; Carlson, J. D.; Chrzan, M. J.; Margida, A. J.: High strength magneto- and electro-rheological fluids. Society of Automotive Engineers Technical Paper Series, Paper No. 932451, 1993.
[222] Manfred Weck, "Handbook of Machine Tools", Page Brothers (Norwich) Ltd ,Vol. 2, 1984
[223] Wen, Y.: Method for random vibration of hysteretic systems. Journal of the Engineering Mechanics Division, **102** (1976), 249-263.
[224] Whittle, M.; Atkin, R. J.; Bullough, W. A.: Fluid dynamic limitations on the performance of an electrorheological clutch. Journal of Non-Newtonian Fluid Mechanics, **57** (1995), 61-81.
[225] Winslow, W. M.: Induced vibration of suspensions. Journal of Applied Physics, **20** (1949), 1137-1140.
[226] Wood D., "Editorial: Tactile Displays: Present and Future," *Displays-Technology and Applications*, Vol. 18, No. 3, 1998, pp. 125-128.
[227]Papalambros Y. P. and Wilde J. D., *Principles of Optimal Design – Modeling and Computation*, Cambridge University Press, 1988.
[228] Yoshikawa, T., Manipulability of Robotic Mechanisms, *International Journal of Robotic Research*, Vol. 4 No. 2, pp. 3–9. 1985.
[229] Asada, H., A geometrical representation of manipulator dynamics and its application to arm design, *Transactions of ASME, Journal of Dynamic Systems.*, Meas. and Control, Vol. 105, pp. 131-135. 1983.
[230] Graettinger T. and Krogh B.H., The acceleration radius: A global performance measure for robotics manipulators, *Journal of Robotics and Automation*, Vol. 4, No 1, Feb 1988.
[231] Bowling A., Analysis of robotic manipulator dynamic performance: Acceleration and force capabilities, PhD-thesis, Stanford University. 1998.
[232] Ma Ou and Angeles J., Optimum Design of Manipulators Under Dynamic Isotropy Conditions, *Proceedings of IEEE International Conference on Robotics and Automation*, Vol. 1, pp. 470 – 475. 1993.
[233] Kahn W.A. and Angeles J., The kinetostatic optimization of robotic manipulators: the inverse and the direct problems, *Transactions of the ASME Journal of Mechanical Design*, Vol.128, No.1, pp.168-178, 2006.
[234] Salisbury, J. K., and Craig, J. J., Articulated Hands: Force Control and Kinematic Issues, *International Journal of Robotics Research*, Vol.1, No.1, pp.4–17, 1982.
[235] Kirkpatrick S., Gelatt C. D., and Vecchi M. P., "Optimization by simulated annealing," *Science*, Vol. 220, pp. 671-680, 1983.
[236] Workspacelt. [Online]. Available: *http://www.workspacelt.com.*
[237] Roboticsimulation. [Online]. Available: *https://robologix.com.*
[238] Ni-robotics. [Online]. Available: *http://www.ni.com.*
[239] Robonaut. [Online]. Available: http://robonaut.jsc.nasa.gov.
[240] Simrobot. [Online]. Available: http://www.informatik.uni-bremen.de.
[241] Open dynamics engine. [Online]. Available: *http://ode.org.*
[242] Bullet physics. [Online]. Available: *http://bulletphysics.org.*

[1243] Nvidia physx. [Online]. Available: *https://developer.nvidia.com/physx- sdk.*
[244] Dart. [Online]. Available: *http://dartsim.github.io*.
[245] RoKiSim − available at: *http://www.parallemic.org/RoKiSim. html*. Accessed in June 2016.
[246] M.A.Gonzalez-Palacios, E.A.Gonzalez-Barbosa, L.A.Aguilera- Cortes, *SnAM: a simulation software on serial manipulators,* Eng. Comput., 29 (2013), 87–94.
[247] M. Quigley, K. Conley, B. Gerkey, J. Faust, T. Foote, J. Leibs, E. Berger, R. Wheeler, A. Ng, ROS: an open-source robot operating system. *In ICRA Workshop on Open Source Software*, Vol. 3, No. 3.2, 2009.
[248] ROS – Gazebo Plugin, available at: *http://wiki.ros.org/gazebo*. Accessed on June 2016.
[249] Eulalie Coevoet, Thor Morales-Bieze, Frederick Largilliere, Zhongkai Zhang, Maxime Thieffry, et al.. *Software toolkit for modeling, simulation and control of soft robots. Advanced Robotics*, Taylor & Francis, 2017, pp.1-26. hal-01649355.
[250] J. Denavit and R. S. Hartenberg, A Kinematic Notation for Lower-Pair Mechanisms Based on Matrices, *Trans. of ASME,Journal of Applied Mechanics,*23:215–221.
[251] J. T. Feddema, Kinematically optimal placement for minimum time coordinated motion, Robotics and Automation, 1996 *IEEE International Conference* on Volume 4, Issue, 22-28 Apr 1996, pp. 3395-3400.
[252] L. Tian and C. Collins, Optimal placement of a two-link planar manipulator using a genetic algorithm, *Robotica Journal*, Cambridge University Press, Issue 02 - Mar 2005, Volume 23, pp. 169-176.
[253] Othayoth RS, Chittawadigi RG, Joshi RP, Saha SK. *Robot kinematics made easy using RoboAnalyzer software.* Comput Appl Eng Educ. 2017;9999:1–12. https://doi.org/10.1002/ cae.21828.
[254] F. A. Candelas, S.T. Puente, F. Torres, F. G. Ortiz, P. Gil, J. Pomares, *A virtual laboratory for teaching robotics,* Int J. Eng. Educ., 19 (2003), 363–370.
[255] C. A. Jara, F. A. Candelas, J. Pomares, F. Torres, *Java software platform for the development for advanced robotic virtual laboratories,* Comput. Appl. Eng. Educ., 21 (2013), 14–30.
[256] Navaraja, N.Jain, D.Sengupta, C.S.Kumar, Web based simulation and remote triggered laboratory for robots, *28th International Conference on CAD/CAM, Robotics and Factories of the Future*, 2016, 665–677.
[257] H. D. Nayar, Robotect: serial-link manipulator design software for modeling, visualization and performance analysis, *7th Int. Conf. Control, Autom., Robot. and Vision*, 2002, 1360–1364.
[257] M. Freese, S. Singh, F. Ozaki, N. Matsuhira, Virtual robot experimentation platform V-REP: a versatile 3D robot simulator, *Int. Conf. Simulation, Modeling, and Programming for Autonomous Robots*. 2010, 51–62.
[259] O. Michel, *Webots: professional mobile robot simulation*, Int J. Adv. Robot. Syst., 1 (2004), 39–42.
[260] A.Gil,O.Reinoso, J.M.Marin, L.Paya, J.Ruiz, *Development and deployment of a new robotics toolbox for education,* Comput. Appl. Eng. Educ., 23 (2015), 443–454. https://doi.org/10.1002/cae.21615.
[261] M.Flanders, R.Kavanaugh, *Build-A-Robot:using virtual reality to visualize the Denavit– Hartenberg parameters*, Comput. Appl. Eng. Educ., 23 (2015), 846–853.
[262] S. Kucuk, Z. Bingul, *An off-line robot simulation toolbox*, Comput. Appl. Eng. Educ.,18 (2010), 41–52.
[263] M. A. Gonzalez-Palacios, Advanced engineering platform for industrial development, *J. Appl. Res. Tech.*, 10 (2012), 309–326.
[264] Olaru, A, Olaru, S. and Mihai, N., Proper Assisted Research Method Solving of the Robots Inverse Kinematics Problem, *Applied Mechanics and Materials,* 555 (2014) 135-147.
[265] A. Olaru, S. Olaru, L.Ciupitu, Assisted research of the neural network by back propagation algorithm, *OPTIROB 2010 International Conference,* Calimanesti, Romania, The Reserch Publishing Services Singapore Book, (2010) 194-200.
[266] A. Olaru, S. Olaru and N. Mihai, Proper Assisted Research Method Solving of the Robots Inverse Kinematics Problem, *Applied Mechanics and Materials,* vol.555, 2014, 135-147.
[267] A. Olaru, S. Olaru and L. Ciupitu, Assisted research of the neural network by back propagation algorithm, *OPTIROB 2010 International Conference,* Calimanesti, Romania, May 28-th–30-th,2010,The Research Publishing Services Singapore Book, ISBN 978-981-08-5840-7, Editors: A. Olaru, L. Ciupitu, and S. Olaru, pp. 194-200, 2010.
***http://cgi.omg.org/news/pr97/umlprimer.html
***http://pigseye.kennesaw.edu/~dbraun/csis4650/
***MATLAB, SIMULINK, STATEFLOW (2003): *Real TimeWorkshop*
***http://www.reatek.com/
****A UML Documentation for an Elevator System*, Embedded Systems, Fall 2000
***http://www.iis.ee.ic.ac.uk/~frank/surp00/article1/ vgpf98/#Activity
***http://www.gdpro.com/what_is_uml.html
***STÄUBLI RX brochure GB.pdf.
***Dassault Systèmes, CATIA Version 5 User's Documentation.
***http://www.kinematics.com
***http://www.easyrob.com
***http://robotworks-eu.com
***http://camelot.dk
***Engineering Note, LORD Corporation.
***Applied Physics, Vol. 21, 1988, pp. 1661.
***Logitech Inc., http://www.logitech.com.

***Microsoft Corp., http://www.microsoft.com/hardware/sidewinder/devices/default.asp .
***http://vesuvius.jsc.nasa.gov/er_er/html/robonaut/robonaut.html .
***http://www.ent.ohiou.edu/~bobw/html/Projs.html.